I. TERNARY PHASE EQUILIBRIA IN THE SYSTEMS Ti-Fe-C, Ti-Co-C, AND Ti-Ni-C

II. PHASE EQUILIBRIA OF THE TY:E METAL CARBONITRIDE + GRAPHITE + NITROGEN IN THE SYSTEMS T - C- N

III. THERMODYNAMIC CONSIDERATIONS OF CHEMICAL VAPOR DEPOSITION REACTIONS FOR SELECTED CARBIDES, NITRIDES, AND OXIDES

Philip Harold Booker
B.S. University of California, Berkeley, 1967
M.S., University of Denver, 1970

A dissertation submitted to the faculty
of the Oregon Graduate Center
inppartial fulfillment of the
requirements for the degree
Doctor of Philosophy
in
Materials Science

July 1979

This thesis has been examined and approved by the following Examination Committee.

Erwin Rudy, Thesis Advisor
Professor

William E. Wood, Dept. Chairman
Associate Professor

Nicholas G. Eror
Associate Professor

Lynwood W. Swanson
Professor

ACKNOWLEDGMENTS

The author wishes to express his sincere appreciation to Professor Erwin Rudy for providing the opportunity for this research to be carried out and for his valuable discussions at points during this work. In addition, the cooperation and suggestions from members of the Faculty and Staff of the Oregon Graduate Center are gratefully acknowledged.

Thanks are due to the following persons for their help in the preparation of the thesis manuscript: Mrs. Janijo Weidner and Mrs. Barbara Ryall for the final typing and the preparation of drawings.

The financial assistance from the Teledyne Wah Chang Albany Corporation, the National Science Foundation, and the D.S. and R. H. Gottesman Tuition Fellowship for various parts of the work conducted is greatly appreciated.

TABLE OF CONTENTS

ABSTRACT

The experimental and theoretical work presented in this thesis was conducted in order to help further the technology associated with the development of composite wear and corrosion resistant tool materials. The information presented, i.e. fundamental data concerning phase equilibria and thermodynamic considerations for the deposition of alloys from multiple vapor sources, may be used for the formulation of well characterized alloy systems belonging to the carbide, nitride, and oxide family.

Specific hard, refractory alloy systems investigated include binary and ternary titanium-ferrous metals with carbon and ternary systems of the group IV transition metals with carbon and nitrogen. The observed phase relationships established during the course of these investigations are discussed

INTRODUCTORY DISCUSSION

The majority of commercial wear-resistant tool steel and sintered (cemented) carbide alloys currently used by industry were developed during the first half of this century. Over the years the use of sintered carbides in place of tool steels has grown; historically, this development process was due to early research which first provided improved wire drawing dies, then better cutting tools, and finally the application of sintered carbides to a variety of other forming dies, tools, and wear parts. Although no single phase is present in sintered carbides, at times they are collectively called "tungsten carbide", since the earliest successful alloys were based on this constituent.

Due to the properties of tungsten carbide and often strategic nature of tungsten, the historical development of sintered carbides for tool and wear applications can be divided into the continued improvement of alloys based on tungsten carbide and alloys designed to avoid or reduce its use. In general, the work presented in the three parts of this thesis should be viewed in this light. The information presented, i.e., fundamental data concerning phase equilibria and phase stabilities, may be used for the formulation of well characterized wear-resistant alloy systems belonging to the carbide, nitride, and oxide family; which may or may not contain tungsten carbide. In order to to efficiently use this data, we must first consider some of the properties associated with current material systems.

Both the tool steels and sintered carbides may be viewed as microcomposites in that they contain a hard phase(s), usually a carbide, embedded in a continuous ferrous metal alloy matrix. The hard, but brittle, carbide phase provides the needed abrasion resistance, and the ductile metal alloy phase adds the needed strength and toughness. In general, the metal matrix in wrought tool steels consists of an iron-base alloy and the hard carbide phase, e.g., carbides of V, Cr, Mo, and W, is usually formed by precipitation reactions. In contrast, carbide tool alloys with metal matrix-hard phase combinations of Co(Ni)-WC, Co-(Ti,Ta,W)C, and Ni(Mo)-TiC, as examples, are made by powder metallurgical techniques, and in all cases the carbide phase is consolidated by the metal binder which is liquid at sintering temperatures.

The wrought tool steels are inherently tougher than the sintered carbides because of their higher metal alloy content. When used as a machine tool, they exhibit good impact strength and wear resistance but are limited to local maximum temperatures of several hundred degrees centigrade. The resulting poor wear characteristics (softening and loss of structural integrity) at higher temperatures are due to dissolution reactions of the hard carbide phases in the iron base matrix or decomposition of the metastable ferrous martensite.

The tool steels are essentially a fixed material system because their carbide content is controlled by the carbon solubility in the steel matrix at subsolidus temperatures. On the other hand, the carbide loading of sintered tool alloys can be varied at will, and hence more abrasion resistant refractory composites can be formulated. For example, some machine tool grades can retain their structural integrity at localized temperatures on the order of 1000°C (generated by high cutting speeds). But for many applications, e.g., during interrupted cutting operations or conditions which produce high impact type loads, the sintered carbides exhibit poor mechanical shock resistance and hence fail accordingly.

In addition to catastrophic failure, thermal deformation, abrasive wear, and chemical interaction between the sintered carbide, workpiece, and gas phase lead to tool failures in many machining operations.

Significant improvements have been made in reducing failures associated with the latter two failure modes by applying protective coatings through the technique of chemical vapor deposition. However, the development of sintered carbide substrate-coating systems still suffers many problems. Reactions involving the gas phase and coating with the substrate during the deposition process can result in the formation of microporosity and low strength phases at the substrate-coating interface. If reactions of this type are not controlled, they will result in the observed cracking and spally tendency of coatings under heavy load conditions plus increase the impact sensitivity of the macrocomposite.

The reported shortcomings associated with current wear-resistant alloys are mainly related to toughness, hot strength, and corrosion resistance. These mechanical and chemical properties must be improved so that the inherent high hardness of these composites is fully realized. Since the choice of suitable hard phases is limited to the transition metal carbides and nitrides, and a few metal oxides which are chemically compatible with iron-group metals and certain refractory transition metal alloys, the metal matrix phase must provide improved toughness and hot strength qualities. By optimizing the mechanical properties of these microcomposites, coatings of either single or multi phase hard alloys based on stable carbides, nitrides, and oxides must provide any improved wear and corrosion resistant qualities.

In general, the higher the stability difference between coexisting phases of a composite tool alloy or constituents of a tool alloy and workpiece, the less will be their mutual solubilities and compositional changes with temperature. This is the desired condition for protective coatings in which the tendency for chemical interaction between tool and workpiece is reduced, and wear and corrosion resistance increased. On the other hand, by decreasing the stability difference between coexisting phases through compositional modifications, the bond strength of the hard phase – metal binder interface may be improved. That is, by providing hard metal microcomposites as well as hard metal-coating macrocomposites where partial solutioning or phase interchange reactions can occur, more coherent systems will result with improved strength and thermomechanical fatigue characteristics.

The above discussions have been presented to point out areas of development for improved wear-resistant alloys. In order to help further this technology, the investigations presented in this thesis on equilibria involving the hard, refractory titanium monocarbide phase and iron-group metals (Part I), and the group IV transition metal carbonitrides (Part II) were conducted. Because the group IV transition metal carbides-nitrides are thermodynamically more stable than higher group transition metal carbides, the carbonitrides are of interest as protective coatings. The stability data presented on these systems (Parts I and II) combined with thermodynamic considerations for their formation from the vapor phase (Part III) may be used to establish deposition conditions for a preselected alloy. In addition, other protective wear-resistant coatings are considered.

PART I

TERNARY PHASE EQUILIBRIA IN THE SYSTEMS Ti-Fe-C, Ti-Co-C, AND Ti-Ni-C

TABLE OF CONTENTS

PAGE

I. TERNARY PHASE EQUILIBRIA IN THE SYSTEMS Ti-Fe-C, Ti-Co-C, AND Ti-Ni-C.

A. Introduction and Summary

B. Literature Review

1. Binary Systems

2. Ternary Systems

C. Experimental Procedures

TABLE OF CONTENTS (Cont'd)

D. Experimental Results

2. The Ti-Co-C System

3. The Ti-Ni-C System

LIST OF FIGURES

LIST OF FIGURES (Cont'd)

LIST OF FIGURES (Cont'd)

LIST OF FIGURES (Cont'd)

LIST OF FIGURES (Cont'd)

LIST OF FIGURES (Cont'd)

LIST OF FIGURES (Cont'd

LIST OF TABLES

PART I

A. INTRODUCTION AND SUMMARY

1. Introduction

The success of wear-resistant materials consisting of a dispersion of a hard, refractory transition metal-interstitial phase(s) in a ductile metal matrix depends upon the intrinsic mechanical and chemical properties of the composite. Before considering the mechanical compatibility of the high and low modulus phases, it is absolutely essential to establish the chemical interactions between alloy constituents under environments of interest.

In general, when service conditions imposed upon the composite are not severe, non-equilibrium phase mixtures may be tolerated. But due to the refractory nature of the alloys considered, coexisting phases must be chemically compatible to ensure the structural integrity of parts subjected to high temperatures during fabrication and service.

Although one can predict the stability of combinations of materials from the principles of chemical thermodynamics, the lack of pertinent thermodynamic data combined with often complex phase relationships make calculations of this type impossible.

Therefore, the best way to obtain phase equilibria data is to systematically investigate systems of interest.

The above discussions present the underlying initiatives for the investigation of the three ternary systems Ti-Fe-C, Ti-Co-C, and Ti-Ni-C which contain the hard and refractory titanium monocarbide phase. If the high-temperature phase characteristics are known, alloys may be formulated that will assure intrinsic chemical stability of the composite. This data will also provide information on the upper temperature service limit for a particular alloy since its melting temperature will be known.

2. Summary

The alloy systems titanium-iron-carbon, titanium-cobalt-carbon, and titanium-nickel-carbon were investigated by means of X-ray diffraction, metallographic, and melting point techniques. In addition, due to conflicting results found in the literature on the constitution diagrams of the systems Ti-Fe, Ti-Co, Ti-Ni, Fe-C, Co-C, and Ni-C, additional investigations were performed in order to better establish the melting behavior and/or homogeneity limits of phases in these systems. These results will be reported in a later section, but they will be included in the summary of the above ternary systems.

For the ternary systems, no ternary phases are formed, and the solid state phase equilibria is governed solely by the respective binary boundary phases. That is, the resulting two-phase equilibria between titanium monocarbide and titanium-ferrous metal phases are directly attributable to the large stability difference between titanium and ferrous metal carbide phases. At and above 900°C, neither titanium carbide nor any of the titanium-ferrous metal binary phases exhibit appreciable mutual solubility among themselves or with graphite.

The phase relationships in the ternary systems Ti-Fe-C, Ti-Co-C, and Ti-Ni-C from 900°C through the melting range are summarized below.

a. Ti-Fe-C System

The solid state equilibria in this system are characterized by the two-phase equilibria between titanium monocarbide and the phases of β-Ti$_{(ss)}$, TiFe, $TiFe_2$, and α, γ-Fe, and Fe_3C*. In the temperature range from 900°C through melting, all eight isothermal reactions which occur involve a liquid phase. Three correspond to class I (ternary eutectic) four-phase reactions, three

---

*(Metastable equilibrium)

to class II four-phase reactions, and two to limiting tie line reactions (pseudobinary eutectic). These reaction isotherms, in order of decreasing temperature, are:

(1) 1475°C: $L \rightleftarrows TiC_{1-x} + \alpha\text{-Fe}$

(2) 1409°C: $L + \alpha\text{-Fe} \rightleftarrows TiC_{1-x} + \gamma\text{-Fe}$

(3) 1370°C: $L \rightleftarrows TiC_{1-x} + TiFe_2$

(4) 1299°C: $L \rightleftarrows TiC_{1-x} + TiFe_2 + \alpha\text{-Fe}$

(5) 1268°C: $L + TiFe_2 \rightleftarrows TiC_{1-x} + TiFe$

(6)* 1240°C: $L + C \rightleftarrows TiC_{1-x} + Fe_3C$

(7)* 1109°C: $L \rightleftarrows TiC_{1-x} + \gamma\text{-Fe} + Fe_3C$

(8) 1058°C: $L \rightleftarrows TiC_{1-x} + \beta\text{-Ti} + TiFe$

*(Metastable equilibrium)

Based on the melting behavior and combined metallographic and X-ray diffraction evaluation of binary Fe-C and ternary alloys within composition regions containing the Fe_3C phase, reactions (6) and (7) are proposed. These results are not consistent with the thermodynamic calculations of Chipman,(45,46) which result in a congruently melting metastable Fe_3C phase. The three-phase equilibrium $L\text{-}Fe_3C\text{-}C$, which originates at the class II four-phase reaction plane of 1240° C (reaction 6), requires the Fe_3C phase to melt peritectically in the Fe-C binary system.

Using the isothermal sections (Figures 40(a) through 40(e), an isometric view of the ternary system was constructed (Figure 1). The three-dimensional space model is supplemented by a reaction diagram of the binary and ternary isothermal reactions (Figure 2); and a diagram illustrating the flow of melting troughs, the compositions of liquid vertices of three-phase equilibria entering into isothermal reactions, as well as the liquidus projections (Figure 3). In addition, an isopleth exhibiting the principal phase equilibria in the metal rich region of the system is presented in Figure 4. For the phase symbols used in the isopleth, a legend may be found in Figure 2.

b. Ti-Co-C System

The experimental data obtained during the investigation of the Ti-Co-C system, as presented in the isothermal sections (Figures 68(a) through 68(f)), were used to construct a three-dimensional space model of the system for temperatures above 900°C (Figure 5). This space model is supplemented by a reaction diagram of the binary and ternary isothermal reactions (Figure 6), a projection of the liquidus surface (Figure 7), and an isopleth (Figure 8) exhibiting the principal phase equilibria in the ternary system. For the phase symbols used in the isopleth, a legend may be found in Figure 6.

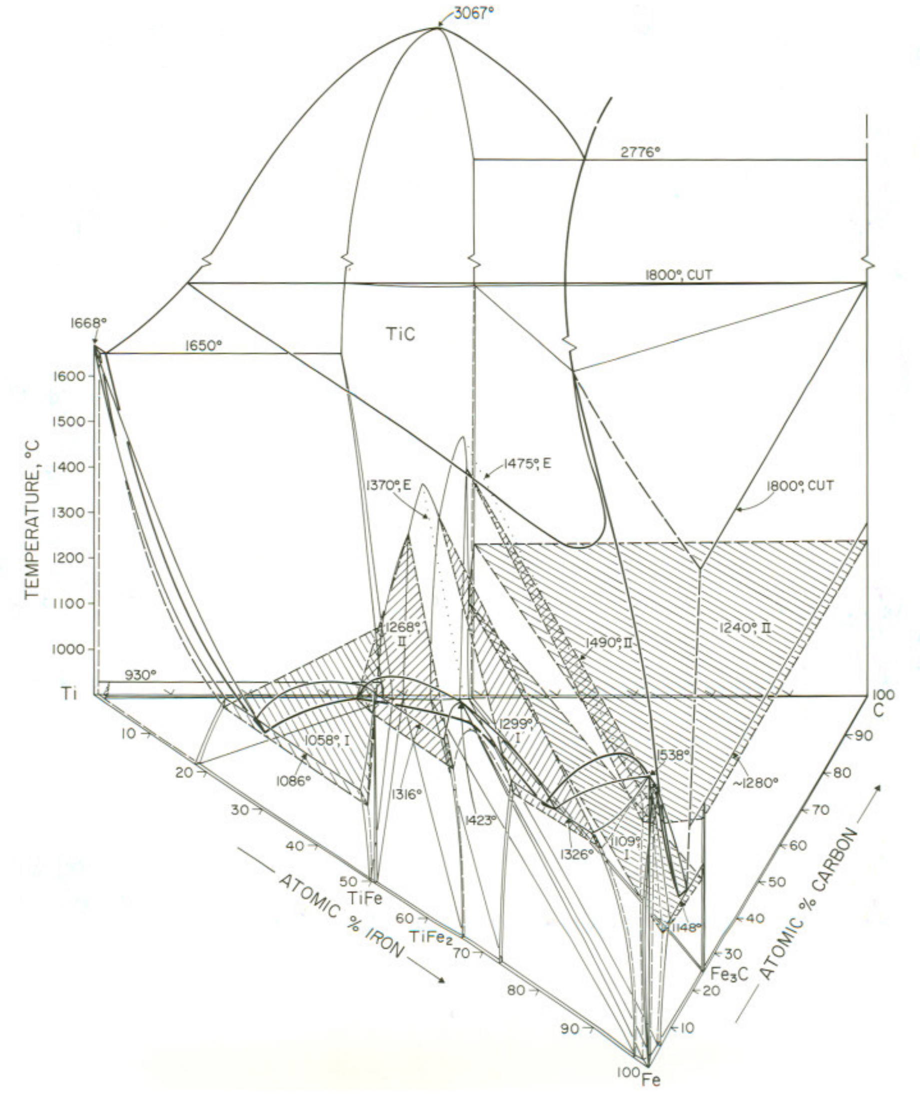

Figure 1. Proposed Metastable Constitution Diagram for the System Titanium-Iron-Carbon.

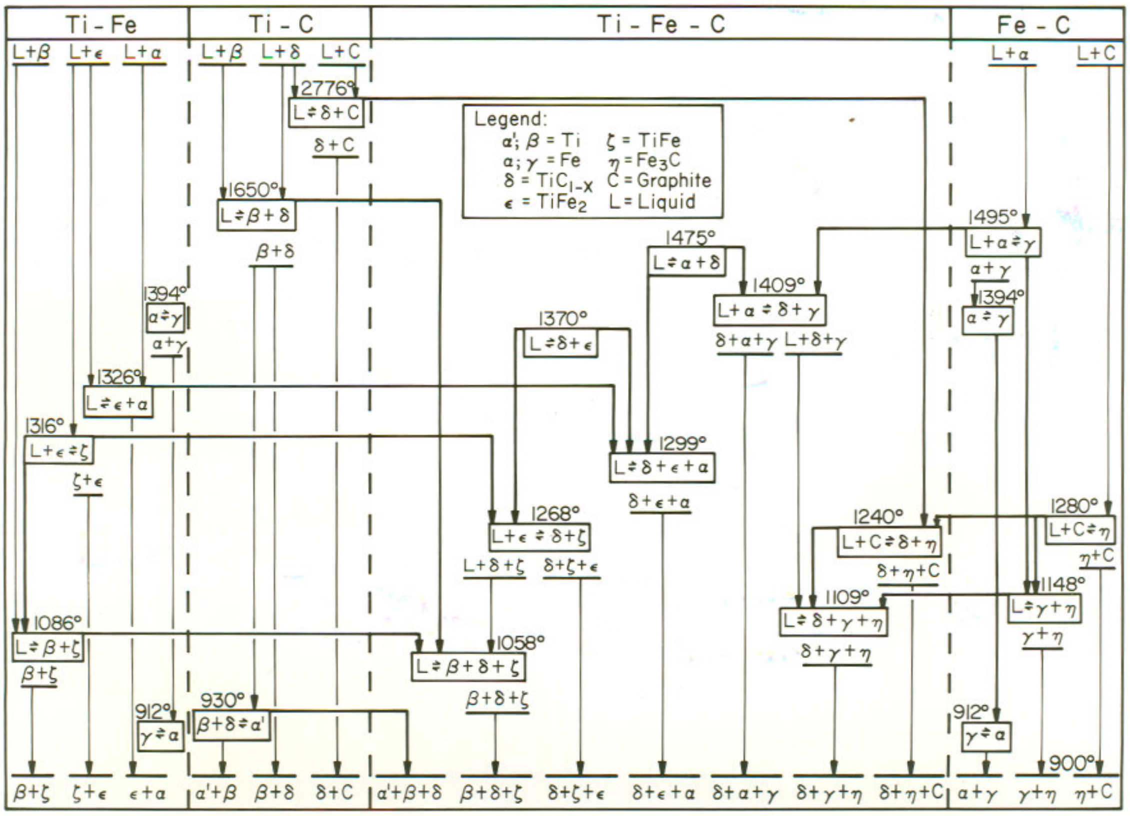

Figure 2. Reaction Diagram for the Ti-Fe-C System Above 900°C.

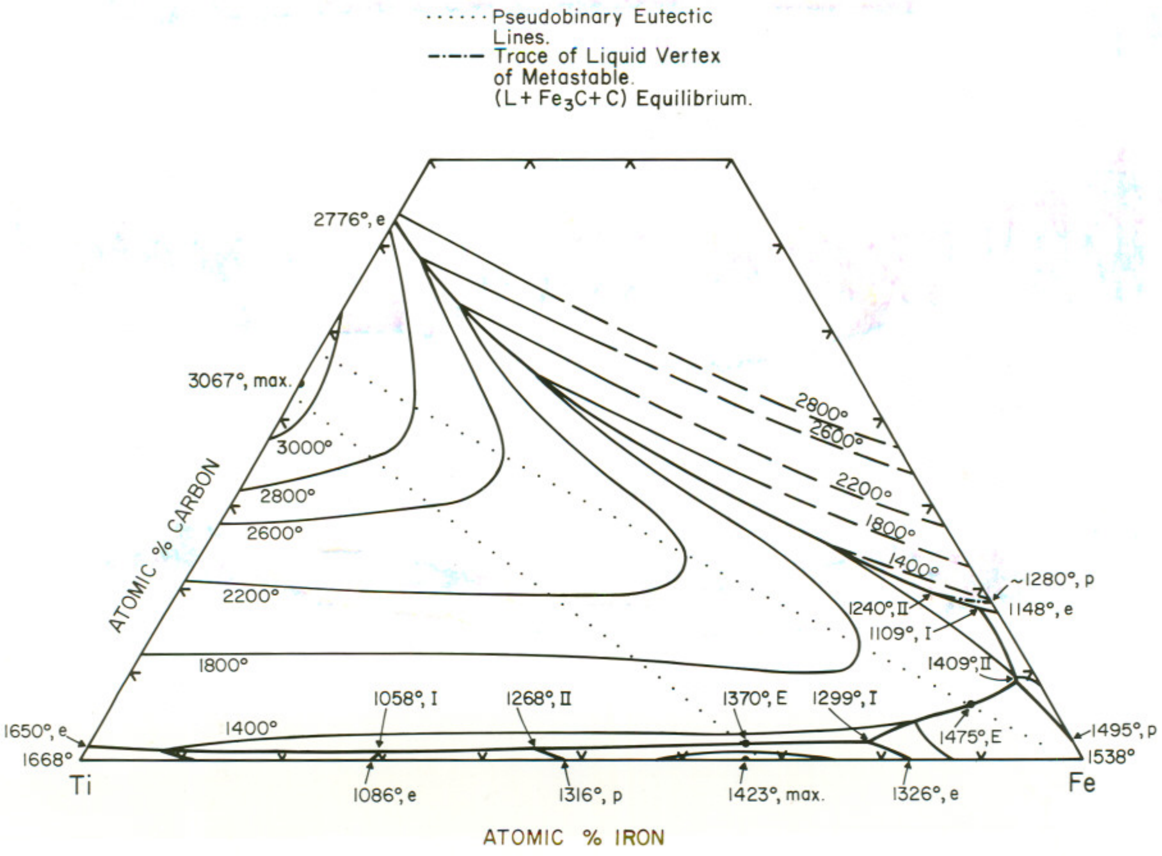

Figure 3. Liquidus Projections in the Ti-Fe-C System.

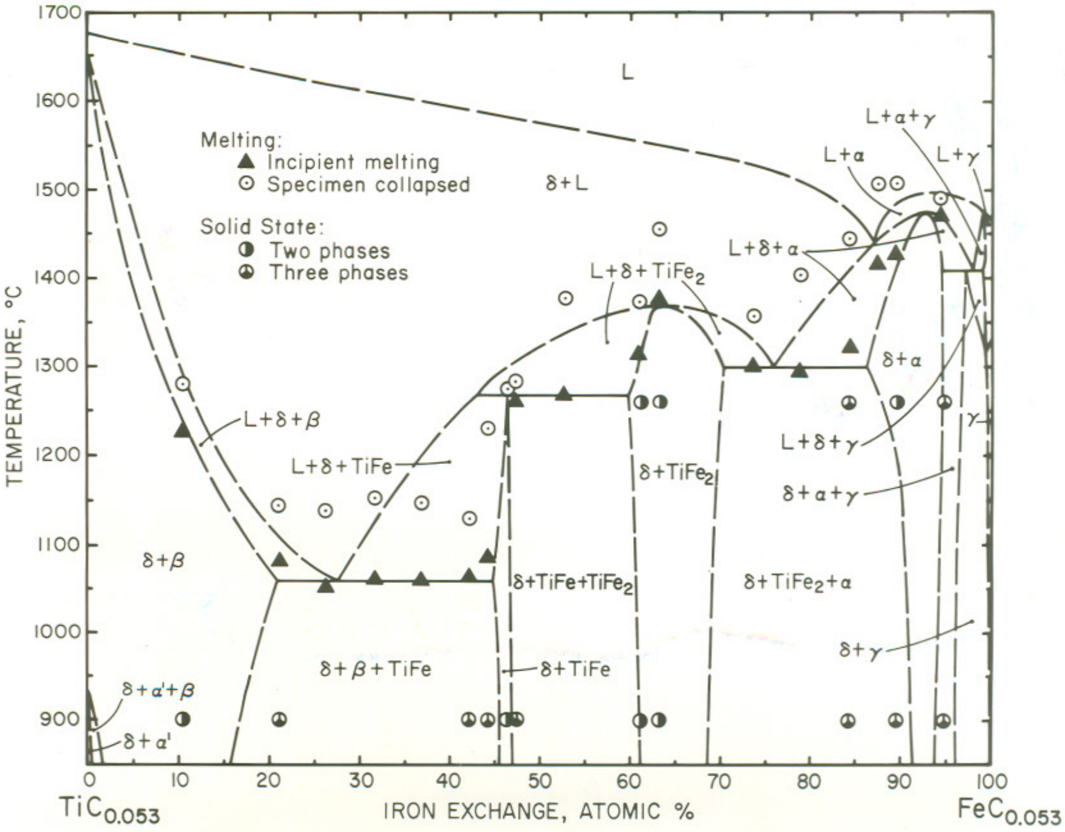

Figure 4. Isopleth at 5 Atomic % Carbon. Experimental Melting Temperatures and Qualitative Phase Evaluation of Ti-Fe-C Alloys.

The solid state equilibria are characterized by two-phase equilibria between carbon-deficient titanium monocarbide and the phases $\beta\text{-Ti}_{(ss)}$, Ti_2Co, TiCo, $TiCo_2$, $TiCo_3$, and $\gamma\text{-Co}_{(ss)}$. In the temperature range from 900°C through melting, ten isothermal reactions occur: four class I (ternary eutectic) four-phase reactions, four class II ternary reactions, and two limiting tie line reactions (pseudobinary eutectic). These reaction isotherms are listed in order of decreasing temperature:

(1) 1372°C: $L \rightleftarrows TiC_{1-x} + \gamma\text{-Co}$

(2) 1293°C: $L \rightleftarrows TiC_{1-x} + TiCo$

(3) 1247°C: $L + TiCo \rightleftarrows TiC_{1-x} + k\text{-}TiCo_2$

(4) 1236°C: $L \rightleftarrows TiC_{1-x} + \gamma\text{-Co} + C$

(5) 1220°C: $L + \gamma\text{-Co} \rightleftarrows TiC_{1-x} + TiCo_3$

(6) ~1215°C: $L + k\text{-}TiCo_2 \rightleftarrows TiC_{1-x} + \epsilon\text{-}TiCo_2$

(7) 1110°C: $L \rightleftarrows TiC_{1-x} + \epsilon\text{-}TiCo_2 + TiCo_3$

(8) 1066°C: $L + TiCo \rightleftarrows TiC_{1-x} + Ti_2Co$

(9) ≃1060°C: $TiC_{1-x} + k\text{-}TiCo_2 \rightleftarrows TiCo + \epsilon\text{-}TiCo_2$

(10): 1033°C: $L \rightleftarrows TiC_{1-x} + \beta\text{-Ti} + Ti_2Co$

The class II four-phase reaction occurring at ≃ 1060°C (reaction 9) results from the three-phase equilibrium $TiC\text{-}k\ TiCo_2\text{-}\epsilon\ TiCo_2$ which originates eutectoidally in the binary

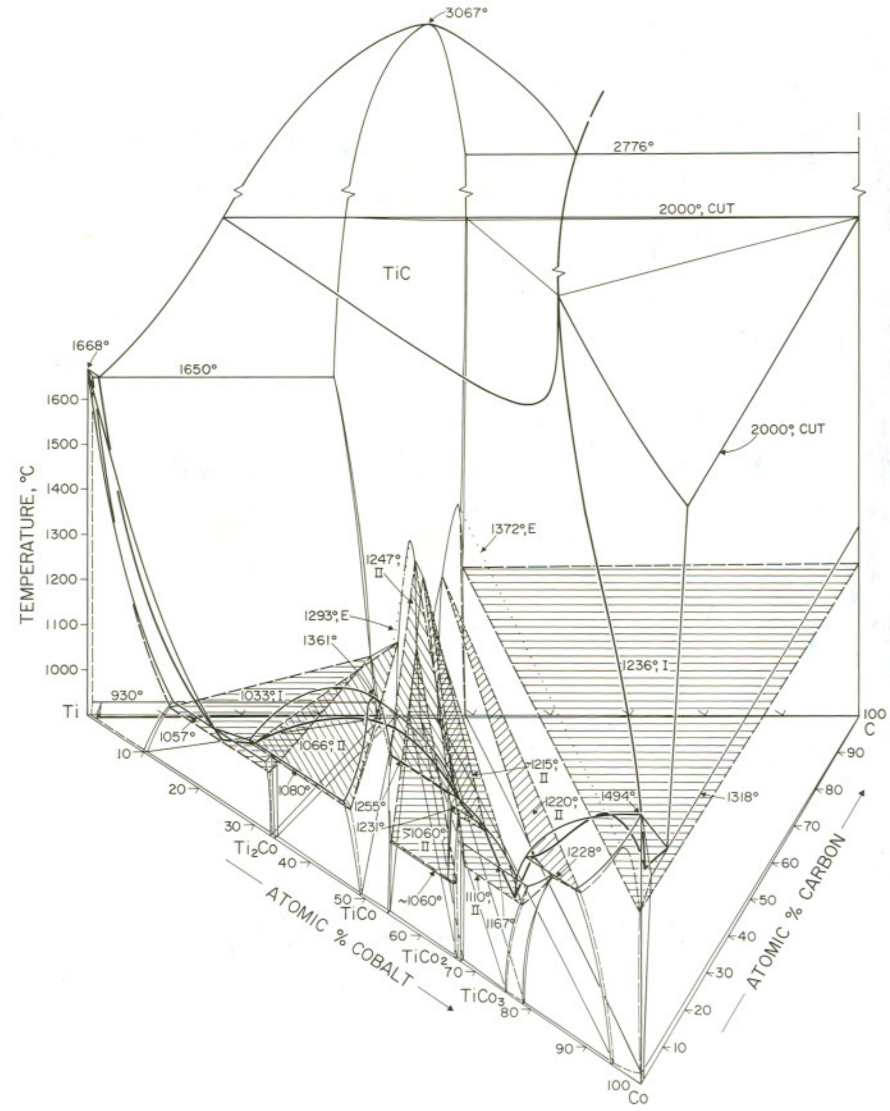

Figure 5. Constitution Diagram for the System Titanium-Cobalt-Carbon.

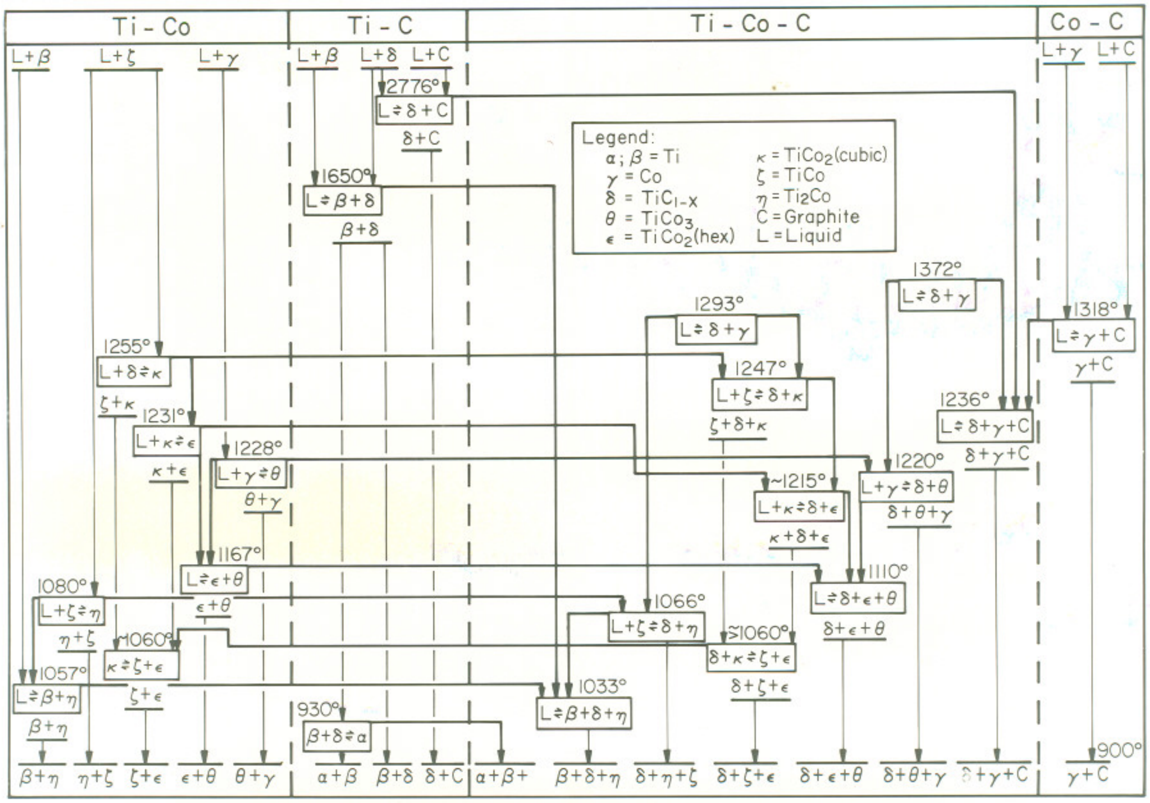

Figure 6. Reaction Diagram for the Ti-Co-C System Above 900°C.

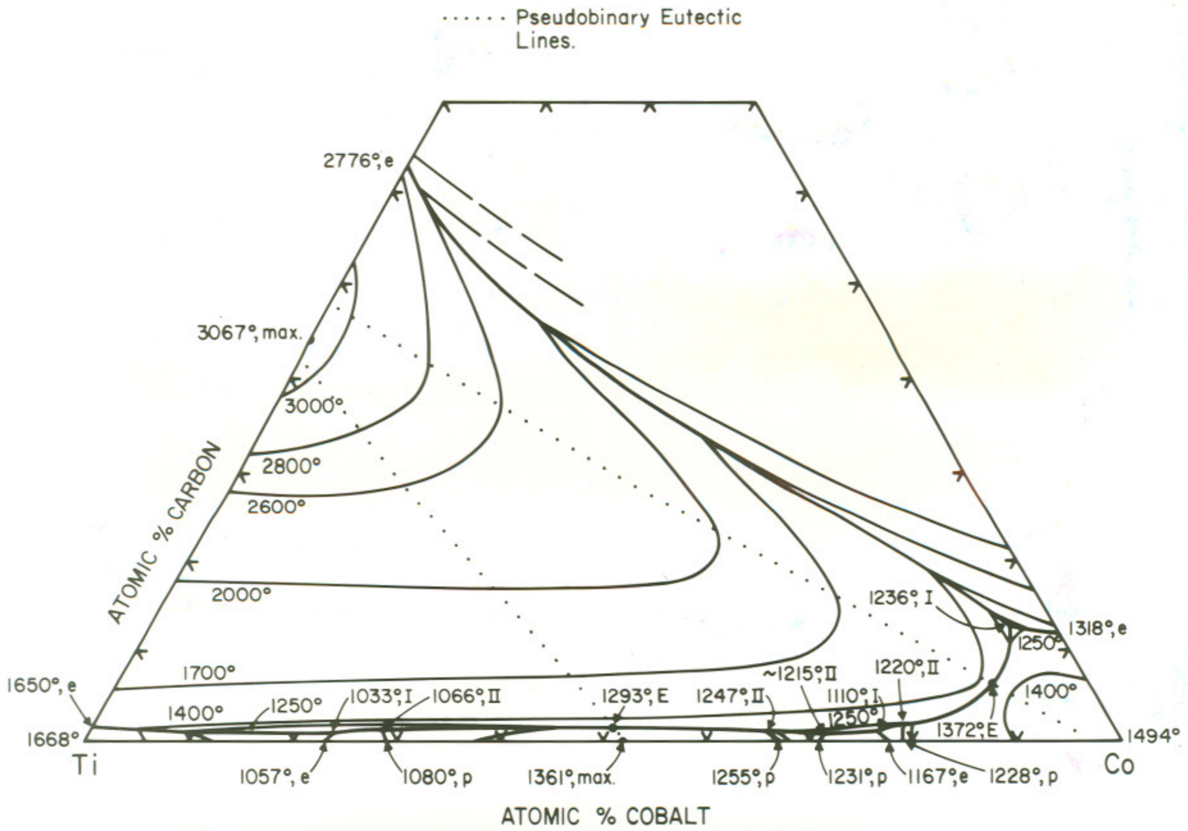

Figure 7. Liquidus Projections in the Ti-Co-C System.

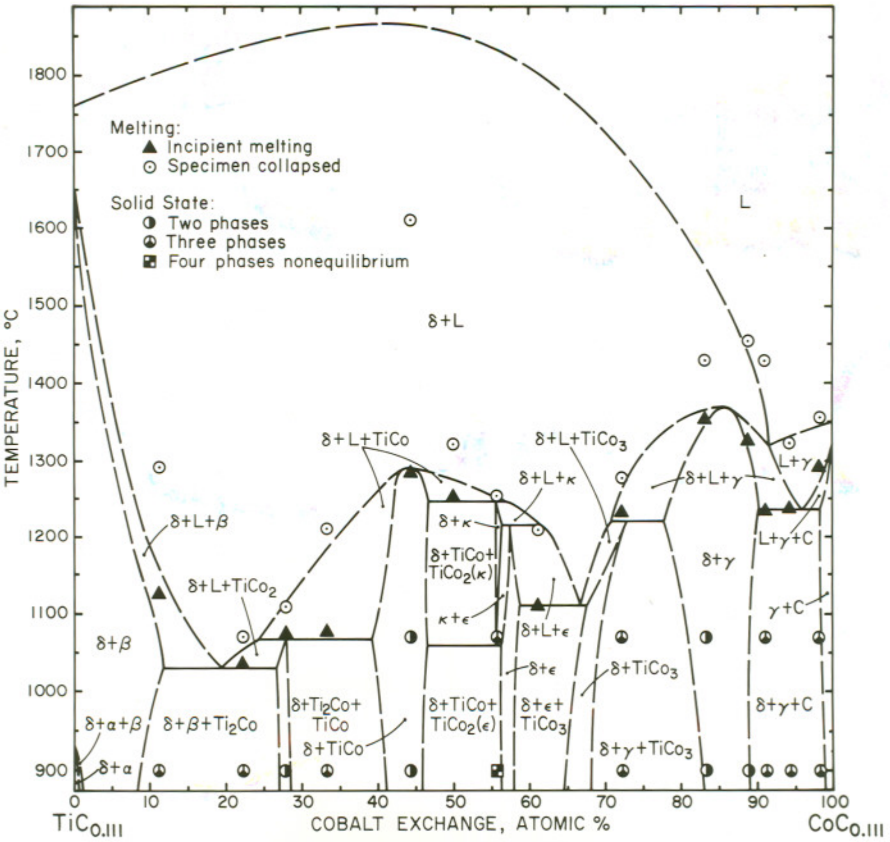

Figure 8. Isopleth at 10 Atomic % Carbon. Experimental Melting Temperatures and Qualitative Phase Evaluation of Ti-Co-C Alloys.

Ti-Co system at approximately the same temperature. The eutectoid decomposition of the cubic modification of $TiCo_2$(k) was established from the combined metallographic and X-ray diffraction evaluation of both as melted and heat treated binary and ternary alloy samples. This result conflicts with the most recently proposed phase diagram of the Ti-Co binary system(4), which shows both the cubic (k) and hexagonal (ϵ) modifications of $TiCo_2$ stable at room temperature.

c. Ti-Ni-C System

The solid state equilibria in this system are characterized by two-phase equilibria between carbon-deficient titanium monocarbide and the phases β-$Ti_{(ss)}$, Ti_2Ni, TiNi, $TiNi_3$, and $Ni_{(ss)}$. In the temperature range from 900°C through melting, eight isothermal reactions occur all of which involve a liquid phase. Four correspond to class I (ternary eutectic) four-phase reactions, one to a class III (ternary peritectic) four-phase reaction, and three to limiting tie line reactions (pseudobinary eutectic). These reaction isotherms, in order of decreasing temperature, are:

(1) 1367°C: $L \rightleftarrows TiC_{1-x} + TiNi_3$

(2) 1302°C: $L \rightleftarrows TiC_{1-x} + Ni_{(ss)}$

(3) 1280°C: $L \rightleftarrows TiC_{1-x} + TiNi$

(4) 1277°C: $L \rightleftarrows TiC_{1-x} + Ni_{(ss)} + C$

(5) 1272°C: $L \rightleftarrows TiC_{1-x} + TiNi_3 + Ni_{(ss)}$

(6) 1124°C: $L \rightleftarrows TiC_{1-x} + TiNi + TiNi_3$

(7) 1030°C: $L + TiC_{1-x} + TiNi \rightleftarrows Ti_2Ni$

(8) 953°C: $L \rightleftarrows TiC_{1-x} + \beta\text{-}Ti + Ti_2Ni$

From the melting behavior of the binary Ti_2Ni phase it was established that this phase decomposes peritectically at a temperature of 985° ± 7°C. This reaction temperature agrees with the value reported by Hawkins(4); Poole and Hume-Rothery(25).

The intermetallic Ti_2Ni phase is stabilized to higher temperatures by additions of carbon. The three-phase equilibrium L-Ti_2Ni-TiNi, which originates at the binary peritectic temperature, participates in the class III (ternary peritectic) four-phase reaction at 1030° ± 17°C (reaction 7). Ternary alloys partaking in the proposed class III reaction consistently melted at a higher temperature when compared to the peritectic Ti_2Ni binary alloys.

Indirectly, the above results agree with the Margolin, Ence, and Nielsen(21) investigation of the Ti-Ni binary system. These investigators conducted their melting point determination with arc melted alloys placed in graphite crucibles and reported that the Ti_2Ni phase melted peritectically at approximately 1015°C. In addition, their reported eutectic solidification temperature of 955° ± 5°C for the binary reaction $L \rightleftarrows \beta\text{-}Ti_{(ss)} + Ti_2Ni$ corresponds quite closely to the temperature of 953° ± 8°C obtained in this investigation for the class I ternary eutectic reaction (8).

Using the isothermal sections (Figures 102a through 102d), a three-dimensional space model of the ternary system was constructed (Figure 9). This three-dimensional view is supplemented by a reaction diagram (Figure 10), a projection of the liquidus surface (Figure 11), and an isopleth at 10 atomic % carbon exhibiting the principal phase equilibria in the system (Figure 12). A legend for the phase symbols used in the isopleth may be found in Figure 10.

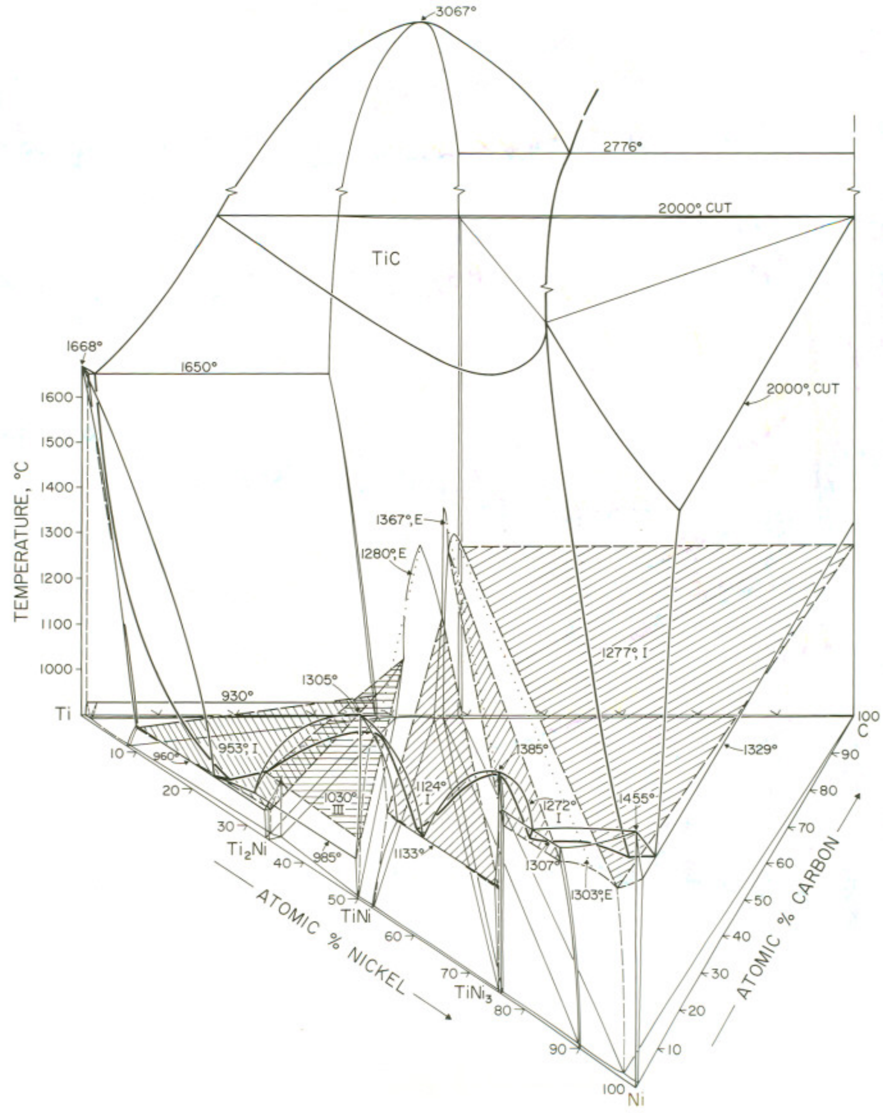

Figure 9. Constitution Diagram for the System Titanium-Nickel-Carbon.

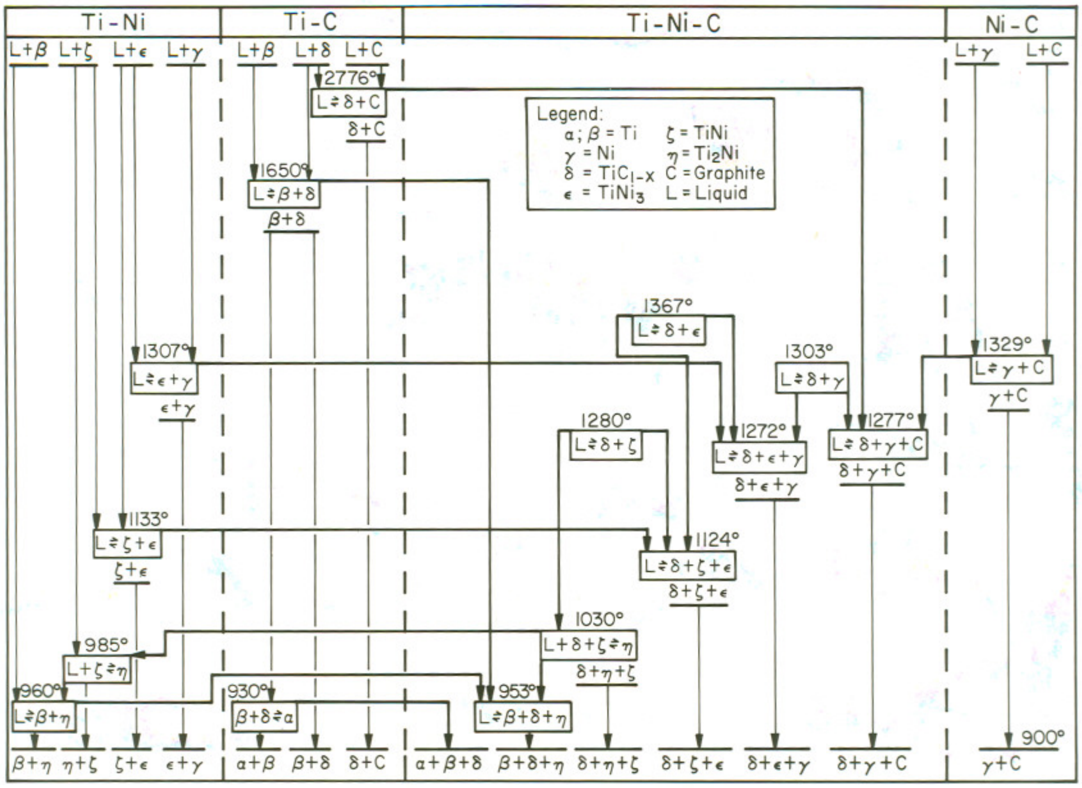

Figure 10. Reaction Diagram for the Ti-Ni-C System above 900°C.

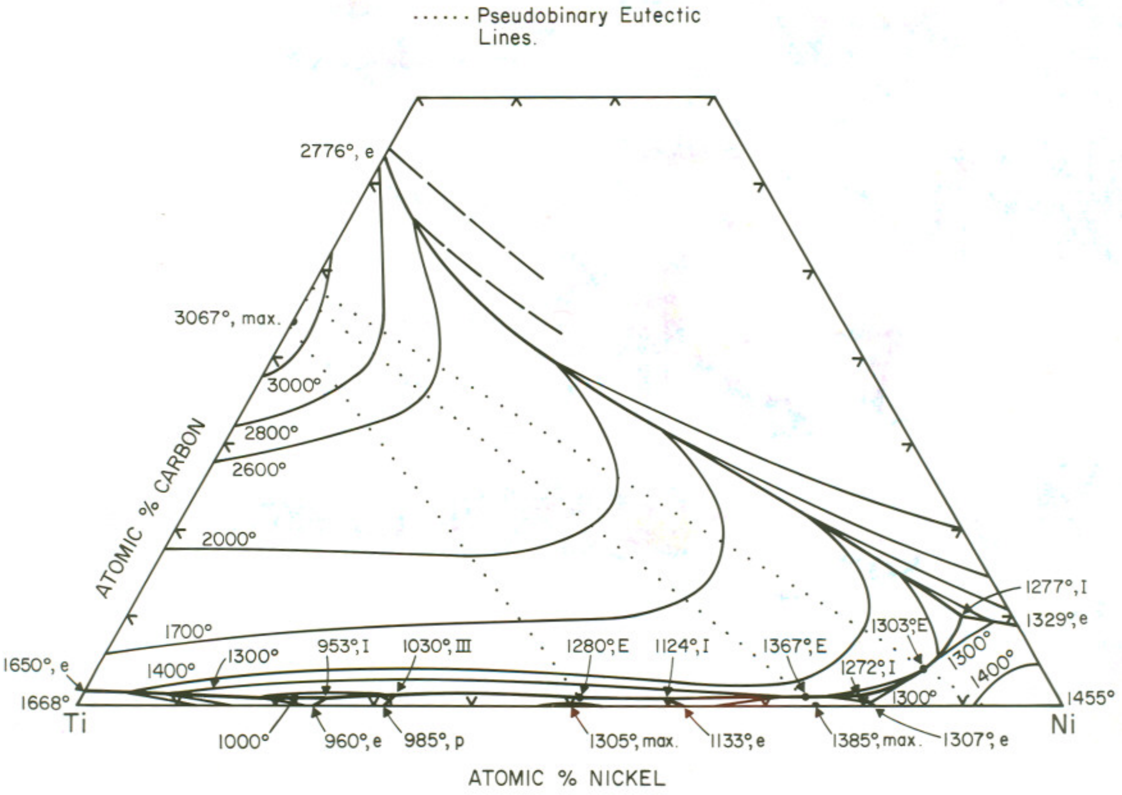

Figure 11. Liquidus Projections in the Ti-Ni-C System.

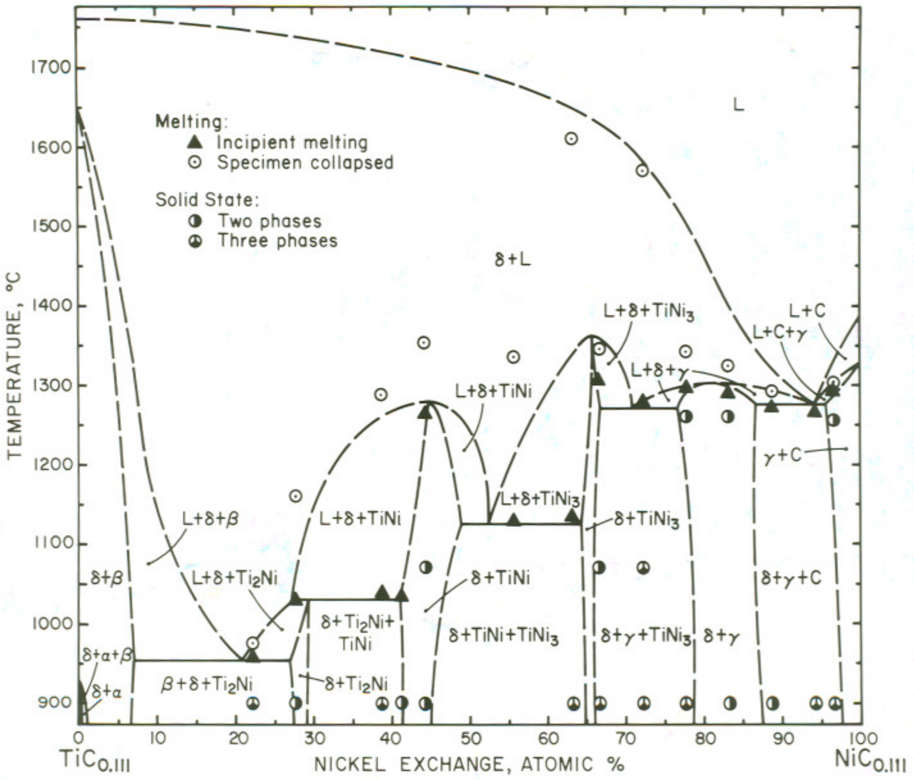

Figure 12. Isopleth at 10 Atomic % Carbon. Experimental Melting Temperatures and Qualitative Phase Evaluation of Ti-Ni-C Alloys.

B. LITERATURE REVIEW

1. Binary Systems

a. The Ti-Fe System

The titanium-iron system has been the object of many investigations; for a detailed account regarding some of the earlier work on this system, the reader is referred to the information compiled by M. Hansen(1). For more recent investigations, the information compiled by R.P. Elliott(2), F. A. Shunk(3), and the American Society for Metals(4) may be consulted.

Phase diagrams for the system were published by R.P. Elliott(2) and P. K. Rohatgi(4). The diagrams constructed were very similar; only slight differences in reaction temperatures and coexisting phase compositions were reported. According to these reviews, the system contains two intermediate phases: TiFe and $TiFe_2$; the former decomposes peritectically at 1319°C and the latter melts congruently at 1429°C. Eutectic equilibria are formed between $TiFe_2$ and Fe at 1290°C, and between Ti and TiFe at 1085°C.

The maximum solubility of titanium in γ-iron, which forms a closed γ phase field, amounts to ~0.76 At.% Ti at 1100°C(2). T. Wada(5) conducted a dilatometric analysis of arc melted iron alloys containing up to 0.8 At.% Ti and showed that the (α-γ) phase boundaries rise continuously from the iron transformation temperature. This result is in agreement with Elliott(2). Previous investigations reported by Hansen(1), showed a minimum in the γ-Fe loop. The iron-stabilized β-Ti solid solution decomposes eutectoidally at ~590°C(1,2,3).

Presented in Table I are the literature values for reaction isotherms in the system; also included are the compositions of the equilibrium phases.

In addition to the intermediate phases of TiFe and $TiFe_2$, the existence of two additional phases, Ti_2Fe and $TiFe_3$, have been reported in the literature(7,8,9). These phases have been shown not to exist(1,3,4,10), and their stabilization has been attributed to either substitutional or interstitial alloying of impurities. Presented in Table II are the structures and lattice parameters of Ti-Fe alloys obtained from the literature.

TABLE I

Isothermal Reactions in the System Ti-Fe(2,4)

Temperature, °C*	Transformation or Reaction Type	Composition of the Equilibrium Phases, At.% Fe		
1668 ± 8° (6)	L ⇄ β-Ti	-	-	-
880 ± 10° (6)	β-Ti ⇄ α-Ti	-	-	-
1085°	L ⇄ β-Ti + TiFe	~29	~23	47.6
~590°	β-Ti ⇄ αTi + TiFe	~13	~0.4	48
1319°	$TiFe_2$ + L ⇄ TiFe	63.3	49.5	50.2
1429°	L ⇄ $TiFe_2$	~66.7	~66.7	-
1290°	L ⇄ α-Fe + $TiFe_2$	84	~90	~75
1538°	L ⇄ α-Fe	100	100	-
1394°	α-Fe ⇄ γ-Fe	100	100	-
912°	γ-Fe ⇄ α-Fe	100	100	-

*Temperature errors are based on estimated overall uncertainty.

TABLE II

Structures and Lattice Parameters of Ti-Fe Alloys

Phase	Structure Type Space Group	Lattice Parameters, Å
Ti	1. T<880°C: hex., Mg (A3), D_{6h}^{4}-P6_3/mmc	a=2.9504; c=4.6833 (10)
	2. T>880°C: cubic, W(A2), O_h^9 - Im3m	a=3.3065 at 900°C (11) a=3.16$_0$ (20.2 At.% Fe) (10)
Ti_2Fe	Cubic, Fe_3W_3C(E9_3) O_h^7 - Fd3m	a=11.328 (9) Not a stable phase in binary. Isomorphous with Fe_2Ti_4O; Fe_3Ti_3O (10)
TiFe	Cubic, CsCl (B2) O_h^1 - Pm3m	a=2.978 (10) a=2.982 (Fe-rich phase boundary (10) a=2.975 (9) a=2.976 (49.5 At.% Ti) (2) a=2.991 (52.5 At.% Ti) (2)
$TiFe_2$	Hex.,$MgZn_2$(C14), D_{6h}^{4}-P6_c/mmc	a=4.759; c 7.831 (11) a=4.78; c 7.80 (1) a=4.779; c 7.761 (1) a=4.760; c 7.831 (1) a=4.77$_4$; c 7.79$_4$ (27.4 At.% Ti) (2) a=4.81$_4$; c 7.85$_0$ (37 At.% Ti) (2) a 4.785$_7$; c 7.799 (3)
$TiFe_3$	Tetrag., $TiAl_3$ (DO), D_{4h}^{17}-14/mmm	a=5.20; c=8.17 (8) Not a stable phase in binary. Alloys contaminated with Al;Si. (1,3)
Fe	1. T<912°C: cubic, W(A2), O_h^9-Im3m	a=2.8662$_1$ (10) a=2.8710$_7$ (2.26 At.% Ti) (10)
	2. 912°C<T<1394°C: cubic, Cu(Al) O_h^5-Fm3m	a= 3.6467 at 916°C (11)
	3. T>1394°C: cubic, W(A2), O_h^9-Im3m	a= 2.9322 at 1394°C (10)

b. The Ti-Co System

According to the reviews of Hansen(1), Elliott(2), Shunk(3), and the investigations conducted by Iannucci et al.(12) and Barton et al.(13), the system contains five intermediate phases: Ti_2Co, TiCo, $TiCo_2$ (two modifications), and $TiCo_3$. The phase equilibria resulting from the first two phases seem to be fairly well established(4). Ti_2Co decomposes peritectically at ~1050°C, and TiCo melts congruently at ~1340°C. A eutectic equilibrium is formed between Ti and Ti_2Co at ~1015°C. The cobalt-stabilized β-Ti solid solution decomposes eutectoidally at ~680°C.

There have been contradictory results from past investigations on cobalt-rich binary alloys. The phase corresponding to the composition $TiCo_2$ was investigated by Wallbaum and Witte(14), and they reported its structure as being cubic ($MgCu_2$ type) for titanium-rich alloys and hexagonal ($MgNi_2$ type) for cobalt-rich alloys. Duwez and Taylor(9) prepared alloys by powder metallurgical methods and sintered them at 1000°C for four hours under vacuum. Their results showed only the hexagonal ($MgNi_2$ type) phase and failed to confirm the existence of a cubic ($MgCu_2$ type) modification for alloys around the composition $TiCo_2$. Pearson(10), Elliott(2), and Iannucci et al.(12) have reported that both modifications are stable at room temperature. A proposed phase diagram for the system(4) shows the cubic and hexagonal modifications of $TiCo_2$ melting peritectically at ~1250°C and ~1230°C, respectively.

A eutectic equilibrium is formed between $TiCo_2$ and $TiCo_3$ at ~1170°C(2,4), and the $TiCo_3$ phase decomposes peritectically at ~1200°C(2,4).

Listed in Table III are proposed literature values for isothermal reactions in the system, and Table IV gives the structures and lattice parameters of Ti-Co alloys.

c. The Ti-Ni System

The phase equilibria resulting in the Ti-Ni system seem to be fairly well established. Phase diagrams constructed from literature reviews by M. Hansen(1) and D.T. Hawkins(4) show that the system contains three intermediate phases: Ti_2Ni, TiNi, and $TiNi_3$. Ti_2Ni decomposes peritectically at 985°C, and both TiNi and $TiNi_3$ melt congruently at 1312°C and 1380°C, respectively. Eutectic equilibria are formed between Ti and Ti_2Ni at 943°C, TiNi and $TiNi_3$ at 1120°C, and $TiNi_3$ and Ni at 1306°C. The nickel-stabilized β-Ti solid solution decomposes eutectoidally at ~770°C.

There has been some doubt concerning the low-temperature stability of the TiNi phase. An investigation conducted

TABLE III

Proposed Isothermal Reactions for the System Ti-Co

Temperature, °C	Transformation or Reaction Type	Composition of the Equilibrium Phases, At. % Co		
1020 ± 5° (1,2)	$L \rightleftarrows \beta\text{-Ti} + Ti_2Co$	~23	14.5	33
1015° (4,12)	"	22.8	14.4	33
685 ± 10° (1,2)	$\beta\text{-Ti} \rightleftarrows \alpha\text{-Ti} + Ti_2Co$	~ 8	0.8	33
1055° ± 5° (1,2)	$TiCo + L \rightleftarrows Ti_2Co$	50	~27	33
~1050° (4,12)	"	46	26	33
~1300° (2)	$L \rightleftarrows TiCo$	50	50	--
~1340° (4,12)	"	51.4	51.4	--
~1250° (2,4)	$L + TiCo \rightleftarrows (\text{cubic})TiCo_2$	~68	55.5	66.7
~1230° (2,4)	$L + (\text{cubic})TiCo_2 \rightleftarrows (\text{hex.})TiCo_2$	~69	~67	~68
~1170°C (2,4)	$L \rightleftarrows (\text{hex.})TiCo_2 + TiCo_3$	77	~68	80
~1200° (4)	$Co + L \rightleftarrows TiCo_3$	89	79	84
~1200° (2)	"	87.2	80.5	84
1494° (4)	$L \rightleftarrows Co$	100	100	--
~450° (10)	$Co\ (\text{cubic}) \rightleftarrows Co\ (\text{hex.})$	100	100	--

TABLE IV

Structures and Lattice Parameters of Ti-Co Alloys

Phase	Structure Type, Spage Group	Lattice Parameters, Å
Ti_2Co	Cubic, Fe_3W_3C ($E9_3$)	a=11.306 (9)
	O_h^7-Fd3m	a=11.30 (10)
TiCo	Cubic, CsCl (B2)	a=2.994 (9)
	O_h^1-Pm3m	a=2.991 (15)
		a=2.987 (16)
		a=2.995 (17)
$TiCo_2$	1. Cubic, $MgCu_2$(C15)	a=6.706 (65 At.% Co) (14)
	O_h^7-Fd3m	a=6.706 (66.7 At.% Co) (18)
		a=6.73 (67 At.% Co) (19)
	2. Hex., $MgNi_2$(C36),	a=4.724; c 15.40 (67.7 At.% Co)(14)
	D_{6h}^4-$P6_3$/mmc	a=4.729; c 15.423 (65 At.% Co) (9)
		a=4.72; c 15.40 (20)
TiCo	Cubic, $AuCu_3$($L1_2$)	a=3.604 (Co-rich) (20)
	O_h^1-Pm3m	a=3.613 (Ti-rich) (20)
Co	1. $T<\sim 450^\circ C$	a=2.5053; c 4.0886 (11)
	hex., Mg(A3)	a=2.5074; c 4.0699 (10)
	D_{6h}^4-$P6_3$/mmc	
	2. $T>\sim 450^\circ C$	a=3.5447 (hex. + cubic) (11)
	cubic, Cu(A1)	a=3.5442 (hex. + cubic) (10)
	O_h^5-Fm3m	a=3.544 (hex. + cubic) (10)
		a=3.626 at 1147°C (cubic only) (10)
		a=3.631 at 1223°C (cubic only) (10)

by H. Margolin et al.(21) showed that TiNi alloys heat treated at 750°C for 48 hours remained single phased. G.R. Purdy and J.G. Parr(22) and F.W. Wang et al.(23) concluded that TiNi is stable at room temperature. On the other hand, P. Duwez and J.L.Taylor(9,24) heat treated alloys at 650° to 800°C for 10 days and noted that TiNi decomposed eutectoidally into Ti_2Ni and $TiNi_3$. D.M. Poole and W. Hume-Rothery(25) also found that the phase decomposed at lower temperatures.

Other investigators(26-29) have shown that TiNi decomposes into one or both of the phases Ti_2Ni and $TiNi_3$ at or below 650°C. In a more recent investigation conducted by D.Koskimaki et al.(30), they placed the eutectoid reaction temperature at ~640°C. These same authors(30) also reported that the decomposition reaction of the body centered cubic (B2-type) phase is preceded by the formation of a metastable cubic precipitate which is accommodated in the B2 matrix by misfit dislocations.

In addition to the transition phase formed by solid state diffusion, M.J. Marcinkowski et al.(31) conducted a detailed transmission electron microscopy investigation of the TiNi phase and found that a monoclinic martensite is formed either thermally or by plastic deformation.

There has been some conflict in the literature as to the location of the eutectic composition between $TiNi_3$ and Ni. As presented in Hansen$^{(1)}$, Vogel and Wallbaum$^{(32)}$ concluded that the eutectic composition was at 80.8 At.% Ni; whereas Poole and Hume-Rothery$^{(25)}$ placed it at 85 At.% Ni, close to the maximum solubility of titanium in nickel, 13.8 At.%. In a more recent investigation on the morphology of directionally solidified $TiNi_3$-Ni eutectic alloys conducted by Sheffler et al.$^{(33)}$, they reported a eutectic composition of approximately 83.6 At.% Ni. Still in an alloy of this composition, primary dendrites of nickel were noted$^{(33)}$ which contained $TiNi_3$ precipitates in a Widmanstatten structure.

Presented in Table V are selected literature values for reaction isotherms in the Ti-Ni system, and Table VI gives the structures and lattice parameters.

d. The Ti-C System

For an exhaustive compilation of earlier work on the Ti-C system, M. Hansen's "Constitution of Binary Alloys"$^{(1)}$, R. Kieffer and F. Benesovsky's "Hartstoffe"$^{(35)}$, as well as E.K. Storms' "Refractory Carbides"$^{(36)}$ may be consulted.

Only one stable intermediate phase is formed in the system, titanium monocarbide with a cubic NaCl-type

TABLE V

Isothermal Reactions in the System Ti-Ni

Temperature, °C	Transformation or Reaction Type	Composition of the Equilibrium Phases, At.% Ni		
955° (21)	$L \rightleftarrows \beta\text{-Ti} + Ti_2Ni$	24.5	11	33
943° (4,25)	"	24.5	10.3	33
770° (1)	$\beta\text{-Ti} \rightleftarrows \alpha\text{-Ti} + Ti_2Ni$	∼5	< 0.2	33
1015° (21)	$TiNi + L \rightleftarrows Ti_2Ni$	49	33	33.3
985° (4,25)	"	49	32	33.3
1240° (21)	$L \rightleftarrows TiNi$	∼50	∼50	--
1312° (4,25)	"	∼50	∼50	--
∼640° (4,30)	$TiNi \rightleftarrows Ti_2Ni + TiNi_3$	∼52	∼33.3	∼75
1110° (21)	$L \rightleftarrows TiNi + TiNi_3$	∼60	∼54	∼75
1120° (4,25)	"	∼61.5	57	∼75
1378° (32)	$L \rightleftarrows TiNi_3$	75	75	0
1382° (4,25)	"	75	75	0
1287° (32)	$L \rightleftarrows TiNi_3 + Ni$	80.8	∼75	∼85
1306° (4,25)	"	85	∼75	86.2
1455° (4)	$L \rightleftarrows Ni$	100	100	--

TABLE VI

Structures and Lattice Parameters of Ti-Ni Alloys

Phase	Structure Type, Space Group	Lattice Parameters, Å
Ti_2Ni	Cubic, $Fe_3W_3C(E9_3)$ O_h^7-Fd3m	a=11.333 (9) a=11.320 (33.3 At.% Ni) (25) a=11.3231 (2) a=11.278 (2) a=11.3193 (3)
TiNi	Cubic, CsCl (B2) O_h^1-Pm3m	a=2.986 (9) a=3.02 (56 At.% Ni) (21) a=3.013, (50 At.% Ni) (25) a=3.015 (2)
$TiNi_3$	Hex., $TiNi_3(DO_{24})$ D_{6h}^4-$P6_3/mmc$	a=5.1010; c=8.3067 (1) a=5.103; c-8.293 (9) a=5.1089; c=8.3188 (25) a=5.106; c=8.321 (34)
Ni	Cubic, Cu (A1) O_h^5-Fm3m	a=3.5241 (11) a=3.5239 (10)

structure. This phase is stable over a wide composition range, e.g. Umanski and Khidekel(37) have shown that it extends from 29 At.% C to ~50 At.% C. Also, its metal-rich homogeneity limit was placed at 33 At.% C at 1750°C by Cadoff and Nielsen(38). In a more recent investigation by Rudy et al.(6), the homogeneity limits of the TiC_{1-x} were shown to extend at 1650°C from 32 ± 1 At.% C to 48.8 At.% C. It was also reported that the phase melts congruently at 3067 ± 25°C at a carbon concentration of 44 ± 1 At.%. Other reported melting temperatures for the monocarbide phase are 3030°C by Geach and Jones(39), 3140°C by Agte and Moers(40), and 3160 ± 100°C by Friedrich and Sittig(41).

The metal-rich equilibrium in the system is characterized by a eutectic occurring between the cubic Ti and TiC_{1-x} phases with the invariant point being placed at ~4.4 At.% C and 1645 ± 8°C as reported by Bickerdike and Hughes(42). These same investigators reported that the carbon solubility in body centered cubic titanium at the eutectic temperature was 0.55 At.%. Rudy(6) reported that the metal-rich eutectic is formed at 1650 ± 7°C at a carbon concentration of 1.5 ± 0.5 At.%. It was also reported in this investigation that the maximum carbon solubility in cubic Ti was less than 1 At.%.

The hexagonal to cubic transformation of titanium in carbon containing alloys is raised to a peritectoid reaction temperature where the hexagonal modification decomposes to cubic titanium plus monocarbide. Jaffee at al.(43) reported the carbon solubility in hexagonal titanium at the peritectoid temperature (900°-920°C) to be between 1.2 and 1.9 At.%. Rudy(6) reported that the hexagonal to cubic transformation is raised from 880 ± 10°C for the metal to 930 ± 15°C for carbon containing alloys. In the carbon-rich region of the system, the monocarbide phase forms a eutectic equilibrium with graphite at 2776 ± 12°C (63 ± 1 At.% C)(6).

Since the investigation of the Ti-C binary by Rudy et al.(6) is the most recent and complete work done on this system, it was selected as the boundary system for the further investigation of the three ternarys Ti-Fe-C, Ti-Co-C, and Ti-Ni-C. Table VII shows the isothermal reactions in the system, and Table VIII gives the structures and lattice parameters of TiC alloys.

e. The Fe-C System

Because of the importance of iron-carbon base alloys to the steel industry, the Fe-C binary system has received extensive investigations as to its constitution. The literature reviews compiled by Hansen(1), Elliot(2), Shunk(3), and Pearson(10) for both

TABLE VII

Isothermal Reactions in the System Ti-C(6)

Temperature °C*	Transformation or Reaction Type	Composition of the Equilibrium Phases, At. % C		
1668 ± 8°	$\mathrm{L} \rightleftarrows \beta\text{-Ti}$	--	--	--
1650 ± 7°	$\mathrm{L} \rightleftarrows \beta\text{-Ti} + \mathrm{TiC}$	1.5 ± 0.5	< 1	32.0 ± 1.0
930 ± 15°	$\beta\text{-Ti} + \mathrm{TiC} \rightleftarrows \alpha\text{-Ti}$	0.8 (4)	37.1(4)	2.3(4)
880 ± 10°	$\beta\text{-Ti} \rightleftarrows \alpha\text{-Ti}$	--	--	--
3067 ± 25°	$\mathrm{L} \rightleftarrows \mathrm{TiC}$	44 ± 1	44 ± 1	--
2776 ± 12°	$\mathrm{L} \rightleftarrows \mathrm{TiC} + \mathrm{C}$	63 ± 1	~49.4	~100

*Temperature errors are based on estimated overall uncertainty.

TABLE VIII

Structures and Lattice Parameters of Ti-C Alloys

Phase	Structure Type, Space Group	Lattice Parameters, Å
α-Ti	1. T<880°C: hex., Mg(A3) D_{6h}^{4}-P6_3/mmc.	a=2.9504; c=4.6833 (10) a=2.95111; c=3.58433 (36) a=2.9550; c=4.7025 (1.6 At% C) (36)
β-Ti	2. T>880°C: cubic, W(A2) O_h^9-Im3m	a=3.3065 at 900°C (11) a≈3.28 (43) a=3.287 (44)
TiC	Cubic, NaCl (B1) O_h^5-Fm3m	a=4.285 (32 At.% C, quenched from 1650°C) (6) a=4.330 (48.8 At.% C) (6) a=4.3280 (50 At.% C) (36) a=4.3305 (~45 At.% C) (36)
C	Hex., (A9) D_{6h}^{4}-P6_3/mmc.	a=2.4612; c=6.7079 (11)

the stable Fe-C and metastable Fe-Fe_3C systems may be consulted for detailed information regarding earlier investigations.

The most recent review of the system was conducted by Chipman(4,45), who published a phase diagram based on direct experimental results combined with the known thermodynamic properties of iron and experimentally determined activity coefficients of Fe-C alloys as a function of composition and temperature. His results are in agreement with past investigations, and the reaction temperatures and coexisting phase compositions to be presented are from this review(4).

The stable iron-carbon system contains only the body centered and face centered cubic modifications of Fe and graphite. The face centered cubic iron phase decomposes peritectically at 1495°C and eutectoidally at 738°C. A eutectic equilibrium is formed between this phase and graphite at 1154°C. When the metastable Fe_3C phase is present, the eutectic and eutectoid reaction temperatures are lowered to 1148°C and 727°C, respectively. The melting point of Fe_3C has not been determined experimentally, since the metastable carbide decomposes at high temperatures. The Fe_3C liquidus and melting point (1227°C) were calculated by Chipman(45,46) from the free energy of formation of Fe_3C and from the equilibrium liquid composition extrapolated into the metastable range below the graphite liquidus.

Listed in Table IX are the compositions of reacting phases partaking in the various isothermal reactions, and presented in Table X are the structures and lattice parameters of Fe-C alloys obtained from the literature. The phase diagram constructed by Chipman(4) was selected as the boundary system for the further investigation of the ternary Ti-Fe-C.

TABLE IX

Isothermal Reactions in the System Fe-C(4)

Temperature, °C	Transformation or Reaction Type	Composition of the Equilibrium (Metastable) Phases, At.% C		
1538°	L ⇄ δ-Fe	--	--	--
1495°	L + δ-Fe ⇄ γ-Fe	2.42	0.42	0.79
1394°	δ-Fe ⇄ γ-Fe	--	--	--
1154°	L ⇄ γ-Fe + C	17.1	8.99	~100
1148°	L ⇄ γ-Fe + Fe_3C	(17.28)	(9.11)	(~25)
912°	γ-Fe ⇄ α-Fe	--	--	--
738°	γ-Fe ⇄ α-Fe + C	3.09	0.096	~100
727°	γ-Fe ⇄ α-Fe + Fe_3C	(3.48)	(0.101)	(~25)

TABLE X

Structures and Lattice Parameters of Stable (Metastable) Fe-C Alloys

Phase	Structure Type, Space Group	Lattice Parameters Å
α-Fe	1. T<912°C: cubic, W(A2) O_h^9-Im3m (ferrite)	a=2.8662 (10) a=2.866 (11) a=2.8677 (1 At.% C) (10)
γ-Fe	2. 912°C<T<1394°C: cubic, Cu (Al) O_h^5-Fm3m (Austenite)	a=3.6467 at 916°C (11) a=3.590 (3.5 At.% C) (10) a=3.634 (8 At.% C) (10)
	3. Martensite, tetra., L'2, I4/mmm	Formed in Fe-C alloys quenched from austenitic region. a=2.861 - 0.013S c=2.861 + 0.116X (47)* o≤X≤1.8 Wt.% C
δ-Fe	4. T>1394°C, cubic, W(A2), O_h^9-Im3m	a=2.9322 at 1394°C (10) a=2.9315 at 1395°C (11)
Fe_3C	1. Cementite, ortho., (DO$_{11}$), D_{2h}^{16}-Pnma	a=5.0890; b=6.7433; c=4.5234 (11) a=4.5244; b=5.0885; c=6.7431 (1) a=4.526; b=5.087 c=6.744 (2)
ε-$Fe_{2-3}C$	2. Hexagonal, Fe_3N, D_b^6-P6$_3$22	Transition phase formed during decomposition of martensite. Cementite is then formed and ε disappears. a = 2.754; c = 4.349 (1) a=2.73 ; c= 4.33 (1) a= 2.752; c = 4.353 (2)

*kx units.

f. The Co-C System

The solid solution of graphite in cobalt forms a eutectic equilibrium with graphite. The following eutectic compositions and temperatures have been reported: 12.75 At.% C at 1309°C(48), 11.6 At.% C at 1315°C(49), ~12 At.% C at 1321°C(50), 11.9 At.% C at 1319°C(51), and 13.2 At.%C at 1319°C(52). The maximum graphite solubility in cobalt at the eutectic temperature is ~4.5 At.%(48).

The solubility of graphite in liquid cobalt has been investigated by Turkdogan et al.(51) and Schenck et al.(53). Their data are in good agreement; the solubility is about 15 At.% C at 1600°C, 14.1 At.% C at 1500°C, and 12.8 At.% C at 1400°C.

The system has also been investigated in order to establish the existence of cobalt carbide phases of the type Co_3C and Co_2C. By the action of carburizing gases on cobalt at low temperatures (<600°C), two orthorhombic phases isomorphous with Fe_3C and Co_2N have been reported(1,2,10). In addition, changes in the slope of the graphite liquidus at approximately 2100°C and ~6 Wt.% C have been attributed to the formation of Co_3C-type molecules in the liquid phase(1).

g. The Ni-C System

The nickel solid solution forms a eutectic equilibrium with graphite at the following reported compositions and temperatures: 10.1 At.% C (1307°-1318°C)(54), 9.9 At.% C (1304°-1325°C)(55), 10.0 At.% (1305-1318°C)(56), 8.9 At.% at 1314°C(51), 9.5 At.% C at 1314°C(52), and ~10 At.% C at 1326°C(50). Some results deviate considerably because of the tendency for the liquid to supercool. The maximum solid solubility of graphite in nickel at a eutectic temperature of 1318°C was placed at 2.7 At.% C(56).

The solubility of graphite in liquid nickel has been investigated by Turkdogan et al(51) and Schenck et al(53). Their data are in good agreement; the solubility is about 15 At.% C at 1700°C, 12.5 At.% C at 1550°C, and 11 At.% C at 1450°C.

Like the cobalt-carbon system, the nickel carbon system has been investigated in order to establish the existence of a nickel carbide phase of the type Ni_3C. Several authors(57,58,59) have reported that a Ni_3C-phase has a close-packed hexagonal structure, and in a more recent publication(60) a rhombohedral structure was reported. On the other hand, Ni_3C was reported to have an orthohombic structure isomorphous with Fe_3C(61,62). There are reports(1,2,3) that the metastable Ni_3C phase is only obtained in very rapidly quenched, superheated melts; there are also reports that the phase is formed by the action of carburizing gases on nickel at temperatures below ~400°C.

Compared to the graphite liquidus in the Co-C system, a more pronounced change in slope of the liquidus in Ni-C system at 2100°C and ~25 At.% C has been reported(1). Again, this has been attributed to the formation of Ni_3C molecules in the liquid phase.

2. Ternary Systems

a. The Ti-Fe-C System

Concerning the complete investigation of this ternary system, no information was found in the available literature.

According to the literature review conducted by Goldschmidt(63), the following equilibria result in iron-rich alloys: ($T < 727°C$) α-Fe + Fe_3C, α-Fe + Fe_3C + TiC, α-Fe + TiC, and α-Fe + TiC + $TiFe_2$; ($T > 727°C$) γ-Fe + Fe_3C, γ-Fe + Fe_3C + TiC, γ-Fe + TiC, γ-Fe + α-Fe + TiC, α-Fe + TiC, and α-Fe + TiC + $TiFe_2$. These equilibrium sequences are consistent with the displacement of the γ-Fe eutectoid reaction to higher temperatures upon titanium addition(63).

Edwards and Raine(64) reported that the solubility of titanium carbide in iron at 1250°C was less than 0.5 wt%. A partial investigation of the system was conducted by Eremenko(65), who studied alloys between stoichiometric titanium carbide and iron. According to his results, a pseudobinary eutectic equilibrium is formed between γ-Fe and TiC with an invariant point of 3.8 Wt.% TiC (~7 mole %) and 1460° ± 10°C. From differential thermal and dilatometric analyses of alloys along the section Fe-TiC, Eremenko also reported that the α-Fe phase decomposed in a peritectoid reaction at ~920°C. The following approximate equilibrium concentrations of the phases partaking in this reaction were given:

$$\alpha\text{-Fe } (0.15 \text{ Wt.\% TiC}) = \gamma\text{-Fe}(0.04 \text{ Wt.\% TiC}) + \text{TiC}$$

Craighead et al.(66) studied the mechanical properties of ternary base titanium alloys containing the following maximum concentrations of iron and carbon: 2 Wt.% Fe and 0.25 Wt.% C. Phase diagram data were limited to the α-β transformation range of titanium.

b. The Ti-Co-C System

No reports were found in the available literature concerning the complete investigation of this ternary system.

Craighead et al.(66) presented phase diagram data on the α-β transformation range of titanium. The ternary titanium base alloys investigated contained a maximum of 0.25 Wt.% C and 3 Wt.% Co.

Schwarzkopf and Kieffer(67) presented a probable phase diagram of the section TiC-Co based on the unpublished data of Brownlee and Raine. According to their results, based on X-ray analysis of sintered alloys, the solubility of TiC in Co reached a maximum of ~3 mole % at a pseudobinary eutectic equilibrium. The invariant point was placed at ~6 mole % TiC and ~ 1260°C. The solubility of Co in TiC was placed at about 10 mole% at temperatures between 1250° to 1500°C. Edwards and Raine(64) found, on the basis of metallographic and X-ray analyses, that the solubility of TiC in Co at 1250°C was ~1 Wt.%.

Eremenko(65) investigated the ternary section TiC-Co and reported that the solubility of TiC in Co was 0.15 Wt.% at 700°C, 0.9 Wt.% at 1310°C, and ~1 Wt.% at a pseudobinary eutectic equilibrium. The following eutectic temperature and composition were given: 1360°C ± 10°C and 6 wt.% TiC (~11 mole %).

c. The Ti-Ni-C System

Partial investigations of this system include the work conducted by Eremenko(65), who investigated alloys between stoichiometric titanium carbide and nickel. From cooling curve data and metallographic inspection of quenched alloys, he reported that the maximum solubility of TiC in Ni was 6.2 Wt.% at a pseudobinary eutectic equilibrium, invariant point at 1280°C and 9.3 Wt.% TiC (~17 mole %). From a series of heat-treated samples at subsolidus temperatures, the following solubilities (Wt.%) of TiC in Ni were reported: 2.0 (700°C), 2.6 (900°C), 3.8 (1050°C) and 5.2 (1250°C). The solubility at 1250°C is consistent with the result of 5.0 Wt.% TiC reported by Edwards and Raine(64).

Stover and Wulff(68) presented a tentative isothermal section of the system at 870°C. Ternary and binary titanium-nickel alloys utilized were arc cast on a water-cooled copper crucible in purified helium and then annealed 100 hours at 870°C. It was shown that TiC forms two-phase equilibria with Ti_2Ni, TiNi, $TiNi_3$, and Ni. They reported that the carbon solubility in TiNi and $TiNi_3$ was negligible, but the solubility in Ti_2Ni was measurable (few At.% C). A ternary alloy annealed at 870°C had a lattice parameter of $a = 11.365$Å for the Ti_2Ni phase.

Stover and Wulff(68) also reported that a pseudobinary eutectic equilibrium exists between TiC and Ni at 1307° ± 3°C. The composition of the eutectic was placed at about 13 At.% Ti and 4 At.% C; the critical tie line intersected the Ti-Ni binary system at 9 At.% Ti, instead of at stoichiometric Ni as reported by Eremenko(65). On either side of this pseudobinary section, the following ternary eutectic equilibria were reported(68):

L = TiC + Ni + C at 1270° ± 3°C (~7 At.% Ti - ~11 At.% C) and
L = TiC + Ni + $TiNi_3$ at 1295° ± 3°C (~17 At.% Ti-2 At.% C). They also reported that ternary alloys containing the Ti_2Ni-phase melted in a peritectic-type reaction at 1050° ± 30°C. In addition, the following invariant temperatures were given for the indicated equilibria, but no reaction-types were given: (L + TiC + Ti_2Ni + β-Ti) at 980° ± 10°C, (L + TiC + TiNi) above 1275°C, (L + TiC + TiNi + $TiNi_3$) at 1120° ± 3°C, and (L + TiC + $TiNi_3$) at 1390° ± 15°C.

The following compositions for the nickel vertex of the three-phase equilibrium (Ni + TiC + C) were given as a function of temperature (At.%): 2.0 Ti-0.2C at 600°C, 3.1Ti-1.2C at 1000°C, and ~3.5Ti-2.6C at 1260°C. These data were based on Curie point measurements and X-ray, metallographic analyses of chemically analyzed nickel solid solution alloys.

In a more recent investigation of the system, Ballamy and Hucke(69) reported on the composition of liquid (Ti-Ni-C) alloys in equilibrium with TiC_{1-x} at temperatures of 1300°, 1400°, and 1500°C. The equilibrium liquid and solid TiC_{1-x} phases were separated by a flotation and filtration technique using graphite as a crucible material. The compositions of the separated phases were determined by wet chemical and microprobe analyses. At the 1300°C section, the experimental results showed that the exact form of liquidus curve could not be determined for ternary alloys in the vicinity of 75 At.% Ni. This is consistent with the results of Stover and Wulff(68), who reported that two-phase alloys of ($TiC + TiNi_3$) experienced melting at 1390°C. At higher nickel contents, pseudo-binary eutectic structures of (TiC + Ni) were noted by Ballamy and Hucke(69). A photomicrograph of an alloy quenched from 1300°C containing ~10 At.% Ti and 5 At.% C exhibited primary monocarbide in a carbide-metal eutectic matrix. All compositions investigated from about 10 to 80 At. % Ni at 1400° and 1500°C showed only TiC_{1-x} to be in equilibrium with a liquid phase.

C. EXPERIMENTAL PROCEDURES

1. Starting Materials

The elemental powders of titanium, iron, cobalt, nickel and graphite as well as titanium monocarbide served as the starting materials for the preparation of the experimental alloys.

Titanium metal powder (<74 micron particle size) was obtained from Wah Chang Corporation, Albany, Oregon. The listed impurities were (in ppm): H-46, N-164, C-190, O-900, Cl-500, and (Si, Cr, Fe, Co, Ni, Cu, Zn)-600. The lattice parameters, determined from an X-ray exposure with Cu-Kα radiation, were $a=2.949_5$Å and $c=4.685_0$Å. These values are in reasonable agreement with literature data of $a=2.9511$Å, $c=4.6843$Å$^{(36)}$ and $a=2.9504$Å; $c=4.6833$Å$^{(10)}$.

Iron metal powder (<149 micron particle size) of 99.9% purity was purchased from the Var-Lac-Oid Chemical Company, Elizabeth, New Jersey. Debye-Scherrer powder photographs taken with both Cu-Kα and Cr-Kα radiations showed only the cubic α-Fe structure with a lattice parameter of $a=2.866_2$Å. Reported literature values are $a=2.8665$Å$^{(10)}$ and $a=2.8662_1$Å (99.969% Fe)$^{(10)}$.

Impurities in the cobalt powder (Var-Lac-Oid of Elizabeth, New Jersey; overall purity $>99.85\%$ and 20 micron average particle size) were as follows (in ppm): C-350, Mg-30, Si-40, S-100, Ca-200, Mn-30, Fe-250, Ni-260, and Cu-20; the weight loss in H_2 was 0.051%. An X-ray (Cu-Kα) powder photograph of this material showed the face centered cubic pattern plus a trace of hexagonal cobalt. A lattice parameter of $a=3.544_1$Å obtained from this exposure is consistent with values given in the literature(10).

The nickel powder (99.9% pure) was also purchased from Var-Lac-Oid Chemical Company. This powder of 5 micron average particle size had the following impurities as listed by the vendor (in ppm): C-500, O-500, S-<10, and Fe-<100. A Debye-Scherrer powder photograph taken with Cu-Kα radiation revealed only the face centered cubic structure with a lattice parameter of $a=3.523_7$Å. Reported literature values are $a=3.524_1$Å(11) and a=3.5239 Å (99.96% pure)(10).

Titanium monocarbide powder was supplied by the Shieldalloy Corporation from the H.C. Starck Company, Berlin, West Germany. This carbide had a total carbon content of 19.50 Wt.%, of which 0.24 Wt.% was present as free graphite. The combined oxygen and nitrogen content was 1500 ppm, and the sum of metallic impurities was less than 800 ppm. The measured lattice parameter of the titanium monocarbide starting material was $a=4.328_5$Å.

Spectrographic-grade graphite powder purchased from the Union Carbide Corporation, Carbon Products Division, New York, had a total impurity content of less than 2 ppm.

2. Alloy Preparation and Heat Treatments

Both binary and ternary alloys fabricated for melting point and solid state section studies were prepared by cold pressing and sintering blended mixtures of the elemental powders of Ti, (Fe, Co, or Ni); C and/or TiC. Also, ternary alloys with a carbon content greater than ~20 At.% were prepared by hot pressing the blended powders in graphite dies.

The cold pressed samples in the form of rectangular bars (~0.6 x 0.6 x 4.5 cm) were pressed in a steel die at 20,000 psi. After cold pressing, the samples were heat treated under vacuum ($<5 \times 10^{-5}$ Torr) for 2 hours at 825°C in a tungsten-mesh element furnace. For added protection of the samples, the tantalum sample container was lined with titanium foil to act as a getter for residual gases.

Initial melting point measurements made with these samples, i.e., metal binary alloys and ternary alloys located near the metal edge binaries, were masked by a very rapid increase in temperature due to strong exothermic reactions of compound formation in the metal binary systems. By extending the heat treating time to 40 hours at ~850°C, both binary and ternary samples for melting point measurements were successfully prepared.

For the hot pressing method, the powder mixtures (10-15 gram samples) were loaded into graphite dies and closed with a graphite piston. The die assembly was then inserted into a graphite heater clamped between water-cooled copper electrodes. The samples were hot pressed for 2 to 5 minutes while under a pressure of ~750 psi. Depending on the melting temperatures of the alloys, hot pressing temperatures varied between ~900° to 1300°C. After hot pressing, the carburized surface layer (typically 0.2 mm thick) and adhering graphite were removed by grinding, and the cores of the samples were then subjected to further heat treatments.

Alloy samples for metallography were prepared from the melted portions of melting point samples. Whenever the melting point samples were not sufficiently dense for metallographic examination, they were arc melted in a nonconsumable tungsten electrode arc furnace.

Samples used for the investigation of the solid state sections of the systems were either portions of melting point samples, or pieces of sample material which had been arc melted. A portion of the heat treated sample was mounted for metallographic analysis while the remainder was crushed and used for both chemical and X-ray analyses. In addition, ductile alloy samples for X-ray analysis were prepared by filing and then heat treating with a sample from metallography of the same composition. The samples to be heat treated were placed in tantalum cups (~2 cm dia. x 1 cm deep) and then stacked in tantalum tubes of slightly larger diameter. The tubes were then placed in a tantalum can lined with titanium foil (6 tubes at a time) and heat treated in a tungsten-mesh element furnace. The temperature was measured pyrometrically through a quartz window on top of the furnace.

The equilibration temperatures for investigating solid state sections were 900°C (240 hrs), 1070°C (100 hrs), and 1260°C (60 hrs). The first two heat treatments were conducted in vacuum (6×10^{-6} Torr), and the 1260°C heat treatment was carried out in one atmosphere of helium.

3. Determination of Melting Temperatures

The melting temperatures of binary and ternary alloys were measured using the technique devised by Pirani and Alterthum(70). With this technique, either the cold pressed and sintered bar specimens or hot pressed cylindrical specimens are placed between two water-cooled copper electrodes within a furnace chember. The specimen is then heated resistively by the passage of current through it. A small black body hole, generally on the order of 0.6 mm in diameter by 3 to 6 mm in depth, located at the reduced center portion of the specimen serves as a reference point for temperature measurements.

The temperature of the black body hole was measured optically with a disappearing-filament type pyrometer sighted through a quartz window in the furnace wall. To check the pyrometer calibration, melting runs were frequently made with in-house melting point standards. For further information on the design details of this furnace as well as temperature calibration and correction data, the reader is referred to the literature(71,72).

A description of the melting behavior of alloys as determined through the use of the melting point furnace is presented next. Because of the steep temperature gradient between the inner and outer portions of the resistively heated sample during the melting point investigation, the formation of liquid first occurs in the interior. The pyrometer filament is matched against the radiation background from the black body hole, and the investigation is completed when the hole either fills with liquid or collapses.

The most precise or reproducible melting data are obtained on isothermally melting alloys, i.e. elements or phases which melt congruently, or eutectic melting alloys with compositions close to or at the invariant point. For alloys located close to the homogeneity boundaries of single phase regions which melt at higher temperatures, incipient melting is difficult to detect.

One disadvantage of this method is that the exact location of liquidus lines for binary alloys and liquidus surfaces for ternary alloys cannot be determined. After incipient melting has been detected, the liquid formed in the black body hole migrates to the cooler outer portion of the sample and solidifies. A cavity is thus created in the center portion of the sample. As the temperature is increased, more liquid is formed and when it reaches the sample surface, the specimen collapses due to loss of strength before the temperature of the liquidus is reached. This effect may be prevented somewhat by minimizing the axial force of the clamping device holding the sample within the furnace chamber.

By combining the collapsing temperature data with metallographic and X-ray data obtained from the melted portions of the melting point samples, the extent and location of solid-liquid tie lines in the binary and ternary systems may be estimated. The relative amount of the unmelted phase present at the collapsing temperature is estimated from metallographic analysis, and the X-ray analysis provided data on its composition.

The melting point investigations were performed under a helium atmosphere of ~1.1 to 1.3 atmospheres; a few binary metal and ternary alloy samples were run in duplicate under vacuum, yielding identical results. Higher positive helium pressures of ~2 atmospheres were utilized in order to minimize both metal and carbon losses at the high collapsing temperatures of ternary alloys located close to the titanium monocarbide phase. Gas impurities contained in the helium and residual gas impurities contained in the furnace chamber when under vacuum were gettered by a strip of titanium foil heated resistively inside the furnace. In addition, binary melting point alloys located at invariant points were run in triplicate. For the invariant reaction temperatures given in this report, the temperature limits attached to the mean temperature values refer to the reproducibility of the measurements.

Prior to making the melting point investigations, the furnace chamber was evacuated three times to a 30-in. Hg vacuum and each time refilled with helium to atmospheric pressure. The melting point samples were then heated under vacuum to temperatures between -800° and 1100°C and then held until the vacuum stabilized. Next, the furnace chamber was filled with helium to the desired pressure or left under vacuum. Finally, the samples were rapidly heated to within ~50°C of their suspected melting temperatures, and then the temperature gradually raised until melting was detected.

The melting behavior of both binary and ternary alloys in the systems Ti-Fe, Ti-Co, Ti-Ni, Fe-C, Co-C, Ni-C, Ti-Fe-C, Ti-Co-C, and Ti-Ni-C was followed using 230 different alloy compositions.

4. Metallographic, X-Ray, and Chemical Analyses

Metallographic examinations were performed on melting point, arc melted, and heat treated alloy samples. For this study, the samples were mounted in a mixture of diallyl-phthalate-lucite coated copper powder and ground on silicon carbide papers with grit sizes varying between 120 and 600. The final polishing was performed on a nylon cloth using a slurry of 0.3 micron alumina in a 5% chromic acid solution.

The etchants and etching procedures varied with both the metal and carbon concentrations of the alloys. For titanium-rich alloys with carbon concentrations <15 At.%, the alloys were electroetched with a 10% aqueous oxalic acid solution. For the iron group metal-rich alloys with carbon concentrations up to ~35 At.%, the alloys were either electroetched with a 5% H_2SO_4 or HNO_3 solution. Also, dip-etching with the above acid solutions produced satisfactory phase contrast between the metal and carbide phases. Some binary and ternary alloys which contained free graphite were examined in the as-polished state.

Photomicrographs of the prepared metallographic samples were made with a Zeiss Ultraphot II microscope with Nomarski interference contrast attachment. The microscopic examination of the alloys was used to locate eutectic troughs in the ternary systems, and invariant compositions and homogeneity boundaries of phases in both the binary and ternary systems.

Debye-Scherrer powder diffraction patterns, using CuKα as well as CrKα radiation, were prepared from all heat treated alloy samples and selected melting point and arc melted samples. The exposures were taken in a 57.4 mm camera on a Siemens-Crystalloflex II X-ray unit. The angles of the diffraction lines on the film strips were measured with a Siemens-Kirem coincidence scale with micrometer dial (0.01 mm scale division) attachment. The measured lattice parameters were corrected for absorption by extrapolation against $\mathrm{Cos}^2\theta/\mathrm{Sin}\theta + \mathrm{Cos}^2\theta/\theta$.

The structures of all phases occurring in the respective binary systems were known from previous work cited in the literature. At the temperature sections investigated in the ternary systems, i.e., temperatures above 900° C, no ternary phases were detected. All film exposures were evaluated with respect to the nature of the phases present; the lattice parameters were measured to determine the compositions of coexisting phases in the various two phase fields, as well as to locate the vertices (boundary tie lines) of three phase equilibria.

Chemical analysis for carbon, performed on post-experimental ternary alloys, was made by the direct combustion of the samples in oxygen followed by measuring the thermal conductivity of the resulting CO_2- O_2 gas mixture, no metal analyses were performed.

It was found that the analyzed carbon content agreed to within one to two atomic percent of the nominal compositions. The analyses also showed that some ternary alloys containing more than ~ 50 mole% titanium monocarbide, which were exposed to high temperatures (>1500°C) during either the arc melting or melting point investigations, showed carbon losses as great as 5 to 10 atomic%. These results were supported by the X-ray findings and were taken into account during the interpretation of the experimental results.

D. EXPERIMENTAL RESULTS

1. The Ti-Fe-C System

a. Ti-Fe System

The constitution diagram of the titanium-iron system is very similar to the ones published by Elliott(2) and Rohatgi(4) in that only slight differences in reaction temperatures and coexisting phase compositions were observed. Only a brief description of the experimental results will be given.

Presented in Figure 13, the constitution diagram established in this investigations, are the measured solidus temperatures of binary alloys and the solid state phase evaluation of alloys equilibrated at 900° and 1260°C.

Arc melted and quenched alloys, as well as samples heat treated at subsolidus temperatures, showed either the cubic (B2-type) TiFe phase or hexagonal (C14-type) $TiFe_2$-phase; no other intermediate phases were observed. From 900°C towards higher temperatures, the TiFe phase exhibits a slight homogeneity range as evidenced by the change in its lattice parameter from a = 2.986Å, for titanium-rich alloys, to a = 2.975Å for excess iron containing alloys. These results are in agreement with the literature(2,4).

The hexagonal $TiFe_2$ phase at 900°C was found to exhibit a noticeable homogeneity range, extending from approximately 66 At.% Fe (a = 4.781Å; c = 7.801Å) to 73 At.% Fe (a = 4.771Å; c = 7.780Å). At higher temperatures, this same homogeneity range extends from approximately 63 At.% Fe at 1316°C to 75 At.% Fe at 1326°C, the observed eutectic temperature isotherm of the equilibrium $TiFe_2$, liquid α-Fe. The previous literature values reported for this reaction isotherm were 1290°C(2) and 1291°C(4). Photomicrographs of alloys participating in this reaction are presented in Figures 14 and 15.

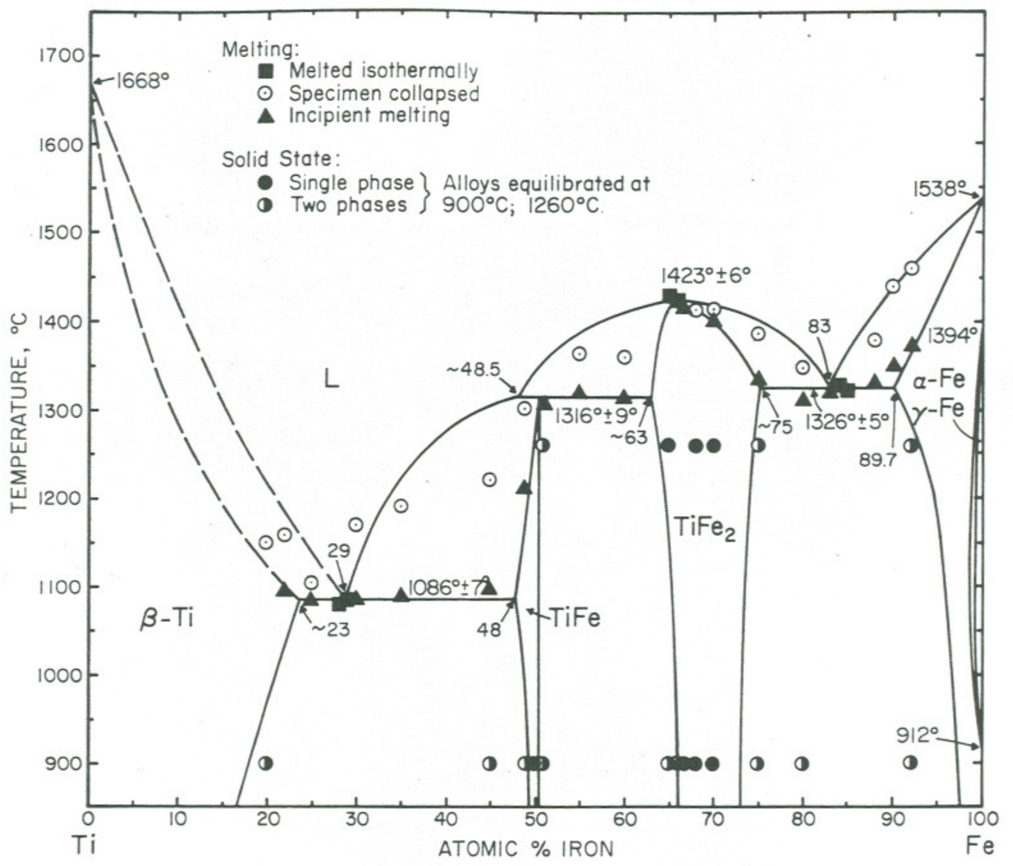

Figure 13. Titanium-Iron Constitution Diagram. Experimental melting temperatures and qualitative Phase Evaluation of Ti-Fe Alloys.

(Transformation temperatures for Ti and Fe obtained from References (6) and (4), respectively.)

The following lattice parameters were obtained for the isomorphic (A2-type) phases of β-Ti and α-Fe in melted and quenched alloys exhibiting two-phase equilibria β-Ti + TiFe and $TiFe_2$ + α-Fe, respectively: β-Ti of approximately 23 At.% Fe, $a \approx 3.075Å$; α-Fe of approximately 90 At.% Fe, $a = 2.875Å$.

b. Ternary System

As determined from metallographic and X-ray diffraction data, the ternary solid solubilities of either titanium, iron, or carbon in the appropriate edge binary phase were extremely small at all temperatures up through melting (1 to 2 atomic percent at the most). For both melted and quenched, and annealed alloy samples; no significant variation in the lattice parameters of phases in ternary alloys could be detected when compared to their binary values.

With respect to the titanium monocarbide phase, metallographic examination of ternary alloys quenched from liquidus temperatures did not reveal any coring of this primary phase; indicating that it has a fairly temperature independent iron-rich phase boundary. Consequently for ternary alloys of the above type, the X-ray patterns obtained for the cubic monocarbide phase were sharp except for some high-angle lines in the back reflection region which were slightly diffuse.

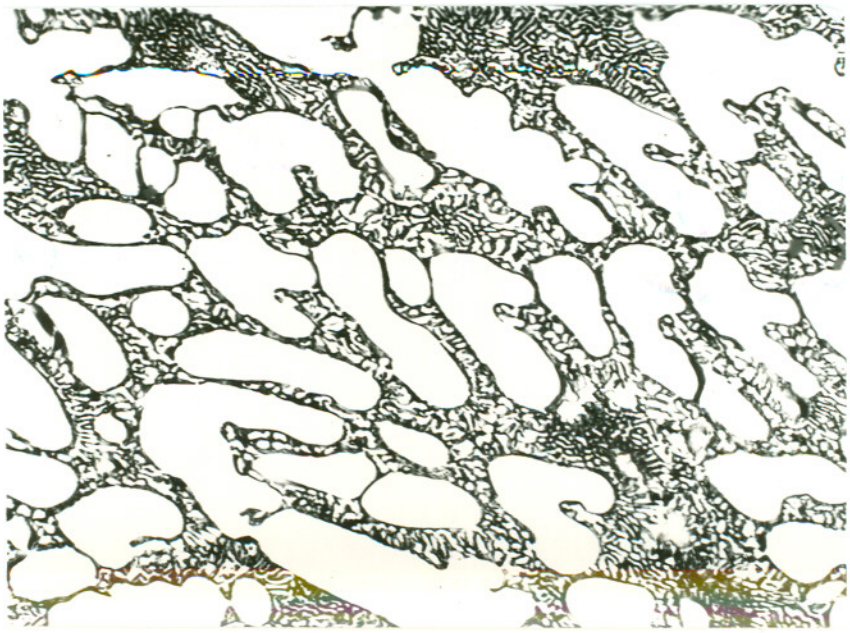

Figure 14. Ti-Fe (20-80 At.%), Arc Melted Sample. X800
Primary $TiFe_2$ in $TiFe_2$ + α-$Fe_{(ss)}$ Eutectic Matrix.

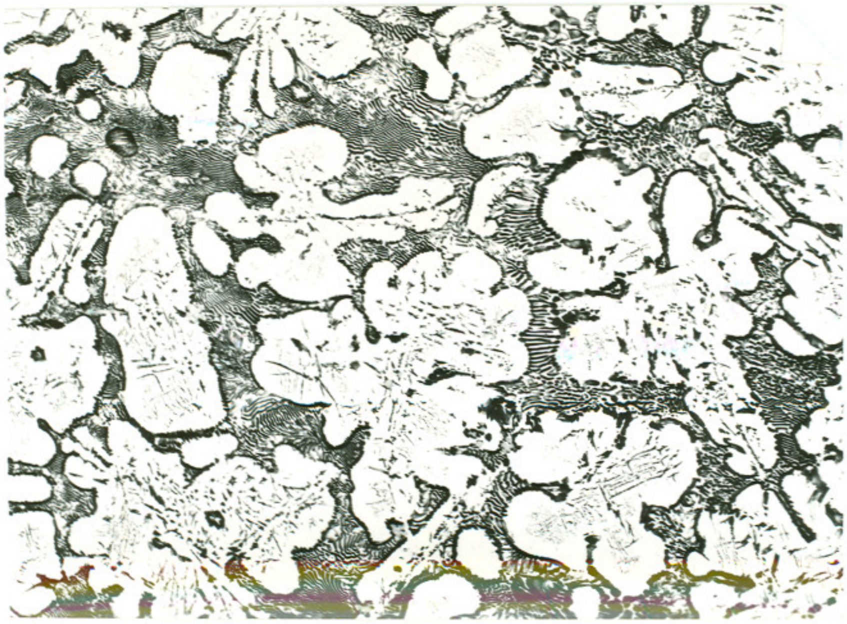

Figure 15. Ti-Fe (14-86 At.%), Arc Melted Sample. X400
Primary α-$Fe_{(ss)}$ in $TiFe_2$ + α-$Fe_{(ss)}$ Eutectic Matrix. Sample Slightly Annealed: Primary α Contains Intragranular $TiFe_2$ Precipitates.

Depending on the ternary alloys carbon concentration and prior thermal history, the lattice parameters of the cubic monocarbide phase varied from approximately a = 4.295Å, at the metal-rich (Ti) phase boundary, to a = 4.327Å, at the carbon-rich phase boundary. This lattice parameter variation corresponds very closely to that of the carbon-deficient binary phase reported in the literature(36,43).

The qualitative phase evaluation of ternary alloys equilibrated at 900° and 1260°C resulted in the phase relationships presented in Figures 16 and 17, respectively. At these temperatures, the resulting phase equilibria are similar, except for the appearance of a liquid phase in titanium and iron-rich alloys at the higher temperature section. Since both of these temperature sections lie close to solidus temperatures of certain ternary alloys, the measured terminal compositions of the solid phases closely correspond to the compositions entering reactions with a liquid phase.

The three-phase equilibrium β-Ti(a ≈ 3.18Å) + TiC_{1-x} (a = 4.311Å) + TiFe (a = 2.987Å) shown in the 900°C temperature section (Figure 16) is terminated at 1058° ± 9°C. At this temperature, the following class I ternary reaction occurs:

$$L \underset{>1058^\circ C}{\overset{<1058^\circ C}{\rightleftharpoons}} TiC_{1-x} + \beta\text{-Ti} + TiFe.$$

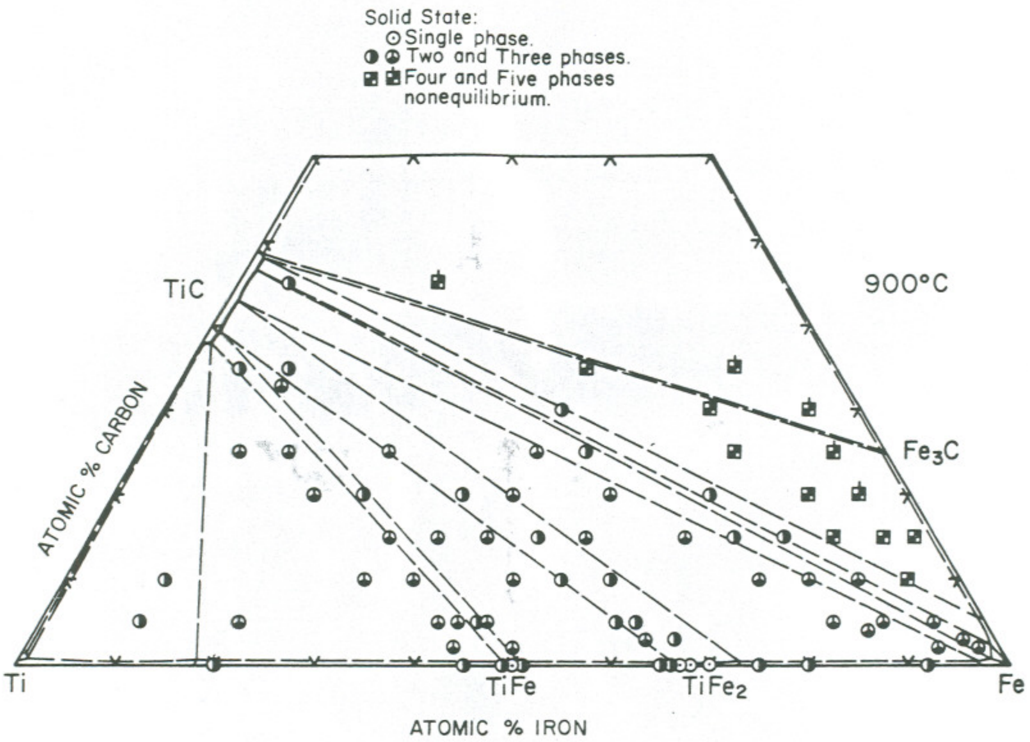

Figure 16. Qualitative Phase Evaluation of Ti-Fe-C Alloys Equilibrated at 900°C.

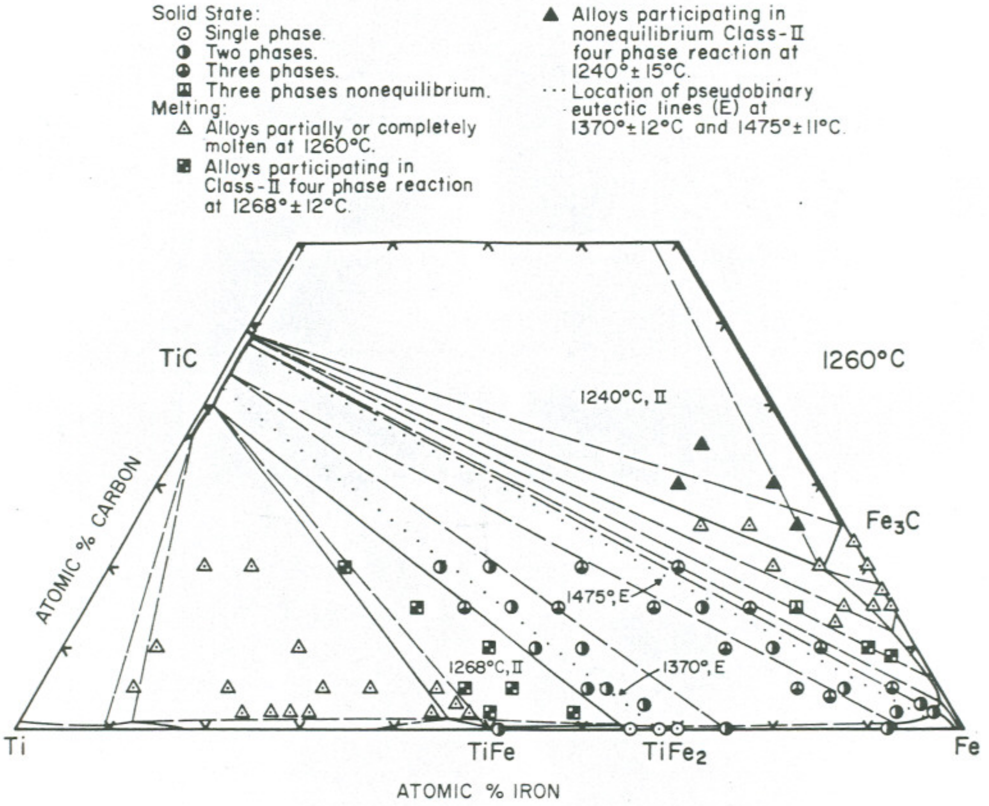

Figure 17. Qualitative Phase Evaluation of Ti-Fe-C Alloys Equilibrated at 1260°C.

The existence of this four-phase temperature plane was determined from the consistency of the incipient melting temperature of ternary alloys participating in this reaction. From the metallographic examination, the composition of the invariant liquid phase was placed at approximately Ti(70) - Fe(29) - C(1) At.%. Figures 4 and 40(a) show the location of the four-phase reaction plane, and a photomicrograph of an alloy partaking in this reaction is presented in Figure 18. Because of the metal-rich position of the eutectic liquid phase, the eutectic monocarbide can not be resolved.

Another class I reaction at 1109° ± 7°C produces the iron-rich liquid phase shown in Figure 17. This reaction involves the metastable Fe_3C phase,

$$L \underset{>1109^\circ C}{\overset{<1109^\circ C}{\rightleftharpoons}} TiC_{1-x} + \gamma\text{-}Fe + Fe_3C,$$

with a eutectic liquid composition of approximately Ti(2)-Fe(81)-C(17) At.%. Figure 40(a) shows the location of this four-phase reaction plane, and quantitative results concerning this reaction and others involving the Fe_3C phase will be presented later.

With increasing temperature, the three-phase equilibrium liquid + TiC_{1-x} + TiFe, originating at the 1058°C eutectic isotherm (Figure 40a), merges with the three-phase equilibrium (Figure 16) of TiFe (a = 2.976Å) + TiC_{1-x} (a = 4.321Å) + + $TiFe_2$ (a = 4.784Å; c = 7.806Å) at a temperature of 1268° ± 12°C

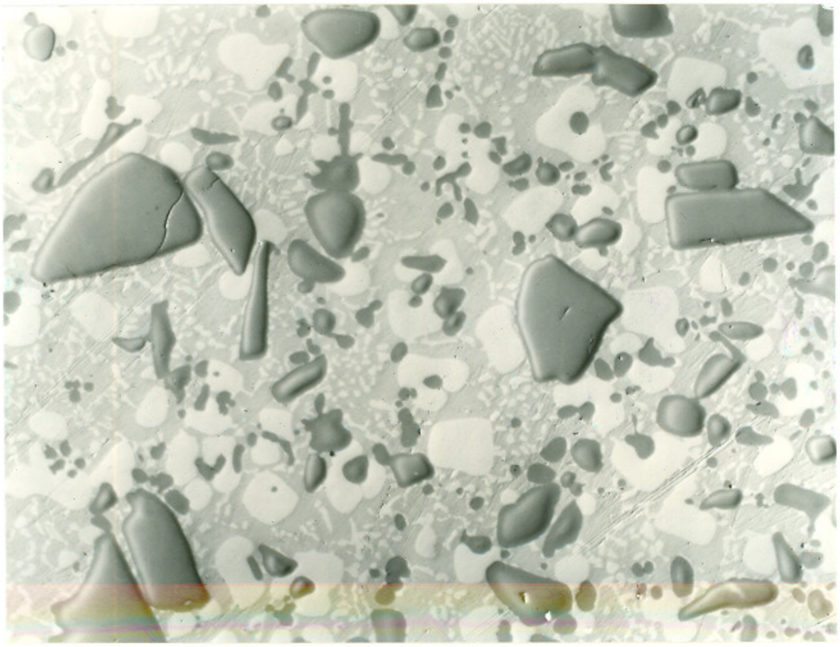

Figure 18. Ti-Fe-C (65-25-10 At.%), Melting Point Sample Quenched from 1178° C. Primary Monocarbide (Dark Phase) and Secondary TiFe (Light Phase) Set in a Eutectic Matrix of Transformed β-Ti (some β retained).

(Figures 17 and 40b). The melting behavior of alloys participating in this class II ternary reaction,

$$L + TiFe_2 \xrightleftharpoons[>1268\,^\circ C]{<1268\,^\circ C} TiC_{1-x} + TiFe,$$

are shown in Figure 17. Alloys located along the section $\mathrm{TiC}_{1-x} + \mathrm{TiFe}$ and within the three-phase field $\mathrm{TiC}_{1-x} + \mathrm{TiFe} + \mathrm{TiFe}_2$ (Figure 16) generally exhibited a nonequilibrium phase mixture of Ti, TiC_{1-x}, TiFe, and TiFe_2 after quenching from temperatures in excess of 1268°C (Figure 19).

The three-phase equilibrium liquid $+ \mathrm{TiC}_{1-x} + \mathrm{TiFe}_2$, which originates at the above 1268°C four-phase temperature plane, is terminated at a temperature of $1370° \pm 12°\mathrm{C}$. At this temperature, the following pseudobinary eutectic reaction occurs:

$$\mathrm{L} \ \frac{< 1370^\circ\mathrm{C}}{> 1370^\circ\mathrm{C}} \ \mathrm{TiC}_{1-x} + \mathrm{TiFe}_2.$$

One additional reaction of this type takes place at a temperature of $1475° \pm 11°\mathrm{C}$ between titanium monocarbide and the α-modification of iron.

$$\mathrm{L} \ \frac{< 1475^\circ\mathrm{C}}{> 1475^\circ\mathrm{C}} \ \mathrm{TiC}_{1-x} + \alpha\text{-}\mathrm{Fe}.$$

The melting behavior of ternary alloys located on or slightly off these pseudobinary selections are presented in Figures 20 and 21, and the location of the critical tie lines are shown in Figures 3 and 17. In addition, typical photomicrographs of alloys from the concentration regions $\mathrm{TiC}_{1-x} + \mathrm{TiFe}_2$ and $\mathrm{TiC}_{1-x} + \alpha\text{-}\mathrm{Fe}$, which were either rapidly cooled from the liquidus range or equilibrated at sub-solidus temperatures, are presented in Figures 22-24. From the melting

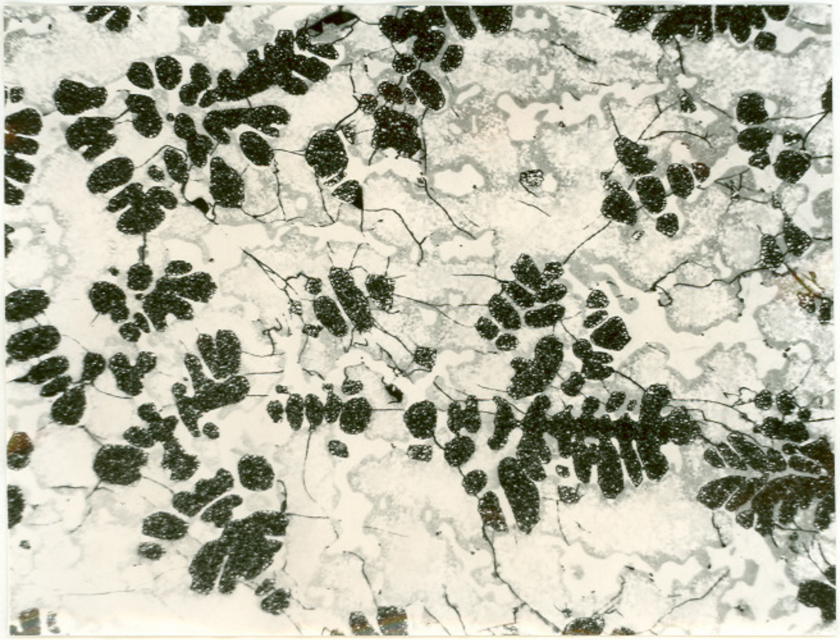

Figure 19. TiFe-C (47-42-11 At.%), Arc Melted Sample Primary Monocarbide Dendrites (Dark, Heavily Etched Phase) plus $TiFe_2$ and TiFe (Light Phase) which Solidified from a Ti-rich Liquid at 1268°C.

(Note cracks in brittle $TiFe_2$ phase which are arrested at the ductile TiFe phase).

behavior and metallographic examinations, the following invariant liquid compositions were obtained: approximately Ti(33)-Fe(65)-C(2) At.% at 1375°C, and Ti(8)-Fe(86)-C(6) At.% at 1475°C. Alloys located along the section TiC_{1-x} + $TiFe_2$ (Figure 20) did not exhibit very characteristic

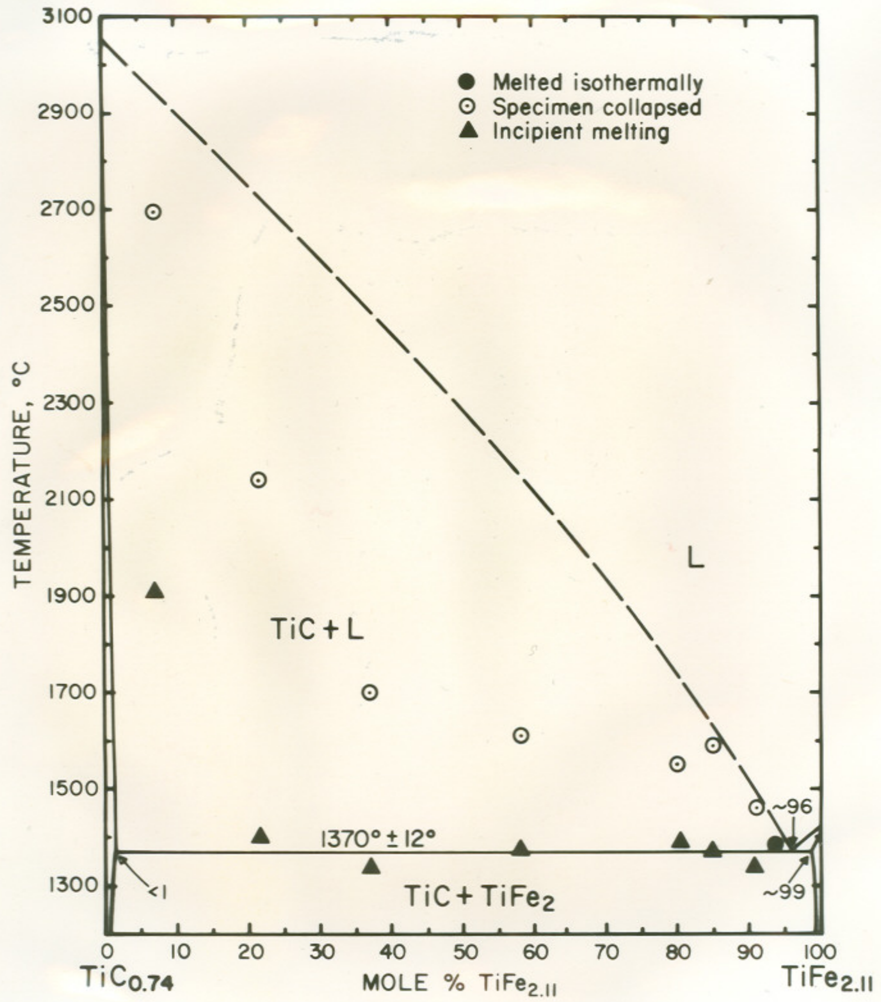

Figure 20. Melting Temperatures of Ternary Alloys Located Along the Pseudobinary Section ($TiC_{0.74}$-$TiFe_{2.11}$).

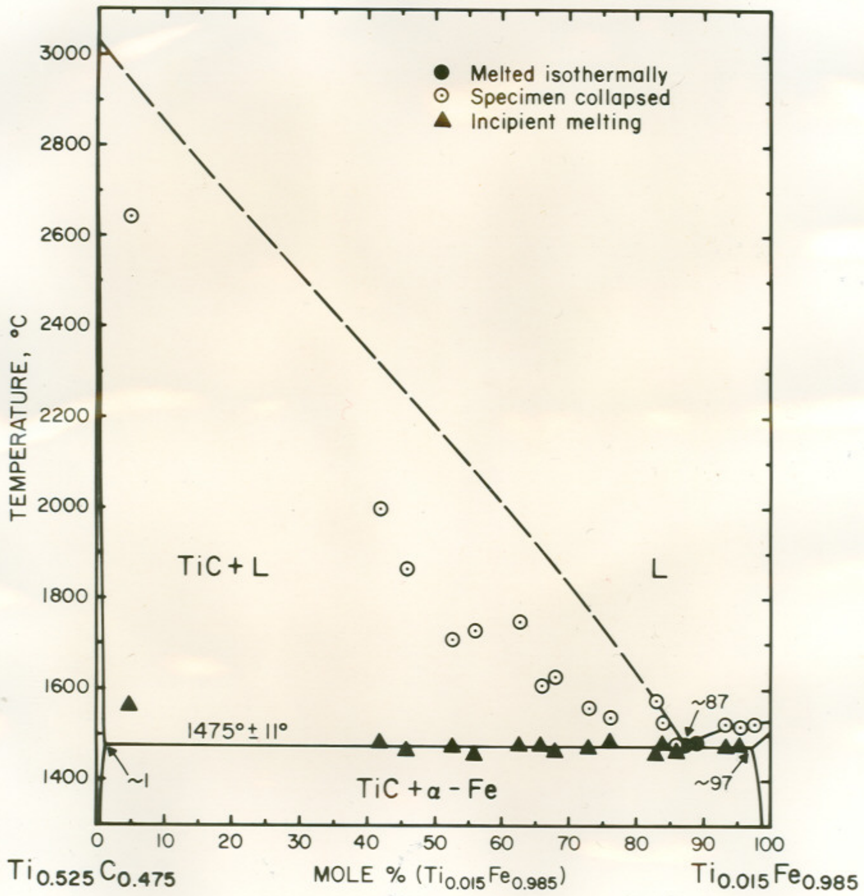

Figure 21. Melting Temperatures of Ternary Alloys Located Along the Pseudobinary Section ($TiC_{0.90}$-$Ti_{0.015}$-$Fe_{0.985}$).

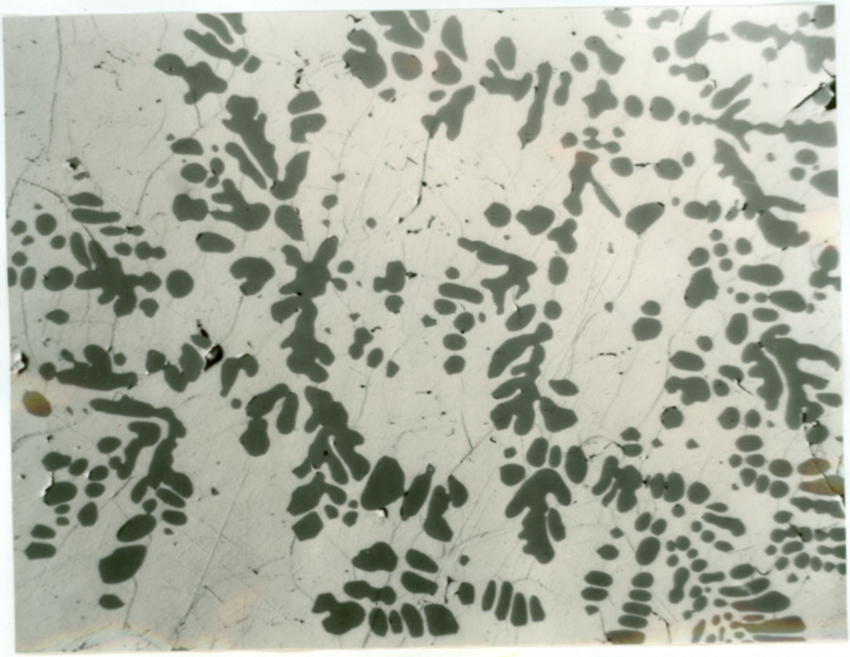

Figure 22. TiFe-C (39-50-11 At.%), Arc Melted Sample. Primary Monocarbide Dendrites (Dark Phase) in $TiFe_2$ Matrix. (Note cracks in brittle $TiFe_2$ phase).

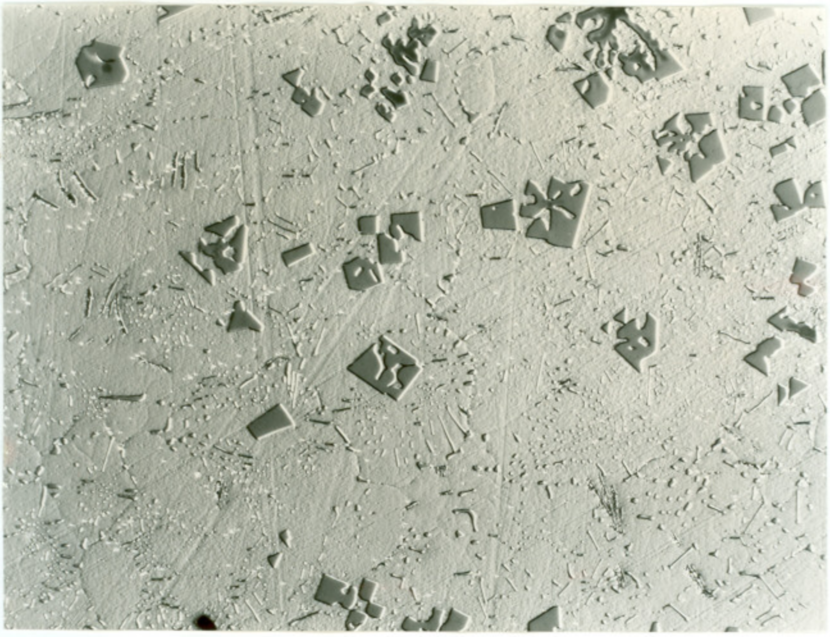

Figure 23. Ti-Fe-C (10-83-7 At.%), Arc Melted Sample. Trace of Primary Monocarbide in TiC_{1-x} + α-Fe Pseudo-binary Eutectic Matrix.

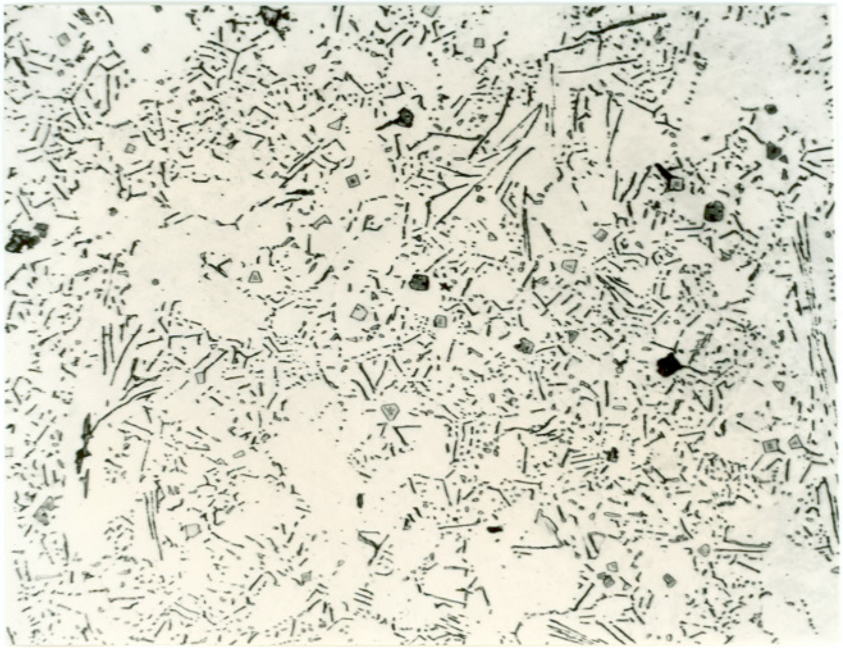

(a) X400

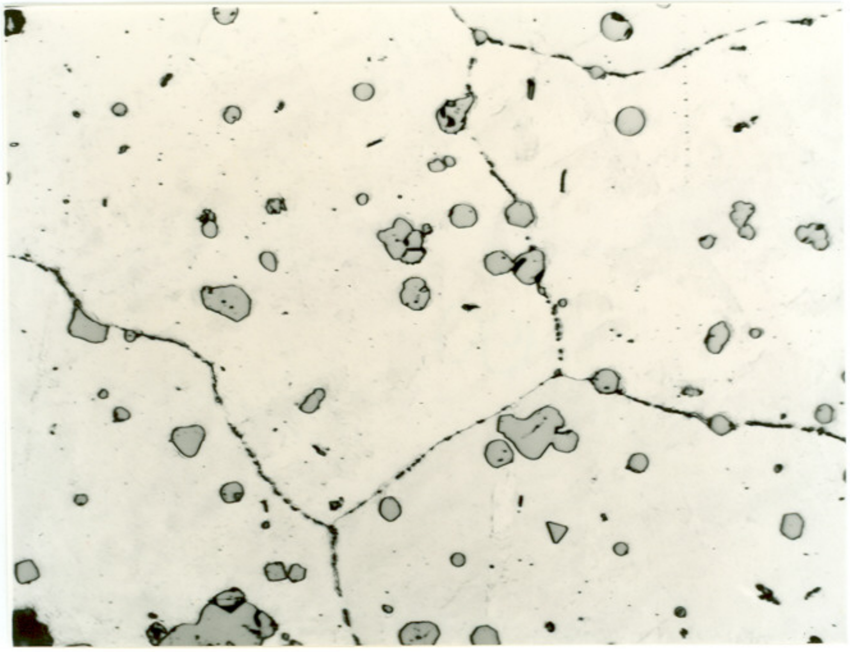

(b) X500

Figure 24. Ti-Fe-C (10-85-5 At.%), Arc Melted Sample.

(a) Primary α-Fe(Light Phase) in a Matrix of Bivariantly Solidified TiC_{1-x} + α-Fe Eutectic.

(b) Same alloy; Heat Treated at 1260°C for 60 hours. Annealed Eutectic Resulting in Spheroidal Monocarbide Within and at α Grain Boundaries.

eutectic structures due to the low carbon concentration of the eutectic liquid (Figure 22).

As shown in Figure 4, the melting temperatures of ternary alloys located between the above two pseudobinary eutectics drop to 1299° ± 10°C. At this temperature, the following ternary eutectic reaction occurs:

$$L \underset{>1299^{\circ}C}{\overset{<1299^{\circ}C}{\rightleftharpoons}} TiC_{1-x} + \alpha - Fe + TiFe_2.$$

From the metallographic analysis, the composition of the liquid phase was placed at approximately Ti(20)-Fe(78)-C(2) At.%; the location of this four-phase reaction plane which yields the three-phase equilibrium TiC_{1-x}(a= 4.325Å) + $TiFe_2$(a= 4.772Å; C = 7.781Å) + α-Fe (a = 2.875Å) is shown in Figure 40(c).

Photomicrographs of melted and heat treated alloys exhibiting the phase morphology characteristic of this reaction are presented in Figures 25, 26 and 27. Again, it is difficult to resolve the eutectic monocarbide phase because of the metal-rich position of the eutectic liquid. The eutectic structure exhibited by the ternary alloys is similar to that of the binary $TiFe_2$ + α-Fe constituents previously shown in Figures 14 and 15.

Figure 25. Ti-Fe-C (22-75-3 At.%), Arc Melted Sample. X400 Trace of Primary Monocarbide Dendrites (Light Gray Phase) in Ternary Eutectic Matrix.

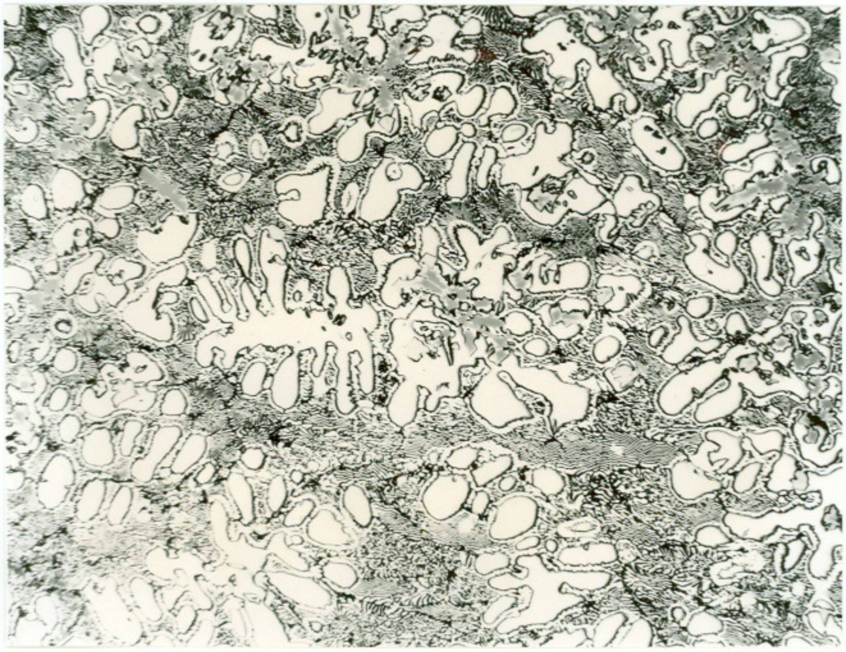

Figure 26. Ti-Fe-C (20-75-5 At.%), Arc Melted Sample. X400 Trace of Primary Monocarbide Plus Secondary α-Fe (Light Phase) in Invariantly Solidified TiC_{1-x} + $TiFe_2$ + α Eutectic.

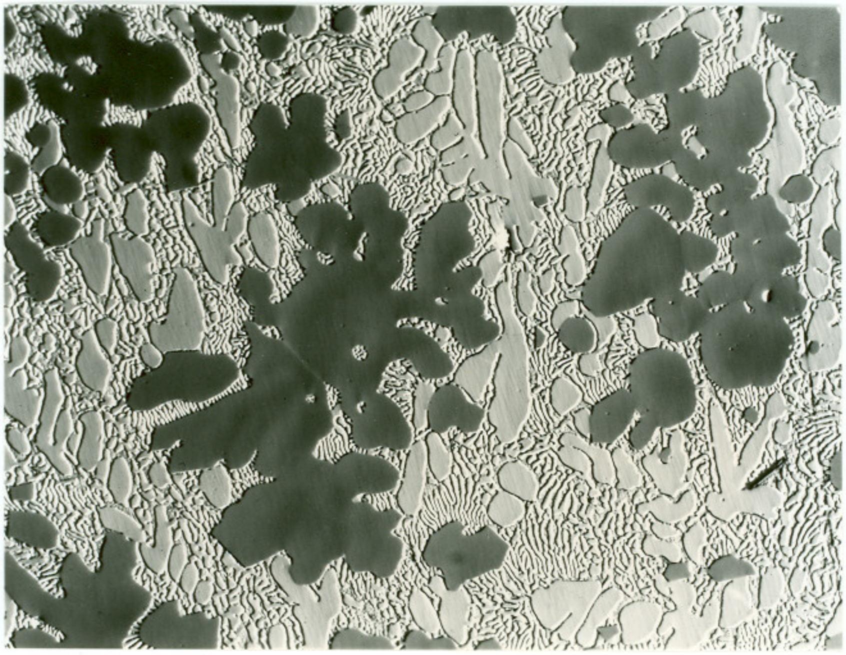

(a) X680

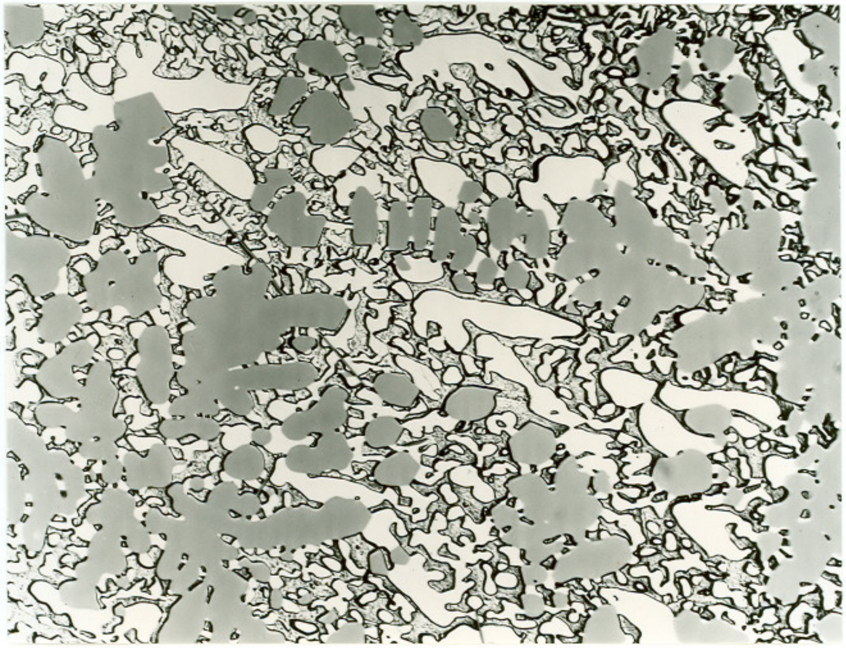

(b) X460

Figure 27. Ti-Fe-C (37-42-21 At.%), Arc Melted Sample.

(a) Primary Monocarbide (Dark Phase) plus Secondary $TiFe_2$ in Metal Matrix Type Ternary Eutectic. X-Ray Analysis. Substoichiometric monocarbide, $TiFe_2$; α-Fe.

(b) Same Alloy; Heat Treated at 900°C for 240 hours. Annealed Eutectic Structure.

With decreasing temperature, the three-phase equilibrium liquid (Fe-rich) + TiC_{1-x} + α-Fe, which originates at the 1475°C critical tie line (Figures 17 and 21), is terminated at $1409^{\circ} \pm 6^{\circ}C$. At this temperature, the following class II type ternary reaction occurs:

$$L + \alpha\text{-Fe} \underset{>1409^{\circ}C}{\overset{<1409^{\circ}C}{\rightleftharpoons}} TiC_{1-x} + \gamma\text{-Fe}.$$

The distribution of phases partaking in this reaction are presented in Figures 4 and 40(d).

The existence of the four-phase temperature plane at 1409°C was determined from the consistency of the incipient melting and collapsing temperatures of ternary alloys with subsequent metallographic and X-ray examination of these alloys in both the melted and quenched, and heat treated condition. As indicated in Figures 3 and 4, alloys located on the iron-rich side of the critical tie line at 1475°C melted increasingly heterogeneously as the solidus temperatures rapidly drop to the four-phase reaction plane at 1409°C and then to the ternary eutectic at 1109°C (Figure 40a).

The microstructures of ternary alloys located just to the iron-rich side of the 1475°C critical tie line were coarse grained and the eutectic slightly divorced (Figures 28 and 29). In Figure 29 which still shows remnance of TiC_{1-x} + α-Fe eutectic colonies after a 240 hour anneal at 900°C, the iron-rich liquid phase which had enveloped the primary α-Fe at 1409°C formed the γ-Fe phase. A similar microstructure of a melted and quenched alloy is presented in Figure 30. Here primary monocarbide is noted in a matrix of TiC_{1-x} + α-Fe eutectic colonies, but the divorced eutectic regions correspond to the γ-Fe phase formed at 1409°C.

Additional photomicrographs of an alloy annealed at 900° and 1260°C are presented in Figure 31. Here the γ-Fe phase which formed at the 1409°C reaction plane has decomposed during furnace cooling at some temperature between 900°C and 727°C (eutectoid decomposition temperature of γ-Fe in the Fe-C binary system). Hence the four-phase nonequilibrium mixture of TiC_{1-x}, α-Fe, γ-Fe, and Fe_3C.

Since no additional studies were conducted to better establish the ternary reaction sequence which accounts for the four-phase alloys of monocarbide + α-Fe + γ-Fe + Fe_3C shown in the 900°C and 1260°C temperature sections (Figures 16 and 17), a proposed reaction sequence derived from the available data is presented.

As presented in photomicrograph 31(a), the γ-Fe eutectoid decomposition structure of α-Fe + Fe_3C is still lamellar in appearance. Even after the 900°C anneal for 240 hours, no spheroidized

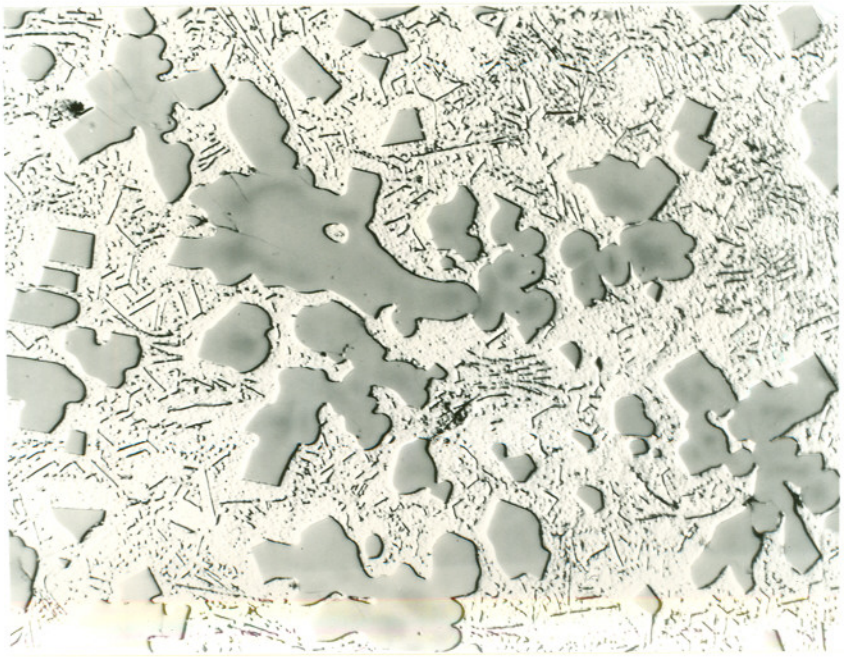

Figure 28. Ti-Fe-C (25-52-23 At.%), Arc Melted Sample. Primary Monocarbide in Slightly Divorced Eutectic Matrix of TiC_{1-x} + α-Fe.

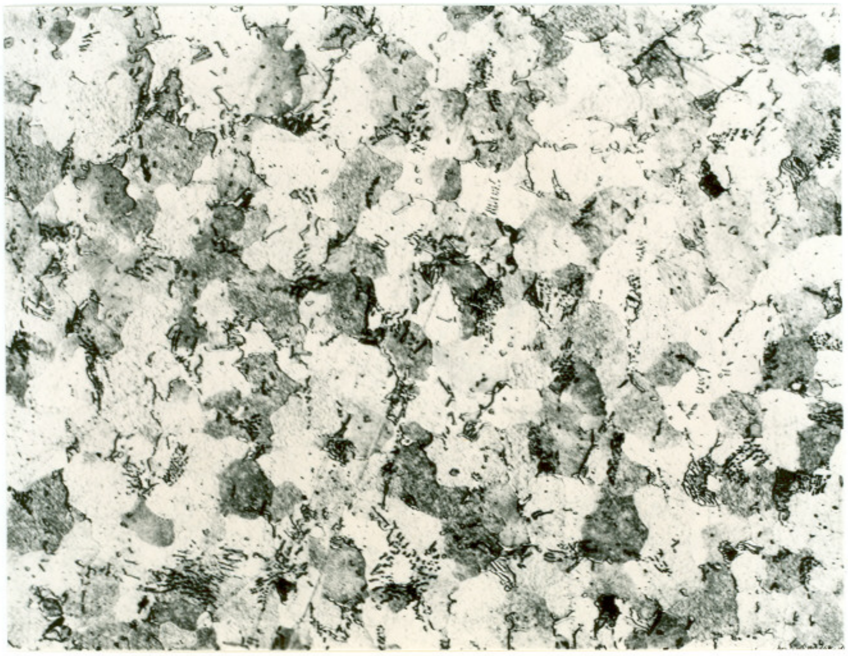

Figure 29. Ti-Fe-C (5-90-5 At.%), Arc Melted Sample Heat Treated at 900°C for 240 hours. Primary α-Fe (Light Phase) and Trace of Annealed TiC_{1-x} + α-Fe Eutectic Colonies; Rest γ-Fe (Dark Phase). X-Ray Analysis: X500

TiC_{1-x} (a = 4.327Å), α-Fe (a = 2.867Å); γ-Fe(a = 3.634Å).

Figure 30. Ti-Fe-C(10-78-12 At.%), Arc Melted Sample. Primary Monocarbide in TiC_{1-x} + α-Fe Eutectic Matrix. γ-Fe Regions Divorced of Eutectic. X-Ray Analysis: TiC_{1-x} and Diffuse, α and γ, Metal Phases. X500

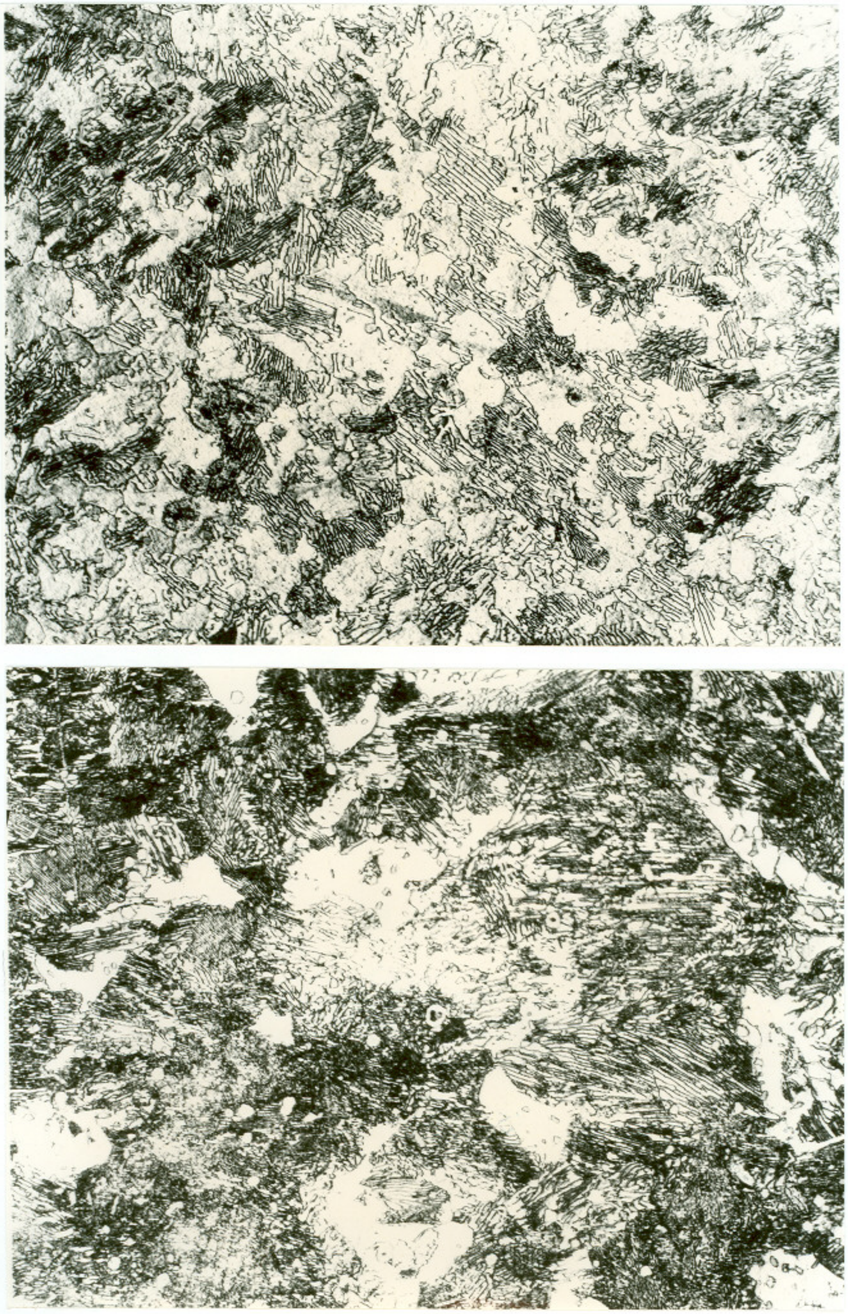

(a) X500

(b) X500

Figure 31. Ti-Fe-C (5-86-9 At.%), Arc Melted Sample.

(a) Heat Treated at 900°C for 240 hours. Trace of Primary Monocarbide in Matrix of α-Fe (Outlining Prior γ Grains) and Retained and Eutectoidally Decomposed γ-Fe. X-Ray Analysis: TiC_{1-x} (a = 4.328Å), α-Fe(a = 2.864 Å), γ-Fe (a = 3.633Å); Fe_3C.

(b) Heat Treated at 1260°C for 60 hours. Same as (a) Except Decomposition Structure is Finer.

Fe_3C can be detected in the matrix. Therefore, the γ phase which is stabilized by titanium to temperatures above the binary eutectoid (727°C) must have decomposed at some critical temperature Tc, $727^\circ C < T_c < 900^\circ C$. Since the solubility of Ti is greater in α than γ at 900°C (Figure 16) for the indicated three-phase equilibrium $TiC_{1-x} + \alpha + \gamma$, the width of the two-phase field $TiC_{1-x} + \gamma$ with decreasing temperature must rapidly reduce to a critical tie line at T_c where a class II-type reaction occurs in the following manner:

$$TiC_{1-x} + \gamma\text{-}Fe \xrightarrow{<T_c} \alpha\text{-}Fe + Fe_3C.$$

Below T_c, the $TiC_{1-x} + \alpha + Fe_3C$ phase field remains at all temperatures, while the $\alpha + \gamma + Fe_3C$ phase field proceeds to the binary eutectoid isotherm at 727°C.

From the binary monocarbide plus graphite eutectic at 2776°C and 63 At.% carbon, the maximum solidus temperatures of ternary alloys decrease rapidly to $1240^\circ \pm 15^\circ C$, the temperature of the proposed class II-type four-phase reaction involving the metastable Fe_3C phase,

$$L + C \underset{>1240^\circ C}{\xrightarrow{<1240^\circ C}} TiC_{1-x} + Fe_3C.$$

The location of this reaction plane is presented in Figure 17. Its accepted temperature and location was based on a correlation of X-ray and metallographic data obtained on both annealed and quenched ternary alloys and the consistency of their incipient melting temperatures.

As shown in the 900°C temperature section (Figure 16), alloys in the critical concentration region exhibited five-phase nonequilibrium mixtures of monocarbide, α -Fe, γ-Fe, graphite, and Fe_3C; and at lower carbon contents four-phase mixtures of monocarbide, α, γ and Fe_3C. Both four- and five-phase alloys located at carbon levels below the metastable two-phase equilibrium $TiC_{1-x}+Fe_3C$ participated in the ternary eutectic reaction at 1109°C (Figure 40a).

For ternary compositions away from the binary TiC + C eutectic isotherm, photomicrographs of alloys exhibiting bivariantly solidified monocarbide + graphite aggregates are presented (Figures 32-34). Figure 34 exhibits the same lamellar eutectoid decomposition structure previously shown in Figure 31, and also a trace of the characteristic phase morphology associated with the class II four-phase reaction at 1240°C. As shown in Figures 35 and 36, this phase morphology becomes more apparent in alloys of higher iron content.

In addition to the three-phase field of $L+TiC_{1-x}+C$ which takes part in the four-phase reaction at 1240°C, two additional melting troughs are associated with this reaction. The liquidus vertex of the metastable three-phase equilibrium $L + Fe_3C + C$ (Figure 3)

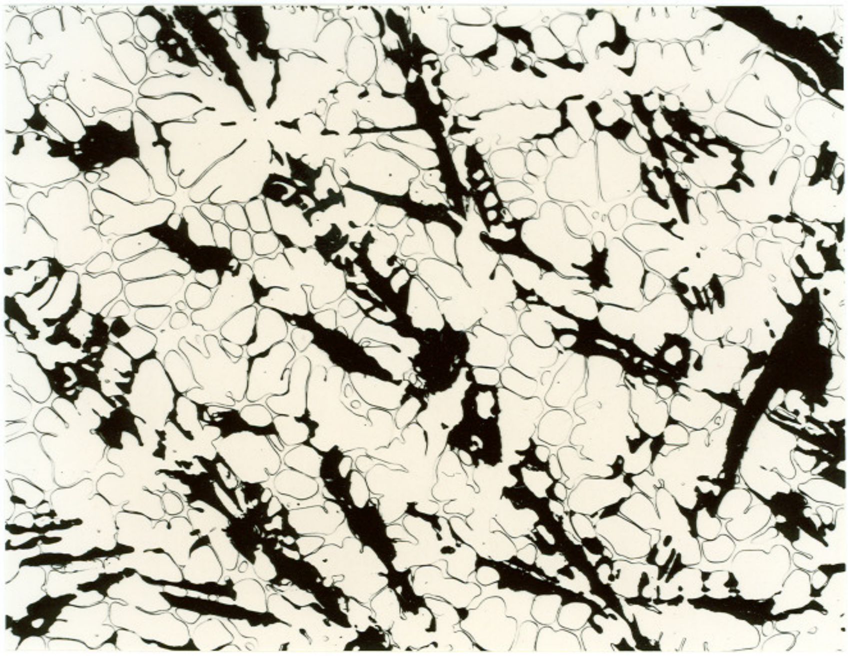

X200

Figure 32. Ti-Fe-C (35-10-55 At.%), Arc Melted Sample. Trace of Primary Graphite (Dark Phase) plus Bivariantly Solidified TiC_{1-x} + C Eutectic.

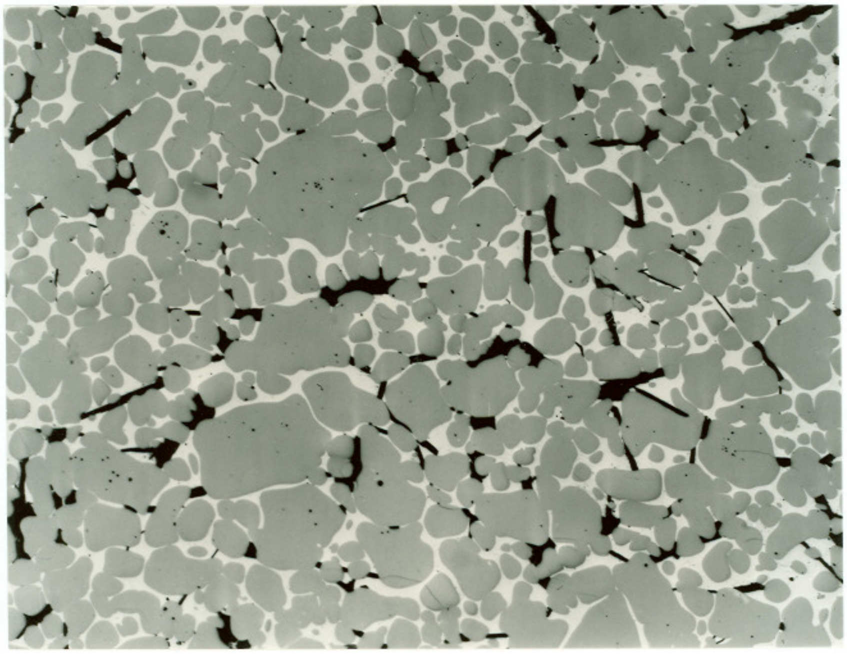

Figure 33. Ti-Fe-C (35-20-45 At.%), Melting Point Sample X200 Quenched from 1700°C. Primary Monocarbide plus Annealed TiC_{1-x} + C Eutectic in a Matrix of Unresolved Fe_3C and α-Fe.

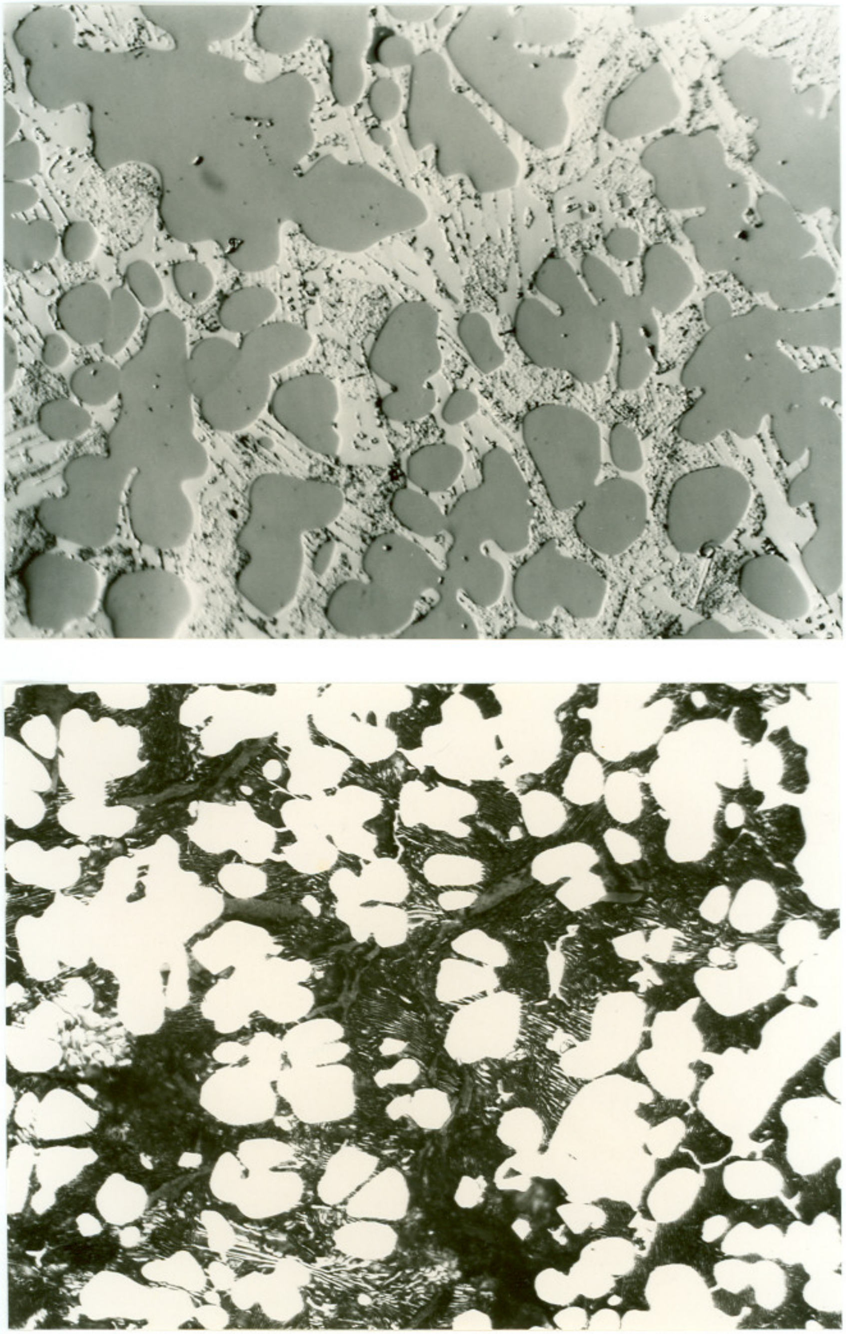

(a) X800

(b) X600

Figure 34. Ti-Fe-C (25-40-35 At.%), Arc Melted Sample

(a) Primary Monocarbide (Gray Phase), Trace of Secondary Graphite (Dark Phase) in Matrix of Fe_3C plus Decomposed γ-Fe (Lamellae unresolved).

(b) Annealed at 900°C for 240 hours. Coarsend Eutectoid Lamellae (formed between 727° and 900°C) and Remnants of Secondary Graphite. X-ray Analysis: TiC_{1-x}(a=4.326Å), α-Fe(a=2.864Å) trace of γ-Fe, and Fe_3C (a=4.53Å, b=5.09Å, c=6.73Å).

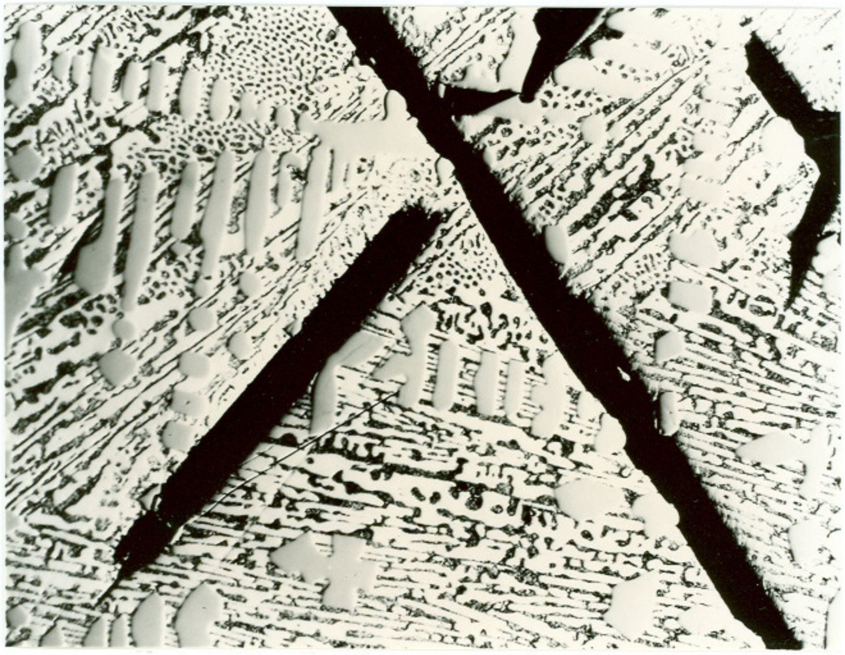

Figure 35. Ti-Fe-C (10-51-39 At.%), Arc Melted Sample. X600 Primary Graphite Needles (Dark) plus Secondary Monocarbide Dendrites (Gray). Matrix Phases: Fe_3C (Light) and Interdendritic Eutectic γ-Fe (Retained and Decomposed) which Solidified at 1240°C and 1109°C, respectively.

originates at 1240°C and with increasing temperature traces back to the Fe-C binary and terminates at the proposed peritectic isotherm of ~1280°C (Figures 1, 2 and 3). The second liquidus vertex associated with the metastable three-phase equilibrium of $L + TiC_{1-x} + Fe_3C$, continues with decreasing temperature towards the Fe-C binary system and finally merges with the three-phase fields of $Fe_3C + L + \gamma$-Fe and $TiC_{1-x} + L + \gamma$-Fe at the 1109°C eutectic plane. The melting behavior of alloys along these melting troughs were noticeably isothermal, and the corresponding microstructures of quenched alloys always exhibited both vibariantly and invariantly solidified Fe_3C, as shown in the Figures 35-39.

The proposed binary peritectic reaction, $Fe_3C \rightarrow L$ (~18 At.%C) + C at ~1280°C, was established from the melting behavior of ternary alloys participating in the class II reaction at 1240°C and hypereutectic Fe-C binary alloys. The binary alloys melted erratically, but their maximum incipient melting temperature tended to indicate a reaction isotherm at ~1280°C, consistently above the class II reaction plane.

When melted and quenched binary alloys were examined, it was noted that during melting the primary graphite in contact with an iron-rich liquid would migrate to the surface of the arc melted buttons leaving their interiors divorced of free graphite. Microstructures similar to those shown in Figures 35-38 were observed after subtracting the monocarbide and graphite constituents. Therefore the liquidus vertex of the metastable three-phase equilibrium $L + Fe_3C + C$ originating at the 1240°C reaction plane was extended to the Fe-C binary system (Figures 2 and 3).

In order to facilitate the reading of the phase diagram data previously presented in Figures 1-4 and also to efficiently use the experimental results presented, a series of isothermal sections were prepared which show more clearly the phase relationships prevailing at different temperatures and the sequence of reactions in the ternary system.

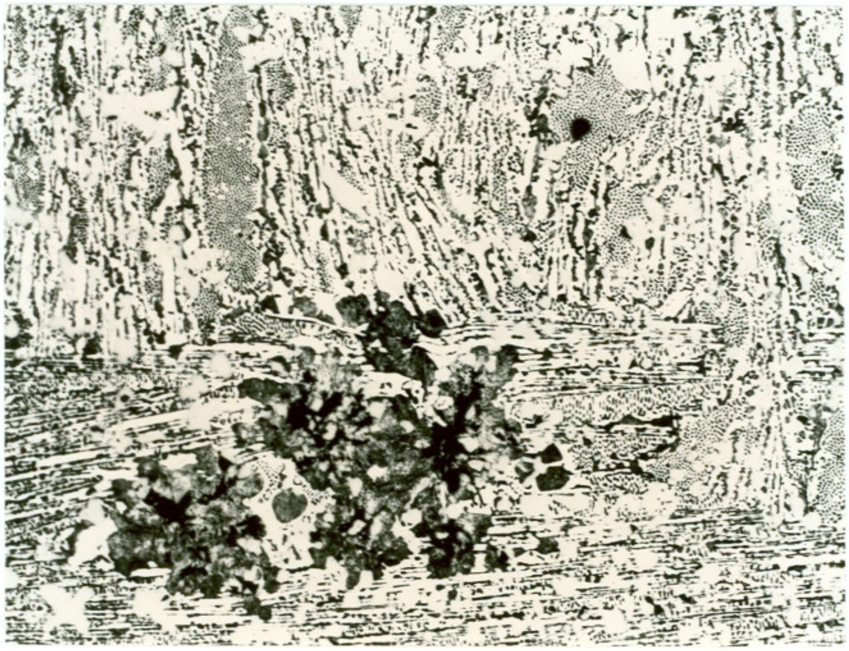

Figure 36. Ti-Fe-C (11-59-30 At.%), Arc Melted Sample. Primary Graphite (Dark Blotchy Regions) Plus Monocarbide. Matrix phases of Fe_3C which solidified at 1240°C according to the reaction: $L + C \rightarrow TiC_{1-x} + Fe_3C$, plus interdendritic eutectic γ-Fe.

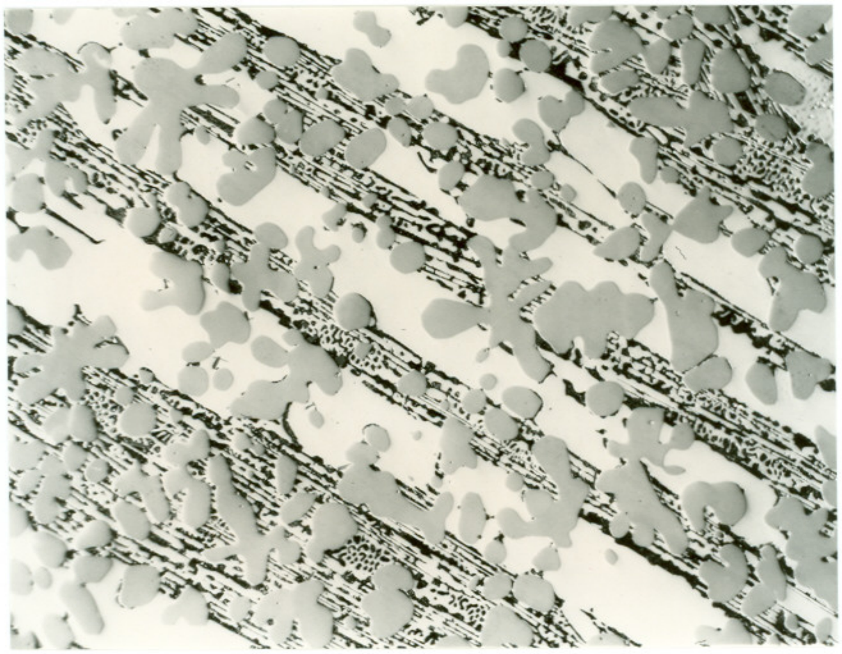

Figure 37. Ti-Fe-C (19-52-29 At.%), Arc Melted Sample. Bivariantly Solidified Monocarbide plus Fe_3C (Light Phase) in Ternary Eutectic Matrix.

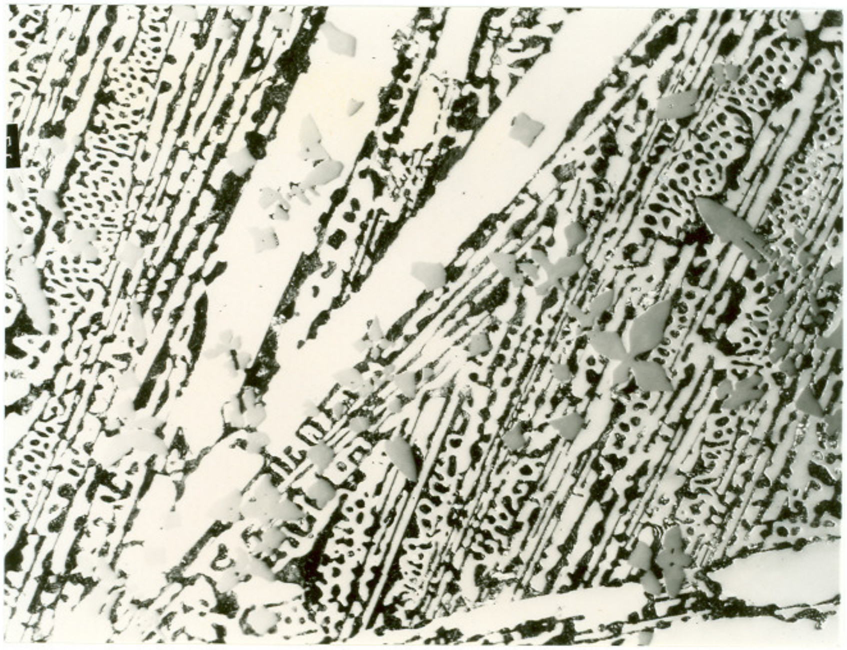

(a) X500

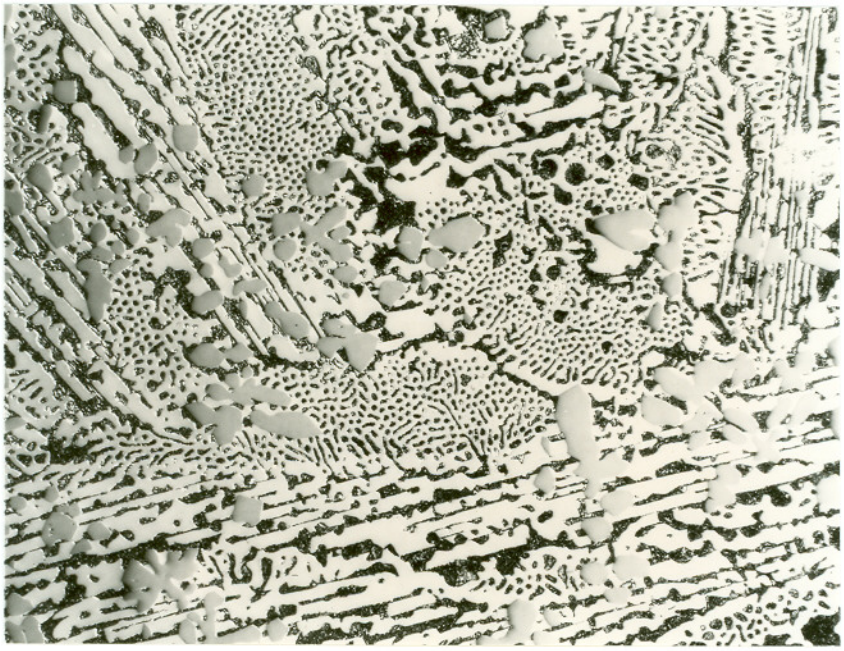

(b) X500

Figure 38. Ti-Fe-C (8-69-23 At.%), Arc Melted Sample

(a) Region Exhibiting Bivariantly Solidified Monocarbide plus Fe_3C in Ternary Eutectic Matrix.

(b) Same Sample Which Exhibits Primary Monocarbide in a Predominantly Ternary Eutectic Matrix of Fe_3C + γ-Fe (decomposed) + TiC.

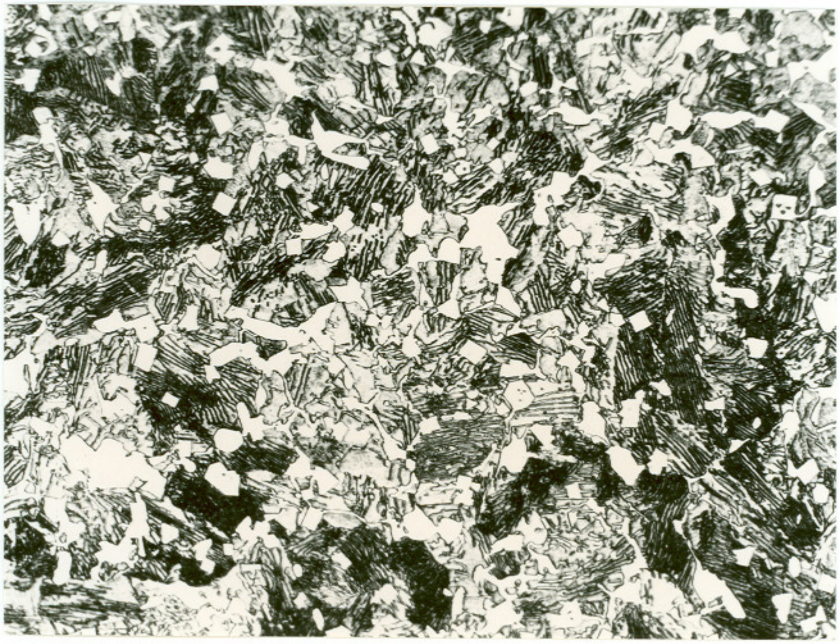

X520

Figure 39. Ti-Fe-C (6-74-20 At.%), Arc Melted Sample Heat Treated at 900°C for 240 hours. Trace of Primary Monocarbide and Fe_3C in an Annealed Eutectic Matrix. γ-Fe Matrix: Trace Retained and Remainder Decomposed During Furnace Cooling.

X-ray Analysis: TiC_{1-x} (a = 4.326Å), α-Fe(a = 2.865Å), γ-Fe(a~ 3.63Å); Fe_3C.

The ternary isotherms, which have been referred to during the presentation of experimental data, are presented in Figures 40(a) - 40(e).

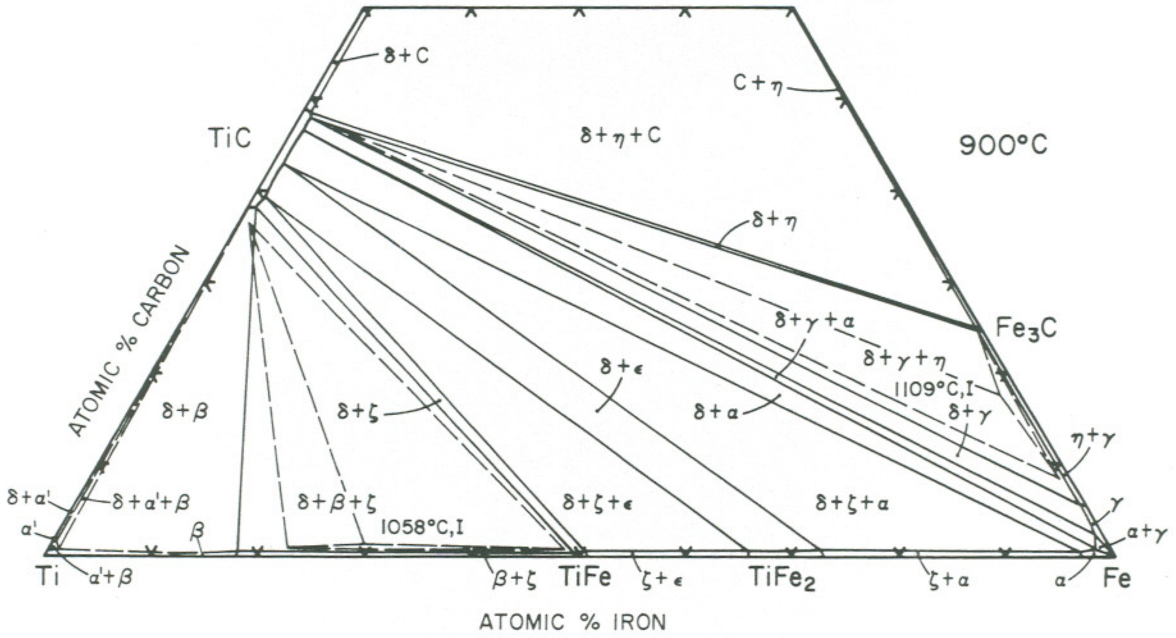

Figure 40(a). Isothermal Section of 900°C. Location of Class I Four-Phase Reaction Planes at 1058° ± 9°C and 1109° ± 7°C.

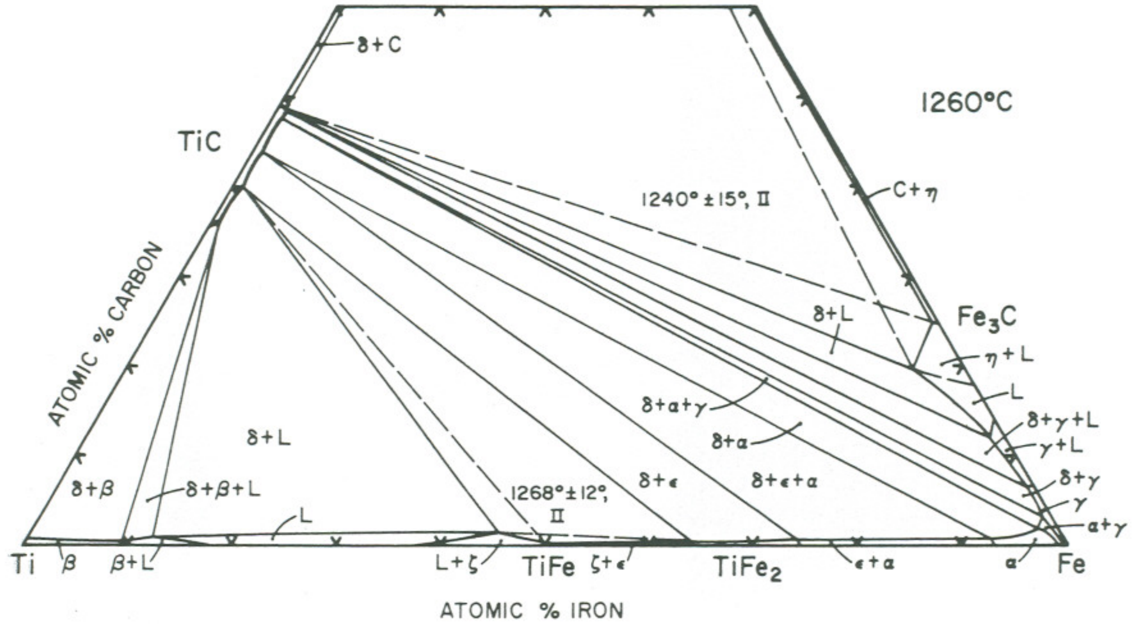

Figure 40(b). Isothermal Section at 1260° C

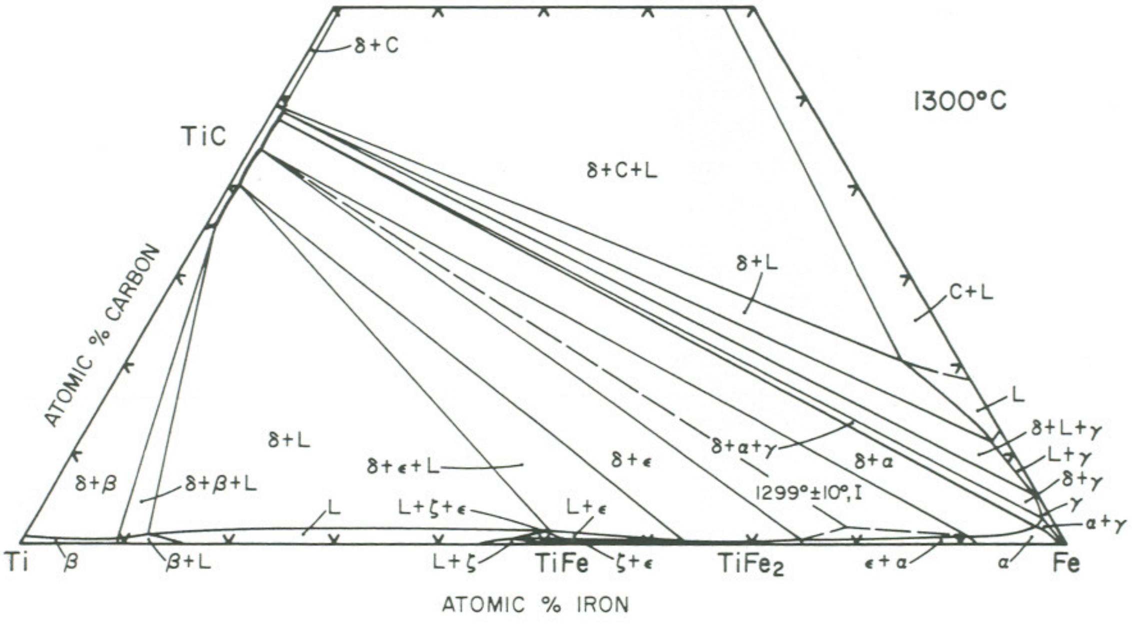

Figure 40(c). Isothermal Section at 1300° C.

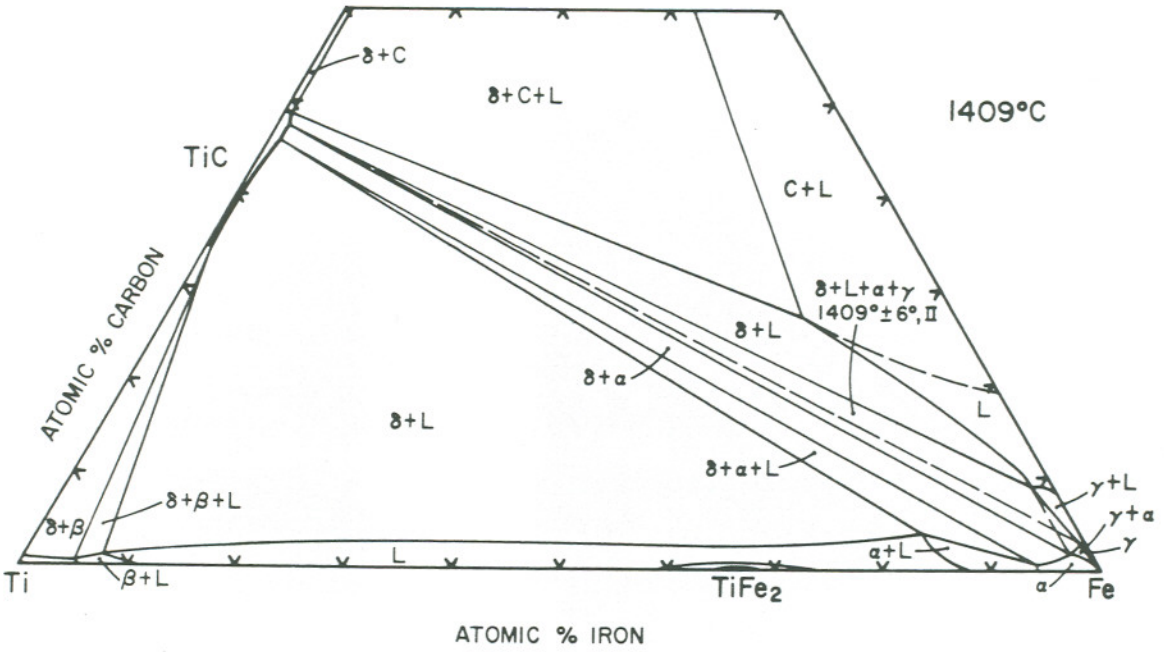

Figure 40(d). Isothermal Section at 1409° C.

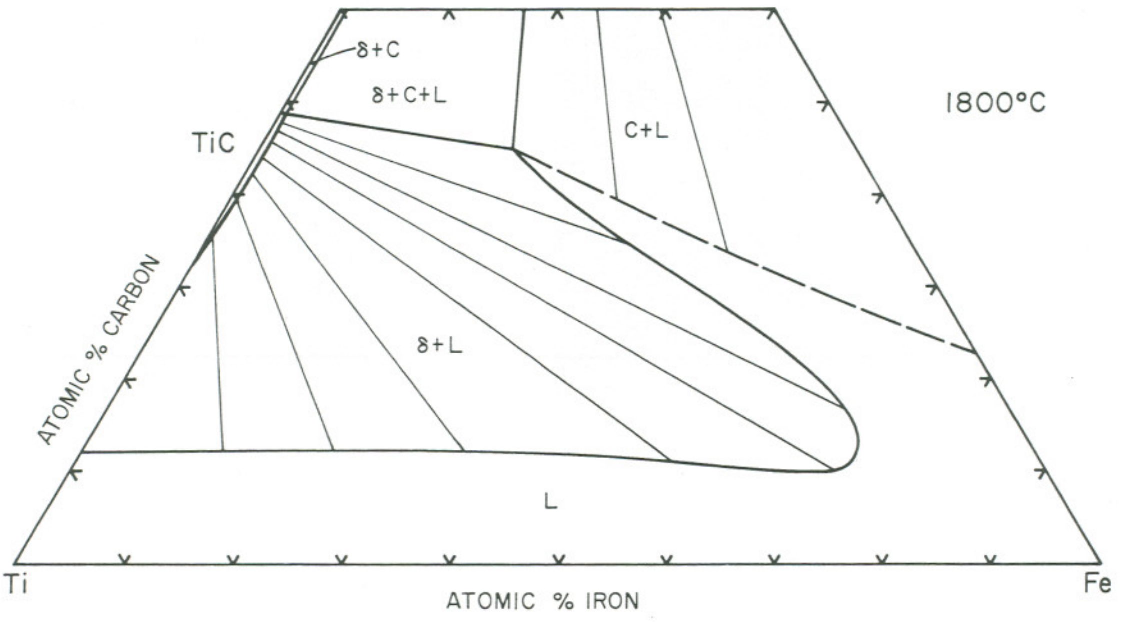

Figure 40(e). Isothermal Section at 1800° C.

2. The Ti-Co-C System

a. Ti-Co System

The constitution diagram of the system titanium-cobalt established in this investigation is similar to the one recently presented by Hawkins.(4) Depicted in Figure 41 are the measured solidus temperatures of binary alloys plus the solid state phase evaluation of alloys equilibrated at 900° and 1070°C.

The melting behavior of binary alloys in the concentration range of 48 to 53 At.% Co indicated that the TiCo phase melts congruently at 1361° ± 14°C. On the titanium-rich side of this intermetallic phase, eutectic and peritectic equilibria are formed between β-Ti and Ti_2Co at 1057 ± 4°C, and Ti_2Co and TiCo at 1080° ± 10°C, respectively. The above melting isotherms are slightly higher than those reported in the available literature(2,4,12).

Above 900°C, the cubic ($E9_3$-type) Ti_2Co phase exhibits a narrow homogeneity range. On the average and independent of the alloys composition and prior thermal history, a lattice parameter of $a = 11.300Å$ was measured. On the other hand at 900°C, the cubic (B2-type) TiCo phase was found to exhibit a noticeable homogeneity range as evidenced by the change in its lattice parameter from $a = 2.997Å$ at approximately 48 At.% Co to $a = 2.877Å$ at 54 At.% Co.

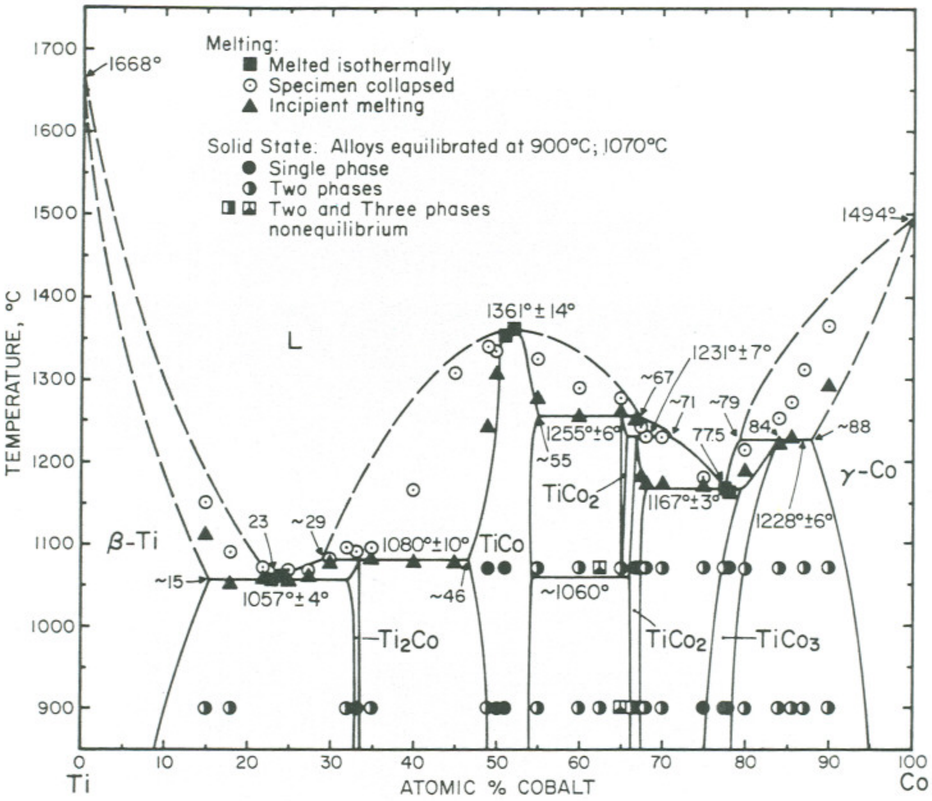

Figure 41. Titanium-Cobalt Constitution Diagram. Experimental Melting Temperatures and Qualitative Phase Evaluation of Ti-Co Alloys.

(Melting Temperatures for Ti and Co obtained from References (6) and (4), respectively.)

At higher temperatures, the cobalt-rich phase boundary of TiCo remains unaffected by temperature; its maximum stability range is terminated at 1255° ± 6°C, the observed peritectic isotherm of the equilibrium TiCo, cubic (C15-type) $TiCo_2$, and liquid. The hexagonal (C36-type) modification of $TiCo_2$ was found to melt peritectically at a slightly lower temperature of 1231° ± 7°C (Figure 41). Previous literature values reported for these proposed reaction isotherms were ~1250°C(2,4) and ~1230°C(2,4), respectively.

A eutectic equilibrium is formed between the hexagonal modification of $TiCo_2$ and the cubic (Ll_2-type) $TiCo_3$ phase at 1167° ± 3°C. Presented in Figures 42-44 are photomicrographs of melted and quenched alloys participating in this reaction. Also presented in Figures 43(b) and 44(b) are photomicrographs of annealed alloys which exhibit the appearance of the $TiCo_3$ phase in bulk from the once fine lamellar eutectic structure. As shown in Figure 41, both the titanium- and cobalt-rich phase boundaries of $TiCo_3$ are strongly temperature dependent above approximately 1070°C. Below this temperature, the phase extends from ~75 At% Co (a = 3.616Å) to 78 At.% Co (a = 3.601Å). This stability range is somewhat less than the 74-80 At.% Co range reported by Iannucci et al.(12).

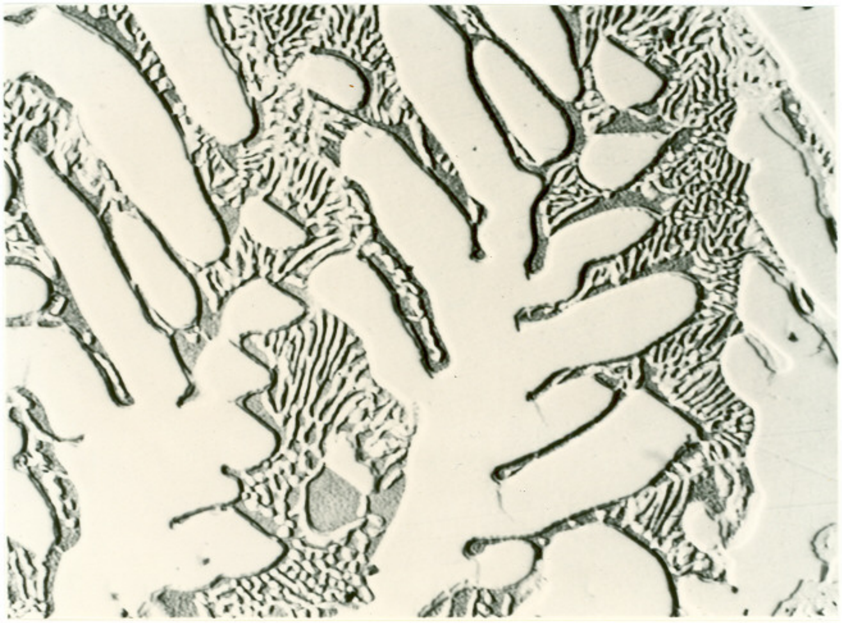

Figure 42. Ti-Co (26-74 At.%), Arc Melted Sample. Primary Hexagonal $TiCo_2$ in $TiCo_2 + TiCo_3$ Eutectic Matrix.

X-Ray Analysis: $TiCo_2$ (a = 4.723Å; c = 15.399Å),
$TiCo_3$ (a = 3.618Å).

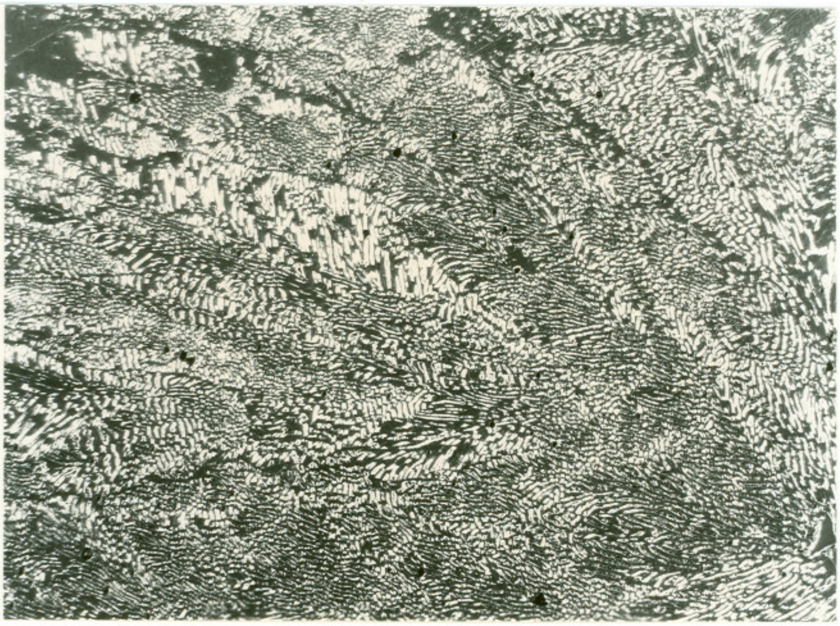

(a) X500

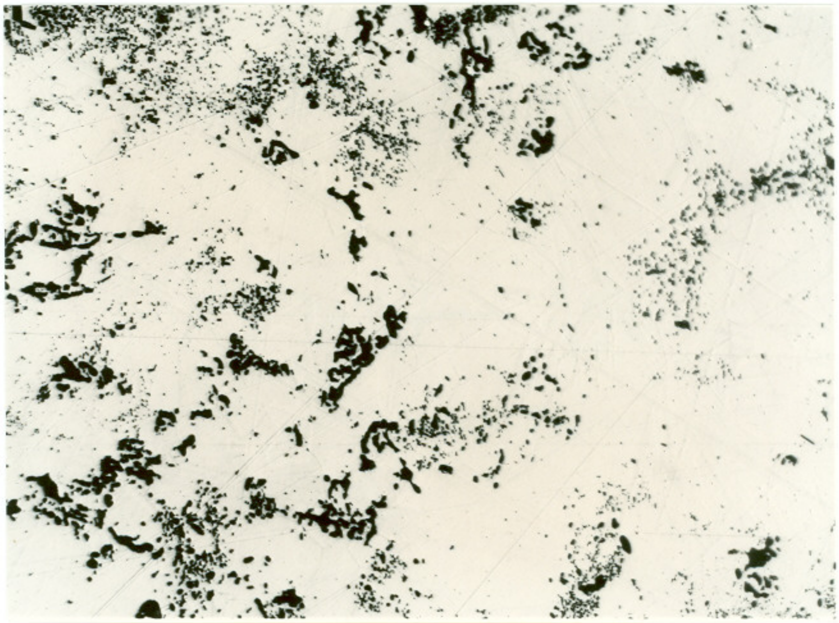

(b) X500

Figure 43. Ti-Co (23-77 At.%), Arc Melted Sample.

(a) $TiCo_2 + TiCo_3$ Eutectic Structure,

(b) Same sample heat treated at 1070°C for 100 hours. $TiCo_3$ (Light Matrix Phase) plus annealed $TiCo_2$. X-ray Analysis: $TiCo_2$ ($a = 4.728Å$; $c = 15.401Å$) and $TiCo_3$ ($a = 3.615Å$).

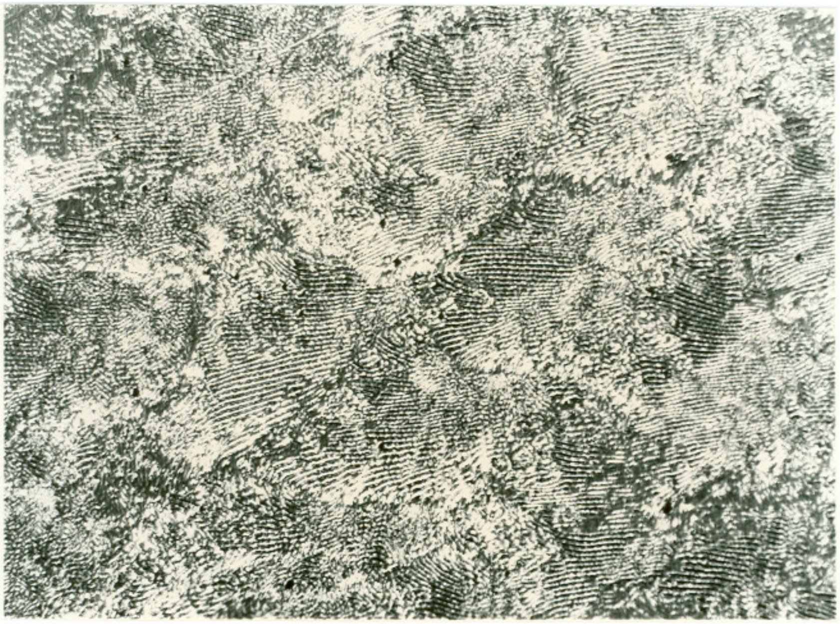

(a) X650

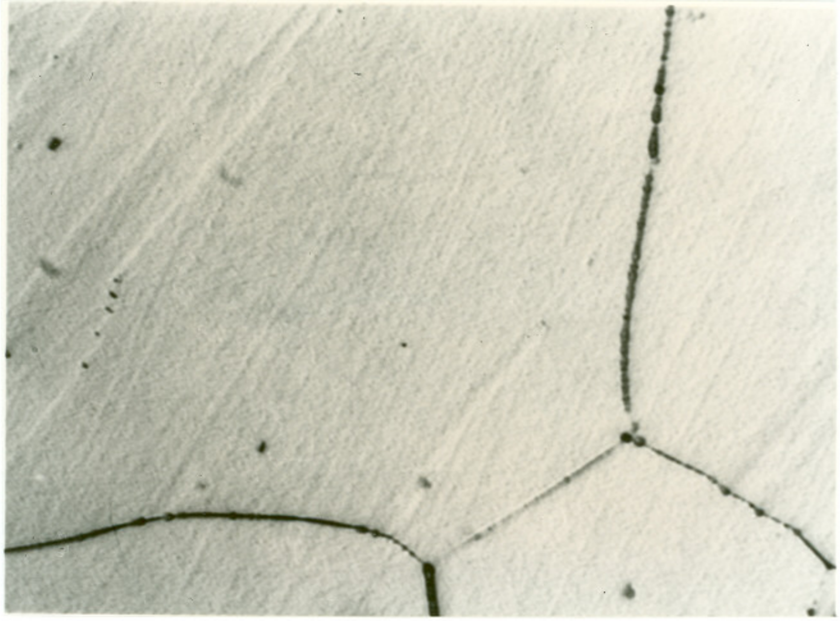

(b) X1800

Figure 44. Ti-Co (22-78 At.%), Arc Melted Sample.

(a) $TiCo_2 + TiCo_3$ Eutectic Structure.

(b) Same Sample Heat Treated at 900°C for 240 hours. Single Phase $TiCo_3$. X-ray Analysis: $TiCo_3$ ($a = 3.610_2$Å).

Above 1070°C, $TiCo_3$ exists at Co-richer compositions and finally decomposes peritectically at 1228° ± 6°C. Typical microstructures of melted alloys which exhibit the phase morphology characteristic of this reaction are presented in Figures 45 and 46; also shown are the precipitation structures which result from the temperature dependent solvus lines for the Co-rich $TiCo_3$ and Ti-rich Co phases.

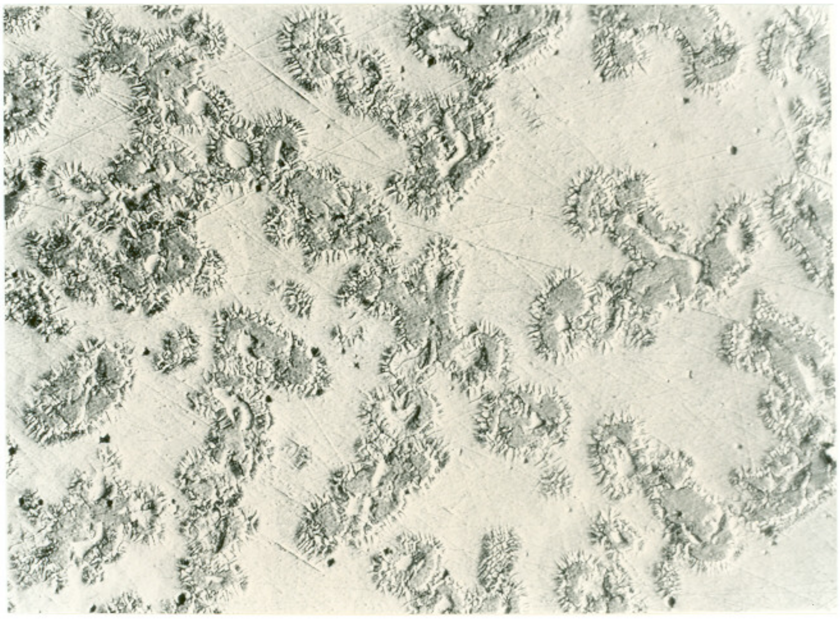

Figure 45. Ti-Co (20-80 At.%), Arc Melted Sample. Primary Co Phase (Dark) in a Matrix of Peritectically Solidified $TiCo_3$ Plus Slight Trace of Eutectic $TiCo_2$. Transition Region Surrounding Primary Phase: Co Precipitates in Secondary $TiCo_3$.

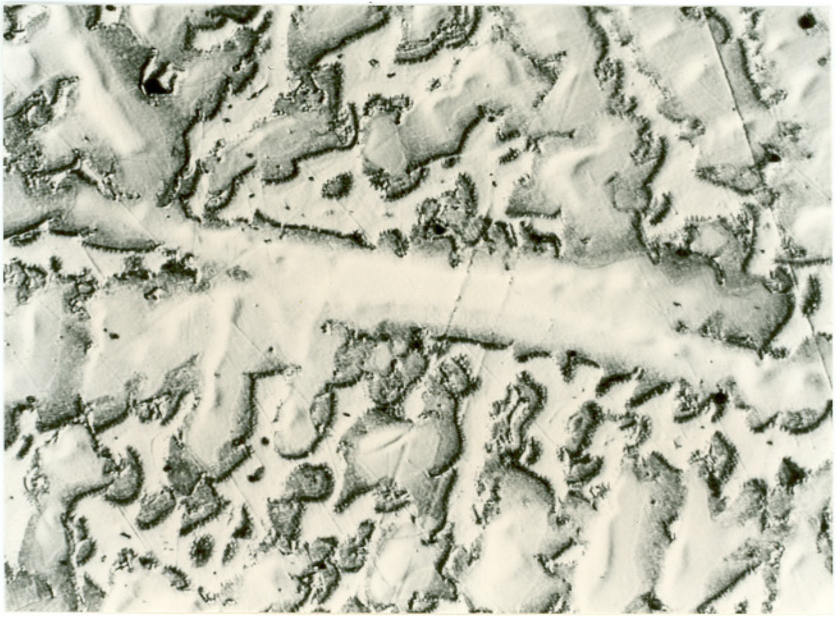

(a) X840

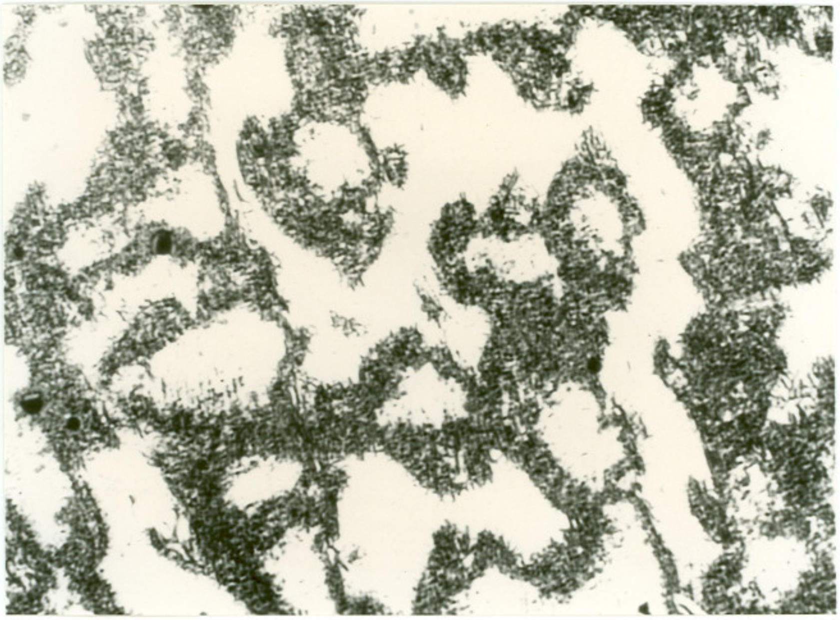

(b) X1700

Figure 46. Ti-Co (16-84 At.%), Arc Melted Sample.

(a) Peritectic-Type Envelopment of Cored Primary Co Dendrites Plus $TiCo_3$ (Light Phase) and Transition Region.

(b) Same Sample Heat Treated at 900°C for 240 hours. Once Single Phase $Co_{(ss)}$ Dendrites (Dark Regions) Heavily Precipitated with $TiCo_3$ Plus Trace of Coarse Co Precipitates in $TiCo_3$ Matrix. X-ray Analysis: $TiCo_3$($a = 3.608$Å); Co ($a = 3.569$Å).

As shown previously in Figure 42, the hexagonal $TiCo_2$ partakes in the eutectic reaction at 1167°C (Figure 41). Melted and quenched alloys invariably showed the presence of only the hexagonal modification at Co-rich compositions, while peritectically melting alloys at Ti-richer compositions showed the presence of secondary cubic $TiCo_2$ plus trace amounts of the hexagonal modification in addition to the primary TiCo phase. From melting temperatures down to 1070°C, it was found that both the cubic and hexagonal phases coexist. The following lattice parameters were obtained from alloys annealed at 1070°C for 100 hours: $TiCo_2$ (a = 6.698Å) plus slight trace of hexagonal phase at 66.7 At.% Co, and $TiCo_2$ (a = 4.730Å; c = 15.429Å) single phase at 67.5 At.% Co.

In disagreement with the results reported by Elliott(2), Hawkins(4), and Pearson(10); the cubic (C15-type) modification of $TiCo_2$ was not detected in any Ti-rich alloys heat treated at 900°C, except for the two- and three-phase nonequilibrium samples depicted in Figure 41. This result is in agreement with the earlier findings of Duwez and Taylor(9) who only observed the hexagonal phase in alloys equilibrated at 1000°C.

In addition to the X-ray diffraction data generated from melted and annealed alloys, metallographic analysis of these same alloys revealed the presence of a reaction structure associated

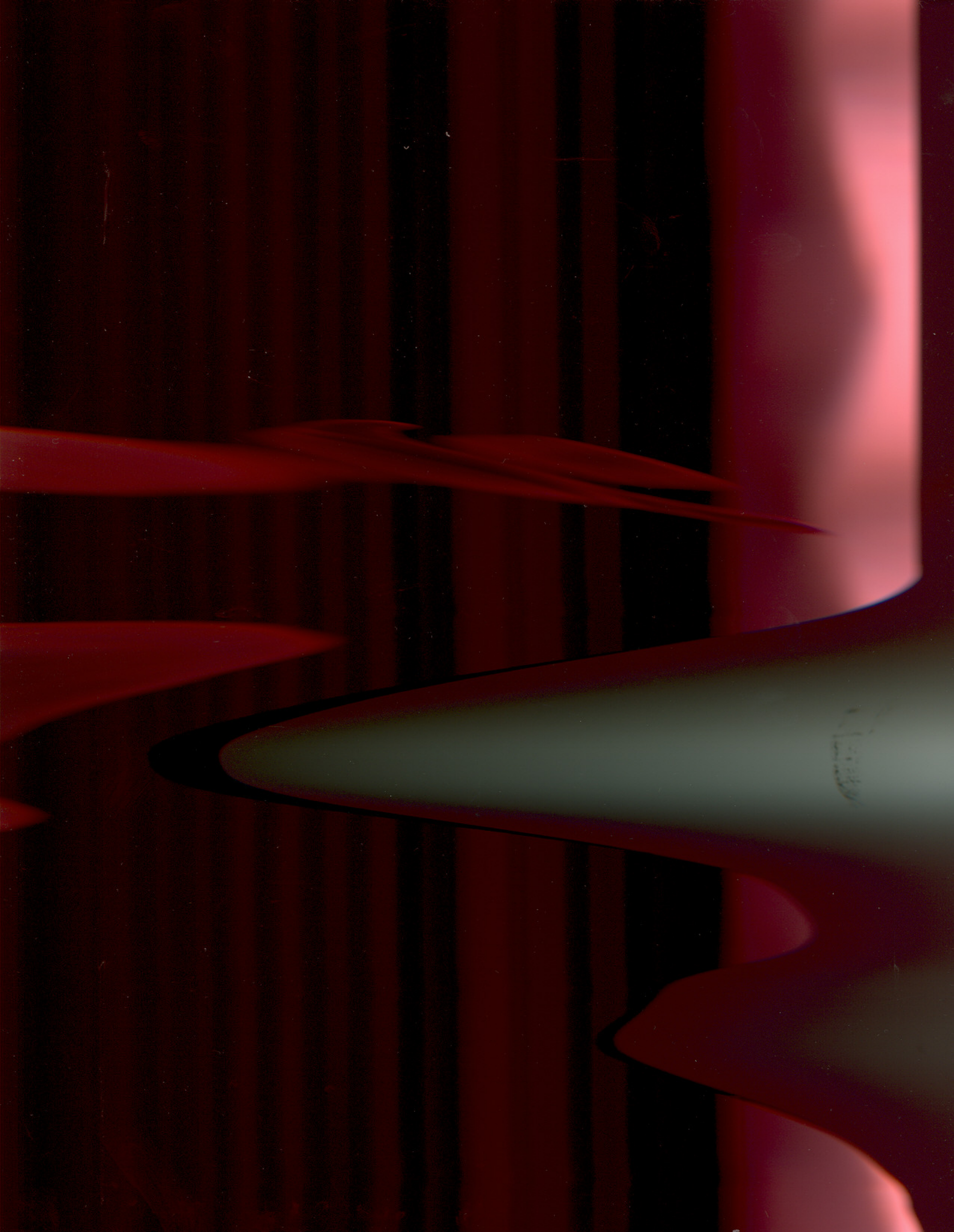

with the $TiCo_2$ phase (Figure 47). This structure was only observed in Ti-rich alloys and not alloys located to the Co-rich side of this phase. Titanium-rich alloys equilibrated at 1070°C usually exhibited either the cubic $TiCo_2$ or cubic $TiCo_2$ plus TiCo. In some instances the hexagonal phase (Figure 41) was noted in the presence of the cubic modification and TiCo; this was interpreted as a nonequilibrium phase mixture.

Because of these observations, a proposed eutectoid decomposition temperature for the cubic $TiCo_2$ phase was placed at ~1060°C, slightly less than the 1070°C equilibration temperature of this investigation and above the 1000°C equilibration temperature of Duwez and Taylor(9). At the lower temperature anneal of 900°C, the eutectoid reaction proceeds to completion rather sluggishly for alloys located close to the stoichiometric $TiCo_2$ phase as evidenced by the two- and three-phase nonequilibrium alloys shown in Figure 41 and photomicrographs 47(a-b).

b. Co-C System

The brief investigation of this binary system was restricted to the determination of its eutectic melting temperature and composition. The melting point investigation yielded a value of 1318° ±3°C; the metallographic analysis of the melted samples yielded a eutectic composition of ~12 At.% carbon. Both these values are in excellent agreement with the literature values of 1321°C and 11.9 At.% carbon(4).

(a) X1450

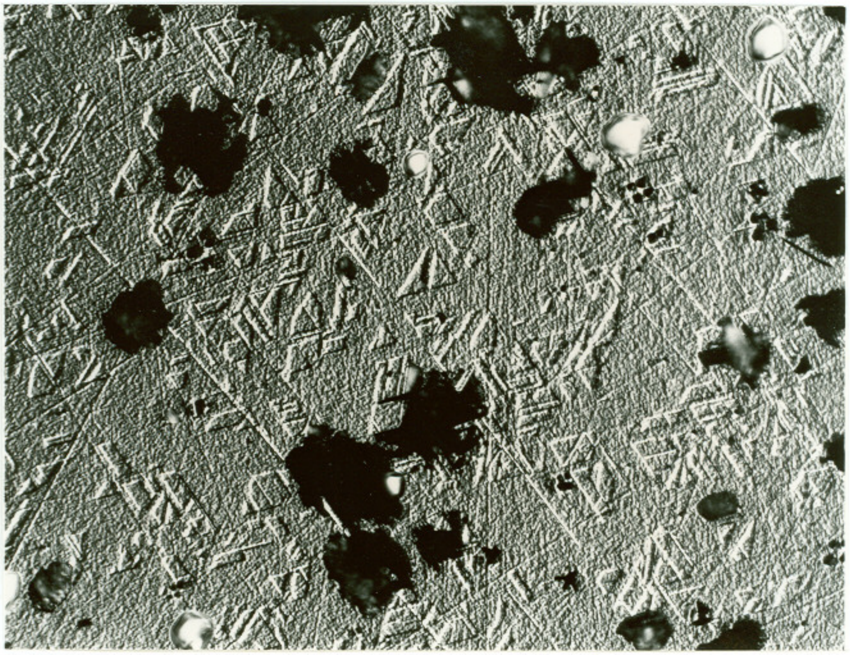

(b) X650

Figure 47. Ti-Co (35-65 At.%), Arc Melted Sample.

(a) Heat Treated at 1070°C for 100 hours. Heavily etched cubic $TiCo_2$ plus slight trace of TiCo (Dark Areas). X-ray Analysis: $TiCo_2$ ($a = 6.703_2$Å).

(b) Same Sample treated at 900°C for 240 hours. Heavily etched $TiCo_2$, both decomposed and retained cubic modification, plus slight trace of TiCo dendrites (small dark areas) and porosity. X-ray Analysis: Cubic $TiCo_2$ ($a = 6.702_2$Å); Hexagonal $TiCo_2$ ($a = 4.731$Å; $c = 15.430$Å).

A phase diagram of the system (Figure 48) was constructed from literature data and results obtained in this investigation. Also presented in Figure 49 is a photomicrograph of a slightly hypereutectic alloy which exhibits the phase morphology characteristic of the cobalt-graphite eutectic reaction.

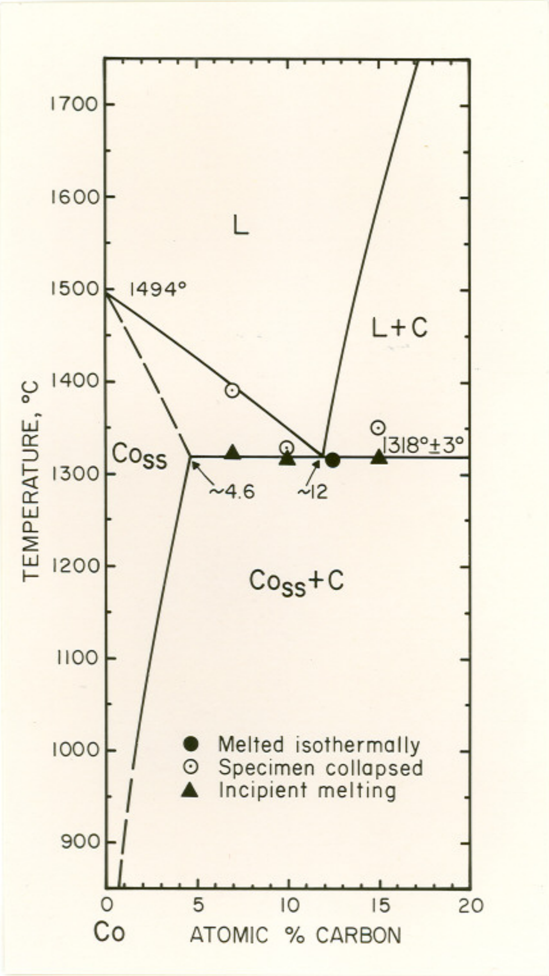

Figure 48. Cobalt-Carbon Constitution Diagram. Experimental Melting Temperatures.

(Melting temperature of Co, and solvus and liquidus curves obtained from References 4,51, and 53).

Figure 49. Co-C (87.5-12.5 At.%), Melting Point Sample Quenched from 1315°C. Slight trace of primary graphite (coarse dark areas) in a cobalt plus graphite eutectic matrix.

c. Ternary System

Qualitative X-ray diffraction and metallographic analyses of Ti-Co-C alloys equilibrated at 900° and 1070°C resulted in the phase relationships depicted in Figures 50 and 51, respectively. From a comparison of these isothermal sections, the principal phase relationships do not vary appreciably, except in the higher temperature section a liquid phase appears in Ti-rich alloys near the Ti-Co boundary system. This Ti-rich liquid originates at a temperature of 1033° ± 5°C from the following class I ternary eutectic reaction

$$L \xrightarrow[\geq 1033\ C]{\leq 1033\ C} \mathrm{TiC}_{1-x} + \beta\text{-Ti} + \mathrm{Ti_2Co}.$$

As determined from the melting point and metallographic analyses, Figures 8 and 68 (a) show the location of the above reaction plane with a eutectic liquid composition of approximately Ti(76)-Co(23)-C(1) At.%. The three-phase equilibrium β-Ti(a = 3.19Å) + TiC_{1-x} (a = 4.313Å) + $\mathrm{Ti_2Co}$ (11.304Å), shown in the 900°C temperature section (Figure 50), is the product of this reaction.

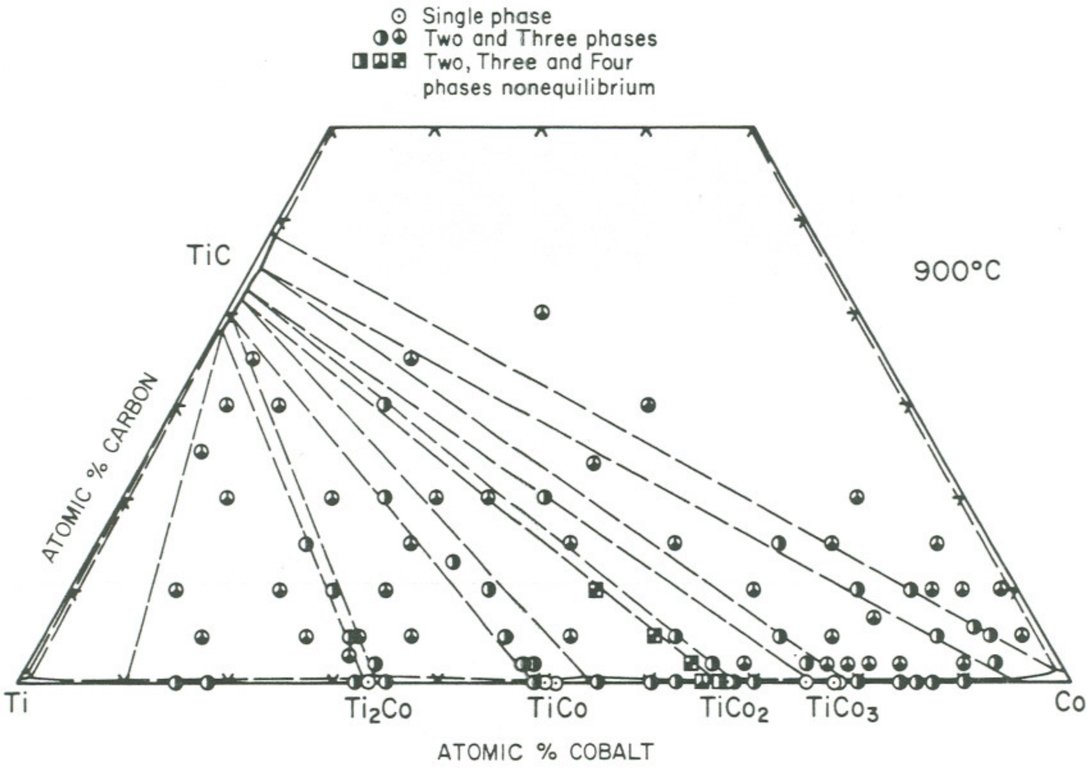

Figure 50. Qualitative Phase Evaluation of Ti-Co-C Alloys Equilibrated at 900°C.

With increasing temperature, the equilibrium liquid + TiC_{1-x} + Ti_2Co which originates at 1033°C merges with the three-phase equilibrium of Ti_2Co (a = 11.303Å) + TiC_{1-x} (a = 4.317Å) + TiCo (a = 2.989Å) at a temperature of 1066°± 4°C. The resulting class II four-phase reaction is depicted in Figures 8, 51, and 68(b), i.e.

$$L + TiCo \underset{>1066^\circ C}{\overset{<1066^\circ C}{\rightleftharpoons}} TiC_{1-x} + Ti_2Co.$$

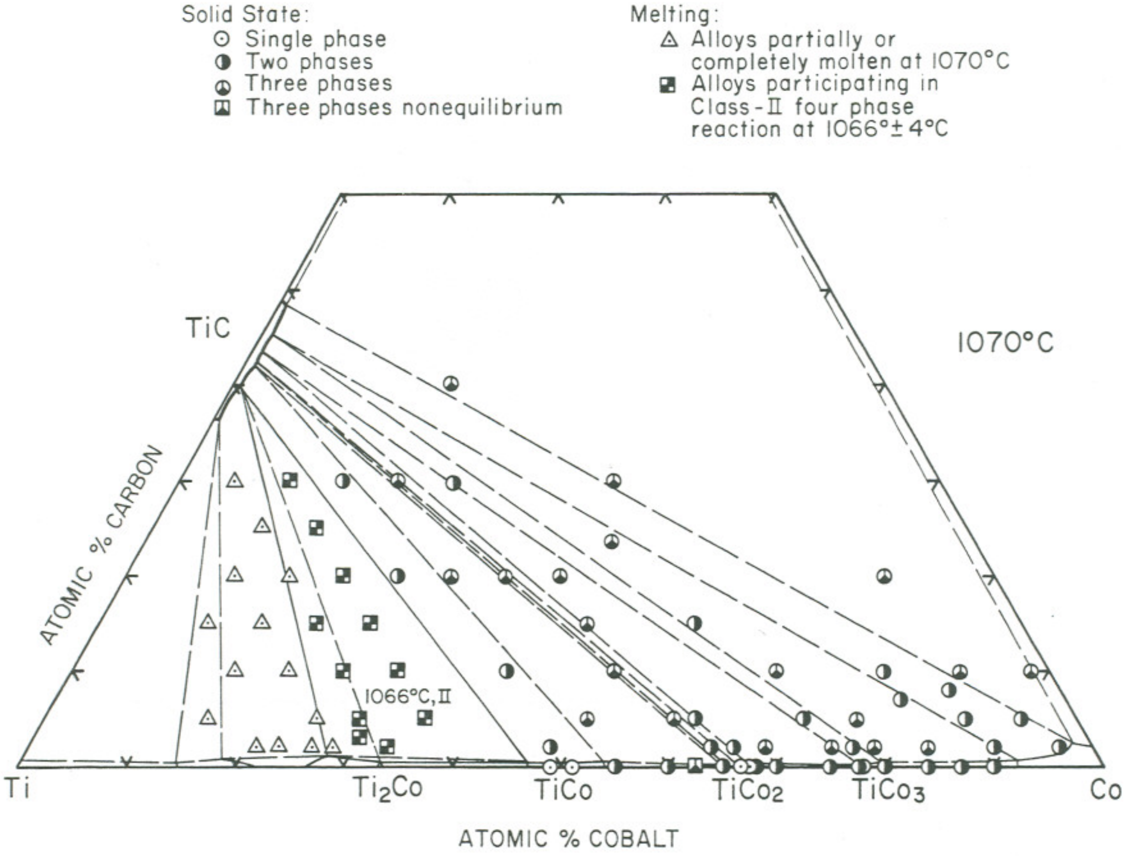

Figure 51. Qualitative Phase Evaluation of Ti-Co-C Alloys Equilibrated at 1070°C.

The existence of this reaction was determined from the consistency of the incipient melting temperatures of alloys located along the section TiC_{1-x} + Ti_2Co and within the three-phase field TiC_{1-x} + Ti_2Co + TiCo.

To the cobalt-rich side of the two-phase equilibrium TiC_{1-x} + TiCo (Figures 50 and 51), another class II ternary reaction occurs at a temperature of 1247° ± 3°C. It involves the cubic (C15-type) modification of $TiCo_2$ in the following manner

$$L + TiCo \underset{>1247^\circ C}{\overset{<1247^\circ C}{\rightleftharpoons}} TiC_{1-x} + (\text{cubic})\ TiCo_2.$$

Below this four-phase reaction plane, the product equilibria of $TiCo_2$ + TiC_{1-x} + liquid and TiCo + TiC_{1-x} + $TiCo_2$ are stable to temperatures of approximately 1215°C and 1060°C, respectively, where again two additional class II reactions are proposed. At the 1215°C invariant plane, the two-phase equilibrium TiC_{1-x} (a = 4.321Å) + $TiCo_2$ (a = 4.734Å; c = 15.431Å) depicted in the 900° and 1070°C isotherms is stabilized, i.e.

$$L + (\text{cubic})\ TiCo_2 \underset{>1215^\circ C}{\overset{<1215^\circ C}{\rightleftharpoons}} TiC_{1-x} + (\text{hex})\ TiCo_2.$$

The location and melting behavior of ternary alloys participating in the 1215°C and 1247°C class II reactions are presented in Figures 52 and 53, respectively. In addition, typical photomicrographs of alloys from the concentration regions TiC_{1-x}+ $TiCo_2$ and TiCo + TiC_{1-x} + $TiCo_2$, which were quenched from liquidus temperatures, are

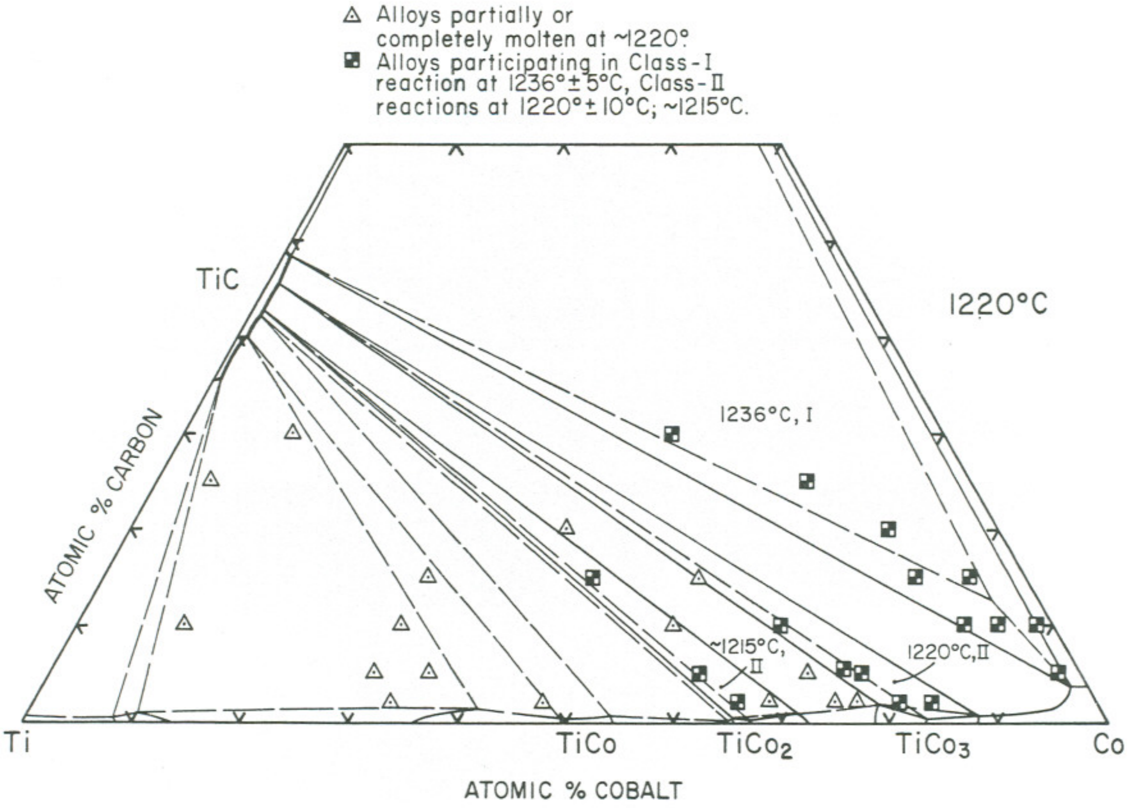

Figure 52. Melting Behavior of Ti-Co-C Alloys at ~ 1220° C.

presented in Figures 54-56. The class II reaction temperature of 1215° C could only be approximated; this was due to the narrow two- and three-phase fields of TiC_{1-x}+(hex)$TiCo_2$ and (cubic) $TiCo_2$ + TiC_{1-x}(hex) $TiCo_2$ combined with the interference of a liquid phase of eutectic origin at lower temperatures (Figure 52).

The previously mentioned class II ternary reaction occurring at 1060° C results from the merging of the three-phase equilibria TiCo + TiC_{1-x} + (cubic) $TiCo_2$ and (cubic) $TiCo_2$ + TiC_{1-x} + (hex) $TiCo_2$ which originate at 1247° C and 1215° C, respectively. The distribution of phases partaking in this reaction,

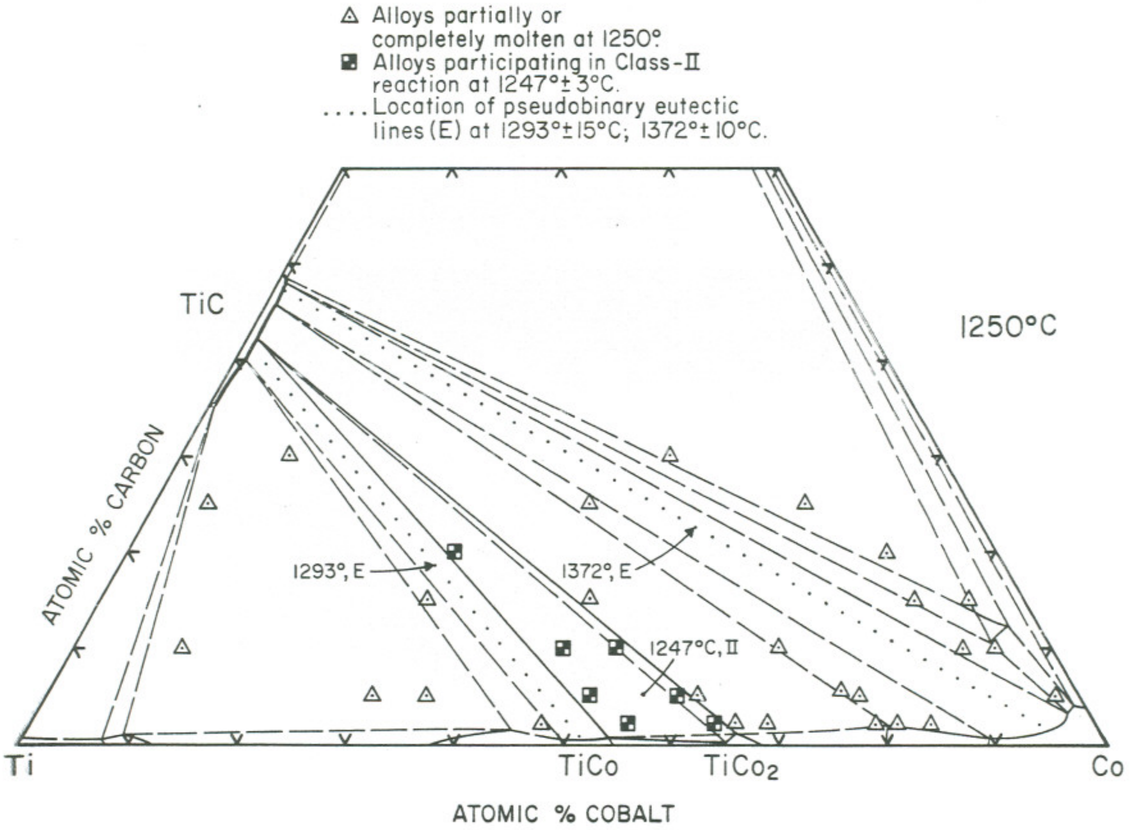

Figure 53. Melting Behavior of Ti-Co-C Alloys at 1250°C and Location of Pseudobinary Eutectic Equilibria at 1293° and 1372°C.

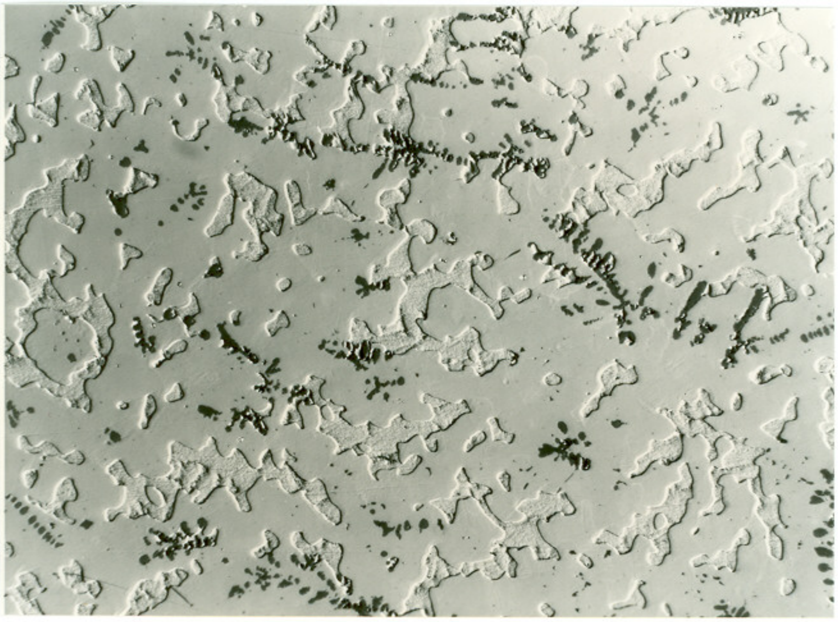

Figure 54. Ti-Co-C (43-55-2 At.%), Arc Melted Sample. Primary Monocarbide Dendrites in Matrix of TiCo Plus Cubic $TiCo_2$ (Light Matrix Phase) which Solidified at 1247°C According to the Reaction

$$L + TiCo \rightarrow TiC_{1-x} + TiCo_2.$$

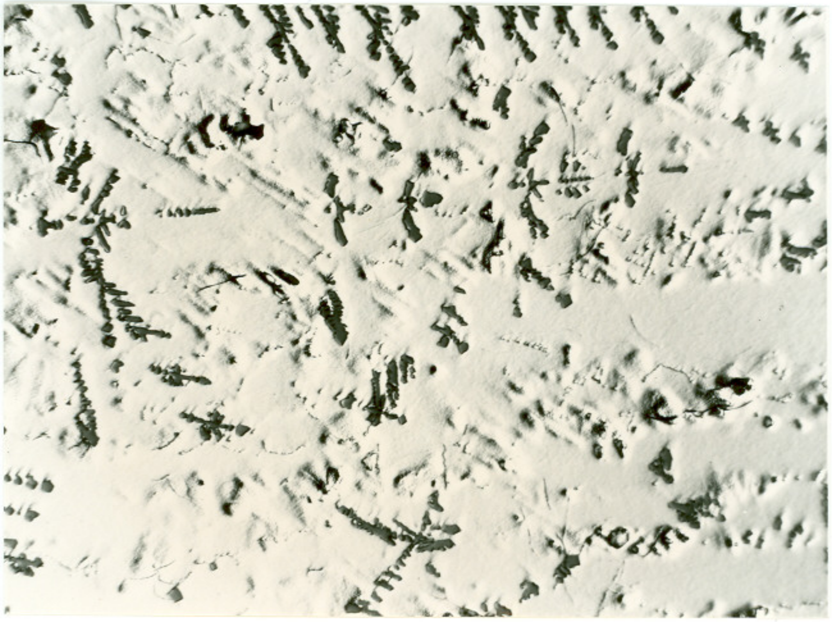

Figure 55. Ti-Co-C (33-65-2 At.%), Arc Melted Sample. Primary Monocarbide (Dark Phase) in Matrix of Dendrite $TiCo_2$ (Cubic Phase). Interdendritic Regions of a once Co-rich Liquid Solidified at ~1215°C According to the Reaction

$$L + (\text{cubic})\ TiCo_2 \rightarrow TiC_{1-x} + (\text{hex } TiCo_2.$$

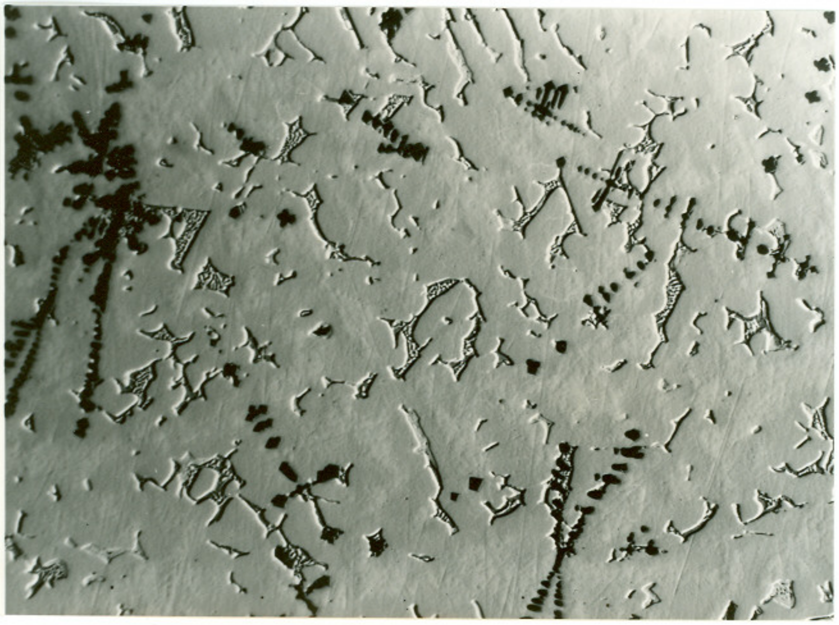

Figure 56. Ti-Co-C (30-68-2 At.%), Arc Melted Sample. Primary Monocarbide Dendrites in Matrix of Secondary $TiCo_2$. Cubic-$TiCo_2$ (Lighter Matrix Phase) Contained within the Hexagonal-$TiCo_2$. Trace of (hex) $TiCo_2$ + $TiCo_3$ + TiC Eutectic at Grain Boundaries.

$$TiC_{1-x} + \text{(cubic) } TiCo_2 \underset{>1060^\circ C}{\overset{<1060^\circ C}{\rightleftarrows}} TiCo + \text{(hex) } TiCo_2,$$

are presented in Figures 6 and 8. This class II reaction is indicated to occur at a temperature slightly above the proposed binary eutectoid decomposition temperature of the cubic $TiCo_2$ phase.

Similar to the results previously presented on the binary $TiCo_2$ phase, the cubic (C15-type) modification was not detected in any Ti-rich ternary alloys within the three-phase field of TiCo + TiC_{1-x} + $TiCo_2$ at 900°C. Exceptions were the four-phase nonequilibrium alloys depicted in Figure 50, along with the observed equilibrium and nonequilibrium distribution of phases in binary alloys. In fact, due to the low carbon solubility in $TiCo_2$, photomicrographs of alloys participating in the 1060°C ternary reaction revealed almost identical microstructures as the binary alloys, compare Figures 57 and 47(b).

The intermetallic phase of $TiCo_3$ participates in two ternary reactions at temperatures of 1110° ± 5°C and 1220° ± 10°C. The location of the first four-phase reaction plane is indicated in Figures 8 and 68(b) and corresponds to the following ternary eutectic reaction

$$L \underset{>1110^\circ C}{\overset{<1110^\circ C}{\rightleftarrows}} TiC_{1-x} + TiCo_3 + \text{(hex) } TiCo_2.$$

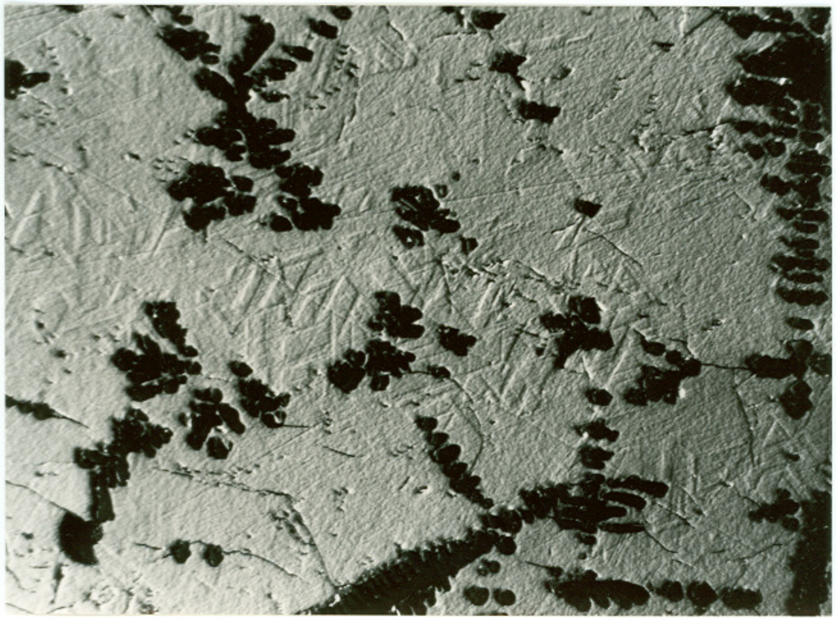

Figure 57. Ti-Co-C (35-63-2 At.%), Arc Melted Sample Heat Treated at 900°C for 240 hours. Monocarbide Dendrites (Dark Phase) plus Trace of TiCo in Matrix of Decomposed $TiCo_2$. X-ray Analysis: TiC_{1-x}, Slight Trace TiCo, $TiCo_2$ (a = 4.734 Å; c = 15.431Å); Trace Cubic-$TiCo_2$.

NOTE:

11/1/88-There is no page 134; this number omitted from page numbering. There is no missing material.

Maureen Sloan

The three-phase equilibrium TiC_{1-x}(a = 4.324Å) + $TiCo_2$ (a = 4.731Å, c = 15.430 Å) + $TiCo_3$ (a = 3.618Å) shown in Figure 51 enters this reaction plane from lower temperatures and produces the Co-rich liquid phase (Fig. 52). The composition of the invariant liquid phase was placed at approximately Ti(23)-Co(76)-C(1) At.%. Evidence of a eutectic-type structure was previously presented in Figure 56.

The second four-phase reaction involving $TiCo_3$ (Figure 52) occurs at a temperature of 1220° ± 10°C and corresponds to a class II-type,

$$L + Co \xrightleftharpoons[>1220^\circ C]{<1220^\circ C} TiC_{1-x} + TiCo_3.$$

Except for the presence of the monocarbide phase, microstructures similar to those previously presented (Figures 45 and 46) for binary alloys partaking in the peritectic reaction at 1228°C were observed. Photomicrographs of both melted and quenched, and annealed alloys revealing the phase morphology characteristic of this reaction are presented in Figures 58 and 59.

Because of the three previously presented Co-rich ternary reactions which occur between ~1215°C to 1247°C, the isotherms at 1220°C and 1250°C (Figures 52 and 53) were constructed to depict the phase equilibria participating in these reactions. In addition,

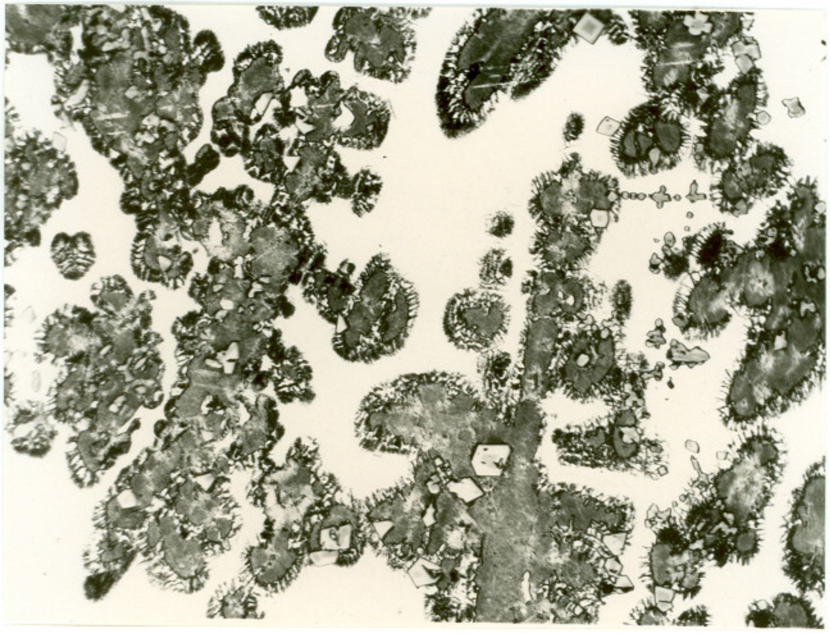

Figure 58. Ti-Co-C (20-75-5 At.%), Arc Melted Sample. Trace of Primary Monocarbide Plus Phase Morphology Resulting from Four-Phase Reaction:

$$L + Co \rightarrow TiC + TiCo_3 .$$

Dark Dendrites: Co
Dendrite Boundaries: $TiCo_3$ with Co precipitations.
Matrix: $TiCo_3$ Divorced of Eutectic TiC and $TiCo_2$.

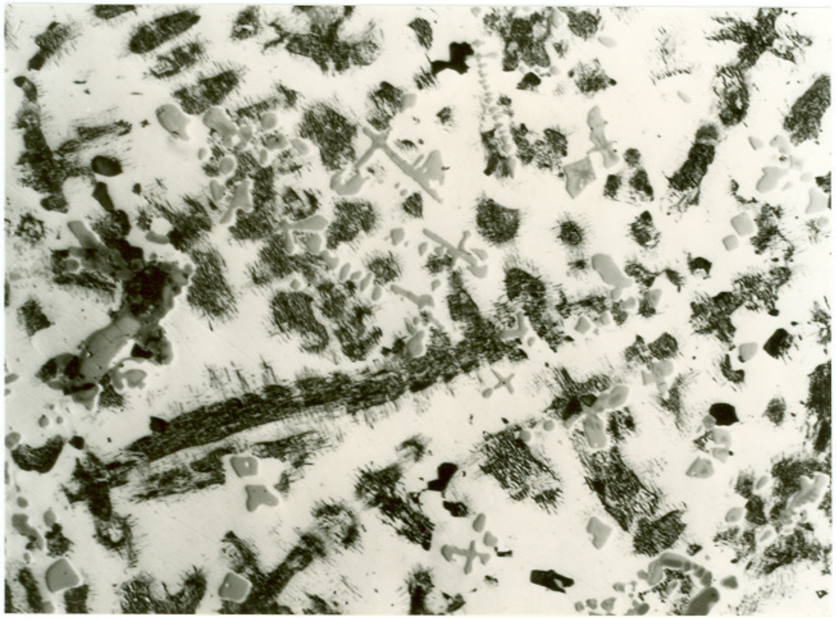

Figure 59. Ti-Co-C (25-65-10 At.%), Arc Melted Sample Heat Treated at 900°C for 240 hours. Bivariantly Solidified Monocarbide and Co Dendrites (Dark Phase). Dendrites Heavily Precipitated with $TiCo_3$ Plus Coarse Co Precipitates in $TiCo_3$ Matrix. X-ray Analysis: TiC (a = 4.324Å), $TiCo_3$ (a = 3.602Å); Co(a = 3.570Å).

alloys located to the Co-rich side of the monocarbide-cobalt join consistently melted at a slightly higher temperature (1236° + 5°C) than the indicated 1220°C isotherm. Since this temperature section lies close to the solidus temperature of ternary alloys within the composition region monocarbide-cobalt-graphite, the 1236°C eutectic plane is depicted in Figure 52. This reaction may be represented by the following equation

$$L \underset{>1236^\circ C}{\overset{<1236^\circ C}{\rightleftarrows}} TiC_{1-x} + Co + C,$$

with an invariant liquid composition of approximately Ti(4)-Co(83)-C(13) At.%.

Three melting troughs associated with the liquidus vertices of the three-phase equilibria L + Co + C, L + Co + TiC_{1-x}, and L + TiC_{1-x} + C originate at the 1236°C reaction plane. With increasing temperature, the first liquidus vertex traces back to the cobalt-carbon binary and terminates at the 1318°C eutectic point; the second merges with another three-phase equilibrium of the type L + Co + TiC_{1-x}, which originates at the 1220°C class II reaction plane, to form a pseudobinary eutectic at 1372° ± 10°C. The third liquidus vertex terminates at the TiC-C binary eutectic of 2776°C. Photomicrographs of melted and quenched alloys within the TiC-Co-C composition triangle are presented in Figures 60-62.

Besides the TiC_{1-x} + Co pseudobinary eutectic isotherm at 1372°C, an additional reaction of this type occurs at a temperature of 1293° ± 15°C between TiC_{1-x} and the intermetallic phase TiCo. The melting behavior of alloys located on or slightly off these pseudobinary sections are presented in Figures 63 and 64, and the location of the critical tie lines are shown in Figures 7 and 53. Typical photomicrographs of alloys from the concentration regions TiC_{1-x} + TiCo and TiC_{1-x} + Co are presented in Figures 65-67.

Eremenko(65) investigated ternary alloys along the join $TiC_{1.0}$-Co and reported the following eutectic temperature and composition of 1360° ± 10°C and ~11 mole % TiC. These results are in agreement with the present investigation (Figure 64) except for the fact that the critical tie line intersects the binary Ti-Co system at ~97 At.% Co and the binary Ti-C system at ~53 At.% Ti. The metallographic examination of melted alloys along the join $TiC_{1.0}$-Co consistently revealed the presence of trace amounts of free graphite (Figure 67). The slightly lower average eutectic temperature reported by Eremenko results from the bivariantly melting alloys between $TiC_{1.0}$ and Co as evidenced by the data presented in the isopleth at 10 At.% carbon (Figure 8).

The results of the experimental studies were used to construct a number of isothermal sections, Figures 68(a)-68(f), in order to depict more clearly the distribution of phases in the ternary system. These isothermal sections are supplemented by the information previously presented in the summary (Figures 5-8).

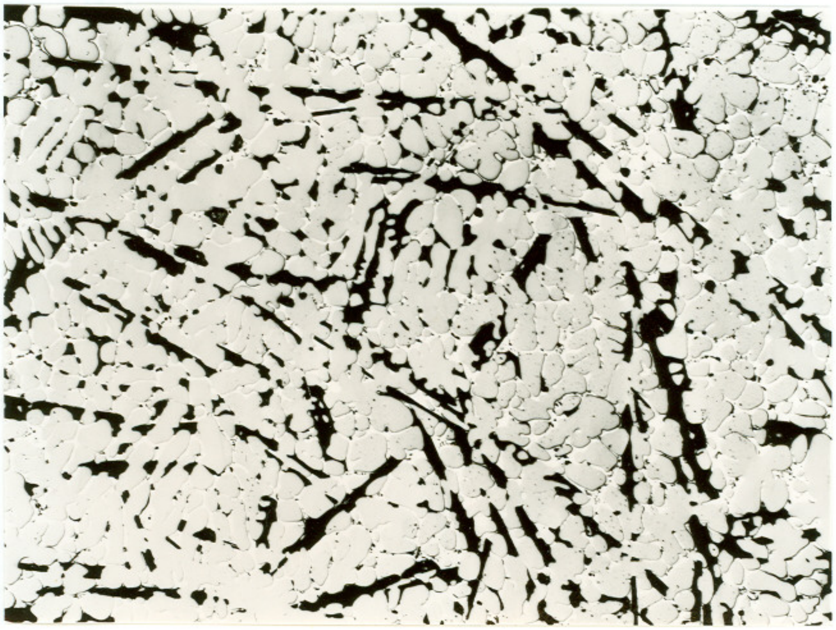

Figure 60. Ti-Co-C (35-15-50 At.%), Arc Melted Sample. Bivariantly Solidified TiC + C Eutectic in Co Matrix.

Figure 61. Ti-Co-C (16-65-19 At.%), Arc Melted Sample. Primary Monocarbide in Matrix of Bivariantly Solidified Cobalt plus Fine Eutectic Structure of TiC + Co + C.

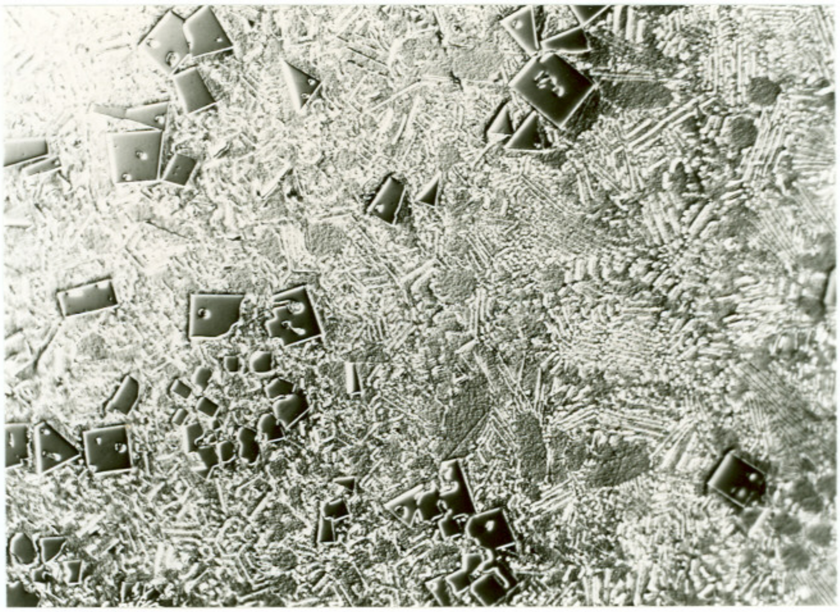

Figure 62. Ti-Co-C (8-82-10 At.%), Arc Melted Sample. Primary Monocarbide and Cobalt (Light Gray Regions Divorced of Eutectic) in Ternary Eutectic Matrix.

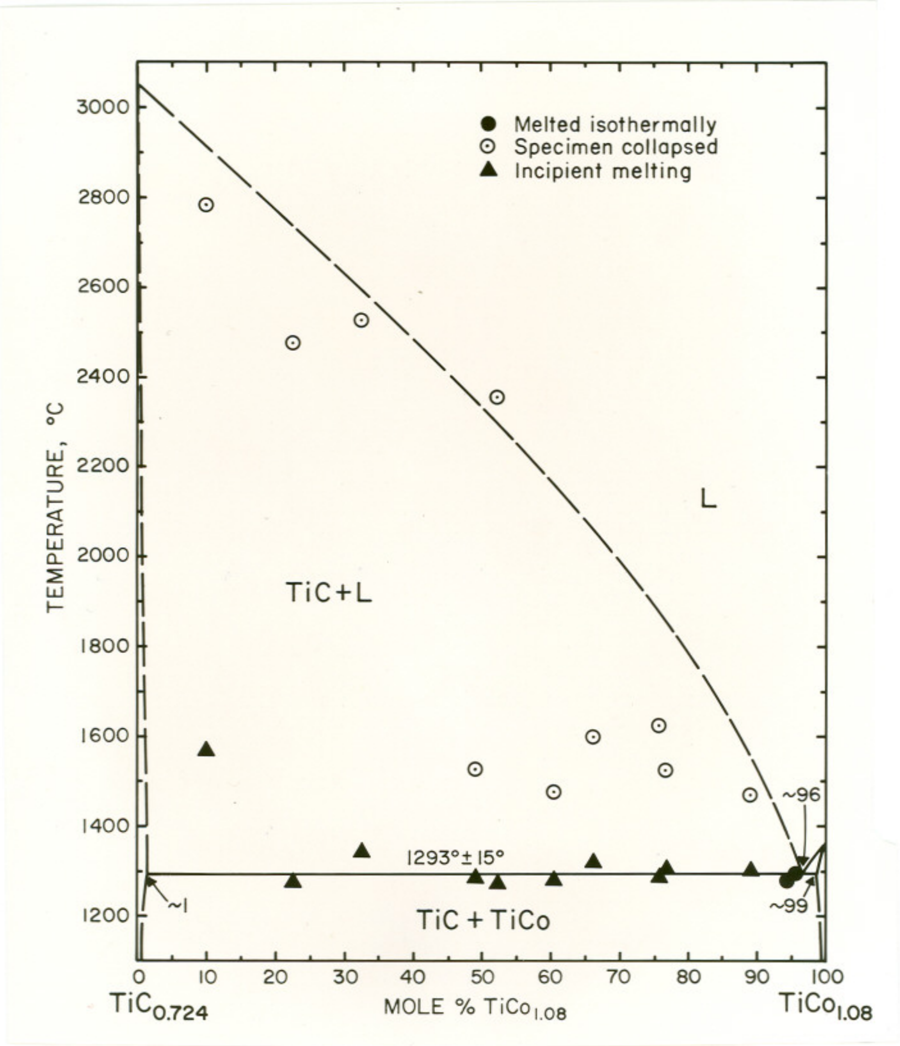

Figure 63. Melting Temperatures of Ternary Alloys Located Along the Pseudobinary Section $(Ti_{0.58}C_{0.42})$-$(Ti_{0.48}Co_{0.52})$.

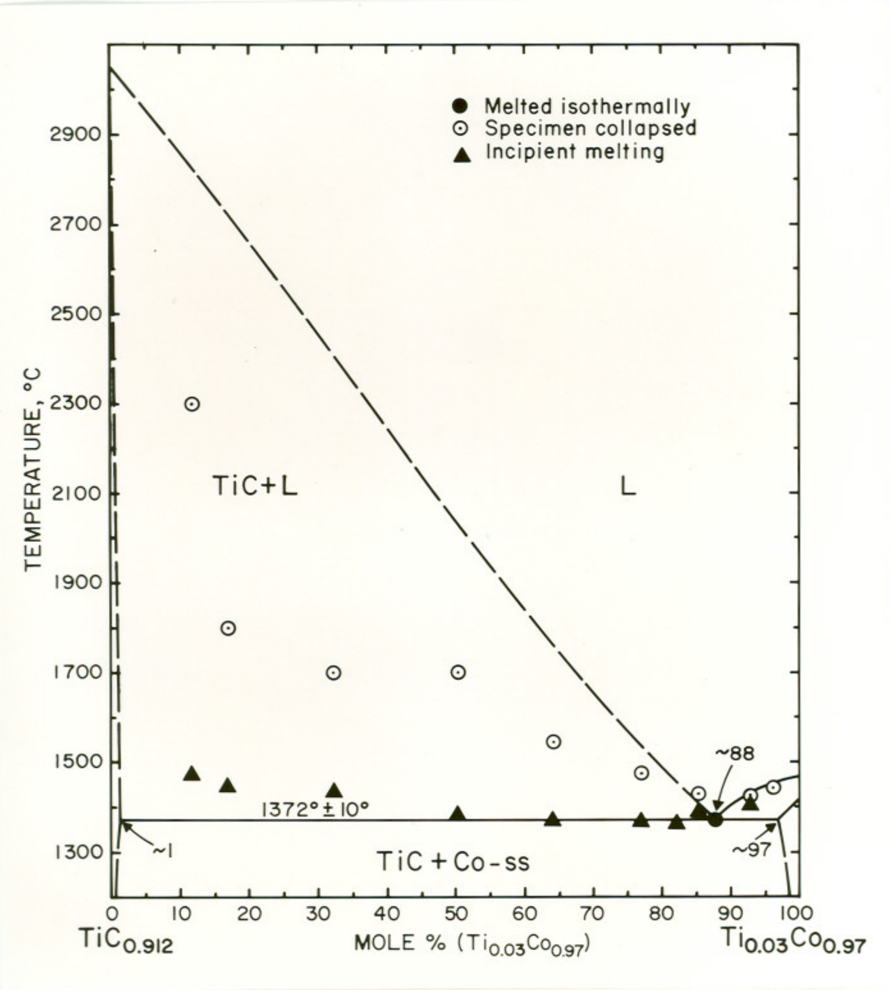

Figure 64. Melting Temperatures of Ternary Alloys Located Along the Pseudobinary Section ($Ti_{0.523}C_{0.477}$)-($Ti_{0.03}Co_{0.97}$)

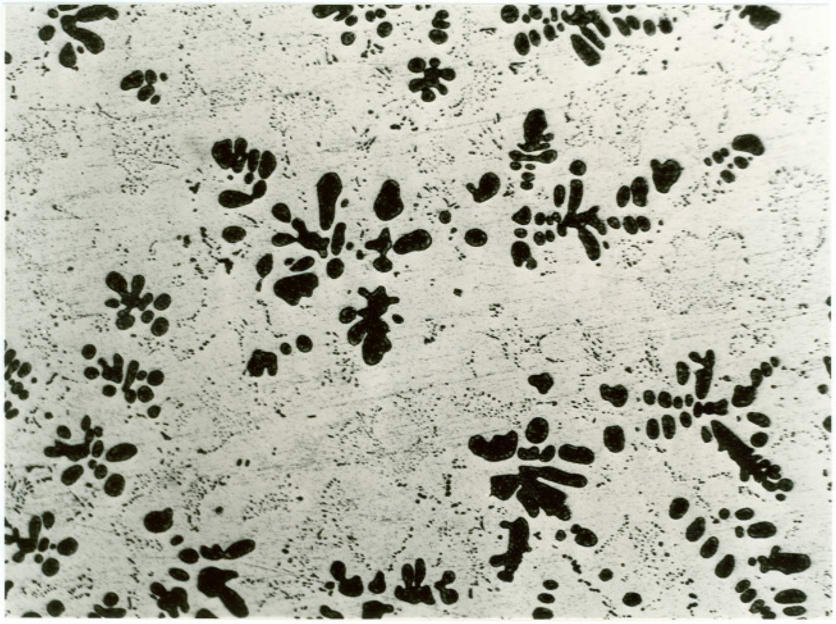

Figure 65. Ti-Co-C (51-44-5 At.%), Arc Melted Sample Heat Treated at 900°C. Primary Monocarbide, TiCo Matrix. Fine TiC + TiCo Eutectic Structure Slightly Annealed. X-ray Analysis: TiC_{1-x} (a= 4.318Å); TiCo (a = 2.990Å).

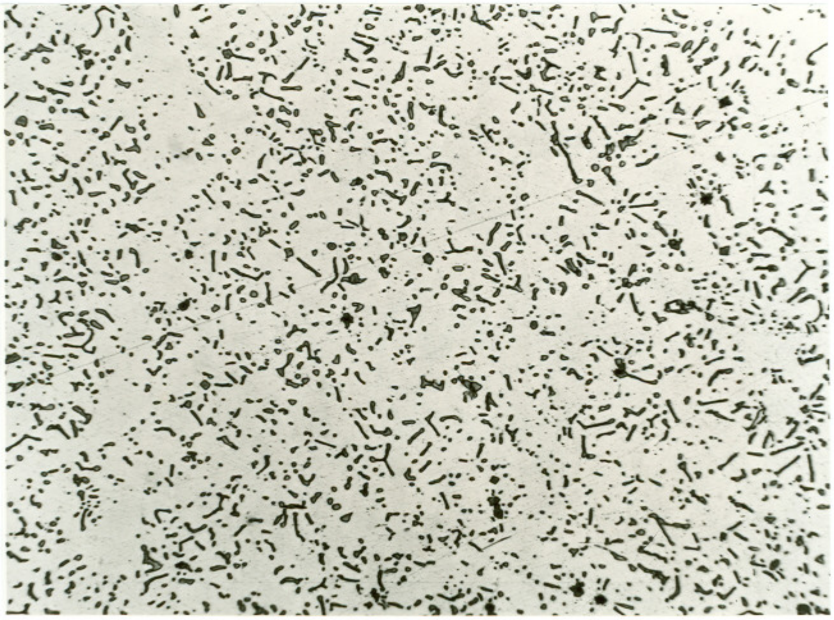

Figure 66. Ti-Co-C (10-85-5 At.%), Arc Melted Sample Heat Treated at 900°C. Trace of Bivariantly Solidified Monocarbide plus Cobalt in Annealed Eutectic Matrix of TiC + Co. X-Ray Analysis: TiC_{1-x} (a = 4.326Å); Co (a = 3.551Å).

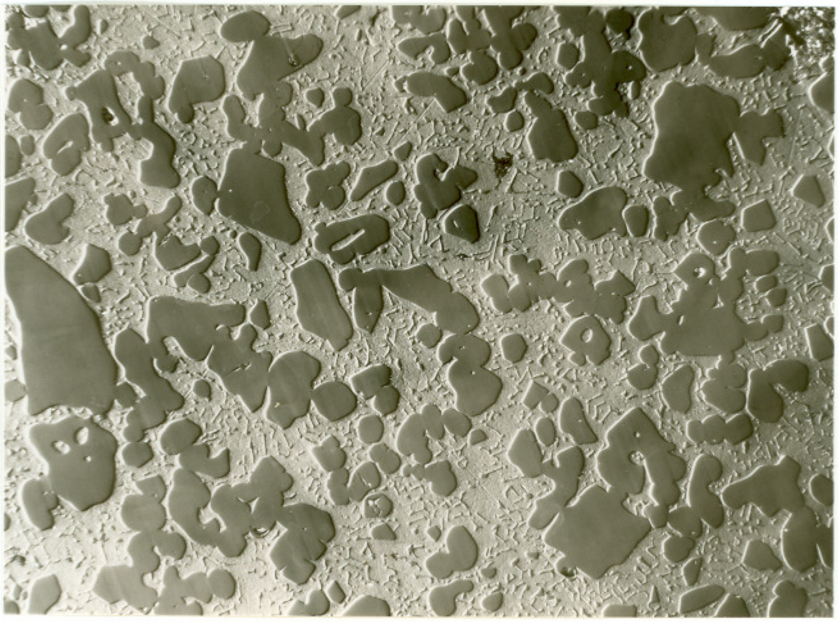

Figure 67. Ti-Co-C (29.8-40.4-29.8 At.%), Arc Melted Sample. Primary Monocarbide in Pseudobinary Eutectic Matrix Containing Trace of Free Graphite.

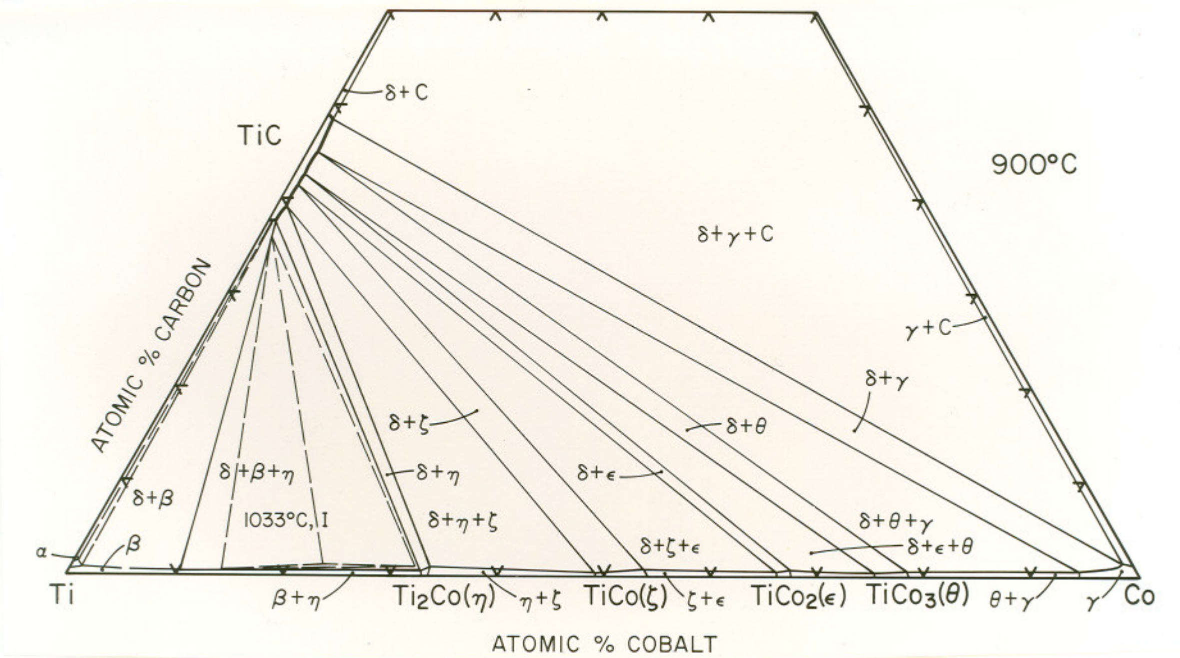

Figure 68(a). Isothermal Section at 900° C. Location of Class I Four-Phase Reaction Plane at 1033° ± 5° C.

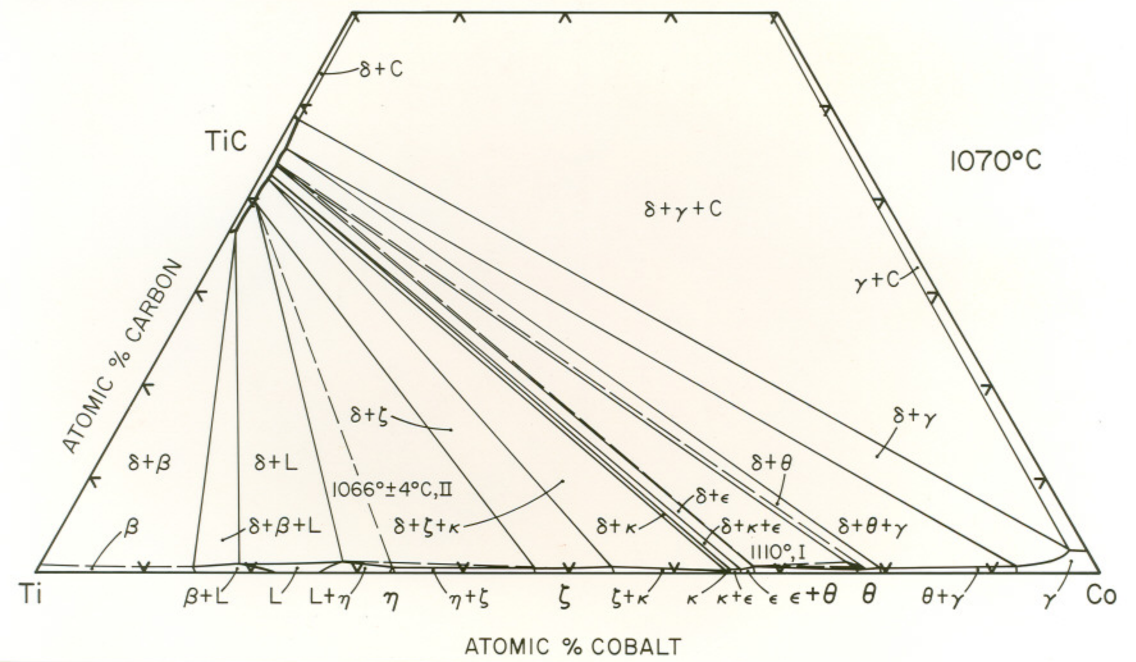

Figure 68(b). Isothermal Section at 1070° C. Location of Class I Four Phase Reaction Plane at 1110° ± 5° C.

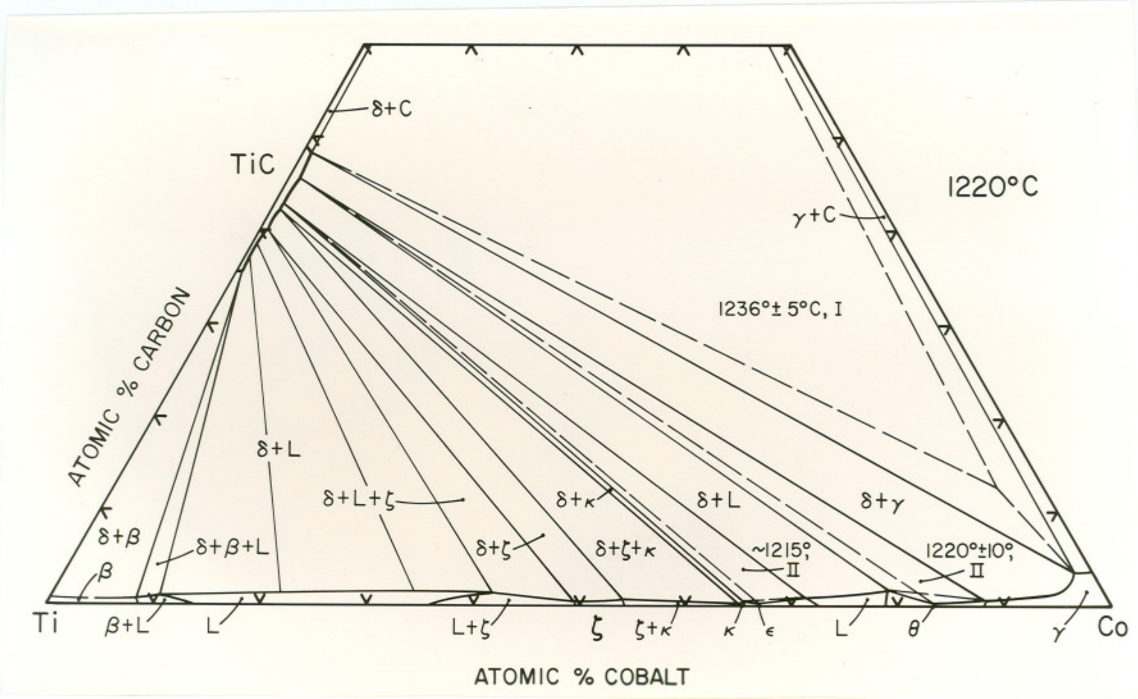

Figure 68(c). Isothermal Section at ~1220°C.

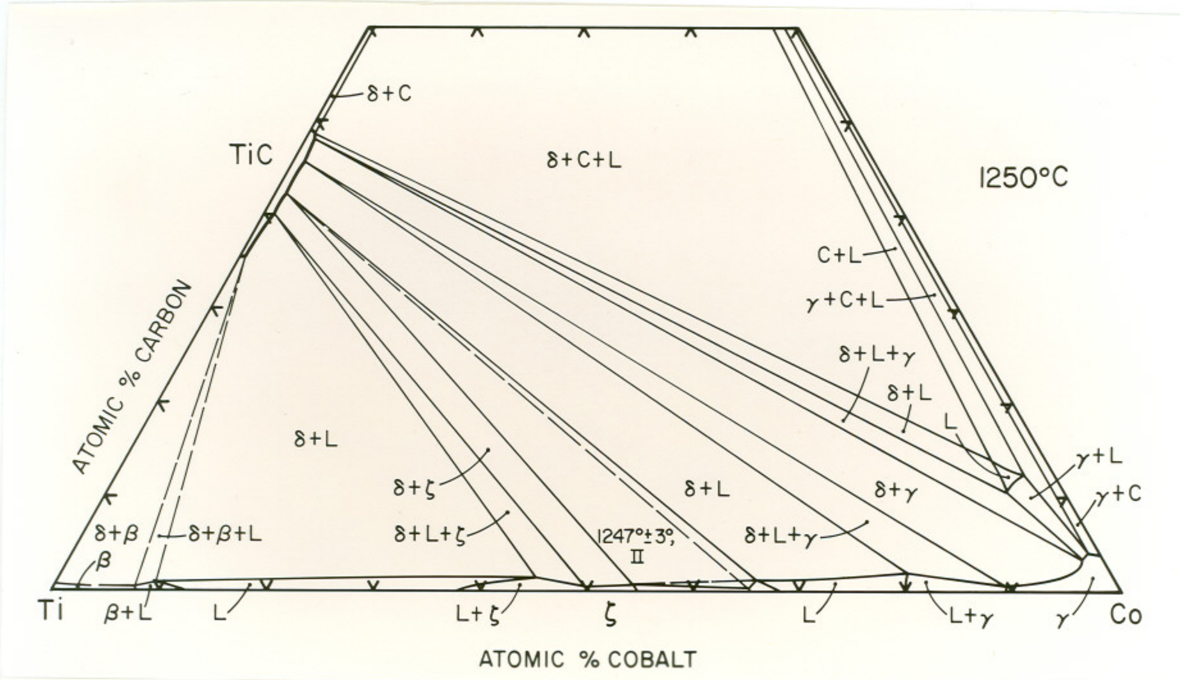

Figure 68(d). Isothermal Section at 1250°C.

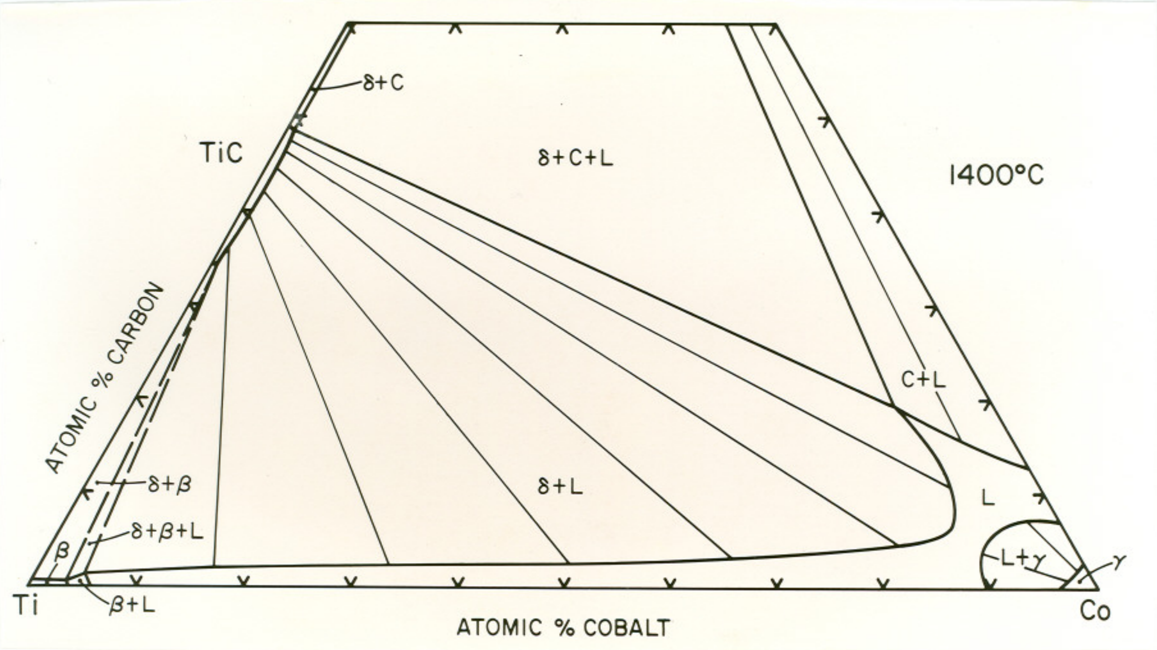

Figure 68(e). Isothermal Section at 1400°C.

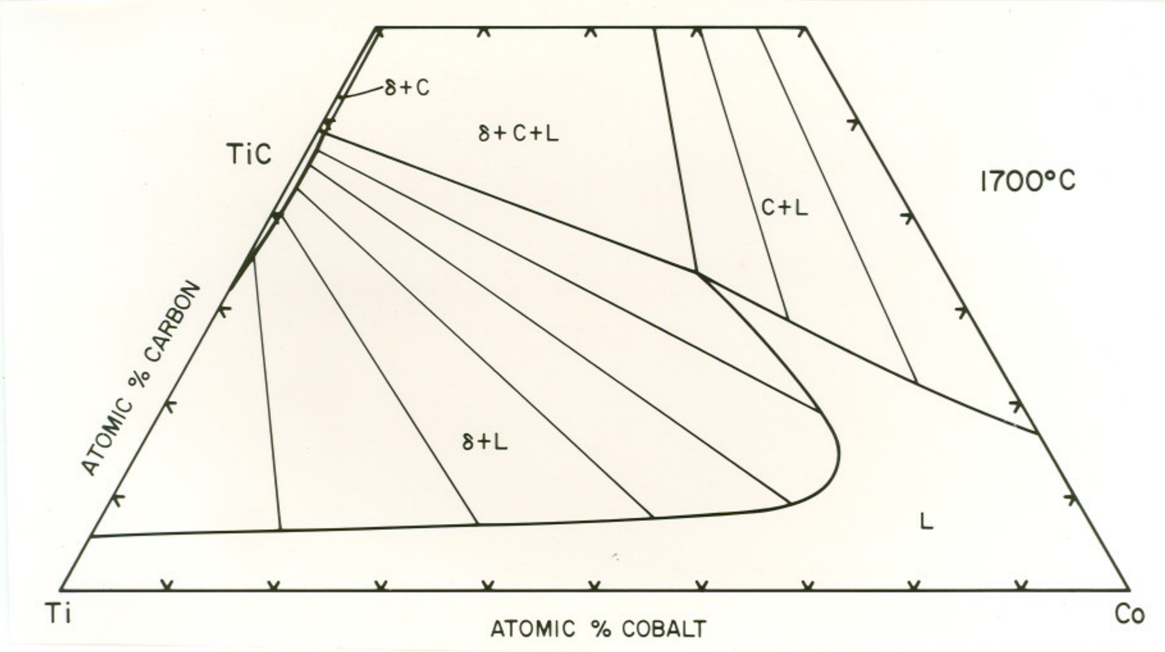

Figure 68(f). Isothermal Section at 1700°C.

3. The Ti-Ni-C System

a. Ti-Ni System

The constitution diagram of the titanium-nickel system established in this investigation is similar to the one recently published by Hawkins(4). Only slight differences in invariant reaction temperatures and coexisting phase compositions were observed. Depicted in Figure 69 are the measured solidus temperatures of binary alloys plus the solid state phase evaluation of alloys equilibrated at 900° and 1070°C.

The melting behavior of alloys located close to or at the stoichiometric compositions corresponding to the phases TiNi and $TiNi_3$ indicated that both melt congruently at temperatures of 1305° ± 8°C and 1385° ± 12°C, respectively. A eutectic equilibrium is formed between TiNi and $TiNi_3$ at 1133° ± 15°C; this reaction temperature is slightly higher than those reported in the available literature(4,21,25). Presented in Figures 70 and 71 are photomicrographs of melted alloys exhibiting the primary end member phases of TiNi and $TiNi_3$ associated with the 1133°C eutectic reaction; Figure 72 of a slightly hypereutectic alloy exhibits the characteristic TiNi matrix-type eutectic structure.

At 900° and 1070°C, the hexagonal (DO_{24}-type) $TiNi_3$ phase exhibits a very narrow homogeneity range. On the average and independent of the alloys composition, lattice parameters of $a = 5.099_0$Å; $c = 8.309_1$Å were measured. For arc melted and quenched

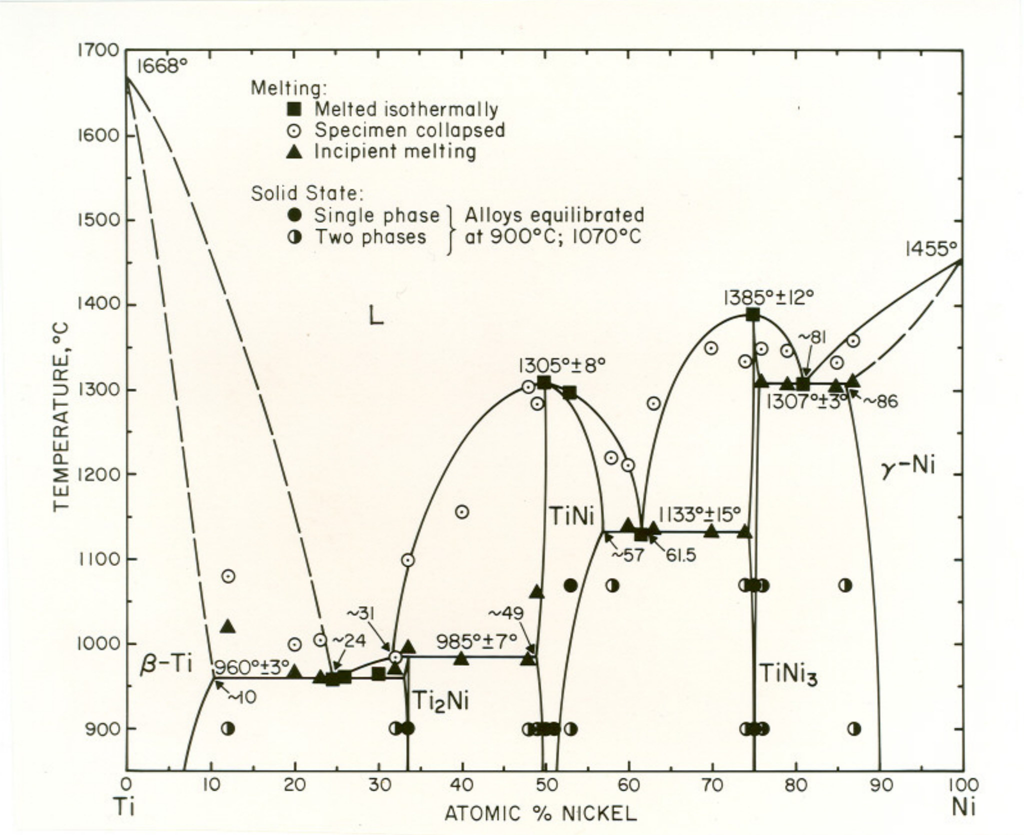

Figure 69. Titanium-Nickel Constitution Diagram. Experimental Melting Temperatures and Qualitative Phase Evaluation of Ti-Ni Alloys.

(Melting temperatures for Ti and Ni obtained from References (6)and (4), respectively.)

alloys, the phase exhibits a slight range of homogeneity as evidenced by its lattice parameter variation from a = 5.108_3Å; c = 8.318_3Å (excess-titanium alloys) to a = 5.097_8; c = 8.301_3Å (excess-nickel alloys). In contrast, the cubic (B2-type) TiNi phase was found to exhibit a noticeable range of homogeneity at all subsolidus temperatures, extending from approximately 49 At.% Ni (a = 3.019Å) to 52 At.% Ni (a = 2.989Å) at 900°C.

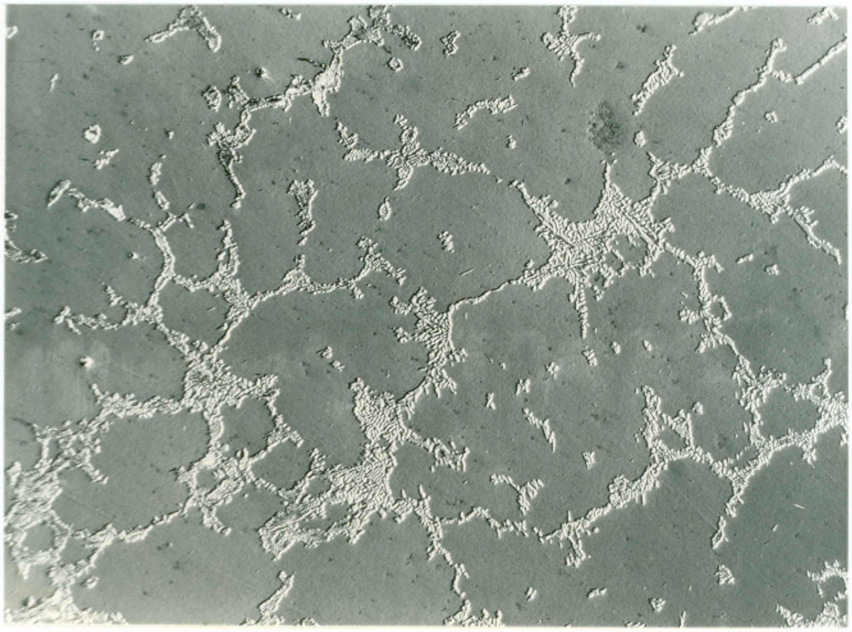

Figure 70. Ti-Ni (42-58 At.%), Melting Point Sample Quenched From 1219°C. Primary TiNi (Dark Phase) plus Intergranular TiN[illegible] + $TiNi_3$ Eutectic.

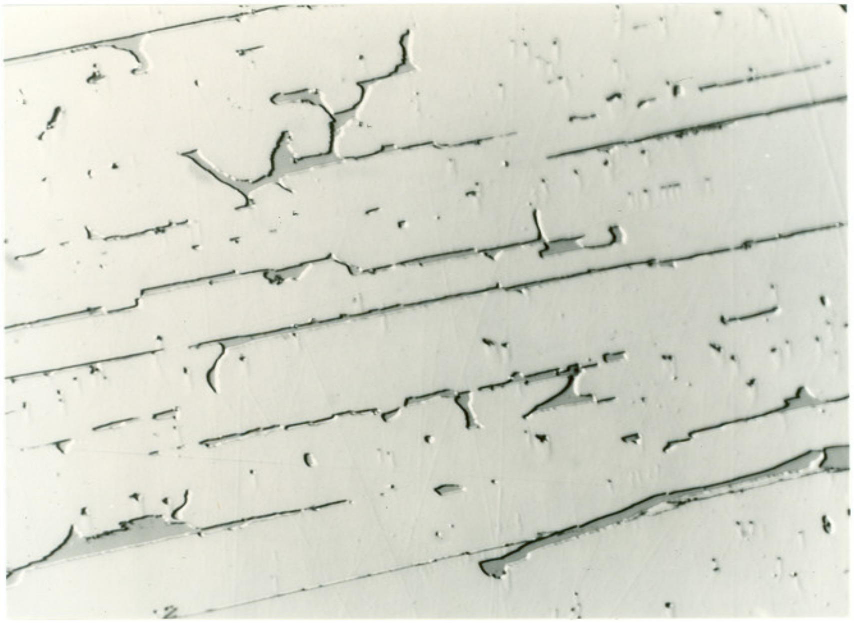

Figure 71. Ti-Ni (26-74 At.%), Arc Melted Sample. Primary $TiNi_3$ in TiNi-Matrix Divorced of Eutectic $TiNi_3$.

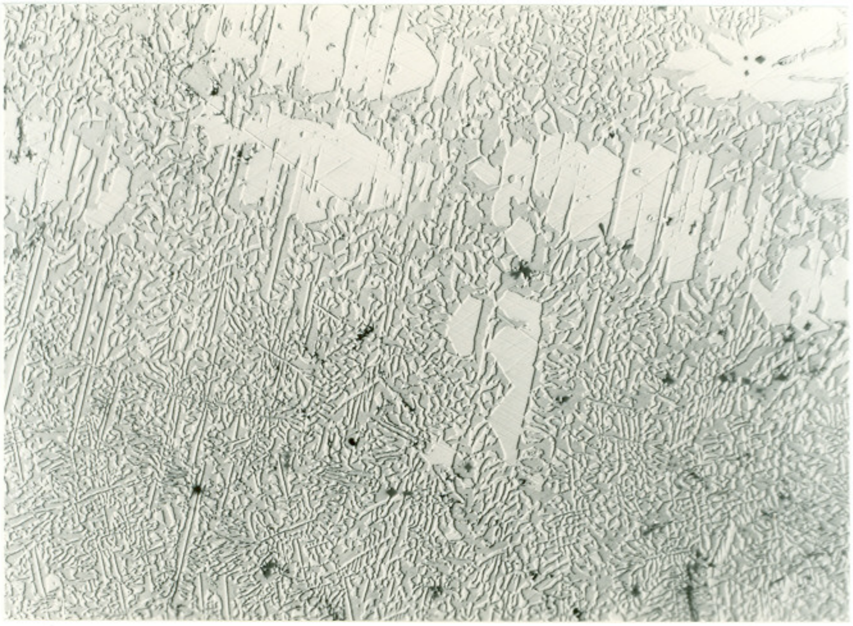

Figure 72. Ti-Ni (37-63 At.%), Arc Melted Sample. Trace of Primary $TiNi_3$ in TiNi Matrix-Type Eutectic.

The only additional intermetallic phase present in this system is the cubic ($E9_3$-type)Ti_2Ni. Independent of composition, an average lattice parameter of $a = 11.324_6$Å was measured. From the melting behavior of alloys containing this phase, eutectic and peritectic reaction temperatures of 960° ± 3°C and 985° ± 7°C, respectively, were obtained (Figure 69).

To the Ni-rich side of the $TiNi_3$ phase, two-phase $TiNi_3$ + Ni alloys melted eutectically at a temperature of 1307° ± 3°C. This reaction temperature agrees with the value of 1306°C reported by Poole and Hume-Rothery(25), but the invariant point of approximately

81 At.% Ni established in this investigation corresponds to the value of 80.8 At.% Ni reported by Margolin et al.(21). Poole and Hume-Rothery(25) placed the invariant point at 85 At.% Ni, a composition close to the maximum titanium solubility in nickel at the eutectic isotherm. A photomicrograph of a melted alloy which participated in the 1307°C eutectic reaction is presented in Figure 73. Figure 74 exhibits the oriented $TiNi_3$ precipitation structure which results from the temperature dependent solvus curve of the Ni solid solution phase. This particular precipitation structure could be interpreted as a eutectic-type.

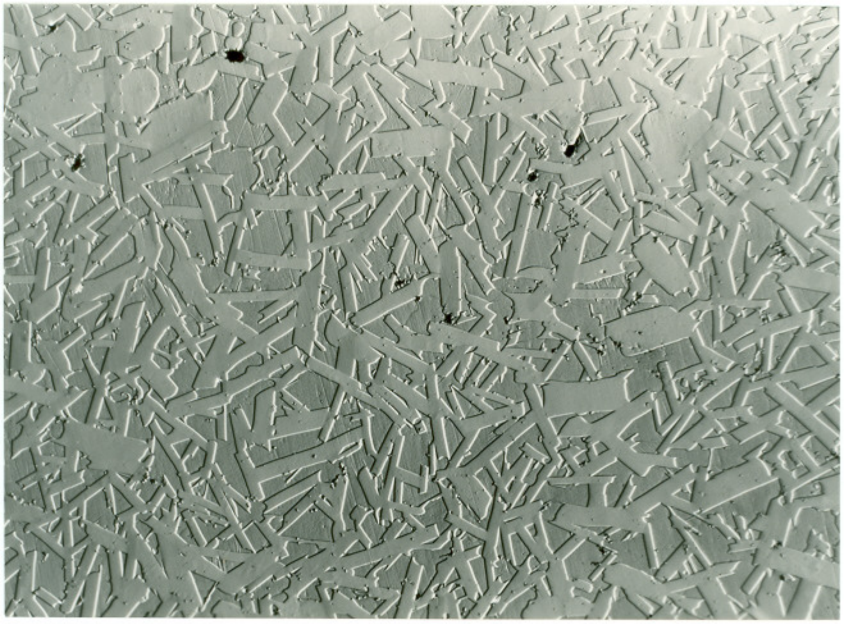

Figure 73. Ti-Ni (20-80 At.%), Melting Point Sample Quenched from 1333°C. Relatively Coarse $TiNi_3$ + Ni Eutectic. Trace of Primary $TiNi_3$ (Blocky Phase). Porosity Dark.

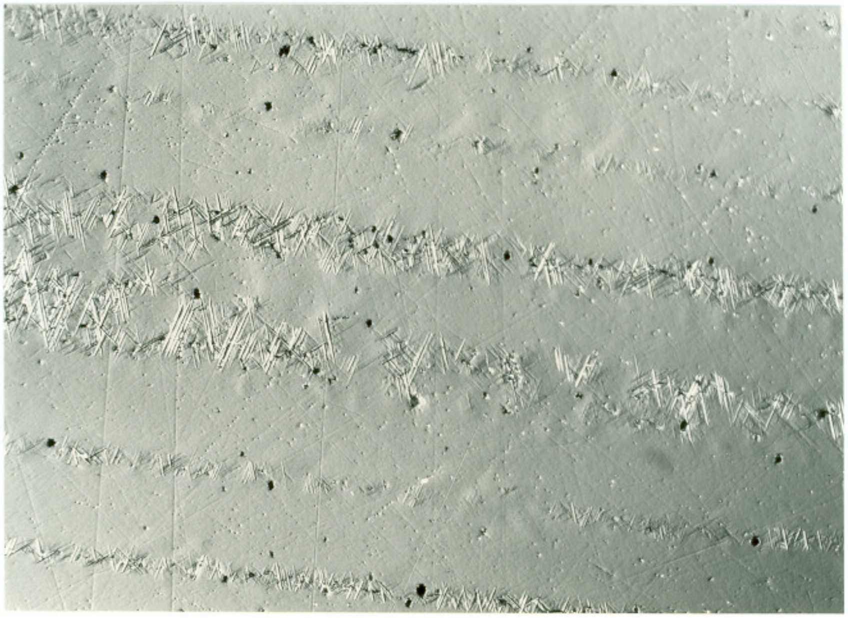

(a) X500

(b) X500

Figure 74. Ti-Ni (14-86 At.%), Arc Melted Sample

(a) Primary Nickel Solid Solution Dendrites plus Fine, Oriented Interdendritic $TiNi_3$ of Eutectic and Solid State Origin.

(b) Same Sample Heat Treated at 900°C for 240 hours. $TiNi_3$ Precipitates in Ni Matrix. Trace of Coarse Eutectic $TiNi_3$. X-ray Analysis: Ni (a=3.561Å); $TiNi_3$(a=5.099Å; c=8.309Å).

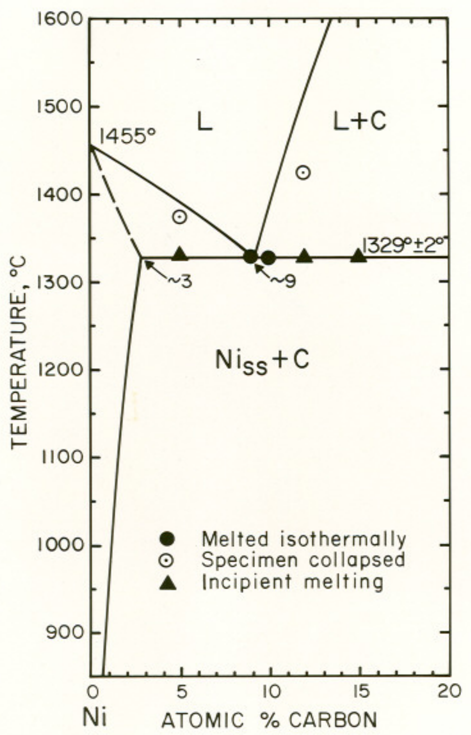

Figure 75. Nickel-Carbon Constitution Diagram. Experimental Melting Temperatures. (Melting Temperature of Ni and Solvus, Liquidus Curves Obtained from References 4,51, and 53).

b. Ni-C System

The results of this investigation to determine the melting temperature and composition of the nickel-graphite eutectic are depicted in Figure 75. From the melting point and metallographic analyses, the invariant temperature and composition were placed at 1329 ± 2°C and approximately 9 At.% carbon, respectively. This Eutectic temperature is slightly higher than values reported in the available literature (50,52,54,55).

Metallographic studies conducted with arc melted alloys as well as the melted portions of melting point samples revealed structures containing agglomerated or spheroidal graphite at both hypo- and hypereutectic compositions (Figures 76 and 77). The occurrence of the spheroidal graphite seems to be related to the amount of superheat and quenching rate experienced by eutectic melting alloys. As evidenced by photomicrographs 76-79, alloys which were quenched ($\geq$ 300°C/min) from temperatures above the 1329°C eutectic isotherm invariably exhibited a greater amount of spheroidal graphite when compared to alloys which were cooled from incipient melting temperatures. This striking difference in phase morphology is demonstrated by a comparison of Figure 78(a) and 78(b).

A plausible explanation for these observations is that a more homogeneous liquid phase results when superheating alloys above their eutectic isotherm, and hence fewer nucleation sites are present for the graphite phase. When the alloys cool through the eutectic temperature, a certain amount of undercooling is required for the nucleation and growth of stable graphite nuclei. Since no differential thermal analysis was conducted, the effect of different melting conditions on the absence or presence of undercooling could not be followed and correlated with the metallographic results.

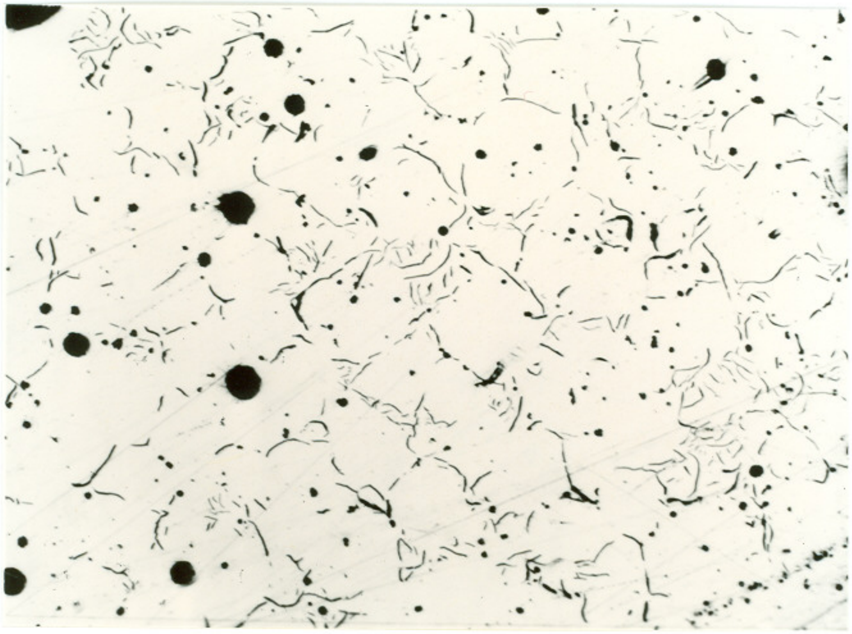

Figure 76. Ni-C (95-5 At.%), Melting Point Sample Quenched from 1370°C. Primary Nickel in a Eutectic Matrix plus Spherulites of Graphite.

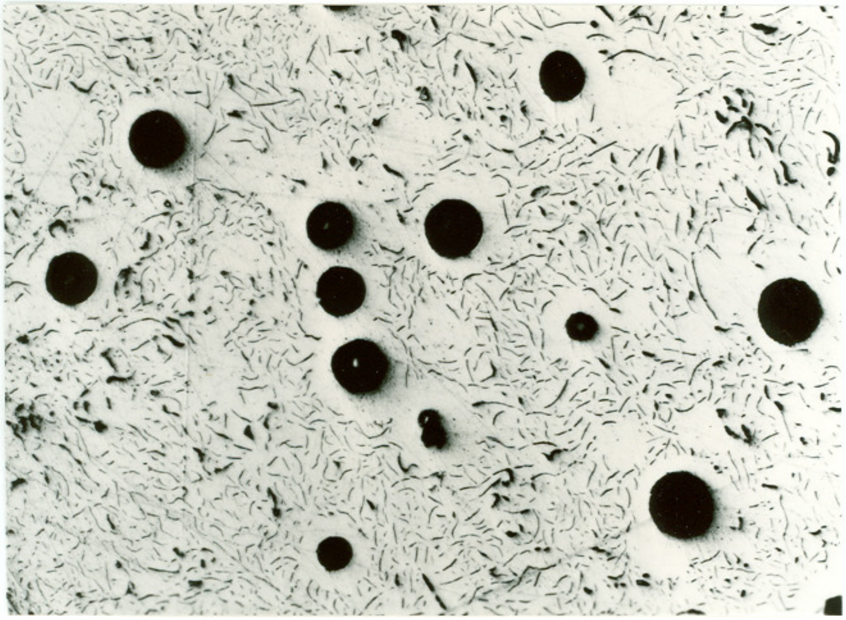

Figure 77. Ni-C (88-12 At.%), Melting Point Sample Quenched from 1430°C. Spheroidal Graphite in Eutectic Matrix plus Metal-Rich Regions Divorced of Eutectic Graphite.

(a) X270

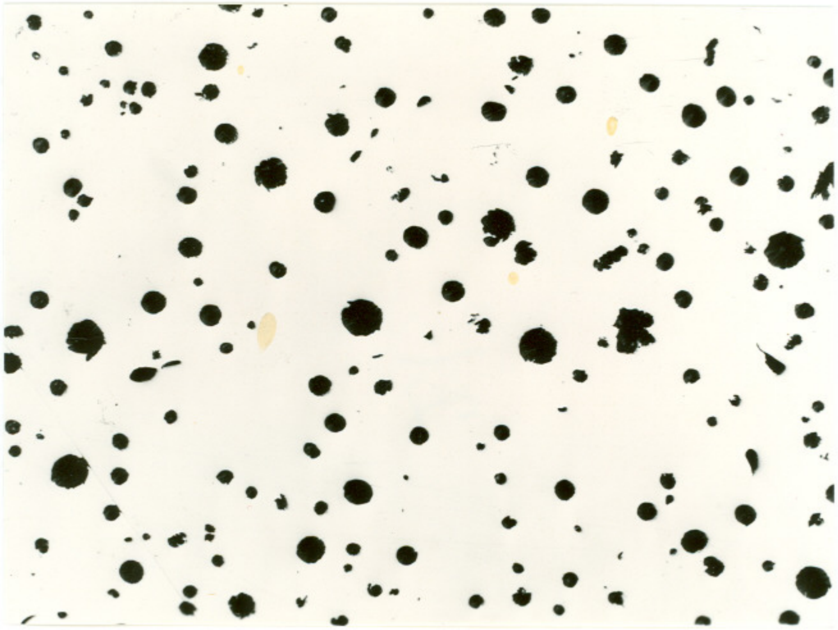

(b) X200

Figure 78. Ni-C (91-9 At.%), Melting Point Sample.

(a) Sample Quenched from Incipient Melting Temperature of 1330°C. Metal Matrix Type Eutectic Structure plus Trace of Spheroidal Graphite.

(b) Same Sample but Arc Melted. Graphite Spherulites in Nickel Matrix Divorced of Eutectic Graphite.

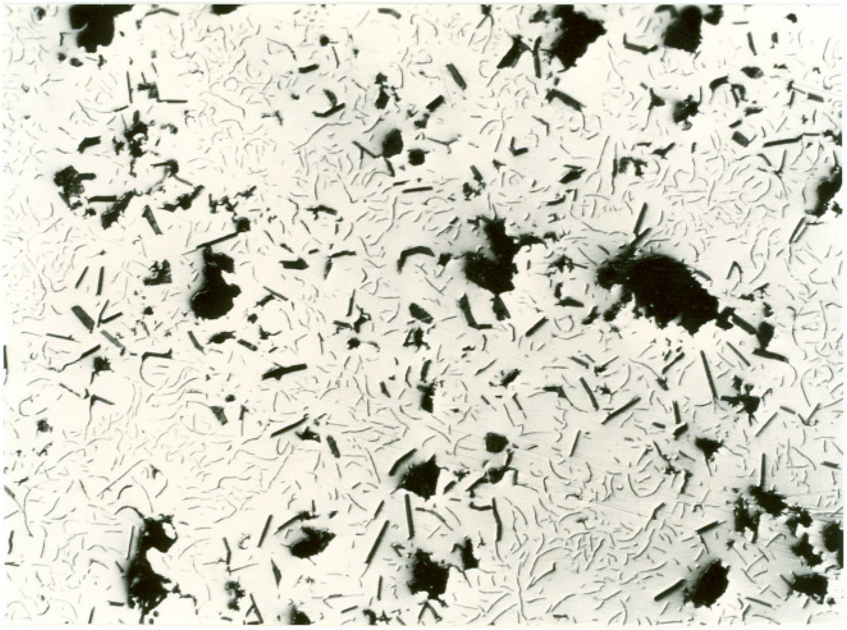

Figure 79. Ni-C (85-15 At.%), Melting Point Sample Quenched from Incipient Melting Temperature of 1329°C. Primary Graphite, Flakes and Agglomerates, in Eutectic Matrix.

c. Ternary System

Qualitative phase evaluation of binary Ti-Ni and ternary Ti-Ni-C alloys equilibrated at 900° and 1070°C resulted in the phase relationships presented in Figures 80 and 81. The principal phase relationships do not vary appreciably, except for the appearance of a liquid phase in Ti-rich alloys at the higher temperature section. Also, since both temperature sections lie close to the solidus temperature of certain ternary alloys, the measured terminal compositions of the solid phases closely correspond to compositions entering reactions with a liquid phase.

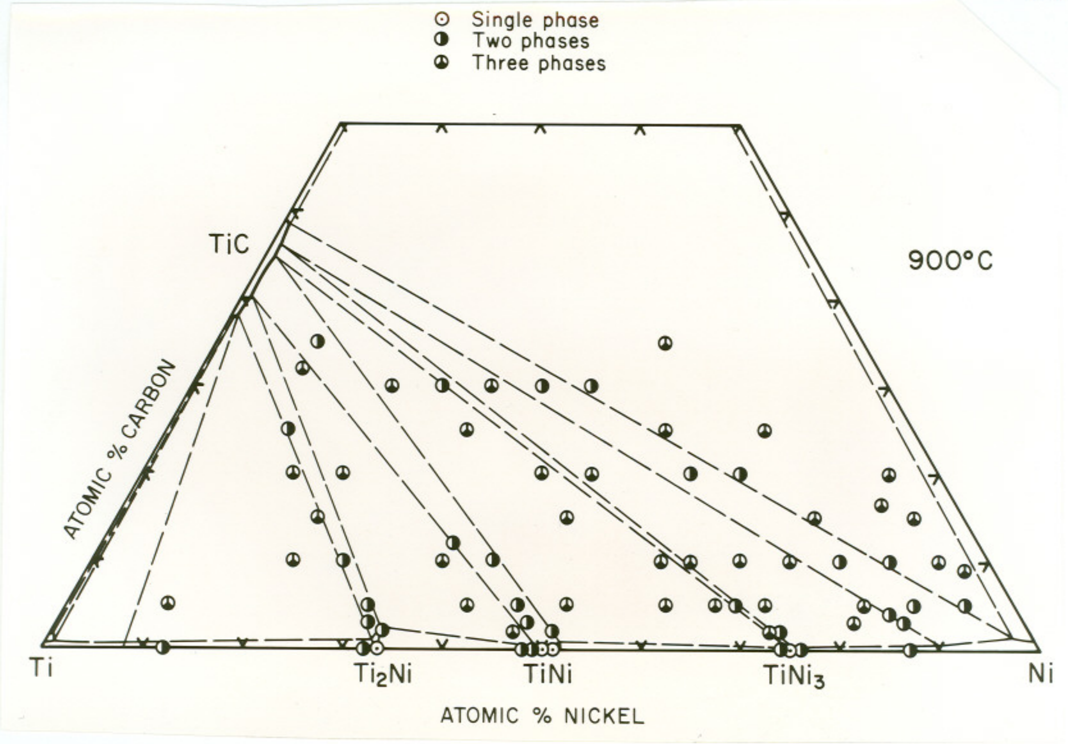

Figure 80. Qualitative Phase Evaluation of Ti-Ni-C Alloys Equilibrated at 900°C.

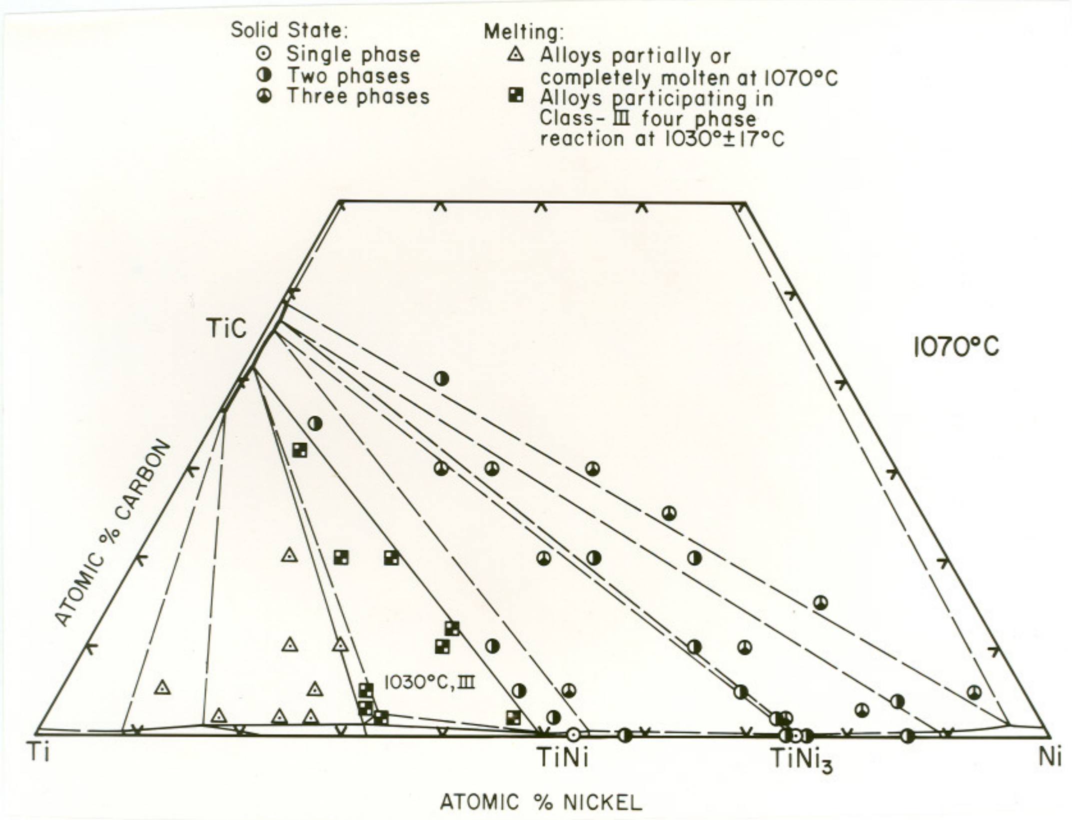

Figure 81. Qualitative Phase Evaluation and Melting Behavior of Ti-Ni-C Alloys at 1070°C.

The phase relationships depicted in the 900°C isothermal section (Figure 80) agree with the 870°C section proposed by Stover and Wulff(68). The Ti-rich liquid phase referred to above originates at a temperature of 953° ± 8°C from the following ternary eutectic reaction

$$L \quad \overset{<953^\circ C}{\underset{>953^\circ C}{\rightleftharpoons}} \quad TiC_{1-x} + \beta\text{-}Ti + Ti_2Ni.$$

As determined from the melting point and metallographic analyses, Figures 12 and 102(a) show the location of the above reaction plane with a eutectic liquid composition of approximately Ti(74)-Ni(25)-C(1) At.%.

To the nickel-rich side of the two-phase equilibrium TiC_{1-x} (a ≃ 4.315Å) + Ti_2Ni (a = 11.344Å) at 900°C, $TiC_{1-x} + Ti_2Ni + TiNi$ three-phase alloys consistently melted at a higher temperature when compared to the 985°C peritectically melting Ti-Ni binary alloys (Figure 69). From the melting point analysis, a reaction temperature of 1030° ± 17°C was established and the proposed four-phase reaction corresponds to a class III-type (ternary peritectic)

$$L + TiC_{1-x} + TiNi \quad \overset{<1030^\circ C}{\underset{>1030^\circ C}{\rightleftharpoons}} \quad Ti_2Ni.$$

The location of this four-phase reaction plane is depicted in Figure 81. On the average, it is slightly lower than the 1050° ± 30°C peritectic-type reaction reported by Stover and Wulff(68).

Indirectly, the above 1030°C reaction temperature agrees with the results of the Margolin et al.(21) investigation of the Ti-Ni binary system. These investigators conducted their melting point determinations with arc melted binary alloys placed in graphite crucibles and reported that the "binary" Ti_2Ni phase melted peritectically at approximately 1015°C. In addition, Stover and Wulff(68) reported that the Ti_2Ni phase in ternary alloys annealed at 870°C had a lattice parameter of a = 11.343Å which is in agreement with the value of a = 11.344Å obtained in this investigation at 900°C. In fact, lattice parameter measurements on alloys quenched from 900°C yielded an average expansion of the cubic ($E9_3$-type) lattice from a = 11.324Å, for the binary phase, to 11.344Å for the carbon-saturated solid solution. For alloys quenched from liquidus temperatures, the measured parameter of the carbon-saturated phase (~3 At.% C, max.) was a = 11.375Å.

With increasing temperature, the three-phase equilibrium TiNi (a = 2.992 Å) + TiC_{1-x} (a = 4.326Å) + $TiNi_3$ (a = 5.106Å; c = 8.309Å) depicted at 1070°C (Figure 81) participates in a ternary eutectic at 1124° ± 9°C, Figures 12 and 102(b). This reaction with an invariant liquid composition of approximately Ti(40)-Ni(59)-C(1) At.% may be represented by the following relationship

$$L \overset{<1124^\circ C}{\underset{>1124^\circ C}{\rightleftharpoons}} TiC_{1-x} + TiNi + TiNi_3.$$

Typical photomicrographs of melted and quenched alloys exhibiting the eutectic-type structure associated with the above reaction are presented in Figures 82 and 83. The phase morphology exhibited is similar to the binary eutectic involving TiNi and $TiNi_3$ previously shown in Figure 72.

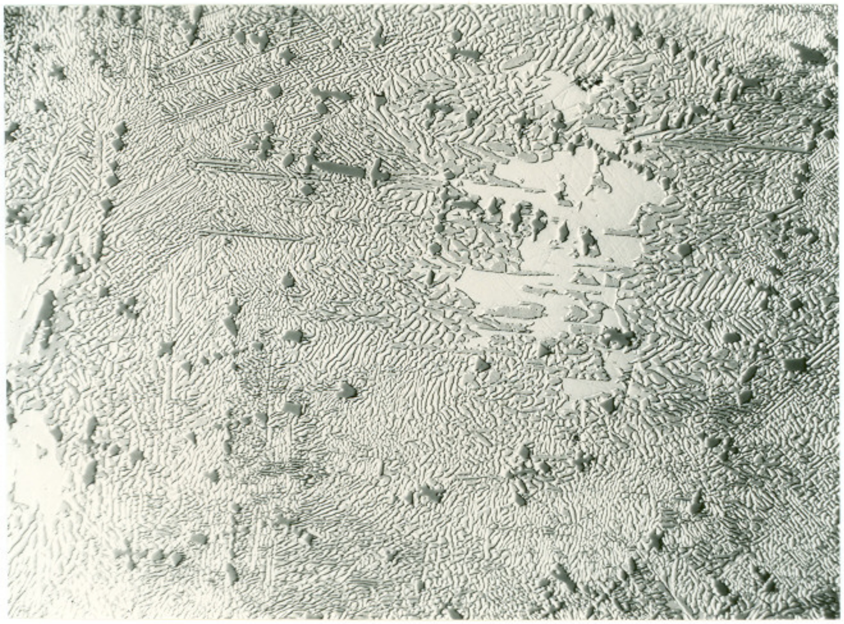
X400

Figure 82. Ti-Ni-C (39-59-2 At.%), Arc Melted Sample. Trace of Primary Monocarbide Dendrites in Eutectic Matrix. Light Regions Divorced of Eutectic $TiNi_3$ and Eutectic TiC_{1-x} Unresolved.

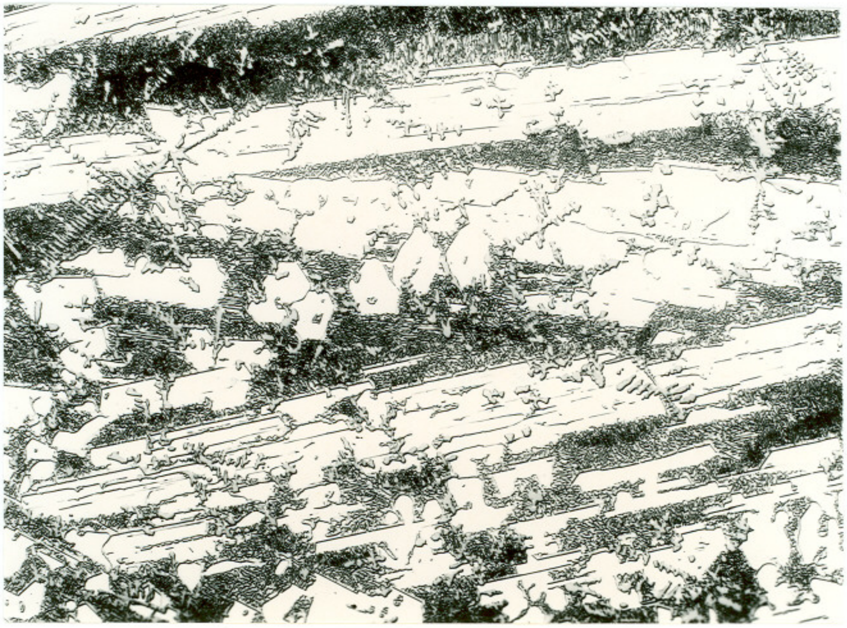

Figure 83. Ti-Ni-C (35-60-5 At.%), Arc Melted Sample. Bivariantly Solidified Monocarbide and $TiNi_3$ Dendrites in Ternary Eutectic Matrix of TiC (unresolved) + TiNi + $TiNi_3$.

Besides the 953° and 1124° C ternary eutectic reactions, two additional reactions of this type involving the three-phase equilibria $TiC_{1-x} + TiNi_3 + Ni$ and $TiC_{1-x} + Ni + C$ occur at 1272° C ± 13°C and 1277° ± 10° C, respectively (Figures 12 and 84). From the melting point and metallographic analyses, the following eutectic liquid compositions were approximated: Ti(20)-Ni(79)-C(1) At.% at 1272° C and Ti(5)-Ni(85)-C(10) At.% at 1277°C and Ti(5)-Ni(85)-C(10) At.% at 1277° C. Photomicrographs of alloys which participated in these reactions are presented in Figures 85-88. Except for the appearance of the titanium monocarbide phase, the above microstructures are similar to the corresponding binary phase morphologies associated with the equivalent binary eutectic reactions, e.g. compare Figures 85 and 86 with 73 and 74; 85 and 88 with 76 and 79. This similarity in structures is due to the low carbon solubility in Ni and $TiNi_3$.

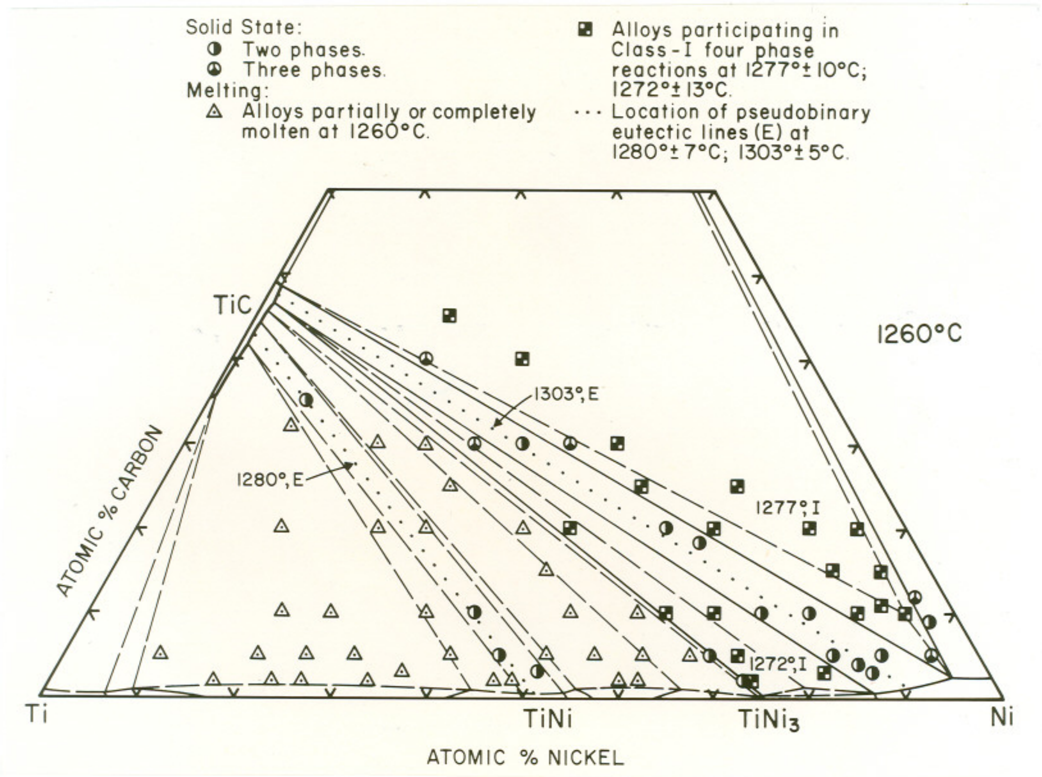

Figure 84. Qualitative Phase Evaluation and Melting Behavior of Ti-Ni-C Alloys at 1260°C.

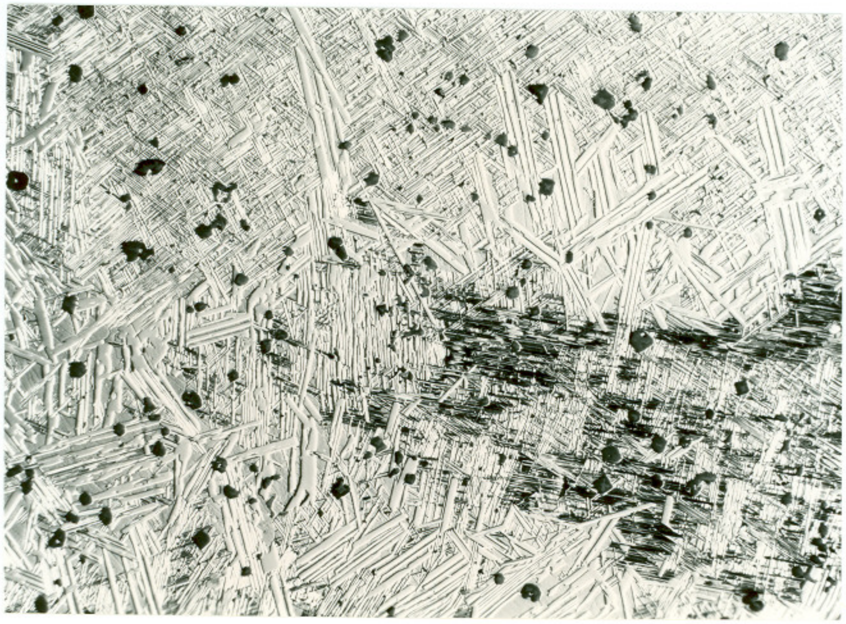

Figure 85. Ti-Ni-C (17-80-3 At.%) Arc Melted Sample Heat Treated at 900°C. Trace of Primary Monocarbide and Once Single-Phase Nickel Containing Fine $TiNi_3$. Precipitates in Eutectic of Ni(Matrix) + $TiNi_3$ (Coarse Needles) + TiC (Unresolved).

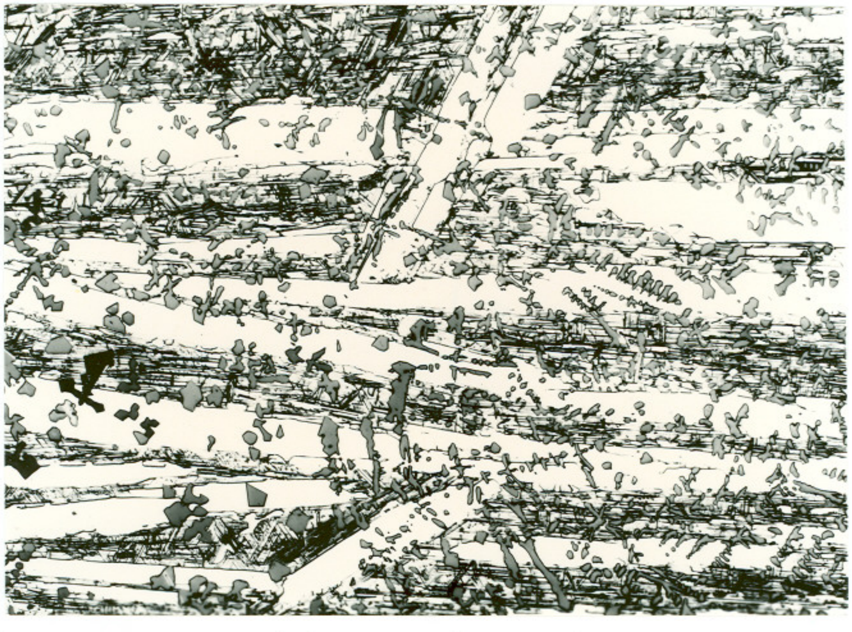

Figure 86. Ti-Ni-C (26-67-7 At.%), Arc Melted Sample. Primary Monocarbide Plus Secondary $TiNi_3$ Dendrites in Nickel Matrix Type Eutectic.

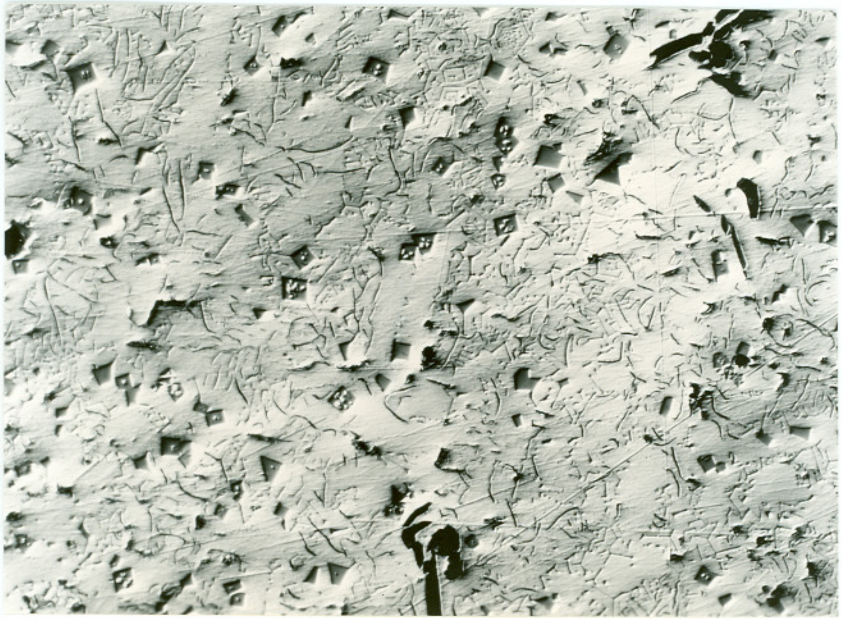

Figure 87. Ti-Ni-C (7-82-11 At.%), Melting Point Sample Quenched from 1292°C. Trace of Bivariantly Solidified Monocarbide and Nickel in TiC + Ni + C Eutectic. Slight Trace of Spheroidal and Flake Graphite.

Figure 88. Ti-Ni-C (3-85-12 At.%), Melting Point Sample Quenched from 1298°C. Trace of Coarse Primary Graphite plus Both Bivariantly and Invariantly Solidified Ni + C and TiC_{1-x} + Ni + C Eutectic.

As presented in Figure 84, melt formation to the carbon-rich side of the TiC-Ni join occurs first at the eutectic temperature of 1277°C. Three melting troughs associated with the liquidus vertices of the three-phase equilibria L + Ni + C, L + TiC_{1-x} + C, and L + Ni + TiC_{1-x} originate at this reaction plane. With increasing temperature, the first liquidus vertex advances towards the Ni-C binary and terminates at the 9 At.% C - 1329°C eutectic point; the second traces back to the Ti-C system and degenerates at the binary eutectic point of 63 At.% C-2776°C. Figure 88 exhibits the bivariantly solidified Ni + C eutectic structure; Figures 89 and 90 exhibit the bivariantly solidified TiC + C eutectic. With the exception of alloys located in the vicinity of the ternary eutectic point, solidification of alloys along the monocarbide + graphite eutectic trough is noticeably bivariant and the resulting microstructures are coarse.

The third liquidus vertex associated with the three-phase equilibrium L + Ni + TiC_{1-x} moves towards the TiC-Ni join with increasing temperature and merges with another three-phase equilibrium of this type to form a pseudobinary eutectic at 1303° ± 5°C. The location of the critical tie line-type reaction is depicted in Figure 84, the melting behavior of alloys along the pseudobinary section are presented in Figure 91, and typical microstructures of alloys from the concentration region TiC_{1-x} + Ni are shown in Figures 92-94.

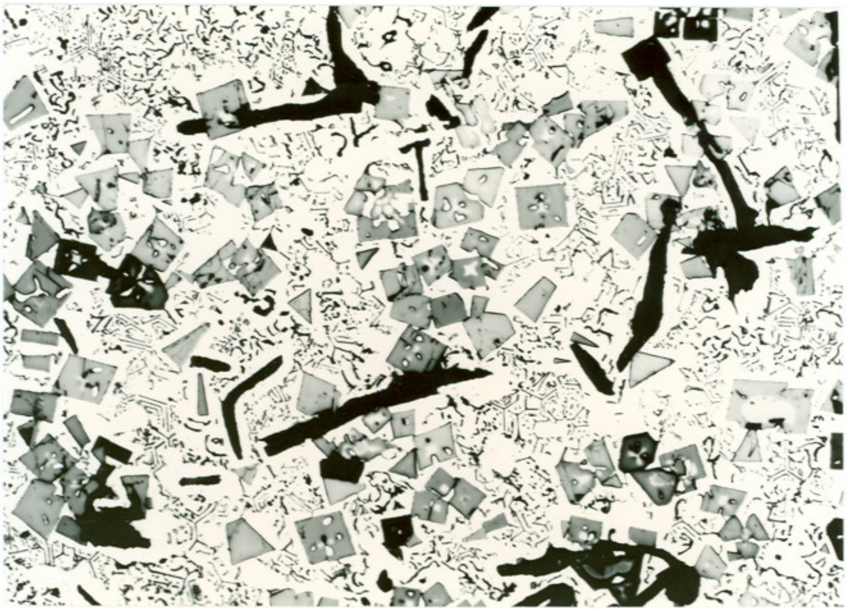

Figure 89. Ti-Ni-C (15-60-25 At.%), Arc Melted Sample Heat Treated at 900°C. Coarse Bivariantly Solidified Monocarbide plus Graphite in Eutectic Matrix of TiC + Ni + C. X-ray Analysis: TiC_{1-x} (a = 4.326Å), Ni (a = 3.539Å); C.

Figure 90. Ti-Ni-C (35-10-55 At.%), Arc Melted Sample. Primary Graphite plus Bivariantly Solidified TiC + C Eutectic and Ni.

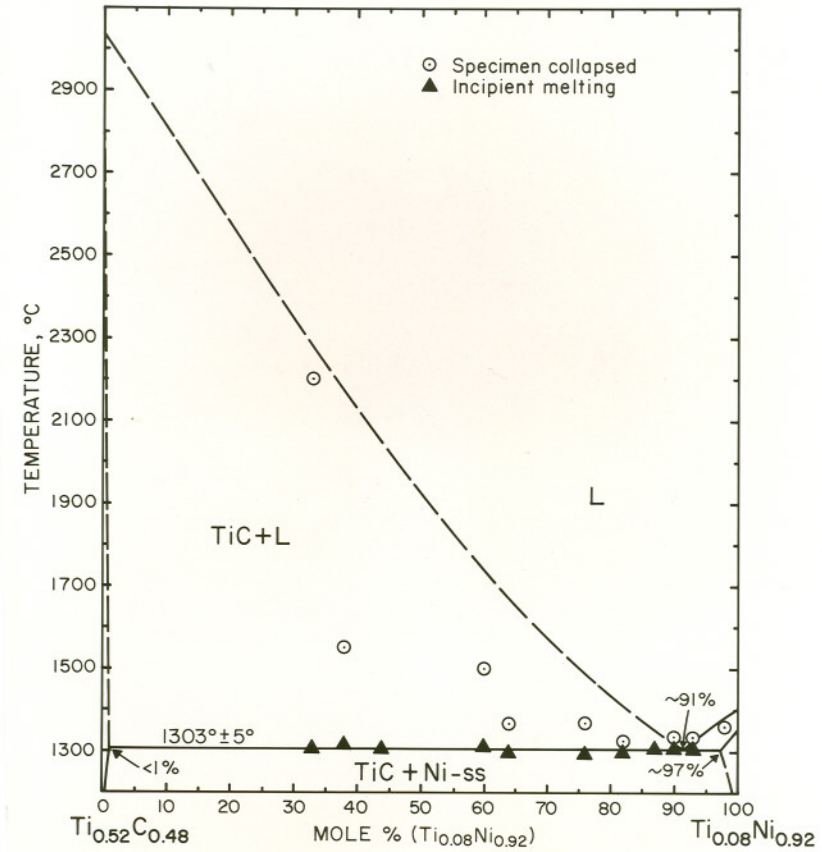

Figure 91. Melting Temperatures of Ternary Alloys Located Along the Pseudobinary Section $(Ti_{0.52}C_{0.48})-(Ti_{0.08}Ni_{0.92})$.

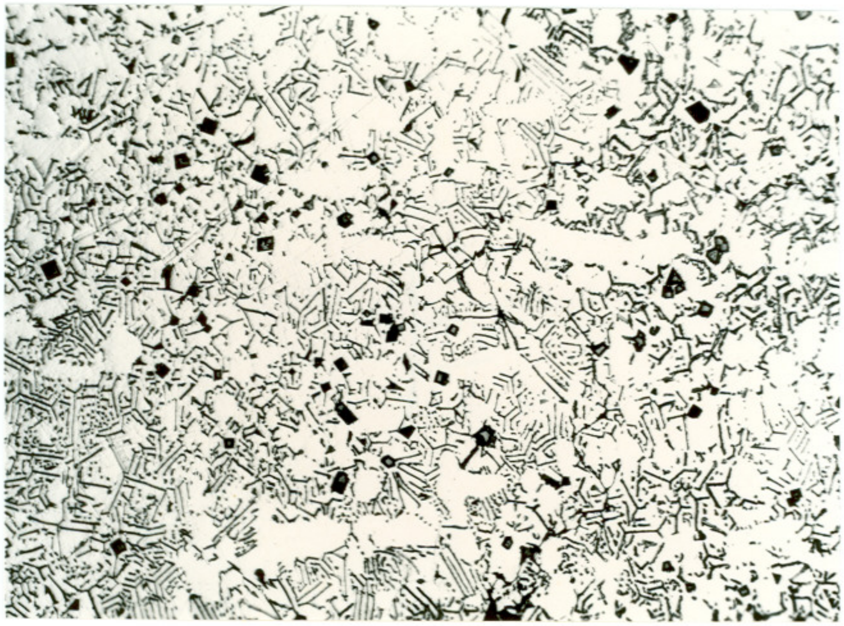

Figure 92. Ti-Ni-C (10-85-5 At.%), Arc Melted Sample. Trace of Bivariantly Solidified Monocarbide plus Nickel in TiC + Ni Pseudobinary Eutectic.

Figure 93. Ti-Ni-C (25-55-20 At.%), Arc Melted Sample. Primary Monocarbide in TiC + Ni Pseudobinary Eutectic Matrix.

Figure 94. Ti-Ni-C (20-60-20 At.%), Arc Melted Sample. Primary Monocarbide in TiC + Ni Eutectic Matrix Containing Trace of Free Graphite.

Eremenko(65) investigated ternary alloys along the join stoichiometric TiC-Ni and reported the following eutectic temperature and composition of 1280°C and ~17 mole % TiC. Stover and Wulff(68) also reported that a pseudobinary eutectic equilibrium existed between TiC and Ni at 1307° ± 3°C. The composition of the eutectic was placed at about Ti(13)-C(4) At.% (~9 mole % TiC); the critical tie line intersected the Ti-Ni binary system at 9 At.% Ti instead of at 100% Ni as reported by Eremenko. The results from the present investigation (Figure 91) agree with Stover and Wulff.

Metallographic examination of melted alloys along the join $TiC_{1.0}$-Ni consistently revealed the presence of trace amounts of free graphite (Figure 94). The lower pseudobinary eutectic temperature of 1280°C reported by Eremenko(65) results from either bivariantly solidifying or invariantly melting alloys along this join as evidenced by the data presented in the isopleth at 10 At.% carbon (Figure 12) and 1260°C isothermal section (Figure 84).

Besides the TiC + Ni pseudobinary eutectic at 1303°C, two additional reactions of this type occur between TiC_{1-x} and the intermetallic phases $TiNi_3$ and TiNi. At 1367° ± 9°C, the two-phase equilibrium TiC_{1-x} + $TiNi_3$ melts eutectically as indicated by the melting behavior of alloys along this section (Figure 95); the eutectic composition was placed at approximately 98 mole % $TiC_{0.87}$. The location of the critical tie line is shown in Figure 11 and presented in Figures 96 and 97 are characteristic microstructures. The photomicrograph of the arc melted sample shown in Figure 96 indicates that this alloy is located to the nickel-rich side of the critical tie line. But in Figure 97, the microstructure exhibits both primary monocarbide and secondary $TiNi_3$. This fact is attributed to the very narrow width of the two-phase equilibrium monocarbide plus $TiNi_3$ as indicated in Figures 12 and 84. Composition fluctuations during arc melting were sufficient to cause bivariant solidification and hence the appearance of the secondary $TiNi_3$ phase.

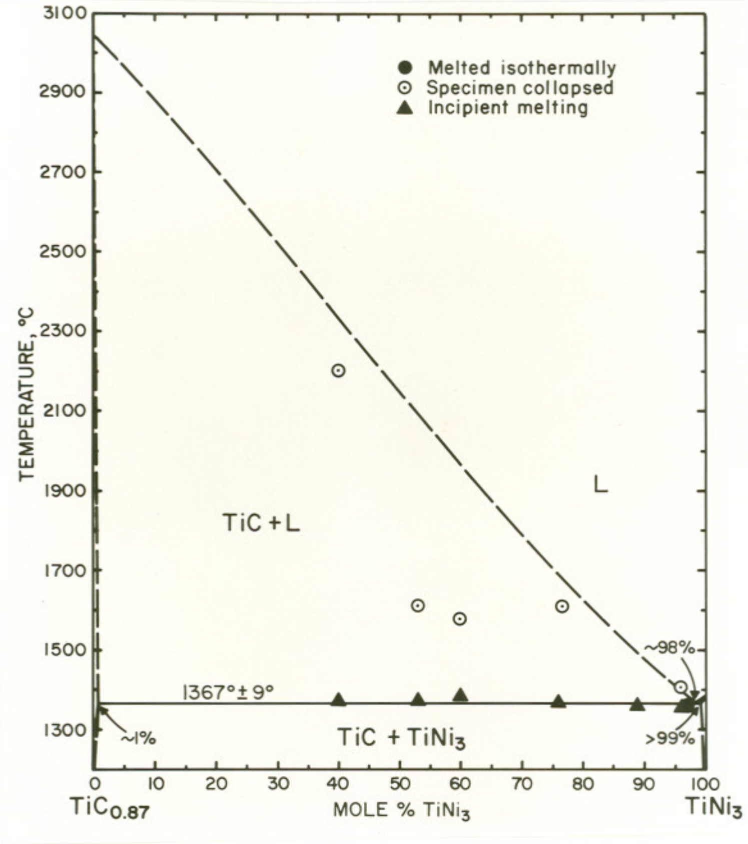

Figure 95. Melting Temperatures of Ternary Alloys Located Along the Pseudobinary Section $(Ti_{0.535}C_{0.465})-(Ti_{0.25}-Ni_{0.75})$.

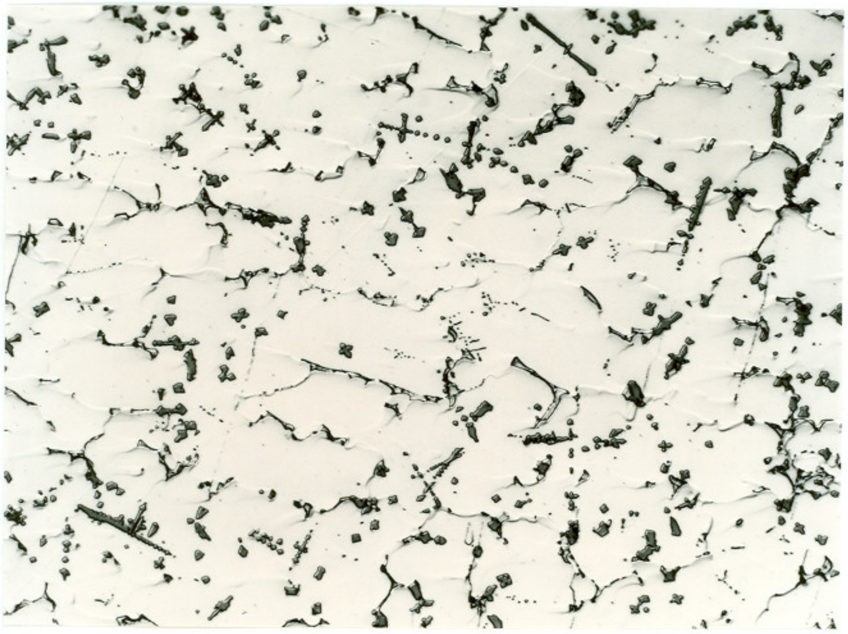

Figure 96. Ti-Ni-C (25-73-2 At.%), Arc Melted Sample. Bivariantly Solidified TiC (Dark Phase) and $TiNi_3$ (Light Phase), Trace of Fine Eutectic and Ni (Third Matrix Phase)

With respect to the two-phase equilibrium TiC_{1-x} + TiNi, the melting point and metallographic analyses yielded the following pseudobinary eutectic parameters: 1280° ± 7°C and approximately 87 mole % $TiC_{0.77}$. The location of the critical tie line is depicted in Figure 84, and the melting behavior of alloys located along this section is presented in Figure 98. Microstructures of both melted and quenched, and annealed alloys are presented in Figures 99-101. In these photomicrographs it is difficult to resolve the eutectic monocarbide because of the metal-rich location of the invariant point (~1 At.% C).

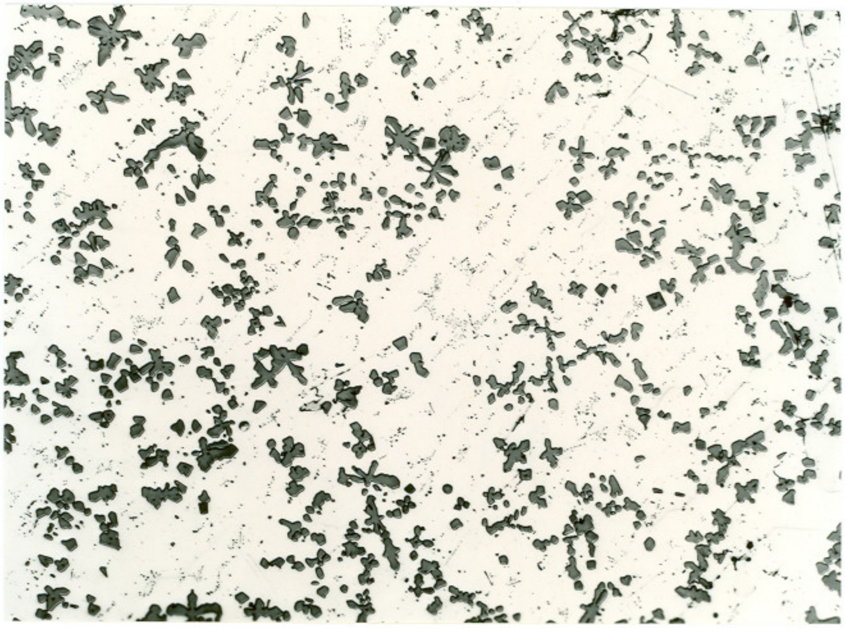

Figure 97. Ti-Ni-C (28-67-5 At.%). Arc Melted Samples. Primary Monocarbide and Secondary $TiNi_3$ plus Monocarbide-$TiNi_3$ Eutectic. X-ray Analysis: TiC_{1-x} (a = 4.324Å); $TiNi_3$ (a = 5.105Å; c = 8.309Å).

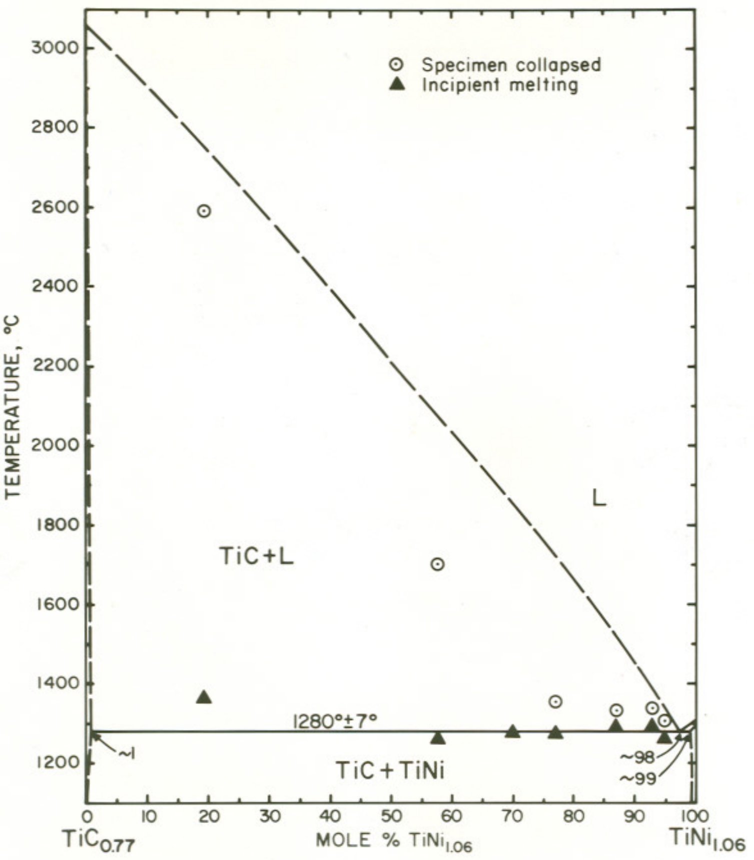

Figure 98. Melting Behavior of Ternary Alloys Located Along the Pseudobinary Section $(Ti_{0.565}C_{0.435})$-$(Ti_{0.485}Ni_{0.515})$.

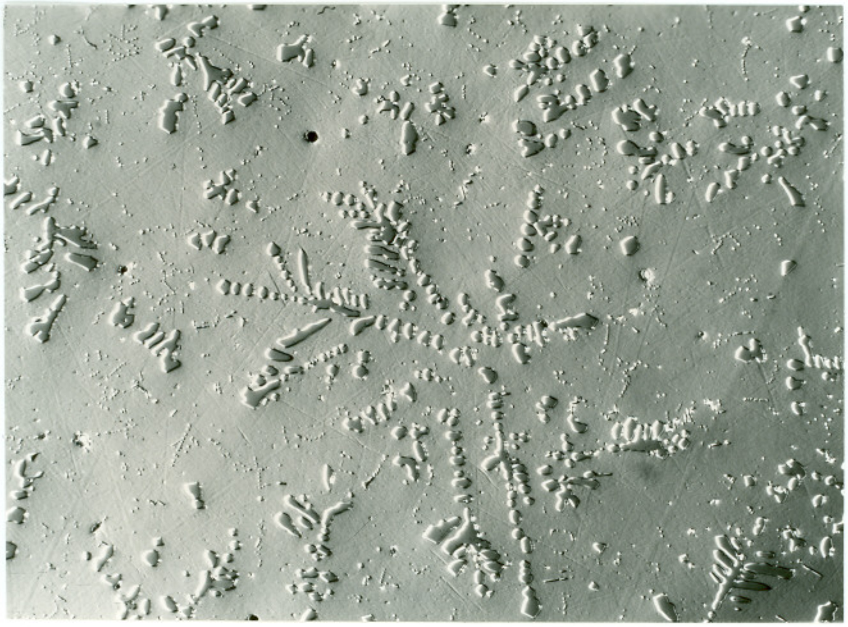

Figure 99. Ti-Ni-C (50-45-5 At.%), Arc Melted Sample. Primary Monocarbide Dendrites in TiC + TiNi Pseudobinary Eutectic Matrix (Slightly Divorced of Eutectic Monocarbide).

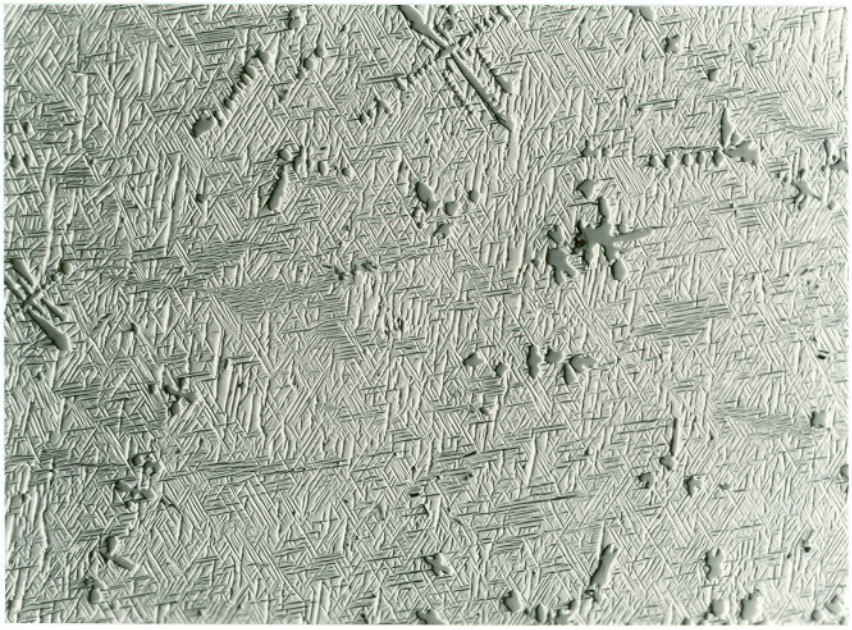

Figure 100. Ti-Ni-C (48-49-3 At.%), Arc Melted Sample Heat Treated at 900°C for 240 hours and Furnace Cooled. Trace of Primary Monocarbide in Transformed Matrix of TiNi Martensite. X-ray Analysis: TiC_{1-x} (4.317Å), Trace TiNi(a≈ 3.0Å, diffuse); TiN Martensite (diffuse).

(a) X400

(b) X500

Figure 101. Ti-Ni-C (50-40-10 At.%), Arc Melted Sample.

(a) Primary Monocarbide in TiNi (B2-type) Matrix.

(b) Same Sample Heat Treated at 900°C for 240 hours and Furnace Cooled. Retained cubic and Martensitic TiNi Matrix Phases.

The shape change or surface relief resulting from the TiNi martensitic transformation is shown in Figures 100 and 101. For both binary and ternary alloys containing the TiNi phase, the cubic (B2-type) to monoclinic (distorted orthohombic, B19-type) transformation structure was observed in heat treated alloys furnace cooled from subsolidus temperatures and not in melted alloys quenched from liquidus temperatures. This observation may be attributed to a lowering of the M_s temperature due to the introduction of substitutional and/or thermal defects during quenching when compared to annealed, slowly cooled alloys(73,74). As shown in Figure 101(b), mechanical deformation of the samples surface during metallographic preparation may account for some stress-induced martensite(31) as evidenced by the untransformed matrix regions protected by the raised, closely spaced monocarbide dendrites.

In order to facilitate the reading of the phase diagram data previously presented in Figures 9-12 and to consolidate the experimental results presented above, a series of isothermal sections were prepared in order to depict more clearly the phase relationships prevailing in the ternary system. These sections are presented in Figure 102(a)-102(d).

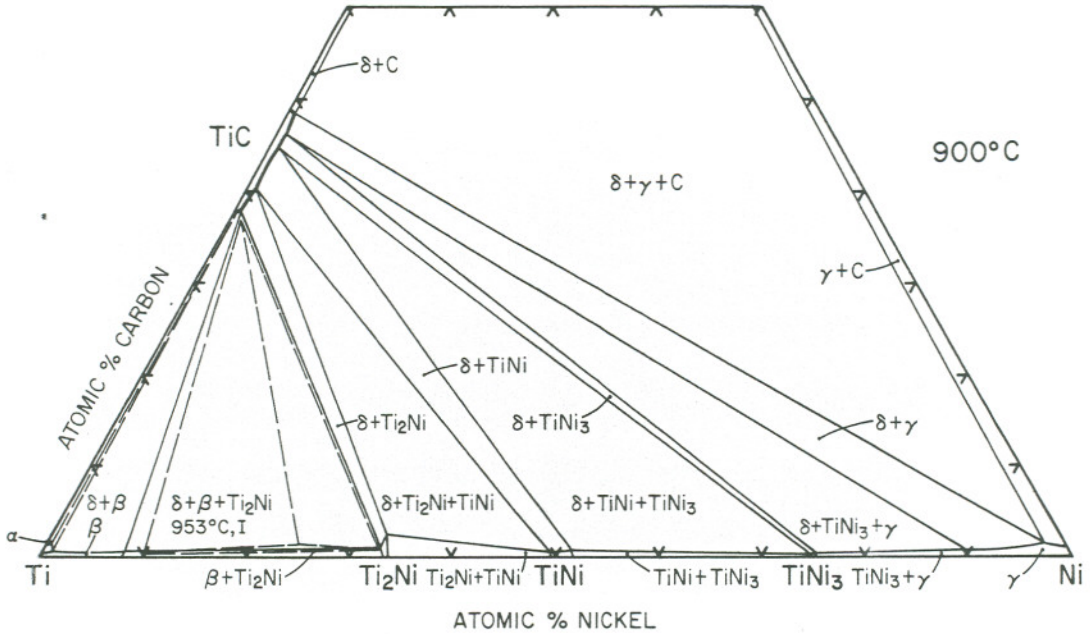

Figure 102(a). Isothermal Section at 900°C. Location of Class I Four-Phase Reaction Plane at 953 ± 8°C.

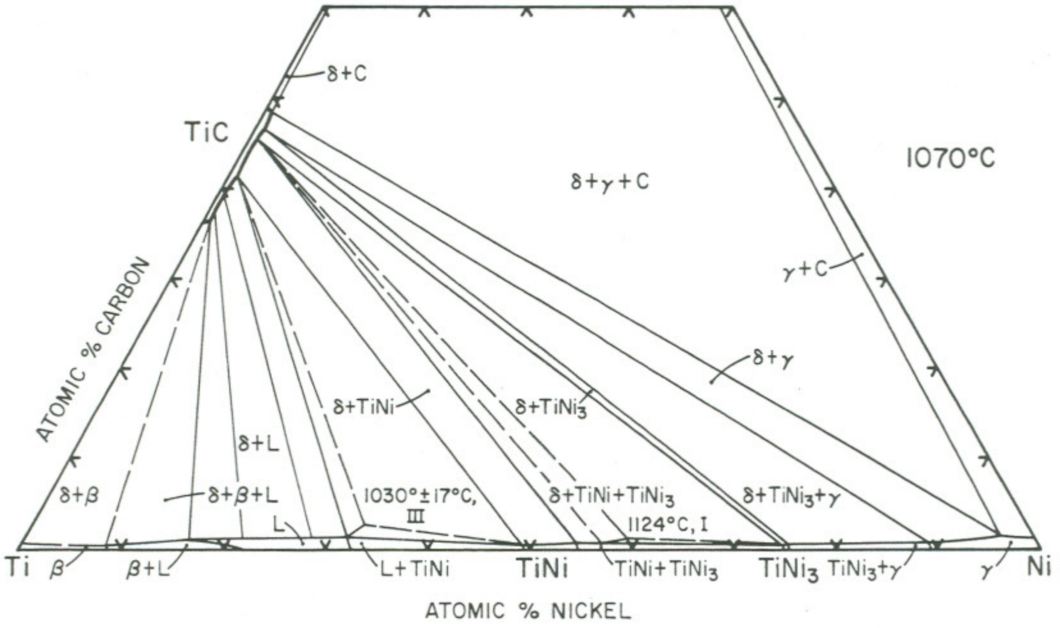

Figure 102(b). Isothermal Section at 1070°C. Location of Class I and Class III Four-Phase Reaction Planes at 1124° ± 9°C and 1030° ± 17°C, Respectively.

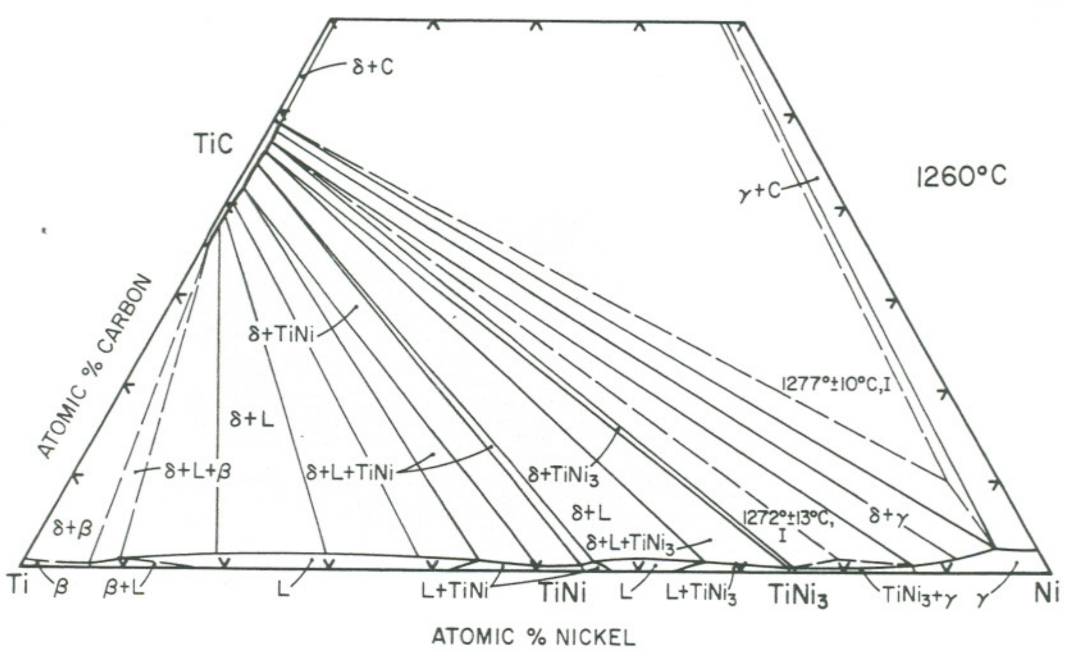

Figure 102(c). Isothermal Section at 1260°C. Location of Class I Four-Phase Reaction Planes at 1272° ± 13°C and 1277° ± 10°C.

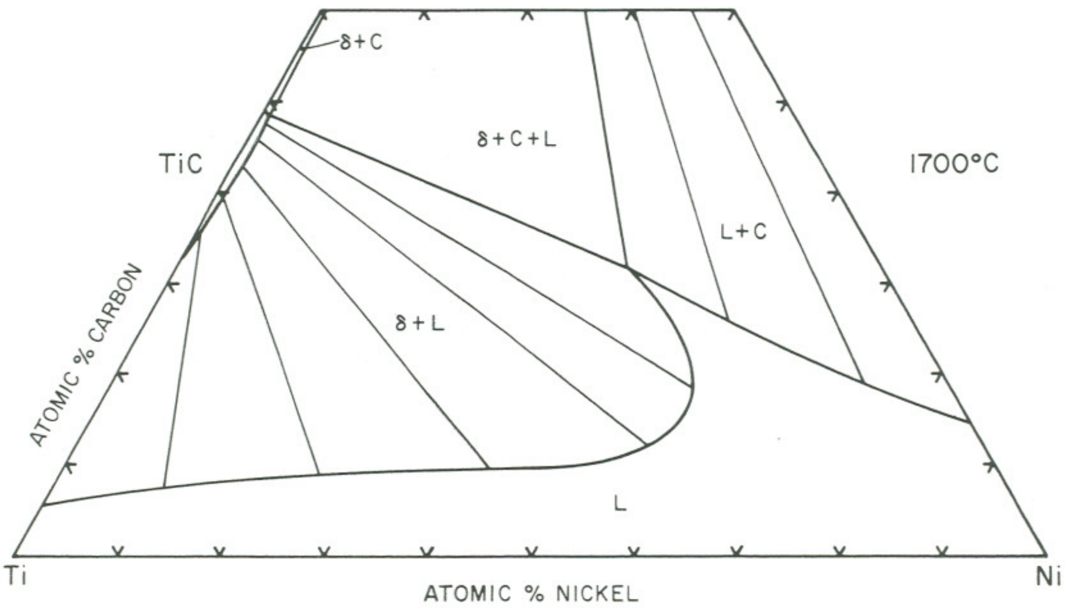

Figure 102(d). Isothermal Section at 1700°C.

E. DISCUSSION

The ternary phase relationships established for the Ti-Fe-C, Ti-Co-C, and Ti-Ni-C systems are similar in that the refractory TiC_{1-x} phase forms pseudobinary eutectic equilibria with the group VIII metals and some Ti_aM_b intermetallic phases (M=Fe, Co, Ni). With decreasing temperature three-phase equilibria of the type TiC_{1-x} + Liquid + Ti_aM_b, which originate at the pseudobinary isotherms, participate in either class I or II four-phase reactions with the exception of one class III reaction which results from the carbon-stabilization of the Ti_2Ni binary phase.

The existence of the metastable Fe_3C phase and the two crystal modifications of $TiCo_2$ accounts for one and two additional four-phase reactions in the respective ternary systems. The established phase relationships also show that the major effect of carbon additions to the Ti-M binary systems is to lower their invariant reaction temperatures involving a liquid phase. In addition, the homogeneity ranges of all edge binary phases remain approximately unchanged and restricted in ternary alloys.

The equilibria existing between a titanium monocarbide phase of increasing interstitial element deficiency and the binary titanium-group VIII metal phases are understandable because of the low-relative stabilities of ferrous metal carbide phases with either an isomorphous or nonequivalent cubic monocarbide (B1-type) structure. This results in the observed restricted ferrous metal exchange in the monocarbide phase. Equiliria of this type will become less selective at high temperatures due to an increase in the energy of mixing which tends to equalize a given free-energy difference. But as is usually the case with systems of this type, solidus temperatures are reached before any noticeable change in the tie-line distribution occurs.

In view of the established phase relationships, the existence of two-phase equilibria of the type TiC-(α,γ)Fe, (γ) Co, and (γ)Ni offer alloy compositions for the fabrication of refractory composite bodies for tool and wear applications. In fact, sintered carbides on the basis of TiC-Mo_2C solid solutions containing 10-15% Ni, Ni-Cr, and Ni-Mo binders are currently used as tools for high speed finishing of steel. In addition, sintered or infiltrated heat-resistant TiC base alloys with high binder contents (up to 60% Ni, Co-Cr alloys) and heat treatable TiC alloys with 50-70% steel binders have found growing interest in the industry.

Besides the alloys currently used in industry as tool materials, future developments could be concerned with the fabrication of useful composites based on the hard, refractory TiC_{1-x} phase and ductile (B2-type) intermetallic phases of TiFe, TiCo, and TiNi; as well as systems based on monocarbide-eta phase (Ti_2Ni- or Fe_3W_3C-types)-metal equilibria.

REFERENCES

1. M. Hansen, "Constitution of Binary Alloys," McGraw-Hill, 1958.

2. R.P. Elliot, "Constitution of Binary Alloys, First Supplement," McGraw-Hill, 1965.

3. F.A. Shunk, "Constitution of Binary Alloys, Second Supplement," McGraw-Hill, 1969.

4. "Metals Handbook, Vol. 8: Metallography, Structures, and Phase Diagrams," American Society for Metals, 1973.

5. T. Wada, Trans. Natl. Inst. Metals (Tokyo), 6, 43-46, (1964).

6. E. Rudy, D.P. Harmon, and C.E. Brukl, Air Force Technical Report, AFML-TR-65-2, Part I, Vol. II, August 1965.

7. F. Laves and H.J. Wallbaum, "The Crystal Chamistry of Titanium Alloys," Naturwissenshaften, 27, 674-675, (1939).

8. W. Jellinghaus, "The Crystal Structure of Fe_3Ti," Ztsch. f. Anorg. und allgem. Chem., 227, (1936), 62-64.

9. P. Duwez and J.L. Taylor, "The Structure of Intermediate Phases in Alloys of Titanium with Iron, Cobalt, and Nickel," Trans. AIME, 188 (1950), 1173-1176.

10. W.B. Pearson, 'Handbook of Lattice Spacings and Structures of Metals and Alloys," Vol. I and Vol. II, Pergamon, 1958 and 1967.

11. A. Taylor and B.J. Kagle, "Crystallographic Data on Metal and Alloy Structures," Dover Publications, 1963.

12. A. Iannucci, A.A. Johnson, E.J. Hughes, and P.W. Barton, J. Appl. Phys., 39, (1968), 2222-2224.

13. P.W. Barton, E.J. Hughes, and A.A. Johnson, "Proceedings of the First International Conference on Electron and Ion Beam Science and Technology," John Wiley & Sons, (1965), 460.

14. H.J. Wallbaum and H. Witte, "The Crystal Structure of $TiCo_2$," Ztsch. f. Metallkunde, 31, (1939), 185-187.

15. T. V. Philip and P.A. Beck, Trans. AIME, 209, (1957), 1269-1271.

16. A. E. Dwight, Trans. ASM, 215, (1959), 283-286.

17. H. P. Stuwe and Y. Shimomura, Z. Metallk., 51, (1960), 180-181.

18. A.E. Dwight, Trans. ASM, 53, (1961), 479-500.

19. W. Rostoker, J. Metals, 4, (1952), 209.

20. R.W. Fountain and W.D. Forgeng, Trans. AIME, 215, (1959), 998-1008.

21. H. Margolin, E. Ence, and J. P. Nielsen, Trans. AIME, 197, (1953), 243-247.

22. G.R. Purdy and J.G. Parr, Trans. AIME, 221, (1961), 636-639.

23. F. W. Wang, W. J. Buehler, and S. J. Pickart, J. Appl. Phys., 36, (1965), 3232.

24. P. Duwez and J.L. Taylor, Trans. AIME, 191, (1951), 551.

25. D.M. Poole and W. Hume-Rothery, J. Inst. Metals, 83, (1955), 473-480; and 84, (1956), 532-535.

26. W. J. Buehler, J.V. Gilfrich, and R.C. Wiley, J. Appl. Phys., 34, (1963), 1475.

27. P. Pietrokovsky and F.G. Youngkin, J. Appl. Phys., 31, (1960), 1763.

28. J.V. Gilfrich, "Advances in X-ray Analysis Vol. 6," W. M. Mueller and M. Fay, eds., p. 74, Plenum Press, 1962.

29. W. J. Buehler and R.C. Wiley, ASM Trans. Quart., 55, (1962), 259.

30. D. Koskimaki, M.J. Marcinkowski, and A.S. Sastri, Trans. AIME, 245, (1969), 1883-1890.

31. M.J. Marcinkowski, A.S. Sastri, and D. Koskimaki, Phil. Mag., 18, (1968), 945-958.

32. R. Vogel and H. J. Wallbaum, Arch. Eisenhuttenwesen, 12, (1938-39), 299-304; H. J. Wallbaum, ibid., 14, (1940-41), 521-526.

33. K. D. Sheffler, R. W. Kraft, and R. W. Hertzberg, Trans. AIME, 245, (1969), 227-231.

34. F. Laves and H. J. Wallbaum, "The Crystal Structure of Ni_3Ti and Si_2Ti," Ztsch. f. Kristallographie, 101, (1939), 78-93.

35. R. Kieffer and F. Benesovsky, "Hartstoffe," Springer-Verlag, Vienna 1963.

36. E. K. Storms, "The Refractory Carbides," Academic Press, New York 1967.

37. J. S. Umanski and S. S. Khidekel, Zh. Fiz. Khim. SSSR, 15, (1941), 983.

38. I. Cadoff and J. P. Nielsen, J. Metals, 5, (1955), 248.

39. G. A. Geach and F. O. Jones, 2nd Plansee Seminar, Reutte, Tirol, (1955), 80.

40. C. Agte and K. Moers, Z. Anorg. Allg. Chemie, 198, (1931), 233.

41. E. Friedrich and G. Sittig, Z. Anorg. Allg. Chemie, 144, (1925), 169.

42. R. I. Bickerdicke and G. Hughes, J. Less-Common Metals, 1, (1959), 42.

43. E. Rudy, Air Force Report, AFML-TR-65-2, Part V, Compendium of Phase Diagram Data, May 1969.

44. P. Donohue, J. Am. Chem. Soc., 85, (1963), 1238.

45. J. Chipman, Met. Trans., 3, (1972), 55-64.

46. J. Chipman, Met. Trans., 1, (1970), 2163-2168.

47. C. S. Roberts, Trans. AIME, 197, (1953), 203.

48. U. Haschimoto and N. Kawai, Nippon Kinzoku Gakkai-Shi, 2, (1938), 26-28.

49. S. Takeda, Science Repts. Tohoku Imp. Univ., (1936), 863-881.

50. H. Morrogh and W.J. Williams, J. Iron Steel Inst., 155, (1947), 321-371.

51. E.T. Turkdogan, R.A. Hancock, and S. I. Herlitz, J. Iron Steel Inst., 182, (1956), 274-277.

52. B.P. Burylev, Zh. Fiz. Khim., 36, (1962), 2230-2232.

53. H. Schenck, M.G. Frohberg, and E. Steinmetz, Arch. Eisenhuettenw., 34, (1963), 37-42.

54. K. Friederich and A. Leroux, Metallurgie, 7, (1910), 10-13.

55. O. Ruff and W. Bormann, Z. Anorg. Chem., 88, (1914), 386-396.

56. T. Kase, Science Rept. Tohoku Univ., 14, (1925), 187-193.

57. L. Hofer, E. Cohn, and W. Peebles, J. Phys. and Colloid. Chem., 54, (1950), 1161.

58. B. Jacobson and A. Westgren, Z. Physik. Chem., B20, (1933), 361.

59. R. Bernier, Ann. Chem., 6, (1951), 104.

60. S. Nagakura, J. Phys. Soc. Japan, 12, (1957), 482.

61. R. Kohlhaas and W. F. Meyer, Metallwirtschaft, 17, (1938).

62. H. J. Goldschmidt, J. Iron Steel Inst., 160, (1948), 347.

63. H. J. Goldschmidt, "Interstitial Alloys," Butterworths (London), 1967.

64. R. Edwards and T. Raine, Proc. First Plansee Seminar, (1953), 232.

65. V. W. Eremenko, Zhur. Neorg. Khim, 1, (1956), 2131-2143.

66. C.M. Craighead, O. W. Simmons, and L. W. Eastwood, Trans. AIME, 188, (1950), 514-538.

67. P. Schwarzkopf and R. Kieffer, "Cemented Carbides," MacMillan, 1960.

68. E. R. Stover and J. Wulff, Trans. AIME, 215, (1959), 127-136.

69. W. C. Ballamy and E. E. Hucke, Journal of Metals, August 1970, 43-50.

70. M. Pirani and H. Alterthum, Z. Elektrochem., 29, (1923), 5.

71. E. Rudy, S. Windisch, and Y. A. Chang, Air Force Technical Report, AFML-TR-65-2, Part I, Vol. I, March 1965.

72. E. Rudy and G. Progulski, "A Pirani-Furnace for the Precision Determination of the Melting Temperature of Refractory Metallic Substances: , Air Force Technical Report AFML-TR-65-2, Part III, Vol. II, May 1967.

73. G. D. Sandrock, A. J. Perkins, and R. F. Hehemann, Met. Trans., 2, (1971), 2769-2781.

74. R. J. Wasilewski, Met. Trans., 6A, (1975), 1405-1418.

PART II

PHASE EQUILIBRIA OF THE TYPE METAL CARBONITRIDE + GRAPHITE + NITROGEN IN THE SYSTEMS Ti-C-N, Zr-C-N, AND Hf-C-N

TABLE OF CONTENTS

PAGE

II. PHASE EQUILIBRIA OF THE TYPE METAL CARBONITRIDE + GRAPHITE + NITROGEN IN THE SYSTEMS Ti-C-N, Zr-C-N, AND Hf-C-N

LIST OF FIGURES

FIGURE PAGE

LIST OF TABLES

PART II

A. INTRODUCTION

For many years, technical grade TiC and HfC, which may be viewed as both oxygen and nitrogen poor monocarbides, have been used as input materials for the fabrication of certain sintered carbide wear resistant alloys.(1) Only recently, true carbonitrides of the group IV transition metals have found extensive use as hard phase and wear, corrosion resistant coating constituents of commercial composite tool materials.(2,3)

As the hard phase for sintered microcomposites, master carbonitride alloys are fabricated by in situ nitriding of either carbide or modified carbide powders, typically at temperatures between 1200° to 2000°C, in nitrogen or a nitrogen-bearing atmosphere. In contrast, the carbides, nitrides, or carbonitrides as dense protective coatings are formed from the gas phase, typically at temperatures between 800° to 1200°C, through the technique of chemical vapor deposition.

In view of the various thermal and gas phase fabrication environments required for the metal carbide-nitride interstitial alloys of interest, it is desirable to know or predict their gross compositions and likely degree of chemical interaction after fabrication. In order to do this, an evaluation of their thermodynamic stability is necessary, i.e., the stabilities of the group IV metal carbides with respect to their mononitrides. In principle, an evaluation of this type can be made by utilizing existing thermodynamic data for the carbide and nitride phases, but the reported literature data seem to be inadequate as evidenced by a past investigation concerned with the calculation of selected carbonitride phase equilibria.(3)

The present investigation is concerned with the establishment of invariant phase equilibria of the type metal carbonitride + graphite + nitrogen in the ternary systems Ti-C-N, Zr-C-N, and Hf-C-N. Using the temperature-composition data from the experimental three-phase equilibria, differences in the free energies of formation of the respective metal monocarbides and nitrides ($\Delta G^{o}_{f,MeC} - \Delta G^{o}_{f,MeN}$) are derived and compared with the literature values. In general, the composition of the carbonitride phase will shift to a lower nitrogen exchange as temperature increases and/or pressure decreases, i.e., the metal mononitride exhibits a more negative enthalpy and entropy of formation when compared to the monocarbides.

B. LITERATURE REVIEW

Thermodynamic property data for the group IV transition metal monocarbides and nitrides have been evaluated and compiled by

Chang(4), Stull et al.(5), Storms(6), Shick(7), and Toth(8). As pointed out by these authors, it is difficult at times to establish reliable high temperature data because of the considerable scatter in reported literature values, e.g. 10% or more. Poorly characterized starting alloys (composition, level and type of impurities) as well as problems of controlling composition at elevated temperatures account for this situation. In general, experimental data for the nitrides are particularly scarce.

From the above compilations, free energy of formation expressions were derived and are presented in Table I. Even though the indicated temperature intervals include the (β-L)Ti, (β-L)Zr, and (α-β) Hf transformation temperatures at 1940°K, 2125°K, and 2073°K, respectively, the ΔG_f^o values as a function of temperature were adequately represented by one linear equation for each of the six alloys. In addition, TlogT terms were not required to correct the ΔG_f^o equations for drastic changes in ΔC_p as a function of temperature.

The standard state for the metal carbide and nitride alloys presented in Table I is the solid interstitial phase with the indicated composition and cubic NaCl (B1-type) structure. These alloys are stable over wide homogeneity ranges which for the carbides extend from near stoichiometric compositions of $TiC_{\sim 0.95}$, a = 4.327Å; $ZrC_{\sim 0.98}$, a = 4.698Å; $HfC_{\sim 0.98}$, a = 4.640Å to metal rich compositions of

TABLE I

Free Energies of Formation of the Group IV Transition Metal Monocarbides and Nitrides. (Compiled from the Literature)(4-8)

$$\Delta G_f^o = A - BT, \text{ calories/g-at. metal}$$

Phase	A*	B	Temperature Range, °K
$TiC_{\sim 1}$	-44,800 ± 4,000	-3.5	1500 - 2300
$TiN_{\sim 1}$	-77,700 ± 3,000	-21.2	1500 - 2300
$ZrC_{\sim 1}$	-48,600 ± 5,000	-3.4	1600 - 2300
$ZrN_{\sim 1}$	-86,900 ± 4,000	-22.3	1600 - 2300
$HfC_{\sim 1}$	-51,700 ± 5,000	-2.2	1400 - 2300
$HfN_{\sim 1}$	-87,200 ± 3,400	-21.6	1400 - 2300

---

*Includes uncertainties associated with only the enthalpy of formation at 298°K

$TiC_{\sim 0.5}$, a ≈ 4.29Å; $ZrC_{\sim 0.58}$, a ≈ 4.69Å; $HfC_{0.61}$, a = 4.619Å (6,9). For the isostructural mononitride phases, the following stability ranges have been reported: $TiN_{\sim 0.45}$, a = 4.218Å to $TiN_{\sim 1.1}$, a = 4.218Å (maximum lattice parameter of a ≈ 4.24Å at $TiN_{\sim 1}$); $HfN_{0.67}$ a = 4.535Å to $HfN_{\sim 1.13}$, a 4.51Å(8,14). The composition range for ZrN is wide but has not been well established; the following lattice parameter values have been reported: $ZrN_{\sim 1.02}$, a = 4.576Å(10); $ZrN_{0.99}$, a = 4.571Å(11).

The pseudobinary sections MeC-MeN for the metals Me=Ti, Zr;Hf are known to form continuous solid solutions(11). The lattice parameter variation of alloys located along the concentration section TiC-TiN exhibits a slight negative deviation from linearity, while for the sections ZrC-ZrN and HfC-HfN slight positive deviations are observed.

C. EXPERIMENTAL PROCEDURES

1. Starting Materials

The monocarbides and nitrides of titanium, zirconium, and hafnium as well as graphite served as starting materials for the preparation of experimental alloys.

The titanium monocarbide powder (Shieldalloy Corporation) had a total carbon content of 19.55 wt% of which 0.31 wt% was present as free graphite. Oxygen and nitrogen contents were 1200 and 660 ppm, respectively; the measured lattice parameter was a= 4.327_2Å.

The zirconium and hafnium monocarbide powders (Wah Chang Albany Corporation) had total carbon contents of 10.73 wt% and 6.23 wt%, respectively. Major impurities included 750 ppm oxygen for ZrC (a = 4.707 Å); 1600 ppm oxygen and 100 ppm nitrogen for HfC (a = 4.633Å).

The mononitrides were prepared by nitriding the respective metal powders in molybdenum containers between 1000° to 1700°C. The nitrided products had analyzed nitrogen contents of 21.80 wt% (TiN, a = 4.240_6Å), 13.42 wt.% (ZrN, a = 4.575Å); 7.41 wt% (HfN, a = 4.515Å).

The spectrographic-grade graphite powder (Union Carbide Corporation) had a total impurity content of < 2 ppm.

2. Alloy Preparation and Heat Treatments

Carbonitride alloys were prepared in the following ways: (1) nitriding cold pressed monocarbide powders, (2) nitriding cold pressed mononitride plus graphite mixtures; (3) nitriding hot pressed carbide plus nitride mixtures of $Me(C_{0.5}N_{0.5})$. In addition, to achieve more rapid equilibration, a separate alloy series containing 2 wt% nickel was fabricated.

The above alloy formulations were reacted under one atmosphere of nitrogen for 200 hours at temperatures of 1400°, 1500°, 1700°, 1800° and 2000°C in covered graphite crucibles (~7.6 cm long x 2.5 cm square). The graphite crucible was heated resistively between two water-cooled copper electrodes within a furnace chamber (refer to Part I, Section C,3). Three black body holes located along the length of the crucible wall served as reference points for temperature measurements.

During the course of and at the end of the 200 hour equilibration runs, Debye-Scherrer powder diffraction patterns using CuK_α radiation were prepared from the reacted alloys. The alloys were also analyzed for total and free carbon, and nitrogen. In general, it was found that an analyzed sample carbon and nitrogen contents were reproducible to within 1 and 2-3 atomic percent, respectively.

D. EXPERIMENTAL RESULTS

Based on the chemical analyses, the carbonitride compositions were expressed in mole fractions of the interstitial elements relative to one gramatom of metal, i.e., $Me(C_uN_v)_w$, $(u + v = 1)$. The terms u and v are the relative mole fractions (interstitial exchange) of carbon and nitrogen, respectively; and w is the combined gramatoms of carbon plus nitrogen per gramatom of metal (stoichiometry parameter). The results of the 200 hour equilibration treatments, derived from nitriding starting alloys of the type $Me(C_{0.5}N_{0.5})$, are presented in Table II.

Even in the presence of low level nickel additions, X-ray analysis revealed that equilibration was much slower for alloys fabricated from either the MeC or MeN + C starting powders when compared to the solid solution master alloy powders, $Me(C_{0.5}N_{0.5})$. For example, the X-ray patterns of the nitrided mononitride plus graphite mixtures were diffuse, i.e., the low angle edges of the diffraction lines corresponding to the carbonitride reaction product were sharp, and the high angle edges corresponding to nitrogen-richer compositions gradually merged with either the film background or the remanence of the mononitride starting material. This same pattern was noted for the monocarbide powders but in the reverse order. For the nitrided $Me(C_{0.5}N_{0.5})$ master alloys, the diffraction lines in the back reflection region were sharp or only slightly diffuse after the 200 hour equilibration (Table II).

The results of the equilibration treatments are also presented in graphical form (Figures 1, 2, and 3) along with data obtained from the literature(2, 3, 12). In addition to the temperature-composition data, the lattice parameter variations of the three carbonitride solid solutions are depicted. The observed parameter variations are consistent with the results of Kieffer et al.(11).

The following chemical reaction represents the resulting three-phase equilibrium of $Me(C_uN_v)_w + C_{(gr)} + N_{2(g)}$ (1 atm):

TABLE II

Mean Compositions and Lattice Parameters of Group IV Transition Metal Metal Carbonitrides, $Me(C_uN_v)$, as a Function of Temperature. (P_{N_2} = 1 atm).

Temperature, °C	Mean Composition $Me(C_uN_v)$	Accuracy* $\pm u$	$\pm v$	Lattice Parameter, Å
1400	$Ti(C_{0.29}N_{0.71})_{0.98}$	0.01	0.02	4.265
	$Zr(C_{0.10}N_{0.90})_{\sim 1}$	0.02	0.01	4.59_7**
	$Hf(C_{0.24}N_{0.76})_{\sim 1}$	0.02	0.02	4.57_0**
1500	$Ti(C_{0.39}N_{0.61})_{0.99}$	0.01	0.01	4.274
	$Zr(C_{0.19}N_{0.81})_{0.98}$	0.02	0.02	4.602
	$Hf(C_{0.34}N_{0.66})_{0.99}$	0.01	0.02	4.565
1700	$Ti(C_{0.57}N_{0.43})_{0.98}$	0.01	0.04	4.288
	$Zr(C_{0.49}N_{0.51})_{0.99}$	0.01	0.03	4.638
	$Hf(C_{0.61}N_{0.39})_{\sim 1}$	0.01	0.04	4.601
1800	$Ti(C_{0.66}N_{0.34})_{0.97}$	0.01	0.04	4.292
	$Zr(C_{0.61}N_{0.39})_{0.99}$	<0.01	0.04	4.653
	$Hf(C_{0.76}N_{0.24})_{1.0}$	0.01	0.05	4.613
2000	$Ti(C_{0.78}N_{0.22})_{0.97}$	<0.01	0.05	4.305
	$Zr(C_{0.84}N_{0.16})_{0.99}$	<0.01	0.05	4.67_0**
	$Hf(C_{0.89}N_{0.11})_{0.99}$	<0.01	0.06	4.62_3**

---

* Standard deviation based on three measurements

**Lines on X-ray pattern slightly diffuse in back reflection region.

$$(MeC_w)_{Me(C_uN_v)_w} + \frac{w}{2} N_2 \rightarrow (MeN_w)_{Me(C_uN_v)_w} + wC \ldots\ldots \Delta G_R \qquad (1)$$

Since there are (w) gram atoms of interstitial solution per gram atom of metal, the free energy difference ($\Delta G^o_{f, MeC_w} - \Delta G^o_{f, MeN_w}$) can be calculated from the following relationship when submitting ideal solution conditions to the carbonitride sublattice.

$$\Delta G_R = \Delta G^o_{f, MeN_w} - \Delta G^o_{f, MeC_w} + wRT \ln \frac{v}{u} P_{N_2}^{-0.5};$$

at equilibrium (T, p = constant)

$$\Delta G^o_{f, MeC_w} - \Delta G^o_{f, MeN_w} = wRT \ln \frac{v}{u} P_{N_2}^{-0.5} . \qquad (2)$$

With the thermodynamic literature data (Table I), ($\Delta G^o_{f, MeC} - \Delta G^o_{f, MeN}$) expressions (Table III) were derived and substituted into (2) for the calculation of the temperature dependence of the metal carbonitride vertices depicted in Figures 1,2,3. Independent of the literature data, the differences in free energies of formation of the MeC and MeN phases were derived from the experimental temperature-composition data and are presented in Table III. For these calculations, the stoichiometry parameter (w) in (2) was set equal to unity since the combined interstitial content remained approximately constant and equal to one at the various equilibration temperatures (Table II).

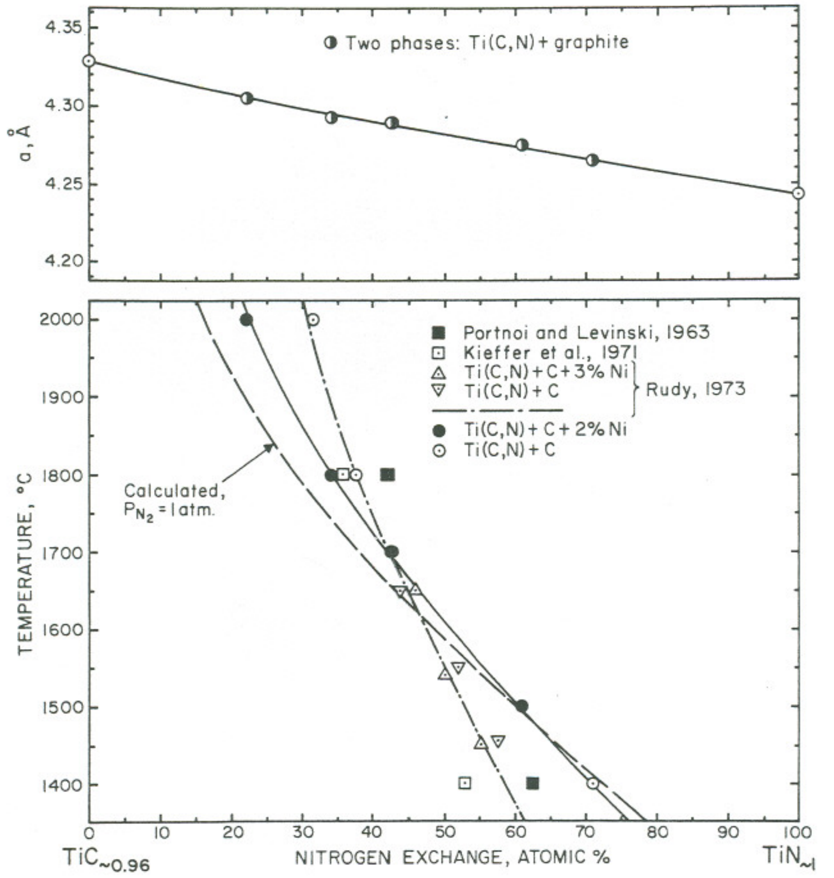

Figure 1. Experimentally Observed Temperature Dependence and Lattice Parameter Variation of the Titanium Carbonitride Vertex of the Three Phase Equilibrium $Ti(C,N) + C_{(gr)} + N_{2(g)}$ (1 atm).

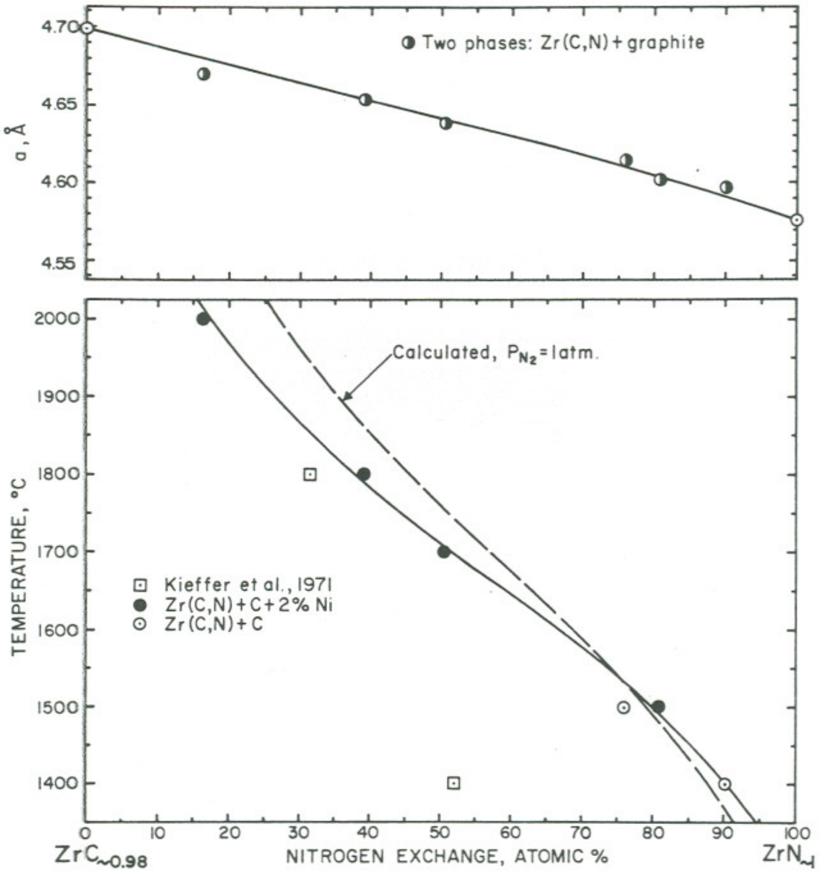

Figure 2. Experimentally Observed Temperature Dependence and Lattice Parameter Variation of the Zirconium Carbonitride Vertex of the Three Phase Equilibrium $Zr(C,N) + C_{(gr)} + N_{2(g)}$ (1 atm).

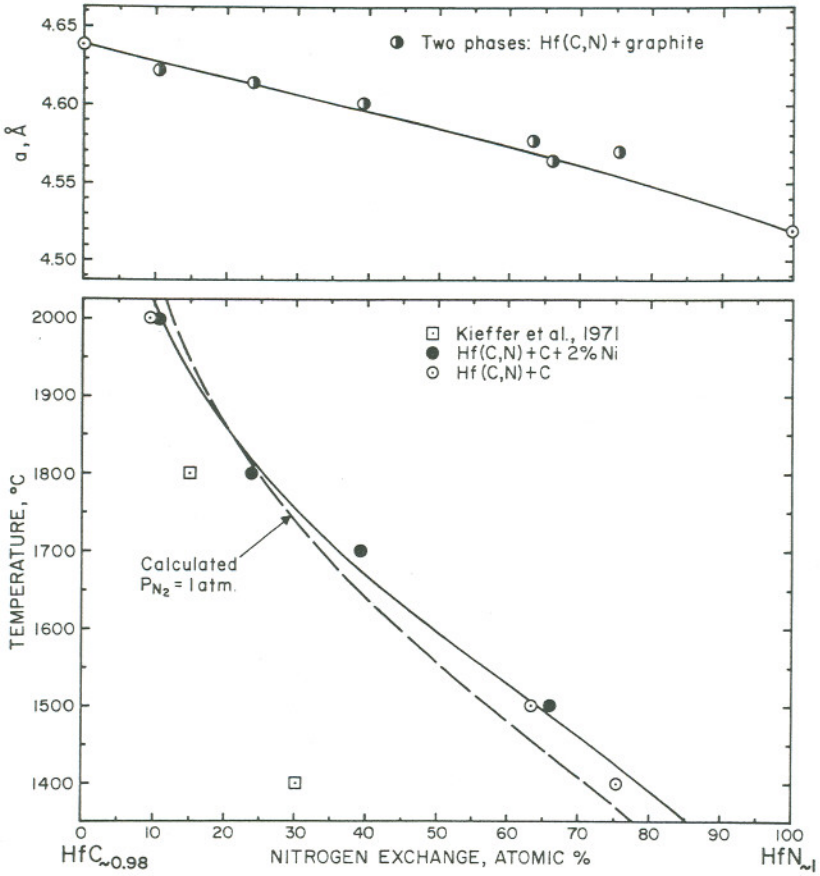

Figure 3. Experimentally Observed Temperature Dependence and Lattice Parameter Variation of the Hafnium Carbonitride Vertex of the Three Phase Equilibrium $Hf(C,N) + C_{(gr)} + N_{2(g)}$ (1 atm).

TABLE III

Calculated Free Energy Differences Between Group IV Transition Metal Carbides and Nitrides

$$\Delta\Delta G = \Delta G^{o}_{f,MeC} - \Delta G^{o}_{f,MeN} = A + BT \text{ cal/gr. At. Me}$$

Carbide-Nitride		A	B	Temperature Range, ° K
TiC-TiN	(a)	32,900	-17.7	1500-2300
	(b)	26,500	-14.1	1673-2273
ZrC-ZrN	(a)	38,300	-18.9	1600-2300
	(b)	45,300	-22.8	1673-2273
HfC-HfN	(a)	35,500	-19.4	1400-2300
	(b)	40,300	-21.6	1673-2273

(a) Calculated from literature (4-8), ideal solution behavior; P_{N_2} = 1 atm.

(b) Calculated from experimental data (Figures 1-3), ideal solution behavior; P_{N_2} = 1 atm.

E. DISCUSSION

Comparing the experimental results of this investigation and the literature$^{(2,3,12)}$ with the calculated temperature dependence of the titanium carbonitride vertex (Figure 1) suggests that true equilibrium for the excess graphite containing alloys may not have been reached. Assuming that the calculated curve under ideal conditions depicts the true temperature dependence, the line fit to the data approaches the calculated but still lies at nitrogen-richer compositions above approximately 1600°C. The nickel additions promoted the equilibration process, and its effect was more noticeable at the higher temperatures. For the zirconium and hafnium carbonitride alloys, nickel additions seemed to have little effect on their final compositions (Figures 2,3).

Over the indicated temperature intervals (Table III), the functions $\Delta\Delta G = (\Delta G^{o}_{f,MeC} - \Delta G^{o}_{f,MeN})$ derived from the experimental data yielded a smaller temperature coefficient for the pair TiC-TiN and larger coefficients for the pairs ZrC-ZrN and HfC-HfN when compared with the literature. As a measure of the error associated with the experimentally derived temperature functions, the composition error figures based on reproducibility (Table II) may be utilized.

Differentiating equation (2) with respect to u and v (constant w, T, P_{N_2}) and setting $du \simeq \Delta u$ and $dv \simeq \Delta v$, the following relationship results for the most probable uncertainty in $\Delta\Delta G$,

$$\Delta(\Delta\Delta G) \simeq \pm \frac{wRT\ln P_{N_2}^{-0.5}}{uv}\left[\,(\Delta u)^2 + (\Delta v)^2\,\right]^{0.5}. \qquad (3)$$

Equation (3) yields values of less than ± 1000 calories at 1400° C to less than ± 3000 calories at 2000° C for each of the three systems investigated. Compared with the literature values (Table I), uncertainties associated with only the reaction enthalpies at 298° K are ± 5000, ± 6000, and ± 6100 calories for the pairs TiC-TiN, ZrC-ZrN, and HfC-HfN, respectively.

While thermochemical data for the elements of carbon and nitrogen are well established, consistent data for well characterized monocarbide and nitride alloys are lacking. Experimentally, a more unsatisfactory situation exists with the nitrides; hence the stability relationships established in this investigation (Table III) should not be discounted. The data suggest that the free energy of formation for the TiN-phase should be less temperature dependent, and the ZrN and HfN phases should exhibit more negative entropies of formation than predicted from the literature for alloys stated to be nearly stoichiometric. Even allowing for deviations from ideality of the carbonitride solid solution, e.g. fitting a regular solution to the experimental data presented in Figures 1-3, the same observations remain.

From the viewpoint of technological applications, the stability data may be utilized to precalculate conditions for the formation of wear and corrosion resistant carbonitride coatings. Selecting an alloy with the desired nitrogen exchange, its nitrogen decomposition pressure is highest when free graphite is present, i.e., with hyperstoichiometric alloys ($w \geq 1$). Since free graphite cannot be tolerated, its formation can be suppressed by establishing initial conditions of temperature and pressure which stabilize single phase substoichiometric alloys ($w < 1$) of lower decomposition pressure. That is, if free graphite were present, it could be consumed by an equivalent loss of interstitial nitrogen according to the exchange reaction (1). Once used up, reaction (1) does not apply and is replaced by

$$(\mathrm{MeN})_{\mathrm{Me}(C_u N_v)_w} \rightarrow \frac{1}{2} N_{2(g)}, \quad w < 1 .$$

REFERENCES

1. P. Schwarzkopf and R. Kieffer, "Refractory Hard Metals," Macmillan Co., 1953.

2. R. Kieffer, P. Ettmayer, and M. Freudhofmeier, in H. H. Hausner (ed.), "Modern Developments in Powder Metallurgy," Plenum Press, 5, 1971.

3. E. Rudy, Journal of the Less-Common Metals, 33, (1973), 43-70.

4. Y.A. Chang, AFML-TR-62-2, Part IV, Vol. I, September 1965.

5. D.R. Stull et al., "JANAF Thermochemical Tables," Dow Chemical Company, 1965.

6. E.K. Storms, "The Refractory Carbides," Academic Press, New York, 1967.

7. H.L. Schick, "Thermodynamics of Certain Refractory Compounds," Vol. I and II, Academic Press, New York, 1966.

8. L.E. Toth, "Transition Metal Carbides and Nitrides," Academic Press, New York, 1971.

9. E. Rudy, "Compendium of Phase Diagram Data," AFML-TR-65-2, Part V, May 1969.

10. R.F. Domagala, D. J. McPherson, and M. Hansen, J. Metals, 8, (1956), 98.

11. R. Kieffer, H. Nowotny, P. Ettmayer, and G. Dufek, Metall., 26, (1972), 701.

12. K. I. Portnoi and Yu. V. Levinski, J. Fiz. Khim, 37, (1963), 2627.

13. R. Kieffer, P. Ettmayer, and M. Freudhofmeier, Metall., 25, (1971).

14. P.H. Booker and C.E. Brukl, AFML-TR-69-117, Part VI, December 1969.

PART III

THERMODYNAMIC CONSIDERATIONS OF CHEMICAL VAPOR DEPOSITION REACTIONS FOR SELECTED CARBIDES, NITRIDES, AND OXIDES

TABLE OF CONTENTS

LIST OF FIGURES

LIST OF TABLES

PART III

A. INTRODUCTION

The technique of chemical vapor deposition constitutes a means of fabricating dense coatings of various elements and compounds from the vapor phase. The actual process considered here relates to the deposition of a solid on suitable substrates at high temperatures (>500° C). Gas phase species, e.g., generated from a source material (liuqid or solid), are transported to the substrate on which they react to form the coating. But for a given temperature and gas phase composition, the formation of nonvolatile deposits resulting from either heterogeneous gas-solid or gas-liquid-solid reactions at the substrate surface must be enhanced.

Alloy systems of primary interest are sintered carbide substrate-metal carbide, nitride, or oxide coating composites for tool and wear applications. As an example, current commercial tool alloys may contain hard refractory coatings of either TiC, TiN, Ti(C,N) or Al_2O_3 which provide improved resistance to mechanical wear and chemical interaction between tool and workpiece.

Although accepted by the industry as a viable tool material, their development and utilization still suffer many problems. Reactions involving the gas phase mixture with the substrate during the deposition process can cause the formation of poorly adhering interface layers and microporosity. When used in applications which tax the strength of the composite, this lack of chemical compatibility or controlled chemical interaction accounts for the coating's tendency to crack and spall. When compared to substrate alloys in the uncoated condition, lower strengths and higher impact sensitivities are observed.

In view of these deficiencies, it is desirable to predict and control the composition of the coating and its likely degree of interaction with substrate phases under the thermal and gas phase environments imposed during fabrication. In approaching this problem, a general calculation method based on equilibrium thermodynamic considerations will be presented and applied to selected systems.

B. LITERATURE REVIEW

For a comprehensive compilation of chemical vapor deposition literature with emphasis on the production of coatings, C. Powell's et al. "Vapor Plating"(1) may be consulted. A more recent book by Powell et al., entitled "Vapor Deposition"(2), is again descriptive in nature and includes many literature citations. Here, emphasis has been placed on developments in transport and nucleation phemonena as applied to the growth of coatings or crystals from the vapor phase by either physical or chemical deposition. In addition, numerous examples are given for the chemical vapor deposition of elemental and alloy phases.

The first investigations concerning the chemical vapor deposition of refractory materials were made in the incandescent lamp industry. Aylsworth(3), de Lodyguine(4), van Arkel(5), van Arkel and de Boer(6), and Moers(7) investigated the formation of refractory metal coatings via various metal halide reduction or decomposition reactions.

For refractory transition metal-interstitial phases, again, van Arkel and de Boer(5,6) reported the first experiments in which the carbides and nitrides of titanium, zirconium, and tantalum were formed from the vapor phase. In addition, Moers(7) extended the method to include several borides, carbides, and nitrides of transition metals. For the phases of titanium carbide and nitride, Pollard and Woodward(8,9) investigated their growth on tungsten filaments. References and examples are given by Powell et al.(2) for the formation of vapor deposited metal oxides on heated surfaces subjected to various oxidizing atmospheres containing either metal halide or organometallic vapors.

Protective coatings constitute the subject of the following references. The vapor phase coating of various transition and ferrous metal elements, a variety of alloy steels, graphite, oxides, and carbides was investigated by Campbell, Powell, Nowicki and Gonser[10].

The general conditions and apparatus for applying coatings of refractory metals, borides, carbides, nitrides, oxides, and silicides on the above substrates were given, and substrate-coating characteristics of grain size, adherence, deposition rate and efficiency, and coating uniformity were evaluated as a function of the deposition temperature, and gas phase composition and purity. The chemical vapor deposition processes consisted of reducing and reacting a volatile metal compound, either a metal halide or carbonyl, at a heated substrate. Munster and Ruppert(11) and Munster and Sagel(12), utilizing the same techniques employed by Campbell et al.(10), investigated the properties of TiC and TiN coatings on steel.

In the above references, little information was presented on utilizing thermodynamic techniques to evaluate and analyze the chemical vapor deposition process. Exceptions were found in the work conducted by Robinson(13), and Nickl and Reichle(14,15). The former investigator studied the kinetics and morphology of TiN coatings on Mo substrates by the overall reaction

$$TiCl_{4(g)} + 1/2N_{2(g)} + 2H_{2(g)} = TiN_{(s)} + 4HCl_{(g)}.$$

The effect of lower chlorides of titanium was also investigated by calculating their equilibrium partial pressures as a function of temperature and initial partial pressures of reactive gas phase species. The latter investigation was similar, except the morphology, yield and thermodynamics of TiC coatings on both graphite and Ta substrates were studied according to the reaction

$$TiCl_{4(g)} + CCl_{4(g)} + H_{2(g,excess)} \rightarrow TiC_{(s)} + HCl_{(g)} \ldots$$

As for the specific technique of applying protective coatings to sintered carbide tool alloys, information in the available literature is scarce. Because of the extreme importance of these macrocomposite systems to the metal working industry, their development has received extensive commercialization. This has resulted in reporting in the form of generalizations as to property and performance data, but a lack of reporting of processing and technical data because of proprietary aspects. In this light, the following development related literature citations may be consulted.

The first titanium carbide coated tool alloys of commercial importance were developed by Swedish(16,17) and German(18) carbide producers. Since their introduction, Schintlmeister and Pacher(19), and Peterson(20) reported on chemically vapor deposited Ti(C,N), and TiN coatings, respectively. Prior to these reports, Kieffer et al.(21) presented some deposition conditions for the formulation of sintered carbide substrate — group IV, V. transition metal nitride and carbonitride coating composites, and their mechanical and wear properties were discussed. Glaski et al.(22) reported on the coating of tungsten carbide with double layers of Ta, Mo, or W plus TiC or HfC; Lee and

and Richman(23) presented information regarding the formation of TiC coatings on a sintered WC + 6 wt.% Co alloy. In addition to the chemical vapor deposition technique, Suh et al.(24-26) reported on increasing the service life of carbide cutting tools by treating their surfaces (vacuum sintering process) with various oxides, e.g., TiO_2, ZrO_2, Cr_2O_3, and Al_2O_3.

C. THERMODYNAMIC CONSIDERATIONS

In this section, the work of Prigogine and Defay(27) may be consulted for background information on derived relationships and also used as an appendix for the derivation of specific thermodynamic formulae. Most of the original work on their approach to chemical thermodynamics was conducted by DeDonder(28,29).

1. Definition of System

For the process of chemical vapor deposition, its thermodynamic interpretation is usually restricted to calculating free energy changes and equilibrium constants for a candidate reaction. The data thus obtained are used to show the relative extent to which a reaction as written will proceed at a given temperature and pressure.

The above approach is primarily used for screening candidate reactions and designing systems, but it can be extended to include the calculation of theoretical yields as a function of the deposition temperature and initial partial pressures of reactive gas phase species.

Since there is currently no way of precalculating the kinetics of chemical vapor deposition reactions without experimental data, deposition rates will be proportional to the total gas feed rate. Hence, these calculations will give an upper limit for the deposition efficiencies and the correct gas phase mixtures to deposit a preselected alloy composition.

In contrast to chemical vapor deposition processes carried out in open thermodynamic systems, the equilibrium calculations to be presented will refer to a closed system of fixed material content. The state of this system will be defined by the two physical variables of temperature (T) and total pressure (p), and a chemical variable (ξ), extent of a reaction or "degree of advancement of a reaction"(27, 29). For establishing whether a given chemical reaction will proceed in a particular direction, consideration of the uncompensated heat or entropy production will be required, and this will introduce the function of state A (affinity)(27, 28).

In order to approximate an open system, one may consider a process in which the initial gas phase reactants exhibit a constant feed rate to and long dwell time in a reaction vessel so that a closed system equilibrium state may be duplicated. That is, in addition to both mechanical and thermal equilibrium, the system is in a state of internal equilibrium with respect to the chemical reaction(s) and distribution of matter in the gas phase.

For the above, inert container walls are assumed, and the following conditions are imposed on the components participating in the reaction: (1) all vapor phase reaction components behave as ideal gases; (2) the vapor pressure of any chemically deposited solid phase is negligible compared to the concentration of gas phase species.

2. Extent of Reaction

The following relationship may be written for a closed system in which a single chemical reaction occurs involving (c) components of which there are (r) reactants and (c-r) products.

$$\nu_1 R_1 + \ldots \nu_r R_r \rightarrow \nu_{r+1} P_{r+1} + \ldots \nu_c P_c \qquad (1)$$

The $\nu_1, \ldots \nu_c$ are the respective stoichiometry parameters for the components 1, ...c. At a given temperature and pressure for which the initial number of reactant moles n_{oi} $(i=1, \ldots r)$ and product moles $n_{\epsilon j}$ $(j=r+1, \ldots c)$ are constant and zero, respectively, the differential increments (dn) for all (c) components at some time $t>0$ can be related to each other through the incremental change in the extent of reaction, $d\xi$. Selecting a reactant and product component with their corresponding stoichiometry coefficients, the following relationship may be written

$$dn_{\epsilon j} = \frac{\nu_j}{\nu_i} n_{oi} \, d\xi , \ (j \neq i). \qquad (2)$$

Upon integrating, equation (2) becomes

$$n_{\epsilon j} = \frac{\nu_j}{\nu_i} n_{oi}\xi, \quad (j=r+1,\ldots.c). \tag{3}$$

By observing stoichiometry and the fact that for the overall reaction the total mass of the closed system remains constant, the increase in number of moles ($n_{\epsilon j}$) of component j is proportional to the number of moles (n_{oi}) of component i which participated in the reaction. The extent of reaction is defined in terms of an arbitrary initial composition of n_{oi} moles of any component $i=1,\ldots r$ for which at time zero, ξ is defined as zero. If at some later time the state of the system can proceed to $\xi = 1$, complete conversion of all reactants to products will have occurred.

Similarly for reactants at some time $t>0$, equation (2) becomes

$$-dn_{\epsilon j} = \frac{\nu_j}{\nu_i} n_{oi}\, d\xi, \; (j= i). \tag{4}$$

If the chemical reaction as written proceeds from left to right, $d\xi>0$, $dn_{\epsilon j}<0$; and vice versa. Integrating (4) and letting $t=0$, $\xi=0$ and $n_{\epsilon j}=n_{oj}$,

$$n_{\epsilon j} = n_{oj} - \frac{\nu_j}{\nu_i} n_{oi}\,\xi, \; (j=1,\ldots r). \tag{5}$$

Instead of selecting a specific reactant n_{oi} to follow the differential increments in $n_{\epsilon j}$ as a function of the change in the extent of reaction, equations (2) and (4) may be combined and equated to a common $d\xi$. Now, $d\xi$ relates the mole changes of all components to their corresponding stoichiometry coefficients, i.e.,

$$-\frac{dn_{\epsilon 1}}{\nu_1} = \ldots -\frac{dn_{\epsilon r}}{\nu_r} = \frac{dn_{\epsilon r+1}}{\nu_{r+1}} = \ldots \frac{dn_{\epsilon c}}{\nu_c} = d\xi \ . \tag{6}$$

This relationship is the same given by Prigogine$^{(27)}$, but its integrated form is more difficult to work with when calculating equilibrium ξ values for selected chemical vapor deposition reactions.

After the introduction of a fixed quantity of reactants into a closed system held at a constant temperature and pressure, the change in ξ as the reaction proceeds will only be a function of time, i.e., $\xi = \xi(t)$. Differentiating (3) with respect to time,

$$\frac{dn_{\epsilon j}}{dt} = \frac{\nu_j}{\nu_i} \ n_{oi} \left(\frac{d\xi}{dt}\right)_{T,p,n_{oi}} . \tag{7}$$

The term $\left(\frac{d\xi}{dt}\right)_{T,p,n_{oi}}$ is defined as the reaction rate or velocity$^{(27)}$. At equilibrium, it equals zero; and the resulting equilibrium extent of reaction, ξ_e, is uniform throughout the system.

In general, the reaction velocity given in (7) and the equilibrium extent of reaction are functions of the independent variables of temperature, pressure, and composition, i.e.,

$$\xi_e = \xi_e\,(T, p, n_{oi}) \tag{8}$$

or

$$\xi_e = \xi_e\,(T, p_{oi}),$$

where $\sum_1^r p_{oi} = p$, total system pressure.

For chemical vapor deposition processes of interest in which at least one of the product phases is a solid, equation (7) only pertains to the rate at which the reaction process approaches equilibrium. Once reached, a deposition rate R_j for the production of a solid product phase $n_{\epsilon j}$ according to (1) and (3) may be defined by

$$R_j = \frac{dn_{\epsilon j}}{dt} = \frac{\nu_j}{\nu_i}\,\xi_e\,\frac{dn_{oi}}{dt}\quad, \tag{9}$$

where ξ_e is from (8). Letting $dn_{oi} = \frac{p_{oi}}{RT}\,dV_o$ and substituting into (9),

$$R_j = \frac{\nu_j}{\nu_i}\,\frac{p_{oi}\xi_e}{RT}\left(\frac{dV_o}{dt}\right)_{T,p,n_{oi}}\,. \tag{10}$$

The validity of (10) is based on the following approximation. By controlling the total gas feed rate $\left(\frac{dV_o}{dt}\right)_{T,p,n_{oi}}$, the dwell time for the initial gas phase mixture in a reaction chamber can be made long compared to the time required for the system to reach equilibrium. Since the consumed reactants are continually replaced, a series of identical closed thermodynamic systems is approximated through an open system.

Therefore for a given total gas feed rate, temperature, and pressure, the deposition rate R_j will be proportional to the product $(p_{oi}\ \xi_e)$. This term may be defined as an effective yield or deposition efficiency. If the calculated value for ξ_e is small for an initial composition, the yield may still be increased by using a higher p_{oi} partial pressure.

Instead of utilizing mole masses, the partial pressure of gas phase components may be calculated from

$$P_{\epsilon j} = \left(\frac{n_{\epsilon j}}{n_{oi}}\right) p_{oi} \left(\frac{Vo}{V\epsilon}\right)_{T,p} . \tag{11}$$

Equation (11) combined with (3) and (5) will give the partial pressures of reactants and products in terms of an initial pressure, the stoichiometry parameters, and extent of reaction for the chemical reaction (1). Since the total system pressure is constant,

$$\left(\frac{Vo}{V\epsilon}\right)_{T,p} = \frac{\Sigma n_{oi}}{\Sigma n_{\epsilon j}} , \tag{12}$$

and for most deposition reactions considered, $\left(\frac{Vo}{V\epsilon}\right)_{T,p} \approx 1$.

If the overall reaction does not represent the process considered, the above relationships may be expanded to include several simultaneous but independent reactions each with its own extensive variable ξ_α , where the subscript refers to a set of α independent equations.

3. Chemical Equilibrium

a. Conditional Equations

A completely general approach of the definition of thermodynamic processes(27), i.e., reversible (equilibrium) and irreversible (natural) processes, is to consider the production of entropy or uncompensated heat resulting from a chemical reaction. This approach introduces the function of state A (affinity) which characterizes the state of the system at a particular instant.

The affinity A may be related to the state functions F(T, V) and G(T,P), as well as U(S,V), S(U,V), and H(S,P), which are suitable indicators for establishing criteria for equilibrium. Since the type of physical change or process considered dictates the choice of the proper indicator, utilization of the previous relationships involving the independent system variables of T,p, n_{oi}, and ξ requires conditional equations which relate the affinity to the Gibbs free energy, G.

It may be shown for a closed thermodynamic system that the affinity relates the change in the uncompensated heat (dQ) of a chemical reaction to the extent of reaction (dξ) at any instant through

$$dQ = A d\xi \geq 0, \tag{13}$$

where A is defined by

$$-A = \left(\frac{\partial G}{\partial \xi}\right)_{T,p} = \left(\frac{\partial H}{\partial \xi}\right)_{T,p} - T\left(\frac{\partial S}{\partial \xi}\right)_{T,p} , \tag{14}$$

the energy change per unit reaction at constant (T,p). Since (dQ) is a measure of the unavilability of energy or production of entropy within a system and equals the difference between the entropy and reversible heat, i.e., $dQ = TdS - dQ_r$, $dQ > 0$ for all irreversible or spontaneous changes, and $dQ = 0$ for all reversible or equilibrium changes. A criterion for equilibrium is then $dQ \leq 0$ and includes unnatural processes that tend away from equilibrium.

The affinity of a given chemical reaction (1) can be represented by the following

$$A = A(T, p, n_{oi} \ldots . n_{or}),$$

or, once all the initial mole masses are fixed and due to the integrated form of (2), (4), or (6),

$$A = A(T, p, \xi). \tag{15}$$

At equilibrium (13), the function

$$A(T,p,\xi) = 0 \tag{16}$$

defines a surface, i.e., variations in T,p, and ξ are no longer independent and equation (16) gives an implicit functional relationship between them. Therefore, (16) may be solved for one variable in terms of the other two, e.g., as previously presented (8), $\xi_e = \xi_e\,(T,p,n_{oi}\ldots n_{or})$.

In order to obtain ξ_e, (15) as a function of (T,p_{oi}) may be calculated from the chemical potentials of elements or phases participating in a reaction. Considering again the chemical reaction (1) and relationships (6) and (14) combined with the total differentials of $G = G(T,p,n_1\ldots.n_c)$ and $G = G(T,p,\xi)$ for open and closed systems, respectively, it may be shown that

$$A = -\left(\frac{\partial G}{\partial \xi}\right)_{T,p} = -\sum_{i=1}^{c}\left(\frac{\partial G}{\partial n_i}\right)_{T,p}\frac{dn_i}{d\xi} = -\sum_{i=1}^{c}\nu_i\mu_i \tag{17}$$

After Gibbs, the partial molar quantity is equal to the chemical potential of component i at constant (T,p).

For A = 0, (17) corresponds to the well known thermodynamic relationship for the equilibrium state,

$$\sum_{i=1}^{c}\nu_i\mu_i = 0\ , \tag{18}$$

i.e., the criterion for equilibrium in a system of c chemically reacting constituents. For a spontaneous reaction (13), the average value of the affinity calculated from (17) equals the decrease in the Gibbs free energy. Therefore, (17) or (18) show that the thermodynamic properties of a system are uniquely defined at any instant if the various μ_i's are known.

By evaluating the equilibrium extent of reaction (ξ_e) as a function of either the temperature, pressure, or composition through (18), upper limits for the deposition efficiency and the correct gas phase composition to form a preselected alloy from the vapor phase can be calculated. As for the evaluation of reaction kinetics, a comparison of theoretical and experimental yields is required.

b. Stability

Though limited in nature, relative kinetic data may be obtained through evaluating the stability of a chemical equilibrium state. A knowledge of the variation in the affinity about an equilibrium state characterized by a certain T,p, and ξ may be used to calculate the energy change of the system per an infinitesimal change in the extent of reaction, i.e., $\left(\frac{\partial A}{\partial \xi}\right)_{T,p}$. The magnitude of this term may then be viewed as an activation energy or driving force for the process.

A continuous transition from state (1) to a second state (2) can be conducted by means of the following infinitesimal changes in the independent variables $\delta T = T_2 - T_1$, $\delta p = p_2 - p_1$, and $\delta\xi = \xi_2 - \xi_1$. From equation (13), $\delta Q = (Q_2 - Q_1) > 0$ characterizes a spontaneous process; but, if state (1) is stable, $\delta Q < 0$.

For either positive or negative perturbations in the extent of reaction combined with the necessary and sufficient condition for equilibrium (16), it may be shown that state (1) is stable if both

$$A_1 = 0$$

and

$$\left(\frac{\partial A}{\partial \xi}\right)_{T_1, p_1} < 0 \tag{19}$$

Comparing (19) with (14).

$$A = -\left(\frac{\partial G}{\partial \xi}\right)_{T,p} = 0 \quad ;$$

$$\left(\frac{\partial A}{\partial \xi}\right)_{T,p} = -\left(\frac{\partial^2 G}{\partial \xi^2}\right)_{T,p} < 0 \quad . \tag{20}$$

(20) signifies that the variation in G as a function of ξ exhibits a concave up free energy surface and a minimum at ξ_e.

c. Equilibrium Displacements

The characterization of a stable equilibrium state by (20) may also be used to investigate how this state is influenced by changes in either the temperature, pressure, or initial composition of a system. Specifically, the change in the extent of reaction as a function of either the temperature, pressure, or composition is of interest.

Consider two stable equilibrium states with affinities $A_1 = A_2 = 0$ that differ by the independent variable changes of δT, δp, and $\delta \xi$. If all intermediate states at any instant during a transition from (1) to (2) exhibit stable equilibria, then $\delta A = (A_2 - A_1) = 0$. Utilizing these arguments and the total differential of $A = A(T,p,\xi)$, the following two relationships may be used to evaluate equilibrium displacements in a closed system for which $\left(\frac{\partial A}{\partial \xi}\right)_{T,p} < 0$.

(1) Constant temperature,

$$\left(\frac{\delta \xi}{\delta p}\right)_T = \frac{\left(\frac{\partial V}{\partial \xi}\right)_{T,p}}{\left(\frac{\partial A}{\partial \xi}\right)_{T,p}} \quad , \tag{21}$$

where the volume change of a reaction is related to the partial molar volume of each reactant and product through (6).

$$\left(\frac{\partial V}{\partial \xi}\right)_{T,p} = \sum_i \left(\frac{\partial V}{\partial n_i}\right)_{T,p} \frac{dn_i}{d\xi} = \sum_i \nu_i v_i \quad .$$

(2) Constant pressure,

$$\left(\frac{\delta\xi}{\delta T}\right)_p = -\frac{1}{T}\frac{\left(\frac{\partial H}{\partial \xi}\right)_{T,p}}{\left(\frac{\partial A}{\partial \xi}\right)_{T,p}} \quad ; \tag{22}$$

likewise for the heat of reaction,

$$\left(\frac{\partial H}{\partial \xi}\right)_{T,p} = \sum_i \left(\frac{\partial H}{\partial n_i}\right)_{T,p} \frac{dn_i}{d\xi} = \sum_i \nu_i h_i \quad .$$

As an example, (22) says that increasing the temperature for an endothermic reaction will advance it to the product side and vice versa for an exothermic reaction.

Similarly for equilibrium displacements in an ideal open system where $A = A\,(T,p,n_i)$, the change in the extent of reaction $(\delta\xi)$ due to the external addition of a component $j(\delta n_j^{ex})$ may be represented by the following relationship

$$\left(\frac{\delta\xi}{\delta n_j^{ex}}\right)_{T,p} = \frac{RT}{\left(\frac{\partial A}{\partial \xi}\right)_{T,p}}\left(\frac{\nu_i}{n_j} - \frac{\nu}{n}\right) \quad . \tag{23}$$

All other composition variations in the components $n_{i \neq j}$ are held constant, ν equals the algebraic sum of the stoichiometry coefficients for the reaction considered, and n equals the total number of moles in the system. Converting from mole masses to pressures, (23) becomes

$$\left(\frac{\delta \xi}{\delta p_j^{ex}}\right)_{T,p} = \frac{RT}{\left(\frac{\partial A}{\partial \xi}\right)_{T,p}} \left(\frac{\nu_j}{p_j} - \frac{\nu}{p}\right) . \qquad (24)$$

Since $\left(\frac{\partial A}{\partial \xi}\right)_{T,p}$ is always negative for a stable system, the sign of the bracketed term on the right side of (23) and (24) must be examined in order to determine the effect of (δn_j^{ex}) on the equilibrium position. Not only will its sign depend on the reaction considered, i.e., the values of ν_j and ν, but at times on the equilibrium concentration of component (j).

Equations (21-24) can be applied to chemical vapor deposition reactions for the purpose of investigating how a coating-gas phase equilibrium is effected by perturbations in any one of the independent variables of temperature, pressure, or composition. The information obtained is in the form of either a positive or negative change in the variable of interest and not its magnitude.

In general, the given thermodynamic relationships based on gross energy changes in equilibrium systems provide a means for evaluating and establishing reaction conditions for complicated deposition processes. They do not, however, predict reaction yields or kinetics in a quantitative manner since no consideration has been given to atomic or molecular processes.

D. SELECTED CHEMICAL VAPOR DEPOSITION SYSTEMS

Refractory transition metal-interstitial alloys (carbides, nitrides or oxides) as protective coatings are readily fabricated through the chemical vapor deposition technique. This process is usually conducted in a resistively heated reaction chamber where the reactive gas feed rate (10) to it is controlled by suitable flowmeters or gas metering system with associated purification train. An example of such an apparatus, utilized to investigate chemically deposited titanium nitride on sintered carbide and tool steel alloys, is presented in Figure 1 (flowmeters not shown).

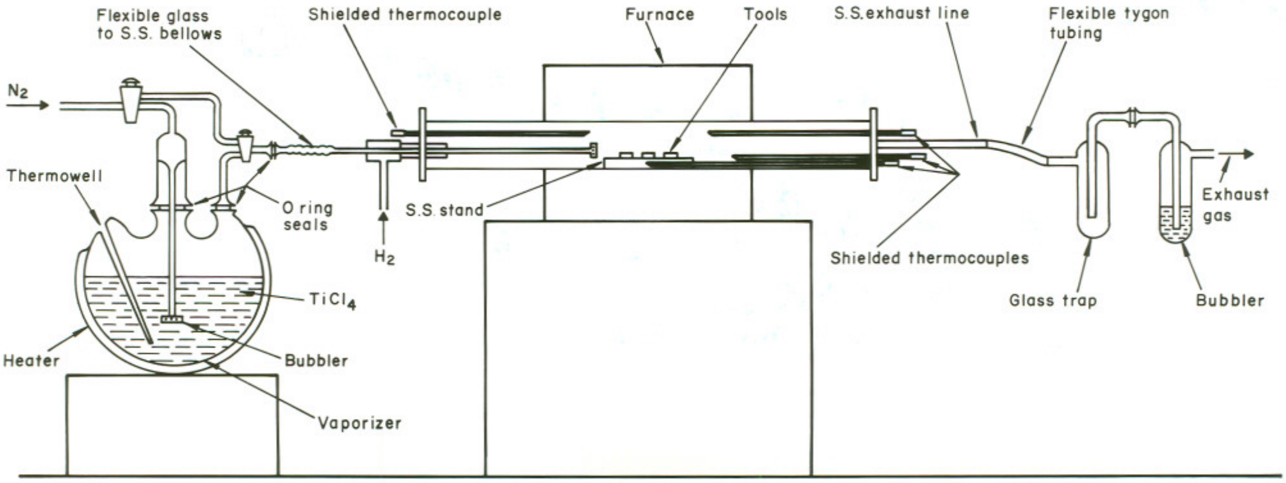

Figure 1. Schematic Diagram of TiN Chemical Vapor Deposition Unit.

As depicted in this schematic diagram, the shielded thermocouples are adjustable so that the temperature profile from input mixing of the reactants to exhaust gases can be continuously monitored and controlled during an experimental run. For coatings other than indicated, different vaporizer systems as well as injectors for the mixing of two or more gas streams can be incorporated into a system of this type. Depending on the volatile metal source, e.g. the chlorination of a metal or the direct use of a metal halide or carbonyl as an input for the formation of a carbide, nitride, or oxide, the type of alloy coating will dictate the choice of suitable mixing gases which may be reducing, oxidizing, and/or neutral in character.

Before proceeding with some example calculations, a listing of terms used is presented in Table I. These symbols are consistent with those previously presented in the text (Section C).

Table I. Listing of Symbols Used in Chemical Vapor Deposition Calculations

T	Temperature, °K
R	Gas constant
$\Delta G^{\circ}_{R(k)}$	Standard Gibbs free energy change for reaction (k).
$K_{p(k)}$	Equilibrium constant determined by a set of partial pressures characterizing the equilibrium state for reaction (k).
n_{oi}	Initial number of reactant moles, component i.
$n_{\epsilon i}$	Final number of reactant or product moles, component i.
P_{oi}	Initial partial pressure of component i.
$P_{\epsilon i}$	Final partial pressure of component i.
P	Total system pressure
ξ_j	Extent of reaction or yield with respect to a component j, i.e. molar fraction of reactant i converted to product j.
$100\ P_{oi}\xi_j$	Relative maximum deposition efficiency (not limited by reaction kinetics).

1. Carbides of the Type MeC

A reaction leading to the formation of transition metal monocarbides may be represented by

$$MeCl_{4(g)} + CH_{4(g)} + (H_2)^{exc.}_{(g)} = MeC_{(s)} + 4HCl_{(g)} + (H_2)^{exc.}_{(g)} \quad , \qquad (25)$$

where the volatile metal source is a tetrachloride, e.g., of a group IV metal (Me = Ti, Zr, Hf), and the carbon source is methane.

As indicated (25), the presence of excess hydrogen is required to suppress the deposition of elemental carbon via

$$CH_{4(g)} \rightarrow C_{(s)} + 2H_{2(g)} \quad , \qquad (26)$$

$$\Delta G_{R(26)} = \Delta G^o_{R\ (26)} + RT \ln \frac{P^2_{\epsilon\ ,H_2}}{P_{\epsilon\ ,CH_4}}$$

Defining the mole fraction of $CH_{4(g)}$ converted to $C_{(s)}$ by ξ_c, expressions (3) and (5) yield

$$\begin{aligned} n_{\epsilon\ CH_4} &= n_{0CH_4}(1-\xi_c) \\ n_{\epsilon\ C} &= n_{0CH_4}\ \xi_c \\ n_{\epsilon H_2} &= 2n_{0CH_4}\ \xi_c \ . \end{aligned}$$

Converting from moles to partial pressures with the aid of (11) and (12),

$$P_{\epsilon CH_4} = P_{0CH_4}(1-\xi_c)\left(\frac{V_o}{V_\epsilon}\right)_{T,p}$$

$$P_{\epsilon H_2} = 2P_{0CH_4}\xi_c\left(\frac{V_o}{V_\epsilon}\right)_{T,p} \quad , \tag{27}$$

where

$$\left(\frac{V_o}{V_\epsilon}\right)_{T,p} = \frac{1}{1+\xi_c} \quad .$$

When the side reaction (26) reaches an equilibrium state characterized by (16), and upon substituting (27) into $K_{p(26)}$ and rearranging terms,

$$\xi_c = \left(\frac{K_p}{4P_{0CH_4} + K_p}\right)^{0.5} \quad . \tag{28}$$

(27) now becomes

$$P^{max}_{\epsilon CH_4} = P_{0CH_4}\left(\frac{1-\xi_c}{1+\xi_c}\right)$$

$$P^{min.}_{\epsilon H_2} = P_{0CH_4}\left(\frac{2\xi_c}{1+\xi_c}\right) \quad , \quad \text{or}$$

$$\left(\frac{P^{min}_{\epsilon H_2}}{P^{max}_{\epsilon CH_4}}\right)_{T,p} = \frac{2\xi_c}{1-\xi_c} \quad . \tag{29}$$

$P^{max}_{CH_4}$ and $P^{min}_{H_2}$ are, respectively, the maximum methane and minimum hydrogen partial pressures necessary to prevent the formation of elemental carbon, or their equilibrium ratio defines the maximum allowable carbon limit.

Using relationships (28) and (29) and letting the system pressure remain constant at one atmosphere, the following data were calculated for the methane pyrolysis reaction as a function of temperature (Table II). The data presented should only be used as a guide, and to be on the safe side the equilibrium hydrogen to methane ratio utilized should be larger than those indicated.

Returning to the chemical vapor deposition of MeC, assume that reaction (26) has gone to completion and now the metal chloride source is introduced to the reactive gas phase mixture. Relabeling with respect to the overall reaction (25), the following relationships characterize an equilibrium state when $A(T,p,\xi) = 0$,

$$\Delta G^{o}_{R\,(25)} = -RT \ln K_{p(25)},$$

$$K_{p(25)} = \frac{P^4_{\epsilon HCl}}{P_{\epsilon MeCl_4} P_{\epsilon CH_4}} \quad . \tag{30}$$

The initial conditions imposed on the reactants are

Table II. Maximum Allowable Carbon Limit in Order to Avoid Deposition of Free Carbon

Reaction: $CH_4(g) = C_{(s)} + 2H_2(g)$

$$\Delta G^o_R = 22{,}022 - 26.60\ T\ \text{(cal per mole)}^{(30,31)}$$

Condition: $P_{0CH_4} = 1$ atm.

T, °K	ξ_c	$\left(\frac{P_{\epsilon H_2}}{P_{\epsilon CH_4}}\right)_{T,p}$
1000	0.845	10.90
1200	0.970	65.67
1400	0.992	249.00
1500	0.995	399.00

$$\left(\frac{P_{0H_2}}{P_{0CH_4}}\right)_{T,p} \geq \left(\frac{K_{p(26)}}{P_{0CH_4}}\right)^{0.5}$$

$$P_{0MeCl_4} + P_{0CH_4} + P_{0H_2} = P \quad ;$$

$$\frac{P_{0MeCl_4}}{P_{0CH_4}} = X\text{(stoichiometry parameter)}.$$

Defining the extent of reaction for (25) by

$$\xi_{MeC} = \frac{n_{\epsilon MeC}}{n_{0MeCl_4}} \quad ,$$

partial pressure relationships of the type previously derived for the methane pyrolysis reaction (27) may be calculated

$$P_{\epsilon MeCl_4} = P_{0MeCl_4}(1-\xi_{MeC})\left(\frac{V_o}{V_\epsilon}\right)_{T,p} \tag{31}$$

$$P_{\epsilon CH_4} = P_{0CH_4}(1-X\,\xi_{MeC})\left(\frac{V_o}{V_\epsilon}\right)_{T,p}$$

$$P_{\epsilon HCl} = 4\,P_{0MeCl_4}\,\xi_{MeC}\left(\frac{V_o}{V_\epsilon}\right)_{T,p}$$

where

$$\left(\frac{V_o}{V_\epsilon}\right)_{T,p} = \left(1+\frac{2P_{0MeCl_4}\xi_{MeC}}{P}\right)^{-1}.$$

Substituting (31) into (30) and rearranging terms, theoretical yields for the deposition of MeC phases are calculable through

$$\xi^4_{\mathrm{MeC}} - \frac{K_{p(25)}(1-\xi_{\mathrm{MeC}})(1-X\,\xi_{\mathrm{MeC}})}{256\ X\ p^2_{0\mathrm{MeCl}_4}} \left(\frac{V_\epsilon}{V_o}\right)^2_{T,p} = 0\ . \qquad (32)$$

As an example, theoretical yield data for TiC are presented in Table III. The volume ratio term from (31) was set equal to unity for these calculations, because the magnitude of $(P_{0\mathrm{TiCl}_4}\xi_{\mathrm{TiC}})$ was considered to be insignificant compared to the total system pressure of roughly one atmosphere. The $P^{\mathrm{max}}_{0\mathrm{CH}_4}$ values are consistent with the data presented in Table II. In addition, TiCl_4 partial pressures normally used during experimental runs are < 0.100 atmosphere.

Table III. Theoretical Yields for the Chemical Vapor Deposition of TiC.

Reaction: $TiCl_{4(g)} + CH_{4(g)} + (H_2)_{(g)}^{\text{exc.}} = TiC_{(s)} + 4HCl_{(g)} + (H_2)_{(g)}^{\text{exc.}}$

$\Delta G_R^o = 70,580 - 58.00\ T$ (cal/formula change)$^{(30,31,3\ell)}$

Conditions: $P_{0TiCl_4} + P_{0CH_4} + P_{0H_2} \approx 1$ atmosphere

$\left(\frac{P_{0H_2}}{P_{0CH_4}}\right)_{\min}$ = Minimum allowable hydrogen to methane ratio to prevent deposition of free carbon.

$X = \frac{P_{0TiCl_4}}{P_{0CH_4}}$ = Stoichiometry parameter.

A. $T = 1000°K, \left(\frac{P_{0H_2}}{P_{0CH_4}}\right)_{\min.} = 10.90$

P_{0TiCl_4}	X	ξ_{TiC}	$100P_{0TiCl_4}\xi_{TiC}$
0.001	10	~0.100	~0.010
0.010		0.099	0.099
0.100		0.068	0.680
0.457(0.045)*		0.037	1.691
0.0001	1	0.965	~0.010
0.001		0.773	0.077
0.005		0.508	0.254
0.010		0.398	0.398
0.050		0.205	1.025
0.077(0.077)*		0.169	1.301
0.0001	0.1	~1.000	~0.010
0.001		0.985	0.099
0.005		0.822	0.411
0.008(0.083)*		0.726	0.581

B. T = 1200°K, $\left(\frac{P_{0H_2}}{P_{0CH_4}}\right)_{min.} = 65.67$

P_{0TiCl_4}	X	ξ_{TiC}	$100P_{0TiCl_4}\xi_{TiC}$
0.001	10	~0.100	~0.010
0.010		~0.100	~0.100
0.100		0.099	0.999
0.130 (0.013)*		~0.099	~1.287
0.0001	1	0.998	~0.010
0.001		0.981	0.098
0.010		0.856	0.856
0.015 (0.015)*		0.809	1.214
0.0001	0.1	~1.000	~0.010
0.0015 (0.015)*		~0.999	~0.150

C. T = 1400, $\left(\frac{P_{0H_2}}{P_{0CH_4}}\right)_{min} = 249.00$

P_{0TiCl_4}	X	ξ_{TiC}	$100P_{0TiCl_4}\xi_{TiC}$
0.038 (0.004)*	10	~0.100	~0.380
0.0001	1	~1.000	~0.010
0.001		0.997	~0.100
0.004 (0.004)*		0.991	0.396
0.0004 (0.004)*	0.1	~1.000	~0.040

D. T = 1500°K, $\left(\frac{P_{0H_2}}{P_{0CH_4}}\right)_{min} = 399.00$

P_{0TiCl_4}	X	ξ_{TiC}	$100P_{0TiCl_4}\xi_{TiC}$
0.024 (0.0024)*	10	~0.100	~0.240
0.0025 (0.0025)*	1	0.998	0.250
0.0002 (0.0025)*	0.1	~1.000	~0.020

*P^{max}_{0,CH_4} = maximum allowable methane partial pressure consistent with $\left(\frac{P_{0,H_2}}{P_{0,CH_4}}\right)_{min}$.

2. Nitrides of the Type MeN

The mononitrides of the transition metals, e.g., the group IV elements, may be formed from the vapor phase via the overall reaction

$$MeCl_{4}(g) + 2H_{2(g)} + \frac{1}{2} N_{2(g)} = MeN_{(s)} + 4HCl_{(g)} \quad . \tag{33}$$

Unlike the deposition of the monocarbides, side reactions resulting in the formation of solid phases other than MeN do not have to be considered.

Proceeding in the same manner as presented for MeC, (31), the following partial pressure relationships consistent with the overall reaction (33) result when ξ_{MeN} is defined by $n_{\epsilon MeN}/n_{0MeCl_4}$:

$$P_{\epsilon MeCl_4} = P_{0MeCl_4} (1-\xi_{MeN}) \left(\frac{V_o}{V_\epsilon}\right)_{T,p} \tag{34}$$

$$P_{\epsilon H_2} = P_{0H_2} (1-2 \frac{P_{0MeCl_4}}{P_{0H_2}} \xi_{MeN}) \left(\frac{V_o}{V_\epsilon}\right)_{T,p}$$

$$P_{\epsilon N_2} = P_{0N_2} (1-\frac{1}{2} Y \xi_{MeN}) \left(\frac{V_o}{V_\epsilon}\right)_{T,p}$$

$$P_{\epsilon HCl} = 4P_{0MeCl_4} \xi_{MeN} \left(\frac{V_o}{V_\epsilon}\right)_{T,p}$$

where

$$\left(\frac{V_o}{V_\epsilon}\right)_{T,p} = \left(1 + \frac{1}{2} \frac{P_{0MeCl_4}\xi_{MeN}}{P}\right)^{-1}$$

$$P_{0MeCl_4} + P_{0H_2} + P_{0N_2} = P$$

$$\frac{P_{0MeCl_4}}{P_{0N_2}} = Y \quad \text{(stoichiometry parameter)}$$

Substituting (34) into the relationship for $K_{p(33)}$ and rearranging terms,

$$\xi^4_{MeN} - \frac{K_{p(33)} P^2_{0H_2} (1-\xi_{MeN})(1-2\,\frac{P_{0MeCl_4}}{P_{0H_2}}\,\xi_{MeN})^2 (1-\frac{1}{2}\,Y\xi_{MeN})^{0.5}}{256\ \ Y^{0.5}\, P^{2.5}_{0MeCl_4}} \left(\frac{V_\epsilon}{V_o}\right)^{0.5}_{T,p} = 0. \quad (35)$$

Following the same considerations as applied to the TiC phase, theoretical yield data for the deposition of TiN were calculated with (35) and are presented in Table IV.

Table IV. Theoretical Yields for the Chemical Vapor Deposition of TiN

Reaction: $TiCl_{4(g)} + \frac{1}{2} N_{2(g)} + 2H_{2(g)} = TiN_{(s)} + 4HCl_{(g)}$

$\Delta G^{o}_{R} = 12,230 - 12.62\ T$ (cal/formula change)$^{(30,31,32)}$

Conditions: $P_{0TiCl_4} + P_{0N_2} + P_{0H_2} \approx 1$ atmosphere

$$Y = \frac{P_{0TiCl_4}}{P_{0N_2}} = \text{Stoichiometry parameter}$$

A. T = 1000°K

P_{0TiCl_4}	Y	ξ_{TiN}	$100\ P_{0TiCl_4}\ \xi_{TiN}$
0.010	20	~0.100	~0.100
0.100		~0.100	~1.000
0.200		~0.100	~2.000
0.001	2	~1.000	~0.100
0.010		0.979	0.979
0.050		0.794	3.970
0.100		0.609	6.090
0.150		0.487	7.305
0.200		0.400	8.000
0.286*		0.294	8.408
0.001	0.2	~1.000	~0.100
0.010		0.999	0.999
0.050		0.902	4.510
0.100		0.578	5.780
0.150		0.199	2.985

B. T ≃ 1200°K

P_{0TiCl_4}	Y	ξ_{TiN}	$100\ P_{0TiCl_4}\ \xi_{TiN}$
0.100	20	~0.100	~1.000
0.001	2	~1.000	~0.100
0.010		0.989	0.989
0.050		0.868	4.340
0.100		0.702	7.020
0.150		0.574	8.610
0.200		0.476	9.520
0.286*		0.352	10.067

P_{0TiCl_4}	Y	ξ_{TiN}	100 P_{0TiCl_4} ξ_{TiN}
0.001	0.2	~1.000	~0.100
0.010		~1.000	~1.000
0.050		0.955	4.775
0.100		0.675	6.750
0.150		0.227	3.405

C. T ≃ 1400°K

P_{0TiCl_4}	Y	ξ_{TiN}	100 P_{0TiCl_4} ξ_{TiN}
0.001	2	~1.000	~0.100
0.010		0.993	0.993
0.050		0.908	4.540
0.100		0.765	7.650
0.150		0.638	9.570
0.200		0.535	10.700
0.286*		0.397	11.354
0.001	0.2	~1.000	~0.100
0.010		~1.000	~1.000
0.050		0.976	4.880
0.100		0.743	7.430
0.150		0.246	3.690

D. T = 1500°K

P_{0TiCl_4}	Y	ξ_{TiN}	100 P_{0TiCl_4} ξ_{TiN}
0.001	2	~1.000	~0.100
0.010		0.995	0.995
0.050		0.921	4.605
0.100		0.788	7.880
0.150		0.664	9.960
0.200		0.559	11.180
0.286*		0.415	11.869
0.001	0.2	~1.000	~0.100
0.010		~1.000	~1.000
0.050		0.982	4.910
0.100		0.770	7.700
0.150		0.253	3.795

*Stoichiometric reactive gas phase mixture at 1 atmosphere: $P_{0,TiCl_4} = 0.286$ $P_{0,N_2} = 0.143$; $P_{0,H_2} = 0.571$ atm.

3. Binary MeX_u(X = C,N, or O) and Ternary Interstitial Phases, et al.

The relationships derived for the deposition of stoichiometric transition metal monocarbides and nitrides may be expanded to include MeX_u(X = C, N, or O) alloys with variable interstitial to metal atom ratios, i.e., u may equal any value within the stability limits of the phase.

For example, reaction (25) leading to the formation of MeC may be split into two simultaneous reactions

$$CH_{4(g)} = (C)_{Me_xC_y} + 2H_{2(g)} \tag{36}$$

$$MeCl_{4(g)} + 2H_{2(g)} = (Me)_{Me_xC_y} + 4HCl_{(g)} , \tag{37}$$

where

$$\xi_{(c)} = \frac{n_{\epsilon\,(c)}}{n_{oCH_4}} \quad ; \qquad \xi_{(Me)} = \frac{n_{\epsilon\,(Me)}}{n_{oMeCl_4}} \quad .$$

Besides the suppression of free graphite through condition (30), an additional constraint is the preassigned composition,

$$u = \frac{y}{x} = \frac{n_{\epsilon\,(c)}}{n_{\epsilon\,(Me)}} = \frac{n_{oCH_4}\,\xi_{(c)}}{n_{oMeCl_4}\,\xi_{(Me)}} = \frac{P_{0CH_4}\,\xi_{(c)}}{P_{0MeCl_4}\,\xi_{(Me)}} \quad . \tag{38}$$

Activities for (Me) and (C) in single phase alloys, if not available from the literature, may be calculated from $\Delta G^{o}_{f,Me_xC_y}$. Combining the Kp relationships for reactions (36) and (37) by means of (38), permissible partial pressures of P_{0MeCl_4} and P_{0CH_4} may be calculated for the deposition of a preselected carbide composition.

The derivation of equations for the deposition of transition metal carbonitrides may be approached in the above manner. A reaction representing the equilibration of a solid solution, $Me(C_uN_v)$, is

$$(MeN)_{Me(C_uN_v)} + CH_{4(g)} = (MeC)_{Me(C_uN_v)} + 2H_{2(g)} + 1/2\ N_{2(g)} \qquad (39)$$

which yields the following partial reactions similar to (25) and (33)

$$MeCl_{4(g)} + CH_{4(g)} = (MeC)_{Me(C_uN_v)} + 4HCl_{(g)}\ ; \qquad (40)$$

$$MeCl_{4(g)} + 2H_{2(g)} + 1/2\ N_{2(g)} = (MeN)_{Me(C_uN_v)} + 4HCl_{(g)} \qquad (41)$$

In addition, $\Delta G^{o}_{R(39)} = \Delta G^{o}_{R(40)} - \Delta G^{o}_{R(41)}$ and $K_{p(39)} = K_{p(40)}/K_{p(41)}$.

With (40) and (41), defining the mole fraction of $MeCl_{4(g)}$ converted to (MeC) by $\xi_{(MeC)}$ and to (MeN) by $\xi_{(MeN)}$ and utilizing (11) for the conversion of moles to partial pressures, $P_{\epsilon i}$ relationships for reactants and products are

$$P_{\epsilon\,\mathrm{MeCl_4}} = P_{\mathrm{oMeCl_4}}\left(1-\xi_{(\mathrm{MeC})}-\xi_{(\mathrm{MeN})}\right)\left(\frac{V_o}{V_\epsilon}\right)_{T,P} \tag{42a}$$

$$P_{\epsilon\mathrm{CH_4}} = P_{\mathrm{oCH_4}}\left(1-X\xi_{(\mathrm{MeC})}\right)\left(\frac{V_o}{V_\epsilon}\right)_{T,P} \tag{42b}$$

$$P_{\epsilon\mathrm{H_2}} = P_{\mathrm{oH_2}}\left(1-2\ \frac{P_{\mathrm{0MeCl_4}}}{P_{\mathrm{oH_2}}}\ \xi_{(\mathrm{MeN})}\right)\left(\frac{V_o}{V_\epsilon}\right)_{T,P} \tag{42c}$$

$$P_{\epsilon\mathrm{N_2}} = P_{\mathrm{oN_2}}\left(1-2^{-1}Y\ \xi_{(\mathrm{MeN})}\right)\left(\frac{V_o}{V_\epsilon}\right)_{T,P} \tag{42d}$$

$$P_{\epsilon\mathrm{HCl}} = 4P_{\mathrm{oMeCl_4}}\left(\xi_{(\mathrm{MeC})}+\xi_{(\mathrm{MeN})}\right)\left(\frac{V_o}{V_\epsilon}\right)_{T,P} \tag{42e}$$

where

$$X = \frac{P_{\mathrm{oMeCl_4}}}{P_{\mathrm{oCH_4}}}\ , \qquad Y = \frac{P_{\mathrm{oMeCl_4}}}{P_{\mathrm{oN_2}}}$$

and with the aid of (12)

$$\left(\frac{V_o}{V_\epsilon}\right)_{T,P} = \left(1+(2\,\xi_{(\mathrm{MeC})}+\frac{1}{2}\ \xi_{(\mathrm{MeN})})\ \frac{P_{\mathrm{oMeCl_4}}}{P}\right)^{-1} .$$

Selecting the partial reaction (40) and substituting 42 (a,b; e) into the expression for $K_{p(40)}$,

$$\xi^4_{(\mathrm{MeC})} - \frac{K_{p(40)}\left(1-(1+Z)\,\xi_{(\mathrm{MeC})}\right)\left(1-X\,\xi_{(\mathrm{MeC})}\right)}{256\ uX\ (1+Z)^4\ P^2_{\mathrm{oMeCl_4}}}\left(\frac{V_\epsilon}{V_o}\right)^2_{T,P} = 0. \tag{43}$$

Constraints imposed on (43) are

(i) Total system pressure:

$$P_{oMeCl_4} + P_{oCH_4} + P_{oH_2} + P_{oN_2} = \mathbf{P} \text{ (constant)}$$

(ii) Suppression of free graphite:

$$\left(\frac{P_{oH_2}}{P_{oCH_4}}\right)_{T,\mathbf{P}} \geq \left(\frac{K_{P(26)}}{P_{oCH_4}}\right)^{1/2}$$

(iii) Preassigned composition of carbonitride phase, $Me(C_uN_v)$:

$$Z = \frac{v}{u} = \frac{n_{\epsilon(MeN)}}{n_{\epsilon(MeC)}} = \frac{\xi_{(MeN)}}{\xi_{(MeC)}} .$$

One additional relationship is required for the calculation of initial nitrogen partial pressures which are consistent with the dependent variables $\xi_{(MeC)}$ and $\xi_{(MeN)}$ from (43). Reaction (39) is used for this purpose, and by substituting 42(a-e) into $K_{p(39)}$ and rearranging terms

$$P_{oN_2} \approx 1/2\, P_{oMeCl_4}\, \xi_{(MeN)} + \left(K_{p(39)} Z P_{oCH_4}\left(1 - X\xi_{(MeC)}\right)\right)^2 \left(\frac{V_\epsilon}{V_o}\right)^3_{T,P} . \quad (44)$$

The approximation $P_{\epsilon H_2} \approx P_{oH_2}$ was used because the magnitude of $(P_{oMeCl_4}/P_{oH_2})\,\xi_{(MeN)}$ is usually insignificant when compared to P_{oH_2} (42c).

Utilizing (43) and (44), initial conditions and yields for the deposition of $Ti(C_uN_v)$ alloys at a temperature of 1000°K are presented in Table V. Also included in Tables VI and VII are the maximum deposition efficiencies as a function of P_{oCH_4} and T for the same ternary alloys plus the edge binary phases of TiC and TiN.

The formation of transition metal oxycarbides and oxynitrides follows the same considerations. Selecting titanium as an example, the following reactions similar to (39) may be written

$$(TiC)_{Ti(C_uO_v)} + \frac{1}{2} O_{2(g)} = (TiO)_{Ti(C_uO_v)} + C_{(s)} \tag{45}$$

and

$$(TiN)_{Ti(N_uO_v)} + \frac{1}{2} O_{2(g)} = (TiO)_{Ti(N_uO_v)} + \frac{1}{2} N_{2(g)} \tag{46}$$

For (45), the formation of free carbon must be suppressed.

In addition, since titanium can form stable oxides besides the cubic TiO modification, the calculated oxygen partial pressures according to (45) or (46) must prevent their formation. The most likely higher oxides are Ti_2O_3 or TiO_2 and, if stabilized, produce three-phase equilibria of the type

$$TiO_{3/2} = (TiO)_{Ti(X_uO_v)} + 1/4\ O_{2(g)} \tag{47}$$

or

$$TiO_2 = (TiO)_{Ti(X_uO_v)} + 1/2\ O_{2(g)} \tag{48}$$

where X = C or N. As indicated, both the carbon and nitrogen solubilities in the higher oxides are restricted. The side reactions (47)

Table V. Theoretical Yields for the Chemical Vapor Deposition of $Ti(C_uN_v)$.

Reaction: $TiCl_{4(g)} + CH_{4(g)} = (TiC)_{Ti(C_uN_v)} + 4HCl_{(g)}$

$\Delta G^o_R = 70,580 - 58.00\ T$(cal/formula change)$^{(30,31,32)}$

Conditions: $P_{oTiCl_4} + P_{oCH_4} + P_{oH_2} + P_{oN_2} \approx 1$ atm.

$$P_{oN_2} \approx 1/2\ P_{oTiCl_4}\ \xi_{(TiN)}$$

$$\xi = \xi_{(TiC)} + \xi_{(TiN)}$$

$$X = \frac{P_{oTiCl_4}}{P_{oCH_4}}, \quad P_{oTiCl_4} = 0.100 \text{ atm.}$$

$$T = 1000°K$$

$Ti(C_{0.1}N_{0.9})$				
X	$\xi_{(TiC)}$	$\xi_{(TiN)}$	P_{oN_2}	$100P_{oTiCl_4}\xi$
200	0.0044	0.0398	0.0020	0.442
100	0.0068	0.0612	0.0031	0.680
10	0.0150	0.1350	0.0068	1.500
1.322^*	0.0249	0.2241	0.0112	2.490
$Ti(C_{0.25}N_{0.75})$				
200	0.0049	0.0147	0.0007	0.196
100	0.0093	0.0279	0.0014	0.372
10	0.0289	0.0867	0.0043	1.156
1.322^*	0.0499	0.1497	0.0075	1.996
$Ti(C_{0.5}N_{0.5})$				
200	~0.0050	~0.0050	0.0003	0.100
100	0.0099	0.0099	0.0005	0.198
10	0.0456	0.0456	0.0023	0.912
1.322^*	0.0836	0.0836	0.0042	1.672

$Ti_{(C_{0.75}N_{0.25})}$

X	$\xi_{(TiC)}$	$\xi_{(TiN)}$	P_{oN_2}	100 $P_{oTiCl_4}\xi$
200	~0.0050	~0.0017	0.0001	0.067
100	~0.0100	~0.0033	0.0002	0.133
10	0.0580	0.0193	0.0010	0.773
1.322*	0.1126	0.0375	0.0019	1.501

$Ti_{(C_{0.9}N_{0.1})}$

200	~0.0050	~0.0006	<0.0001	0.056
100	~0.0100	~0.0011	0.0001	0.111
10	0.0640	0.0071	0.0004	0.711
1.322*	0.1285	0.0143	0.0007	1.428

---

*$P_{0CH_4}^{max.}$ = maximum allowable methane partial pressure to prevent deposition of free carbon at 1000° K (P_{0TiCl_4} = 0.100 atm).

Table VI. Maximum Deposition Efficiencies ($100P_{0TiCl_4}\xi$) for $Ti(C_uN_v)$ Alloys as a Function of the Methane Partial Pressure and Temperature (P_{0TiCl_4} = 0.100 atm).

		P_{0CH_4}, atm		$P_{0CH_4}^{max}$
A. T = 1000°K				
Mole % TiC	0.0005	0.0010	0.0100	0.0756
10	0.442	0.680	1.500	2.490
25	0.196	0.372	1.156	1.996
50	0.100	0.198	0.912	1.672
75	0.067	0.133	0.773	1.501
90	0.056	0.111	0.711	1.428
100	0.040	0.077	0.398	1.301
B. T = 1200°K				
				0.0135
10	0.500	1.000	5.030	5.520
25	0.200	0.400	3.308	3.916
50	0.100	0.200	1.932	2.500
75	0.067	0.133	1.320	1.756
90	0.056	0.111	1.104	1.478
100	0.049	0.098	0.856	1.214
C. T = 1400°K			0.0020	0.0036
10	0.500	1.000	1.990	3.590
25	0.200	0.400	0.800	1.440
50	0.100	0.200	0.400	0.720
75	0.067	0.133	0.267	0.480
90	0.056	0.111	0.222	0.400
100	0.050	0.100	0.199	0.396

Table VII. Maximum Deposition Efficiencies ($100P_{0TiCl_4}\xi$) for $Ti(C_uN_v)$ Alloys as a Function of Temperature

Conditions: $P_{0TiCl_4} = 0.100$ atm

$P_{0CH_4} = P^{max}_{0CH_4}$

$P_{0N_2} \simeq 1/2\ P_{0TiCl_4}\ \xi_{(TiN)}$

	Mole % TiC						
T, °K	0	10	25	50	75	90	100
1000	6.090	2.490	1.996	1.672	1.501	1.428	1.301
1200	7.020	5.520	3.916	2.500	1.756	1.478	0.999
1400	7.650	3.590	1.440	0.720	0.480	0.400	0.380
1500	7.880	2.250	0.900	0.450	0.300	0.250	0.240

and (48) also provide a method for precipitating a second phase after the formation of a $Ti(X_uO_v)$ alloy from the vapor phase.

In terms of a practical application, present refractory and hard coatings deposited on commercial tool alloys have been restricted to TiC, TiN, Ti(C,N), and Al_2O_3. In addition to the established coatings, the remaining group IV transition metal - interstitial phases are of interest because of their chemical and structural similarity to the proven titanium containing alloys. For the more restricted or stoichiometric phases of nontransition metals, such as Al_2O_3; coating materials are the stable, refractory silicon carbide and nitride, and aluminum nitride. AlN exhibits low decomposition pressures at elevated temperatures and is chemically similar to TiN.

Also, many possibilities exist for the improvement of substrate-coating compatibilities by reducing stepwise changes in physical properties. Through the thermodynamic relationships presented, it is technically feasible to design composite systems of the following type:

(i) substrate/MeC/Me(C,N) or Me(O,N)

(ii) substrate/MeN/Me(C,N) or Me(O,N)

(iii) substract/interchanging position of transition and surface layers in (i) and (ii).

(iv) substrate/mechanical mixtures of dissimilar nitrides, nitrides-oxides, carbides-oxides, etc.

E. DISCUSSION

Fundamental considerations for the deposition of alloys from multiple vapor sources were applied to specific systems, and theoretical yields and deposition efficiencies as a function of temperature and pressure were calculated for preselected compositions.

As evidenced by the yield data presented in Tables III, IV, and V for the deposition of TiC, TiN, and $Ti(C_uN_v)$, respectively, maintenance of the stoichiometric ratios $X = 1$ and $Y = 2$ is not necessary. It may also be noted that with increasing temperature when holding the initial concentration of reactants constant, the yields increase as would be expected from the temperature dependence of the free energy changes. But more important is the change in both the yields and deposition efficiencies under isothermal conditions. ξ_j (Tables III, IV; VI) is more sensitive to change as a function of the chloride, methane, and/or nitrogen partial pressures than as a function of the temperature.

Depending on the relative magnitudes of P_{oi} and ξ_j, their product $(P_{oi}\xi_j)$, defined as the deposition efficiency (10), may either increase or decrease with increasing P_{oi}. In general, if P_{oi} is small compared to ξ_j, increasing it will result in a higher deposition rate (Tables III, IV, VI). This trend might not result as evidenced by the efficiency maxima for the deposition of TiN (Table IV, Y = 0.2). $(P_{oTiCl_4}\xi)$ maxima may also be noted for carbonitride alloys as a function of temperature (Table VII).

The theoretical deposition data presented in Table VI for $Ti(C_uN_v)$ alloys show how composite coatings with variable interstitial contents may be formulated. For example, select a system substrate/TiC/Ti(C,N) where the carbide and carbonitride phases exhibit equivalent deposition efficiencies at the same temperature. The transition from carbide to carbonitride outer layer may be made through decreasing the hydrocarbon partial pressure (shorter furnace dwell time) to a value which gives a nitrogen-rich phase of the desired composition. This observation is consistent with the experimental results of Schintlmeister and Pacher(19).

With an apparatus of the type shown in Figure 1, a quantitative check on the theoretical yield calculations was made by coating sintered carbide tool alloys with nitrides of titanium and hafnium. The results for selected deposition conditions are presented in Tables VIII and IX. The conditions used for TiN at $P_{0TiCl_4} = 0.080$ and 0.100 were based on the calculated $(P_{0TiCl_4}\xi_{TiN})$ maxima noted in Table IV at approximately the same temperatures and stoichiometry parameters. The experimental yields due to the method used for their calculation (Table VIII) are considerably lower than the theoretical values, but the same trends in ξ_{TiN} as a function of P_{0TiCl_4} and Y are observed, i.e., coating rates are higher at the lower chloride partial pressures.

Table VIII. Experimental Yields for TiN at 1250° and 1350°K.

Conditions: $P_{0TiCl_4} + P_{0N_2} + P_{0H_2} \approx 1$ atm

$$Y = \frac{P_{0TiCl_4}}{P_{0N_2}}$$

		ξ^*_{TiN}	
P_{0TiCl_4}	Y	1250°K	1350°K
0.020	0.041	0.50	0.61
0.050	0.105	0.13	0.21
0.080	0.174	0.07	0.11
0.100	0.222	0.04	0.08

---

*Estimated by comparing weight gain of coated tools with tetrachloride consumed.

For HfN, both the theoretical and experimental yields are compared under identical deposition conditions (Table IX). Here the total amount of nitride deposited was estimated by comparing the hafnium recovered as tetrachloride with the hafnium consumed and by measuring the hydrogen chloride partial pressure in the off-gas with a gas chromatograph. Thus with $P_{0HfCl_4} = 0.004$, the extent of reaction calculated from the amount of unreacted $HfCl_4$ is 0.49 ± 0.12, and from the measured partial pressure $P_{\epsilon HCl} = 0.007 \pm 0.001$ is 0.44 ± 0.06, in comparison to the theoretical value of 0.505. The theoretical equilibrium HCl partial pressure calculated from (34) with $P_{0HfCl_4} = 0.004$ and $\xi_{HfN} = 0.505$ is $P_{\epsilon HCl} = 0.008$ atmospheres.

Even in light of the uncertainties associated with the experimental ξ_{HfN}, it is evident that the overall deposition reaction is not going to completion. Provided that the thermodynamic data used are correct, with increasing P_{0HfCl_4}, both the theoretical and experimental yields decrease with ξ_{HfN} (exp) decreasing more rapidly; hence indicating that the deposition process becomes more kinetically limited at higher P_{0HfCl_4} values. Improvements in the experimental yields may be made by either allowing longer time for conversion (increase dwell time of reactants by decreasing total gas flow-rate) or increasing the reaction temperature.

Table IX. Theoretical and Experimental Yields for the Chemical Vapor Deposition of HfN

$$\Delta G^{o}_{R} = 45,980-10.59\ T\ \text{(cal/formula change)}^{(30-32)}$$

Conditions: $P_{0HfCl_4} + P_{0N_2} + P_{0H_2} \approx 1$ atm

$$Y = \frac{P_{0HfCl_4}}{P_{0N_2}}\ ; \quad T = 1400^\circ K$$

P_{0HfCl_4}	Y	ξ_{HfN}(Theoretical)	ξ_{HfN}(Experimental)
0.004	0.006	0.505	0.49 ± 0.12*, 0.44 ± 0.06**
0.007	0.012	0.326	N.D.
0.015	0.025	0.195	0.11 ± 0.03*

---

* Estimated by comparing Hf recovered as tetrachloride with Hf consumed.

** Estimated by measuring $P_{\epsilon HCl}$ in the off-gas.

N.D. Not determined.

In addition to the generated yield data, other considerations such as coating morphology (fine, equiaxed or columnar grain structure), substrate-gas phase interactions, and reaction rates and times to deposit a given layer have to be considered in order to optimize the process. Also, the flow characteristics of the reactive gas phase mixture is an important consideration in obtaining even deposition rates and coating uniformity from point to point in the furnace, e.g., laminar versus turbulent flow conditions and convective back-mixing of reactants.

REFERENCES

1. C. F. Powell, I. E. Campbell, and B. W. Gonser, "Vapor Plating," John Wiley and Sons, 1955.

2. C. F. Powell, J. H. Oxley, and J. M. Blocher, Jr., "Vapor Deposition," John Wiley and Sons, 1966.

3. J. W. Aylsworth, U. S. Pat. 553,296, June 1880.

4. A. deLodyguine, U.S. Pats. 575,002 and 575,668, January 1897.

5. A. E. vanArkel, Physika, 4, (1924), 286.

6. A. E. vanArkel and J. H. deBoer, Z. Anorg. Chemie, 148, (1925), 345.

7. K. Moers, Z. Anorg. Chemie, 198, (1931), 243.

8. F. H. Pollard and P. Woodward, Trans. Faraday Soc., 46, (1950), 190-199.

9. F. H. Pollard and P. Woodward, J. Chem. Soc., (London), (1948), 1709-1713.

10. I.E. Campbell, C. F. Powell, D. H. Nowicki, and B. W. Gonser, J. El. Chem. Soc., 96, (1949), 318.

11. A. Munster and W. Ruppert, Z. f. Electrochem., 57, (1953), 564-571.

12. A. Munster and K. Sagel, Z. f. Electrochem, 57, (1953), 571-579.

13. M. Robinson, "Kinetics of Vapor Deposition of Titanium Nitride," Ph.D. Thesis, M.I.T., 1967.

14. J. J. Nickl and M. Reichle, J. Less-Common Metals, 24, (1971), 63-72.

15. M. Reichle and J. J. Nickl, J. Less-Common Metals, 29, (1972), 241-251.

16. BISRA Conference on Materials for Metal-Cutting, Scarborough, England, 1970.

17. C. S. G. Ekemar, U.S. Pat. 3,616,506, Jan. 1970.

18. G. Schuhmacker, T. Z. fur Prakt. Metallbearbeitung, 63, (1969), 275.

19. W. Schintlmeister and O. Pacher, 8th Plansee Seminar, Reutte, Austria, 37, (1974).

20. J. R. Peterson, J. Vac. Sci. Technol., 11, (1974), 715-718.

21. R. Kieffer, D. Fister, H. Schoof, and K. Mauer, Powder Metallurgy International, 5, No. 4, (1973), 188-191.

22. F. A. Glaski, R. A. Holzl, and R. B. Kaplan, U.S. Pat. 3,640,689, March 1970.

23. M. Lee and M. H. Richman, J. Electrochem. Soc., 120, (1973), 993-996.

24. N. P. Suh and S. K. Naik, J. of Engineering for Industry, Trans. ASME, 93, No. 4, (1971), 1106-1112.

25. N. P. Suh and B. J. Sanghvi, J. of Engineering for Industry, Trans. ASME, 93, No. 2, (1971), 455-460.

26. N. P. Suh, S. Shyam, and S. K. Naik, J. of Engineering for Industry, Trans. ASME, 94, No. 4, (1972), 979-984.

27. I. Prigogine and R. Defay, "Chemical Thermodynamics", Logmans, Green and Co., Ltd., 1967.

28. Th. DeDonder and P. VanRysselberghe, "The Thermodynamic Theory of Affinity," Stanford, 1936.

29. Th. DeDonder, "Lecons de Thermodynamique et de Chimie physique," F. H. van den Dungen and G. vanLerberghe, editors, Paris, 1920.

30. D. R. Stull et al., "JANAF Thermochemical Tables," Dow Chemical Co., 1965.

31. H. L. Schick, "Thermodynamics of Certain Refractory Compounds," Vol. I and II, Academic Press, New York, 1966.

32. E. Steinmetz and H. Roth, Journal of the Less-Common Metals, 16, (1968), 295-342.

BIOGRAPHICAL NOTE

The author was born in Corpus Christi, Texas, on February 12, 1944. After moving to Redwood City, California in 1949 and attending public schools there, he entered the University of California at Berkeley in 1964. During the academic years 1965-1966 and 1966-67, the author held the Gladding McBean Scholarship in Ceramic Engineering and the Edwin Letts Oliver Scholarship, respectively. He was awarded the Bachelor of Science Degree in Ceramic Engineering in June 1967.

From 1967 to 1969, the author was employed as an associate engineer at the Materials Research Laboratory of the Aerojet-General Corporation in Sacramento, California. During this time, he did both basic and applied research work on transition metal carbide and nitride systems, and he contributed the following coauthored technical reports:

> W. Bradley and P. Booker, "Development of a Temperature-Indicating Sensor for Use in Ablative Rocket Nozzles," Air Force Technical Report AFRPL-TR-69-172, July 1969.
>
> P. H. Booker and C. E. Brukl, "The Phase Equilibria in the Metal-Rich Region of the Hafnium-Tantalum-Nitrogen System", Air Force Technical Report AFML-TR-69-117, Part VI, December 1969.
>
> P. Booker and E. Rudy, "Phase Equilibria in the Nb-Ta-C System", Air Force Technical Report AFML-TR-69-117, Part III, May 1970.

In September 1969, the author was admitted to the Graduate School in Metallurgy at the University of Denver. During the academic year 1969-1970, he held a National Defense Graduate Fellowship (NDEA Title IV). Upon completion of his course and thesis work, entitled "Ternary Phase Equilibria in the System Titanium-Chromium-Carbon", he was awarded the Master of Science Degree in Physical Metallurgy in December 1970.

From January 1971 to March 1974, the author was a resident student at the Oregon Graduate Center in the Department of Materials Science. Since March 1974, the author has been employed as a carbide development engineer at the Teledyne Wah Chang Albany Corporation in Albany, Oregon; during this time, work was conducted on completing his thesis manuscript.